SANDIA REPORT

SAND2004-4899
Unlimited Release
Printed September 2005

Spatial Analysis of Hypocenter to Fault Relationships for Determining Fault Process Zone Width in Japan

Barry L. Roberts, Timothy C. Coburn, Bill W. Arnold, and Sean A. McKenna

Prepared by
Sandia National Laboratories
Albuquerque, New Mexico 87185 and Livermore, California 94550

Sandia is a multiprogram laboratory operated by Sandia Corporation,
a Lockheed Martin Company, for the United States Department of Energy's
National Nuclear Security Administration under Contract DE-AC04-94AL85000.

Approved for public release; further dissemination unlimited.

Sandia National Laboratories

Issued by Sandia National Laboratories, operated for the United States Department of Energy by Sandia Corporation.

NOTICE: This report was prepared as an account of work sponsored by an agency of the United States Government. Neither the United States Government, nor any agency thereof, nor any of their employees, nor any of their contractors, subcontractors, or their employees, make any warranty, express or implied, or assume any legal liability or responsibility for the accuracy, completeness, or usefulness of any information, apparatus, product, or process disclosed, or represent that its use would not infringe privately owned rights. Reference herein to any specific commercial product, process, or service by trade name, trademark, manufacturer, or otherwise, does not necessarily constitute or imply its endorsement, recommendation, or favoring by the United States Government, any agency thereof, or any of their contractors or subcontractors. The views and opinions expressed herein do not necessarily state or reflect those of the United States Government, any agency thereof, or any of their contractors.

Printed in the United States of America. This report has been reproduced directly from the best available copy.

Available to DOE and DOE contractors from
U.S. Department of Energy
Office of Scientific and Technical Information
P.O. Box 62
Oak Ridge, TN 37831

Telephone: (865)576-8401
Facsimile: (865)576-5728
E-Mail: reports@adonis.osti.gov
Online ordering: http://www.osti.gov/bridge

Available to the public from
U.S. Department of Commerce
National Technical Information Service
5285 Port Royal Rd
Springfield, VA 22161

Telephone: (800)553-6847
Facsimile: (703)605-6900
E-Mail: orders@ntis.fedworld.gov
Online order: http://www.ntis.gov/help/ordermethods.asp?loc=7-4-0#online

SAND2004-4899
Unlimited Release
Printed September 2005

Spatial Analysis of Hypocenter to Fault Relationships for Determining Fault Process Zone Width in Japan

Barry L. Roberts[1], Timothy C. Coburn[2], Bill W. Arnold[1], and Sean A. McKenna[1]

[1]Sandia National Laboratories
Albuquerque, New Mexico

[2]Professor of Statistics
Abilene Christian University
Abilene, Texas

Abstract

Preliminary investigation areas (PIA) for a potential repository of high-level radioactive waste must be evaluated by NUMO with regard to a number of qualifying factors. One of these factors is related to earthquakes and fault activity. This study develops a spatial statistical assessment method that can be applied to the active faults in Japan to perform such screening evaluations. This analysis uses the distribution of seismicity near faults to define the width of the associated process zone. This concept is based on previous observations of aftershock earthquakes clustered near active faults and on the assumption that such seismic activity is indicative of fracturing and associated impacts on bedrock integrity. Preliminary analyses of aggregate data for all of Japan confirmed that the frequency of earthquakes is higher near active faults. Data used in the analysis were obtained from NUMO and consist of three primary sources: 1) active fault attributes compiled in a spreadsheet, 2) earthquake hypocenter data, and 3) active fault locations. Examination of these data revealed several limitations with regard to the ability to associate fault attributes from the spreadsheet to locations of individual fault trace segments. In particular, there was no direct link between attributes of the active faults in the spreadsheet and the active fault locations in the GIS database. In addition, the hypocenter location resolution in the pre-1983 data was less accurate than for later data. These pre-1983 hypocenters were eliminated from further analysis.

GIS processing involved developing automated methods to associate fault polylines with specific faults in the fault attribute data set. The earthquake hypocenter data were filtered with regard to distance from active faults, depth, and approximately perpendicular offset from active faults. Only attributed faults and those earthquake hypocenters near them were retained in the analysis. Histograms of normal distances from hypocenters to active faults were plotted for different active faults. This task revealed several types of the distributions, including symmetric, bimodal, and skewed. In addition, it was observed that many of the distributions were not centered on the fault plane. Examination of the earthquake characteristics of depth and magnitude was conducted, revealing that most of the earthquakes in the filtered data set were from 5 to 15 km depth and the highest frequency of occurrence was for magnitudes of 1 to 1.5. No consistent relationship between associated active fault length and depth or magnitude was observed.

Three alternative statistical measures considered to be potentially representative of the width of the seismic process zone around active faults were evaluated: 1) twice the mean of all hypocenter distances, 2) twice the median of all hypocenter distances, and 3) sum of the medians of the hypocenter distances on the two sides of the fault. Based on the distributions of these three alternative measures among the faults, the sum of the medians of the hypocenter distances on the two sides of the fault was determined to be the most reasonable measure of the width of the seismic process zone. The 50th percentile value of this measure among the active faults evaluated is about 8700 m. Cross plots of the sum of the medians of the hypocenter distances on the two sides of the fault and the fault length showed no correlation between these two variables. This lack of positive correlation could be due to lack of validity of this measure of the width of the seismic process zone or it is possible that the width of the process zone is relatively invariant with fault length. The conceptual model of identifying the width of the process zone around active faults using seismic data is supported when applied in an aggregate sense to all active faults. However, when these data on distances from hypocenters to faults are analyzed statistically for individual active faults, the analysis is confounded by non-ideal distributions for many faults. These non-ideal distributions are likely due to the inaccurate hypocenter-fault relationships due to faults not included in the GIS database. More complete data sets would improve the analyses.

Acknowledgments

The work described in this report was performed under the Discrete Feature Mapping Methodology Project funded by the Nuclear Waste Management Organization of Japan (NUMO) through an agreement with Sandia National Laboratories. We acknowledge the efforts of Hiroyuki Tsuchi and Junichi Goto in providing guidance and assistance in moving the project forward. F. B. Nimick reviewed and provided many useful comments on this document.

Contents

Abstract 3

List of Figures 7

List of Tables 10

Introduction 11
- Objectives 11
- Background 11
- Initial Concept for Analysis 14
- Revised Concept for Analysis 15
- Potential Sources of Error and Limitations in the Analysis 16

Available Data Sets 19
- Original Source Data 19
- Fault Attribute Data Source Properties 19
- Hypocenter Data Source Properties 20
- Fault Location Data Source Properties 21
- Data Set Anomalies 22
- Fault Attribute Data 22
- Hypocenter Data 23
- Fault Location Data 26

Geographic Information System Analysis 29
- Data Processing 29
- Fault Endpoint Polyline Creation 31
- Hypocenter Filtering 37
- Hypocenter Limiting Polygons 38
- Distance Computations 38
- Limitations and Assumptions 46
- Summary of GIS Analysis and Processing 47

Statistical Analysis 49
- Initial Descriptive Assessment of Hypocenter Distance and Further Screening of Hypocenters 49
- Descriptive Characteristics of Hypocenters 70
- Fault Length Considerations 78
- Relationship of Fault Length to Number of Hypocenters 79
- Relationship of Fault Length to Depth of Hypocenters and Earthquake Magnitude 82
- Relationship of Hypocenter Distance to Hypocenter Depth and Earthquake Magnitude 84
- Estimating the Width of the Process Zone 90
- Relationship between Fault Length and Width of the Seismic Process Zone 98
- Other Considerations 102

Summary and Conclusions 108

References.....111

Appendix A.....112
ArcView GIS Processing Codes.....112
Endpoints2polylines.ave.....112
Associate_attributes.ave.....113
Limit_polygons.ave.....114
Data dictionary.....117

Appendix B.....122
Statistics on Earthquake Hypocenters Associated with Individual Faults.....122

Appendix C.....162
Percentage Histograms of “Signed” Normal Distance from Hypocenters to Fault Planes162

Appendix D.....226
Errors in the Location of Earthquake Hypocenters.....226

List of Figures

Figure 1. Active fault traces (red lines) in Japan. 13

Figure 2. Conceptualization of the distribution of fracture intensity around a fault..... 14

Figure 3. Histogram of seismic events. 16

Figure 4. Map of all hypocenter locations, shown in red, available for this study. 23

Figure 5. Map showing clustering of pre-1983 hypocenter locations.. 25

Figure 6. Map showing locations of 1983 and later hypocenter locations. 25

Figure 7. Map showing example fault traces.. 26

Figure 8. GIS process flow chart. 30

Figure 9. Example of fault location polyline data..... 31

Figure 10. Example of Polylines Representing Fault Traces..... 32

Figure 11. Relationships between polylines.. 33

Figure 12. Example of using fault endpoint buffer. 35

Figure 13. Example of small isolated fault trace.. 36

Figure 14. Hypocenter locations (red points) remaining after spatial filtering..... 37

Figure 15. Example hypocenter limiting polygon. 38

Figure 16. UTM Zones and projection test locations. 39

Figure 17. Schematic cross-sections showing depth-corrected planimetric distances.. 42

Figure 18. Hypocenter fault block determination.. 43

Figure 19. Depth correction where hypocenter projection penetrates fault plane.. 44

Figure 20. Geometry used to compute the fault normal distances..... 45

Figure 21. Percentage histograms of normal distance from hypocenters to fault planes. Four different faults with an increasingly larger number of associated hypocenters: (a) A 43-1 (Unnamed), with n=23; (b) A 92-2 (Iyo), with n=41; (c) A 29-5 (Oohira), with n=105; and (d) A 71-1 (Atsumi), with n=179. 52

Figure 22. Percentage histograms of normal distance from hypocenters to fault planes. Four different faults for which the associated histograms exhibit one of four recurring patterns: (a) A 51-2 (unknown name), skewed left, with n=318; (b) A 106-1 (Ono, Hinaku), skewed right, with n=10,532; (c) A 87-3 (Okamura), bimodal, with n=208; and (d) A 70-1 (Takashimizu), symmetric, with n=88. 54

Figure 23. Box plots of normal distance from hypocenters to fault planes (truncated at zero on the lower end). The data set is restricted to faults having 50 or more associated hypocenters. Plots are presented in order of increasing fault length, beginning with B60-1 in (a) having a total length of 6,964.1 m and ending with A87-2 in (d) having a total length of 107,204.8 m. Statistical outliers shown as empty squares; statistical extremes shown as filled squares. 57

Figure 24. Percentage histogram of hypocenter distance associated with Fault A 65-5 (Sansyu). The distribution encompasses no outliers. 58

Figure 25. Percentage histogram of hypocenter distance associated with Fault A 75-7 (Satomura). The distribution encompasses outliers on the right side. 59

Figure 26. Percentage histogram of hypocenter distance associated with Fault A 64-4 (Sakai-toge). The distribution encompasses outliers and extreme values on the left side. 59

Figure 27. Percentage histogram of hypocenter distance associated with Fault A 106-4 (Yhazutoge, Kiminagawa, Uchikiba). The distribution encompasses outliers and extreme values on both sides. 60

Figure 28. Box plots of normal distance from hypocenters to fault planes, after eliminating outliers and extreme values. 62

Figure 29. Percentage histogram of normal distances from hypocenters to Fault A65-5 (Sansyu). 64

Figure 30. Percentage histogram of normal distances from hypocenters to Fault A75-7 (Satomura). 65

Figure 31. Percentage histogram of normal distances from hypocenters to Fault A64-4 (Sakai-toge). 66

Figure 32. Percentage histogram of normal distances from hypocenters to Fault A106-4 (Yhazutoge, Kiminagawa, Uchikiba). 67

Figure 33. Frequency histogram of (a) unsigned distance and (b) signed distance from hypocenters to fault planes, all of Japan.. 69

Figure 34. Histogram of the percentage of all hypocenter distances (all Japan), by depth category, with corresponding cumulative percentage histogram. 70

Figure 35. Stacked histograms of the percentage of the hypocenters associated with each fault, by depth category. 73

Figure 36. Histogram of the percentage of all hypocenters (all Japan), by magnitude category, with corresponding cumulative percentage histogram. 74

Figure 37. Stacked histograms of the percentage of the hypocenters associated with each fault, by magnitude category.. 76

Figure 38. Side-by-side frequency histograms showing the number of hypocenters in magnitude categories within depth categories.. 77

Figure 39. Illustration of the situation in which some fault segments have no associated hypocenters after hypocenter filtering. 78

Figure 40. Bar chart of the number of hypocenters attributed to each of the 68 faults.. 81

Figure 41. Relationship of Type I fault length (m) to number of attributed hypocenters..... 82

Figure 42. Relationship of fault length (Type I) to median depth (km) of hypocenters attributed to faults..... 83

Figure 43. Relationship of fault length (Type I) to median earthquake magnitude associated with the hypocenters attributed to the faults.. 83

Figure 44. Box plots of normal distance from hypocenters to fault planes, by depth category, after one pass of eliminating distance outliers.. 84

Figure 45. Box plots of normal distance from hypocenters to fault planes, by magnitude category, after one pass of eliminating distance outliers.. 85

Figure 46. The relationship between hypocenter depth, earthquake magnitude, and distance to the fault plane for A71-9 (n=168). 87

Figure 47. The relationship between hypocenter depth, earthquake magnitude, and distance to the fault plane for A29-5 (n=100). 88

Figure 48. The relationship between hypocenter depth, earthquake magnitude, and distance to the fault plane for A58-2 (n=219). 89

Figure 49. Frequency histogram and cumulative percentage histogram of mean normal distance of hypocenters to fault planes.. 90

Figure 50. Illustration of (a) the initial concept of the spatial distribution of hypocenters around a fault, and (b) how the IQR would be used to estimate the width of the process zone..91

Figure 51. Spatial arrangement of hypocenters around two faults for which: A) all attributed hypocenters are on the same side, and B) attributed hypocenters are located on both sides, approximating spatial symmetry. 93

Figure 52. Illustration of (a) the actual spatial distribution of hypocenters relative to the nearest fault, and (b) potential spatial locations of the 25th and 75th percentiles.. 94

Figure 53. Histograms of three different measures of the width of the seismic process zone, with corresponding cumulative distribution curves.. 96

Figure 54. Scatter diagrams of fault length (X) versus the sum of the medians of hypocenter distance associated with the two sides of faults (Y). 100

Figure 55. Scatter diagrams of fault length (X) versus twice the median of all hypocenter distances associated with a fault (Y). 102

Figure 56. Scatter diagrams of fault length (X) versus the sum of the medians of hypocenter distance associated with the two sides of faults (Y) for four shapes of faults. 105

Figure 57. Percentage histograms of hypocenter distance for two faults in the same fault system: (a) A44-3 and (b) A44-4. 106

List of Tables

Table 1. Data Sources. 19

Table 2. Fault Data Attributes. 20

Table 3. Seismic Event Attributes. 21

Table 4. Fault Attribute Data Filtering. 22

Table 5. Occurrences of fault relationship types with a strict intersection rule. 34

Table 6. Occurrences of fault relationship types with 300 m tolerance at endpoints. 34

Table 7. Fault relationship type counts with processing of all fault trace polylines within 300 m. 36

Table 8. UTM projection errors. 40

Table 9. Comparative Descriptive Statistics for the Distributions of Three Different Measures of the Width of the Seismic Process Zone. 97

Introduction

The Nuclear Waste Management Organization of Japan (NUMO) is responsible for soliciting areas to explore the feasibility of constructing a repository for high-level radioactive waste. These Preliminary Investigation Areas (PIAs) must be selected based on specific siting factors to meet legal requirements in the "Specified Radioactive Waste Final Disposal Act" of Japan. The evaluation factors for qualification of a site as a PIA include earthquake and fault activity, igneous activity, uplift, erosion, unconsolidated Quaternary deposits, and mineral resources (NUMO, 2002). It is intended that these factors will be evaluated on a nationwide basis using a consistent set of criteria. Any area that has a record of significant impact from these evaluation factors would be excluded from consideration as part of a PIA.

The evaluation factor for qualification related to earthquakes and fault activity is relevant to repository safety because of potential associated destruction and fracturing of host rock. In particular, fault movements could impact the disposal system by creating or enhancing pathways of groundwater movement near a repository (JNC, 2000). Locations near active faults should be excluded from PIAs if they are: 1) where active faults are identified, 2) within the fault crushed zone or surrounding deformation zone, 3) within a zone of likely fault bifurcation, or 4) within a zone of folds or flexures that have been active for the past hundreds of thousands of years (NUMO, 2002).

Objectives

The objective of this project is to develop a spatial statistical assessment method for estimating the confidence needed in avoiding negative impacts from key geometrical features. The key geometrical features of interest for this application are the active faults in Japan. It is also the objective of this report to apply the statistical assessment method to an active fault dataset supplied by NUMO to Sandia National Laboratories (SNL). An overarching goal of this project and the associated project on disruptive influence probability mapping (related to volcanism) is to advance the development of spatial data assessment and extrapolation numerical tools making use of an array of precise (hard) and imprecise (soft) data sets.

Background

Active faulting is related to the tectonic setting of Japan. A majority of active faults are related to the generally east-west compressive stress field resulting from convergent plate tectonics. Although significant regional variations in tectonics are responsible for variability in active faulting across Japan, studies indicate that the current stress state is relatively stable and has been in place for at least the last 500,000 years (JNC, 2000). Consequently, it is expected that future fault activity relevant to repository performance will occur primarily along existing, identified active faults. The distribution of active faults in Japan is shown by the map in Figure 1.

Given that the locations of active faults relevant to the screening of PIAs are known, the important question is the width of the active fault zones. Investigators have distinguished between the "fault crushed zone" near the fault and a wider zone of deformation referred to as the "process zone" (JNC, 2000). The fault crushed zone consists of intensely fractured and altered bedrock including such material as fault gouge, fault breccia, and cataclasite. The process zone is a generally much wider band of bedrock that has been subjected to more subtle

deformation, possibly related to strain relief along the margins of the active fault zone. Observations in tunnels following earthquakes along active faults have indicated such deformation extending up to 1.5 km outward from the crushed zone (JNC, 2000).

The width of the fault crushed zone along active faults is variable and is related to fault characteristics. There is a well established relationship between the width of the crushed zone and the fault length and/or cumulative displacement, based on data from Japan and elsewhere (JNC, 2000 and Otsuki, 1978). The width of deformation associated with active faults may also be related to direction of displacement (e.g., reverse, normal, or strike-slip), position in the hanging or foot wall, average fault slip rate, mechanical characteristics of the bedrock, and flexures on the fault surface. Significant variability in the width and intensity of fracturing associated with faults, as reflected in ore localization, has been recognized in mineral deposits (Guilbert and Park, 1986).

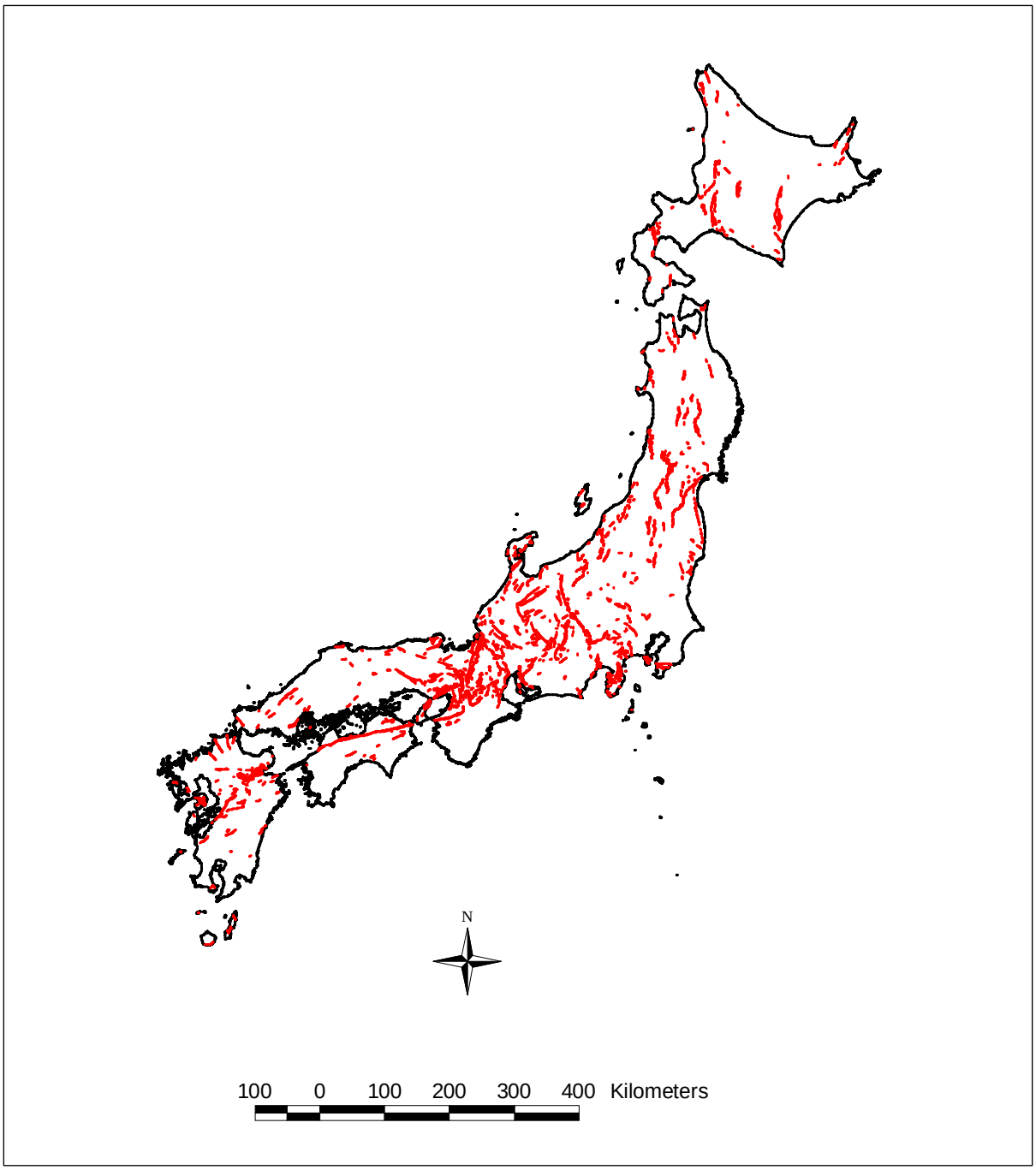

Figure 1. Active fault traces (red lines) in Japan.

Initial Concept for Analysis

The initial concept for the statistical assessment method of determining the zone of influence around faults was to use field observations of fracture intensity adjacent to active faults. It is expected that the fracture intensity is higher near active faults, relative to the background fracture intensity of the bedrock. The distribution of fracture intensity outward from the axis of the fault could be analyzed statistically to estimate the width of the process zone associated with the fault at a particular location. This conceptualization of the system is illustrated in Figure 2. As an example, the fracture intensity around a fault may be approximated by a Gaussian probability density function (pdf) as a function of distance. The parameters of the Gaussian model are the mean and the standard deviation. The mean corresponds to the location of the center of the core of the fault and the standard deviation controls the width of the fracture zone away from the fault (see Figure 2). These two parameters could be defined for each fault in the database of active faults. These parameters could then be correlated against large-scale characteristics of the fault.

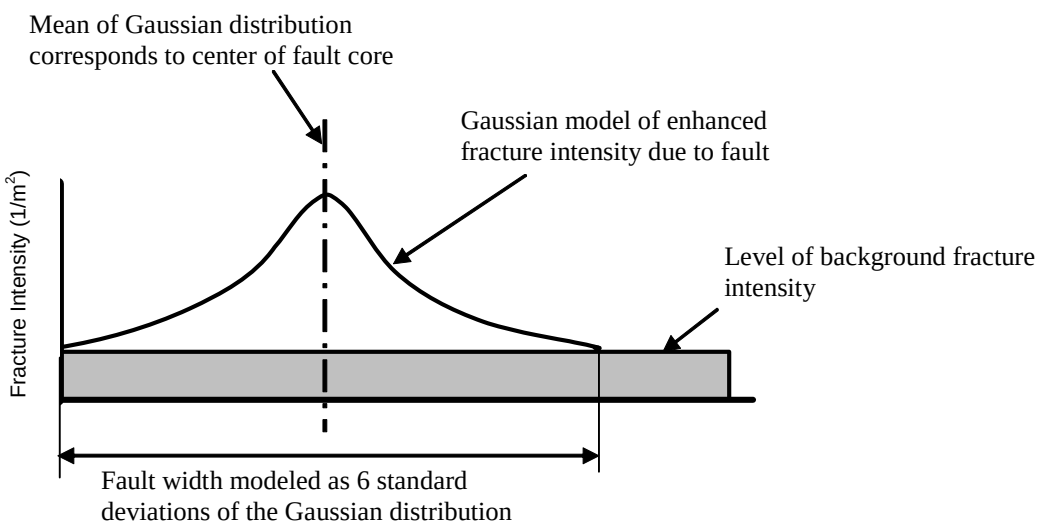

Figure 2. Conceptualization of the distribution of fracture intensity around a fault.

Initial discussions with NUMO staff indicated that there is an extensive database of trenching studies along active faults in Japan. It was anticipated that these data were numerous enough for the statistical analysis described above. However, detailed examination of the trenching data sets showed that few of these contained measurements of fracture intensity in the bedrock. This is because most trenching studies are focused on Quaternary deposits and the determination of recurrence intervals and displacement events along the active faults. Examination of other potential data sources indicated that detailed geological mapping along some major active faults and mapping in some tunnels did include information on fracture

intensity, but these data were too few to support the statistical analyses in the initial concept. Because of the limitations in the available data on fracture intensity this initial concept of the analysis was revised, as described below.

Revised Concept for Analysis

The revised concept for the analysis is based on the use of seismic data to estimate the width of the process zone adjacent to active faults. This concept for the analysis was suggested by data on the distributions of aftershocks along active faults, which show a clear association with the fault location (Yoshida, 2003). These observations of earthquake aftershock hypocenters scattered around the fault surface are consistent with strain relief in the process zone following a major earthquake along the fault itself. This is also consistent with the conceptual model of the fault formation process in which a series of minor faults and fractures are formed within the process zone during the early history of the fault. After formation of the main fault, slip along these minor faults is limited to the accommodation of strain induced by major movements along the main fault. It is thus reasonable to use these hypocenter locations near major faults as an indication of the deformation within the process zone of the active fault.

This revised concept for the analysis was applied to all active faults in Japan using the database of earthquakes from the Japan Meteorological Agency. This extensive database contains hypocenter locations and other information on seismic events. High-resolution data on hypocenter locations are available for earthquakes as small as magnitude 1, particularly since the mid-1980s. The analysis is based on the concept that there is a background density of seismic events and that seismicity associated with active faults is superimposed on this background level.

A preliminary analysis was conducted of the relationship between the seismic data and the locations of active faults to assess the feasibility of this approach. A subset of the seismic database for the years 1996 to 2000 was chosen because of the presumed greater accuracy of the hypocenters from these more recent observations. Shallow earthquakes at depths to 20 km were extracted from the database because of their more probable association with surface, active fault traces. For this preliminary analysis, hypocenters further than 5,000 m from active fault traces were also excluded. The results of this analysis are shown in the histogram in Figure 3.

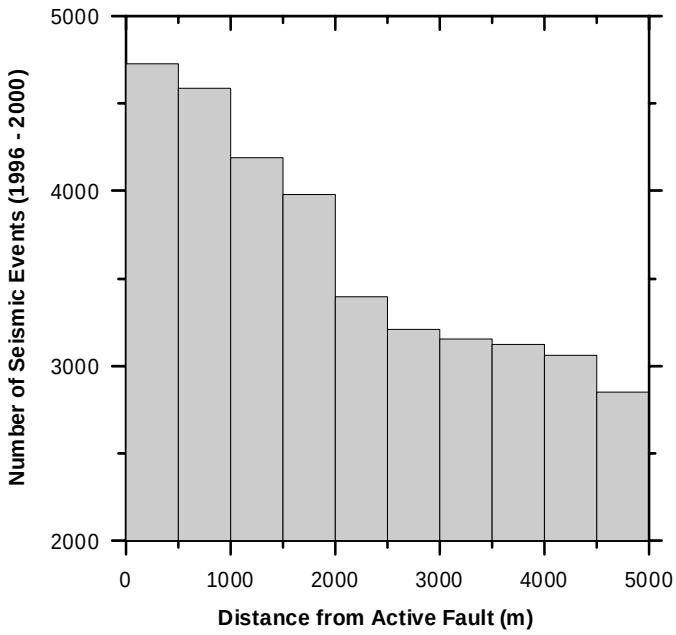

Figure 3. Histogram of seismic events. For seismic events at less than 20 km depth (1996 – 2000) for all of Japan as a function of distance from the nearest active fault.

The results of the preliminary analysis for all of Japan shown in Figure 3 indicate that there is a higher density of earthquakes near active faults, as anticipated. In addition, the large aggregate number of seismic events apparently associated with active faults should be able to support statistical analyses using subsets of the active faults.

Figure 3 also indicates that the width of the process zone may extend several thousand meters from the active faults. It is important to note that the analysis of the aggregate data may be dominated by the larger faults and may thus reflect a maximum width to the process zone. In addition, there are several potential sources of error that may alter the distribution shown in Figure 3. These sources of error are discussed below.

Potential Sources of Error and Limitations in the Analysis

There are several potential sources of significant error and limitations to the analysis using the seismic data. Some of these do not have a large impact on the analysis, some are addressed in the final analysis of the data, and others cannot be resolved. Those potential sources of error that cannot be resolved contribute to the uncertainty in the results, but left unresolved they may overestimate or underestimate the spread of earthquake hypocenters around active faults and thus unduly affect the width of the inferred zone of influence or process zone associated with active faults.

The first source of error is the uncertainty in the locations of the earthquake hypocenters, which are based on seismic data. This uncertainty is a complex function of multiple factors, including the locations and accuracy of the seismographs relative to the earthquake, magnitude

of the earthquake, and depth of the earthquake. The database contains estimates of the standard error of latitude, longitude and depth of the hypocenters, but there is not a straightforward method for incorporating this information in the analysis. However, the magnitudes of these standard errors are not large relative to the apparent spatial distribution of hypocenters around active faults, particularly for onshore earthquakes after the year 1983. In the data analysis no attempt is made to correct hypocenters for location error. A theoretical discussion of the potential impacts of errors in the locations of earthquake hypocenters is presented in Appendix D.

A second source of error is related to the dip of faults and the offset between the hypocenters and the fault surface at depth. In the preliminary analysis presented above the distances between hypocenters and the nearest fault were calculated using the surface trace of the fault. This is equivalent to assuming that the faults are vertical and this assumption introduces significant error for dipping faults and deeper earthquakes. A correction is made for this error in the final data analysis, as described in the GIS Analysis section of this report. Estimated fault dip and dip direction are taken from the active fault database and used to make this correction. The fault was assumed to be vertical if no estimate of the dip was provided. It should be noted that there is significant uncertainty associated with this source of error, even after the dip corrections are applied. Fault dip can vary with depth and values of dip estimated from near-surface measurements may not be accurate for the fault at greater depths. Fault dip can also vary along the strike of the fault and there is not enough dip information to account for this potential complexity in the final analysis.

A third source of error is related to the uncertainty in the association between a given earthquake and a particular active fault. In the final data analysis, automated filtering of earthquake hypocenters was performed in a geometrically reasonable manner, as described in the GIS Analysis section of this report. Distances from hypocenters were calculated in an approximately normal direction relative to the nearest active fault. However, there are residual uncertainties regarding the associations made and distances estimated between hypocenters and active faults. In addition, there are probably instances in which earthquakes are associated with faults other than the identified nearby active fault. Such earthquakes contribute to the "background" seismic frequency conceptualized for the system. However, for individual faults with a limited number of associated earthquakes, statistical fluctuations associated with background events can significantly confound the analysis.

A fourth source of error or limitation to the analysis is the relatively short time period of the high-resolution seismic database. Although a large number of individual earthquakes were recorded for 1983 and later in the database, individual active faults and segments of active faults can remain quiescent for periods of time longer than this. Consequently, the seismic data may contain little or no information associated with some faults or fault segments. Conversely, bursts of seismic activity in some specific areas may bias the results for the associated active fault.

A fifth source of error is the uncertainty related to the location of the mapped fault traces. Faults which branch at depth or have other complex subsurface geometries may have active zones that are not well represented by the mapped fault traces. Some deeper faults may not exhibit any surface expression and therefore are completely unrepresented in the GIS fault

database. An incomplete mapping of fault locations can result in inaccuracies in developing hypocenter-to-fault relationships.

The combined effects of these and other sources of uncertainty on the specific calculation of distance between hypocenters and fault planes is discussed in the section on statistical analysis.

Available Data Sets

This section describes the types and quality of the data available for this project. Details regarding anomalies found in the data and some of the actions taken to address these anomalies are also given.

Original Source Data

The original data files available for this project consisted of three independent data sources containing information related to seismic activity throughout Japan. These data sources were: 1) fault attribute information, 2) seismic event hypocenter information, and 3) fault location information. In some cases, each data source was composed of multiple data files. These data files were either in spreadsheet table format (*xls* files), or as Geographic Information System (GIS) files in ESRI shapefile format (*shp* files). A summary of the available files for each of the data sources is presented in Table 1 below.

Table 1. Data Sources.

Information Type	File Names	Description
Fault attributes	Fault Data SNL 20040616.xls	Spreadsheet containing fault attribute information including fault dip and direction. Also contains limited spatial data providing the latitude and longitude of the end points of the fault locations.
Hypocenter information	0323_1926_1982.shp 0323_1983_1994.shp 0323_1995_1996.shp 0323_1997_1998.shp 0323_1999_2000.shp 0323_2001.shp 0323_2002.shp 0323_200301_09.shp	ESRI shapefiles containing points representing the locations of seismic events dating back to 1926. Various attributes are associated with each hypocenter, including the estimated depth of the seismic event.
Fault locations	AFT_Concealed.shp AFT_Site_Ind.shp Active_Fault_Trace.shp Estimated_AF.shp	ESRI polyline shapefiles containing the geographic location of various fault traces. Attributes are limited to the general classification of the fault trace.

Each of these data sources was independent from the others in the sense that there was no common attribute defining a relationship between the different data files. Only the spatial location information (geographic latitude and longitude), in varying degrees of exactness, was available to provide a link between the data sources. The properties of these different data sources are described below.

Fault Attribute Data Source Properties

Detailed information regarding a number of faults in Japan was provided in tabular format within the file *Fault Data SNL 20040616.xls*. This file contained a total of 277 records (rows) with 25 attributes (columns). In some cases a single fault was repeated in more than one

record, and not all attributes were available for all faults. Table 2 shows the 25 attributes contained in this spreadsheet table and the number of records containing data for that attribute. As shown in Table 2, six of the 25 attributes had a data entry for every record; 19 attributes had less then 100% data coverage; and 11 attributes had less than 50% data coverage.

Table 2. Fault Data Attributes.

Attribute	**Non-Blank Records**	
	Count	**Percentage**
No.	277	100 %
Fault Type	277	100 %
Fault Number	277	100 %
Fault ID	233	84 %
Fault Name	229	83 %
Fault System Name	234	84 %
Northern End (Latitude)	265	96 %
Northern End (Longitude)	265	96 %
Southern End (Latitude)	267	96 %
Southern End (Longitude)	267	96 %
Eastern End (Latitude)	55	20 %
Eastern End (Longitude)	55	20 %
Western End (Latitude)	59	21 %
Western End (Longitude)	57	21 %
Length (km)	277	100 %
Net Length (km)	56	20 %
Strike	277	100 %
Dip	52	19 %
Shape	277	100 %
Maximum Zone Width (m)	17	6 %
Type of Zone	11	4 %
Net Displacement (m)	0	0 %
Maximum Lateral Displacement (m)	101	36 %
Maximum Vertical Displacement (m)	243	88 %
Maximum Average Displacement Rate (m/10^3 years)	129	47 %

Hypocenter Data Source Properties

A comprehensive set of seismic event hypocenter information was provided in a series of eight ESRI point format shapefiles (Table 1). Each record of these shapefiles contains the latitude and longitude of the epicenter, along with multiple attributes, including the depth to the hypocenter. The total range of dates covered by these files spans from January, 1926 to September, 2003; a total of 77 years and nine months. A total of 928,288 individual seismic events are contained in these files for the region encompassing the Japanese Islands. Table 3 shows the 33 attributes contained in the shapefiles and the total number of records containing data for that attribute.

Table 3. Seismic Event Attributes.

Attribute	Total for All Files	
	Count	Percentage
X	928,288	100%
Y	928,288	100%
Header	928,288	100%
Years	928,288	100%
Months	928,288	100%
Days	928,288	100%
Hours	928,288	100%
Minutes	928,288	100%
Seconds	928,288	100%
Time	928,288	100%
Latitude	928,288	100%
Minutes0	928,288	100%
Error_lat	928,288	100%
Longitude	928,288	100%
Minutes1	928,288	100%
Error_lon	928,288	100%
Depth	928,288	100%
Error_dep	928,288	100%
Magnitude1	928,288	100%
Magnitud0	819,482	88%
Magnitude2	928,288	100%
Magnitud1	1,531	0.2%
Traveltime	928,118	< 100%
Precisiono	348,310	38%
Subsidiary	928,121	< 100%
Intensity	928,288	100%
Class	10,653	1%
Class0	69	<0.1%
Epicenter	928,288	100%
Number	928,288	100%
Name	908,724	98%
Observatio	928,288	100%
Flag	607,416	65%

Fault Location Data Source Properties

Fault location data were available from a series of four ESRI shapefiles (Table 1). These files contain polyline features showing the surface expression of numerous faults throughout Japan. Each fault trace has two attributes associated with it. The first attribute is a text description of the general activity level and visibility of the fault surface (i.e. Active, Active Concealed, etc.),

the second is a numeric coding of the first attribute. These attributes are 100% populated for each record in the data files.

Data Set Anomalies

A comprehensive review of the individual data sources discussed above was performed to determine the suitability and completeness of the data sets. This effort was focused on confirming that the available data sets had the necessary data in sufficient quantity to allow the needed computations to go forward. Results from these analyses identified pre-processing and filtering procedures that were then applied to the data sets to prepare them for use in the final computations.

Fault Attribute Data

The original spreadsheet *Fault Data SNL20040616.xls* was examined for anomalies, and inappropriate records were removed from the data set. A crucial part of the GIS analysis involved relating the information in the *Fault Data SNL20040616.xls* table to the polyline fault traces. These represent two independent data sources, therefore some linkage between the files was needed. The one common link between the two data sources is their spatial location information. The fault trace shapefiles inherently contain spatial location information (latitude and longitude for each vertex of the fault trace polylines). The fault attribute table, while not inherently a spatial data file, does contain attributes describing the spatial extent of each fault (the latitude and longitude of the end points of each fault). Therefore, the spatial location information contained in the fault attribute table is critical.

Only records containing the necessary location information are of use, therefore records with missing, duplicate, or spatially inconsistent location information were removed from the data table. In addition, the fault dip magnitude and direction information in this file was critical in later processing, therefore records with very low average dip angles (<45˚) or inconsistent dip directions were also removed from the table since they were considered potential data entry errors.

A summary of how the original data were filtered is given in Table 4 below. After filtering, the final spreadsheet was then converted to a comma-delimited text file for use in GIS processing.

Table 4. Fault Attribute Data Filtering.

Data Set Observation	Records Removed	Record Count
Original number of records		277
Entries with no location information	3	274
Entries with spatially inconsistent information	2	272
Entries with duplicate coordinates	2	270
Entries with suspect fault dip information	3	267

Hypocenter Data

The hypocenter data files contained information for approximately 928,000 onshore and offshore seismic events throughout the area of Japan (Figure 4). A review of the attributes associated with these hypocenters revealed two major data anomalies. The first anomaly involved seismic magnitude data associated with hypocenters spanning a time frame from 1926 to 1996. The second anomaly was related to inconsistencies in the accuracies of the spatial location information for hypocenters with dates ranging from 1926 to 1982.

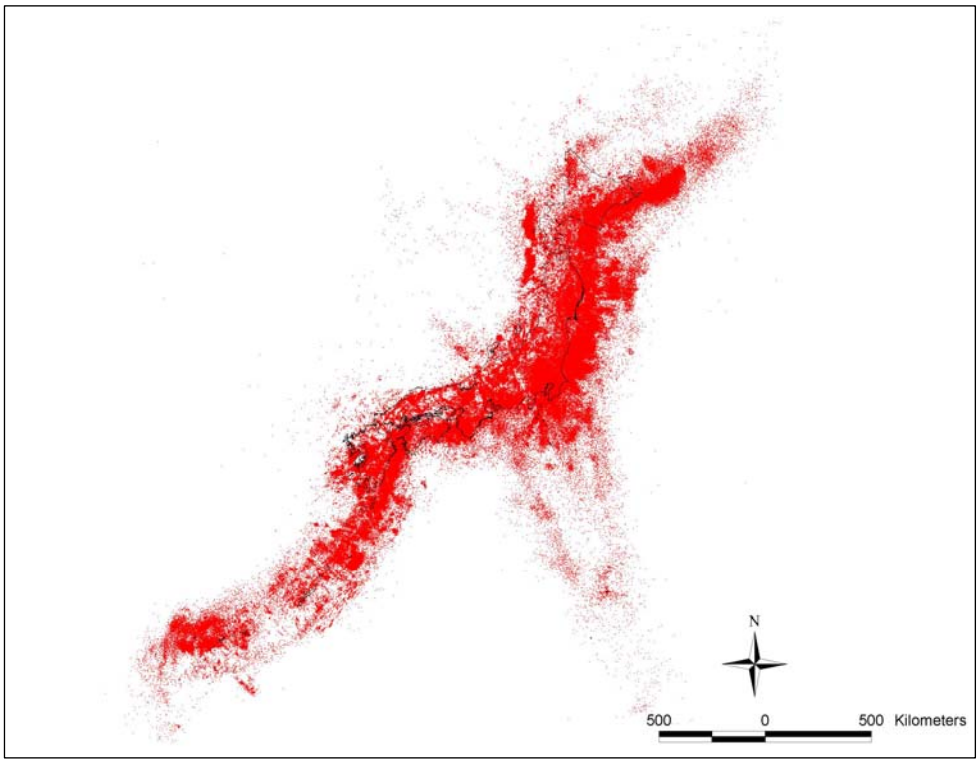

Figure 4. Map of all hypocenter locations, shown in red, available for this study.

The anomalous magnitude data were reveled by a review of the data which indicated magnitude values greater than 9.9. These large magnitude values included values as large as 66.0. Clearly these large values are erroneous; the largest historic earthquake is listed as a 9.5 magnitude event which occurred in Chile in 1960 (Kanamori, 1977). Further investigation, including comparison against alternate data sets, reveled that the suspect magnitude data was restricted to dates prior to 1997. Eliminating hypocenters with dates prior to 1997 would have resulted in the removal of 283,329 hypocenters from the data set; a reduction of 31%. To maximize the number of hypocenters available for analysis, a process was undertaken to correct the errant magnitude data entries.

The process to correct the erroneous magnitude data involved comparisons of the current data set against similar data sets from previous investigations. These alternate data sets contained

reliable magnitude data for the time period of interest, but were incomplete in other terms. The alternate data sets provided a method to compare and correct the magnitude information for the current hypocenter data set, and thereby help to retain as much hypocenter data as possible for the statistical analyses. The process to correct the magnitude data involved a record-by-record comparison between the current and alternate data sets; if the alternate data set and current data set had differing magnitude values, then the current data set magnitude value was replaced by that from the alternate set. This process was only applied to hypocenters with suspect magnitude values. If an identical record for a given hypocenter could not be found in the alternate data set, then no correction was possible and the original magnitude value was maintained. The alternate data set only contained reliable magnitude values for years after 1960, so no corrections prior to this date were possible.

The second anomaly identified in the hypocenter data set was related to the spatial resolution of the hypocenter latitude and longitude values. This issue initially revealed itself as an unexpected spatial pattern in planimetric displays of the hypocenter data. At the scale of display shown in Figure 4, no regular spatial patterns are detectable. At a larger scale (Figure 5) some regular patterning of the data points is evident. Further investigation of the points responsible for this patterning, shows that these points are associated with dates prior to 1983, and that the patterning is the result of the latitude and longitude values being reported only to a minute of a degree. From 1983 and onward, latitude and longitude values are reported to a second of a degree. The increased spatial resolution of the later data results in a random appearance when the spatial locations are plotted. Similar issues in the alternate data sets prevented the use of the alternate data sets to rectify this issues as was done with the magnitude data.

The reduced spatial resolution in the pre-1983 hypocenter locations results in a clustering of multiple hypocenters at a common location. In addition, inconsistent spatial locations may lead to bias in the distance calculations and potential bias in the statistical analyses. In order to avoid the introduction of bias into the distance calculations from differing spatial resolutions, the pre-1983 hypocenter data were excluded from the distance calculations and subsequent statistical analyses. This limits the analysis to only being able to determine the width of faults that have been active since 1983. If patterns of seismicity have changed since 1983, the fault widths identified will not be representative of fault widths that would be calculated from historical seismic records and faults that have not been active since 1983 are excluded from the analysis. A positive aspect of using only more recent seismic data is that the seismic monitoring network in Japan has become more refined with time and therefore the more recent hypocenter locations are those with the greatest precision in the hypocenter locations

The exclusion of pre-1983 hypocenters removed 45,140 hypocenters from the data set. The removal of this small percentage (~5%) of hypocenters should not have a major impact on the project goals due to the large number of remaining hypocenter data. This action also filters out the pre-1961 hypocenters which were determined to contain invalid magnitude errors (see above). Figure 6 shows the distribution of the 1983 and later hypocenters.

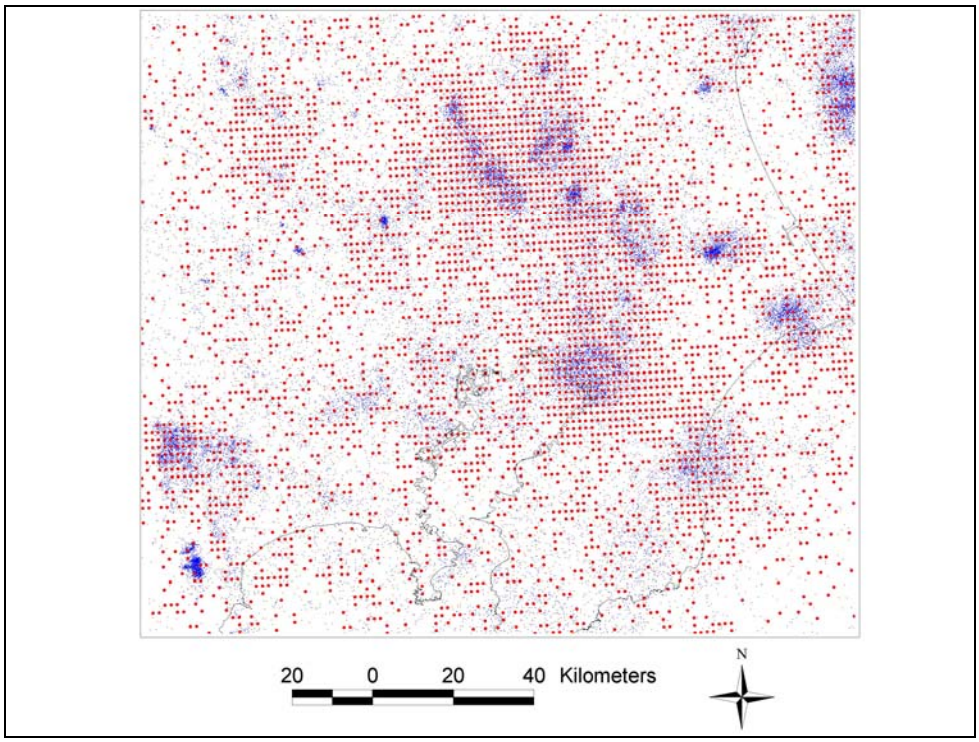

Figure 5. Map showing clustering of pre-1983 hypocenter locations. Pre-1983 hypocenters shown in red; 1983 and later hypocenters shown in blue.

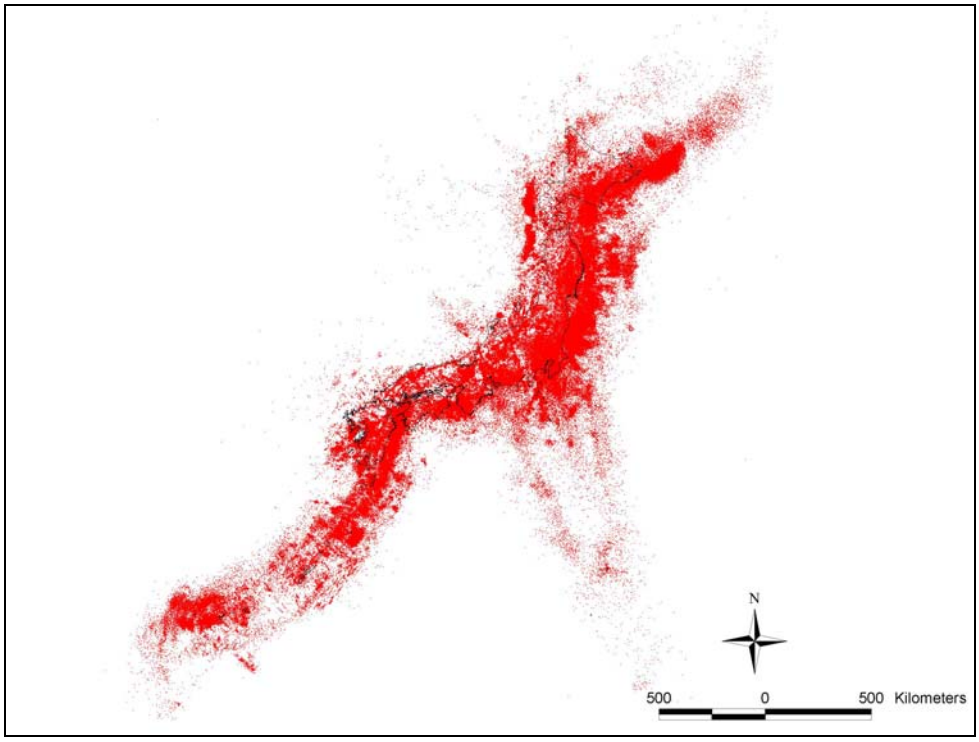

Figure 6. Map showing locations of 1983 and later hypocenter locations.

Fault Location Data

The detailed fault location information available for this study was contained in a series of four ESRI shapefiles (see Table 1). These shapefiles contained many individual records each representing a section of a fault trace. In many instances what appears visually as a single fault trace, is in actuality composed of many individual polyline segments. Although this is not typically problematic, it does add some computational overhead during the GIS processing. This condition also complicates interactive investigation of the fault traces since what appears to be a single fault line is actually composed of many small individual segments (Figure 7).

Further investigation of the polyline fault location data revealed that some of the polyline records were duplicated resulting in multiple polyline segments overlying one another. Additionally, many short (< 10 m) polyline segments were found which appear to be over-shoots created during the original digitizing of the fault traces. These short segments are spurious in that they are an artifact of the digitizing process and do not necessarily depict the intended fault trace.

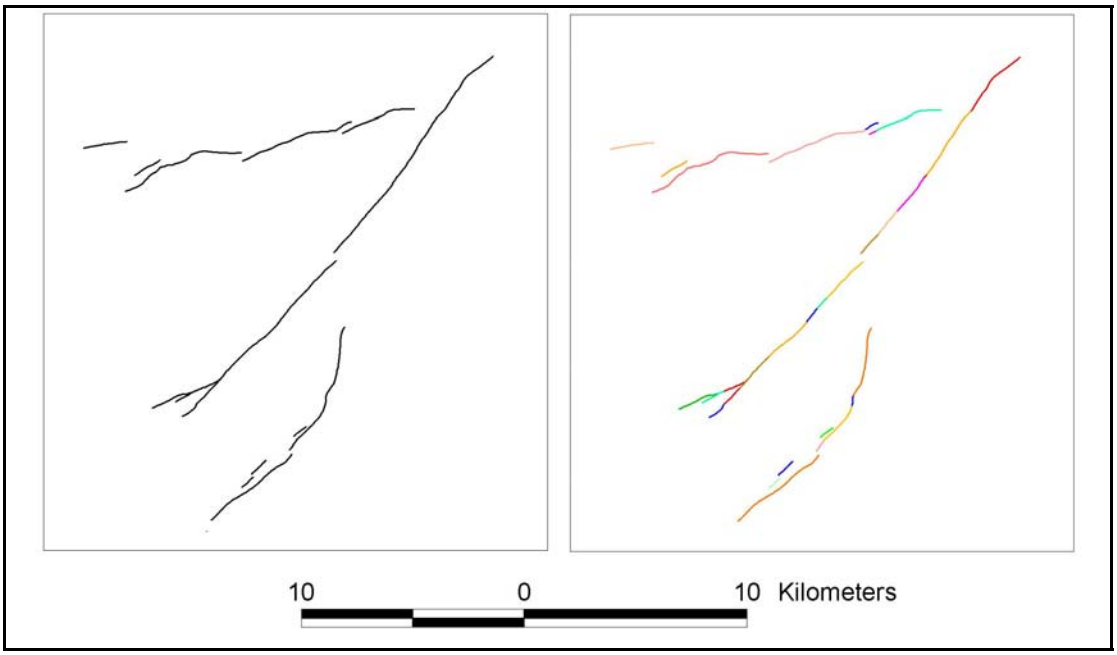

Figure 7. Map showing example fault traces. Traces shown as a single color (left) and color-coded by individual polyline segments (right).

Several steps were taken to address these issues. To minimize the number of individual polyline segments contained in the shapefiles, the four individual shapefiles were combined into one file, and a polyline consolidation procedure applied to them. The consolidation procedure examined each polyline and determined if any other polyline shared a common endpoint. All polylines sharing a common endpoint were combined into a single polyline segment. The limited attributes associated with the fault location data in the *shp* files were not

of use for the analyses presented here, so the consolidation of polyline segments and potential loss of individual segment attribute information was not a concern.

Additionally, an analysis was performed to identify identical, overlying polyline segments. Once identified, the duplicate polyline segments were deleted from the shapefiles. The length of each polyline was also computed and used as a guide for the identification of digitizing artifacts. Unusually short polyline segments were investigated and those determined to be spurious or artifacts from digitizing were deleted.

This page intentionally left blank

Geographic Information System Analysis

This section describes the procedures used during the GIS analysis of the data sets. All the procedures described here were performed using the 3.1 version of the ESRI ArcView GIS software product. These procedures involved the use of standard ArcView features, third-party extensions, and custom-designed Avenue programs.

The primary objective of the GIS analysis task was to provide depth-corrected, normal distance measurements between each hypocenter and its nearest fault plane. These distances and relationships could then be used to develop statistical inferences relating seismic activity and distance from known fault traces.

Data Processing

To meet the above objectives, it was necessary to combine information from the original three independent data sources (Fault Attributes, Hypocenter Information, and Fault Location Information). The merging of this information was performed at the spatial and attribute levels, and was necessary because each of the data sets contained some information essential for the analysis.

The general steps performed to meet the objectives were:

1. Create a spatial representation of the fault attribute table
2. Assign the fault attribute information to the fault location data
3. Filter the hypocenter data to extract points relative to the analysis
4. Compute the hypocenter-to-fault distances

A general flow diagram showing the above steps with some additional detail is shown in Figure 8.

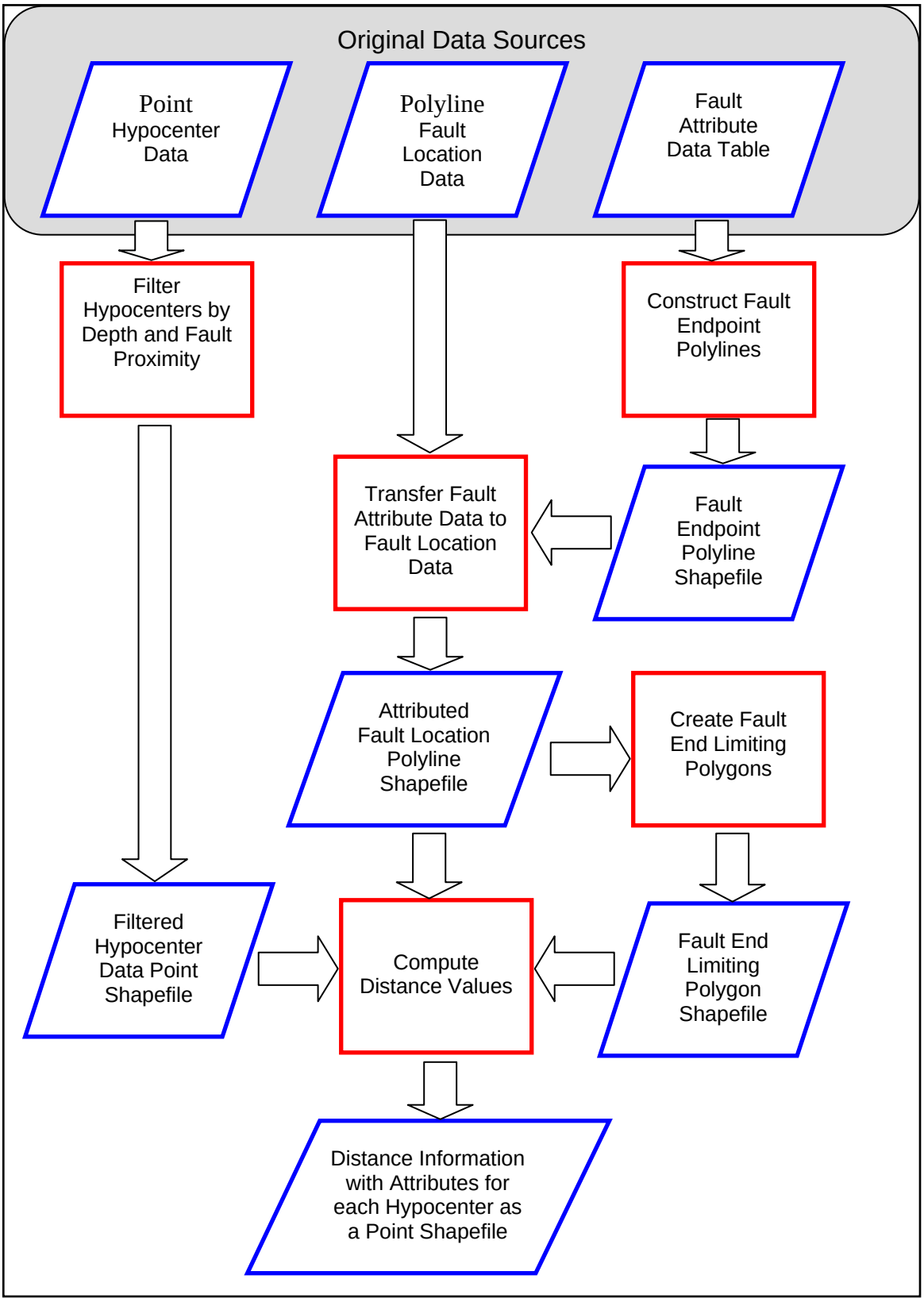

Figure 8. GIS process flow chart.

Fault Endpoint Polyline Creation

The fault location data (fault trace shapefiles) contained detailed information regarding the geographic location of the mapped fault locations (Figure 9). However, these files contained none of the fault attribute information essential for this project (e.g. fault dip angle, fault name, fault system, etc.). Conversely, the fault attribute file contained detailed information regarding the characteristics of each fault, but held very limited information regarding the geographic location of the fault (see Table 2).

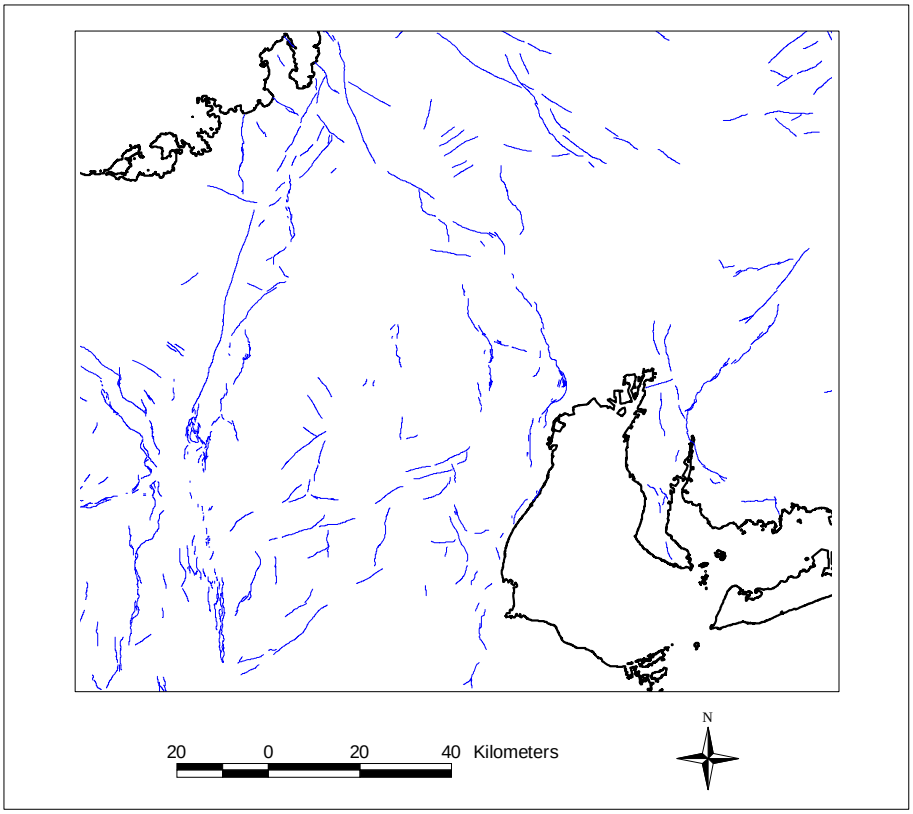

Figure 9. Example of fault location polyline data. Faults shown in blue, coastline shown in black

The geographic information contained in the fault attribute file was limited to latitude and longitude values indicating the endpoints of the fault. It was therefore necessary to use this limited spatial information to correlate the fault attribute information to the fault location data. The first step in this process was to create a GIS-compatible polyline shapefile from the fault endpoint information contained in the fault attribute file. This procedure was accomplished within the ArcView GIS using a custom program written in the ArcView programming language Avenue. This script created a single polyline feature for each record in the fault attribute table that contained valid geographic coordinates. In addition, all attributes contained in the fault attribute table were transferred to the new shapefile. In some instances there were more than two coordinate pairs per point. In these cases, all the pairs were joined in a systematic order and then manually edited to provide an optimal intersection with the

surrounding fault trace polylines. Figure 10 shows an example of the results from this polyline creation procedure. In this figure, the fault location polylines are shown in blue and the polylines constructed from the endpoint information in the fault attribute file are displayed in red.

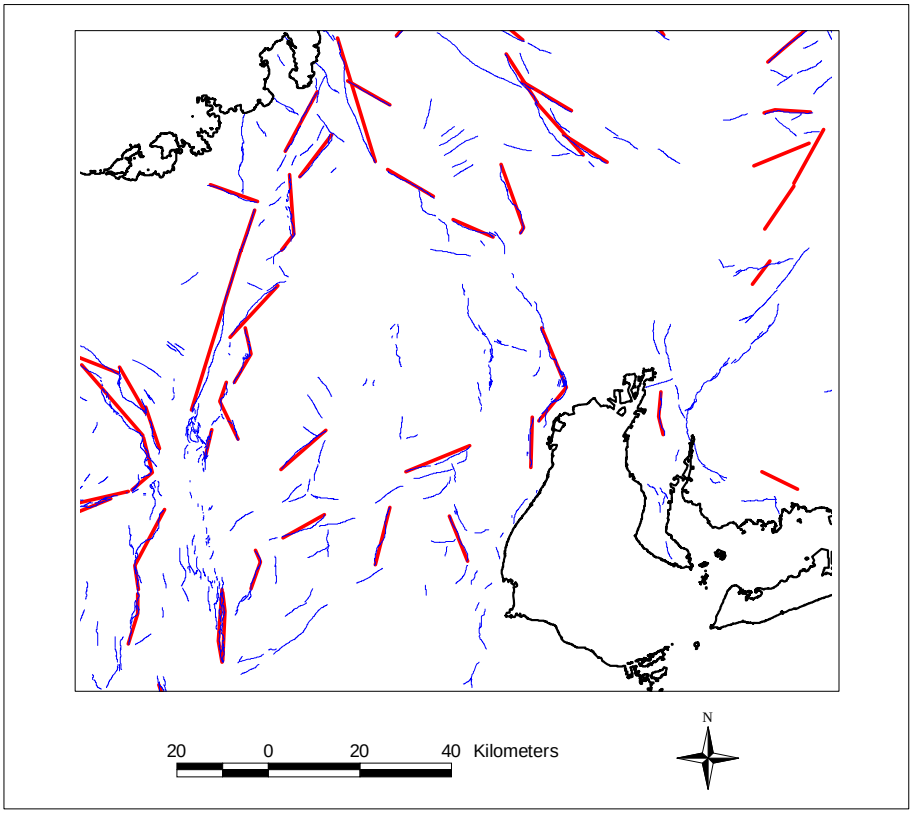

Figure 10. Example of Polylines Representing Fault Traces (Blue Lines) and Fault Endpoint Locations (Red Lines), Coastlines Shown in Black.

This process resulted in the creation of 267 individual polyline features. Each polyline record contained all the attribute information in the original fault attribute file. Details regarding the Avenue code used for this procedure and the input and output files can be found in Appendix A.

Attribution of Fault Location Data

The next step in the GIS data processing was to transfer the fault attribute information from the fault endpoint polylines created above to the detailed fault location polylines (fault traces). This step involved spatially relating the two polyline data sets so that the attribute information

could be transferred to the most appropriate fault trace. This process relies on the assumption that spatially proximate polylines are related and so should share common attributes.

The two polyline files used in this process, the fault location (fault trace) and fault endpoint locations from the fault attribute file, are independent and therefore do not necessarily have a common spatial coverage. Overlaying the new fault endpoint polylines with the fault location traces shows three distinct relationships as shown by Figure 11 below. A type I relationship is defined by the existence of a polyline defined by fault end-point locations but without any nearby fault traces; a type II relationship is defined as a fault location trace without any nearby endpoint defined polylines; a type III relationship is defined by a location with a fault trace and an endpoint defined polyline in close proximity to one another.

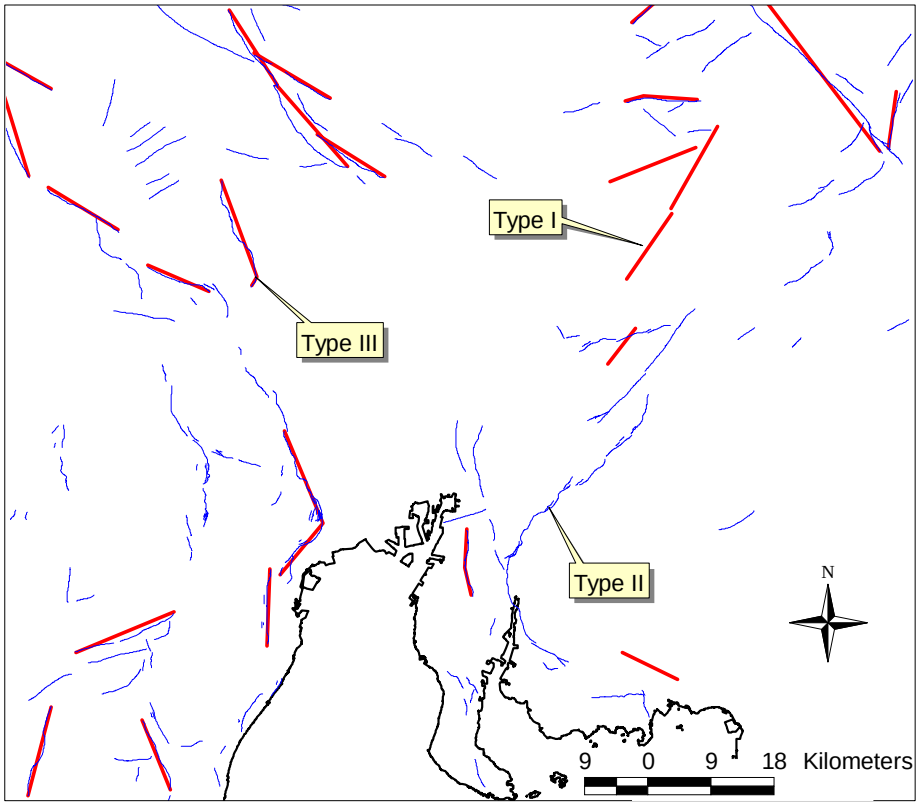

Figure 11. Relationships between polylines. Fault traces are shown in blue and fault endpoint locations are shown in red.

The importance of these spatial relationships is that fault location and fault attribute data having either a type I or type II relationship will not be represented in the final statistical analyses. The type I and type II relationships represent a mismatch between the fault location and fault attribute data sets and so are locations where only one of the two different data sets

were available. Table 5 below shows the count and percentage of total of these different type relationships when based on a strict intersection rule to define the relationship.

Table 5. Occurrences of fault relationship types with a strict intersection rule.

Data Set	Relationship Type	Polyline Count (Percentage of Total)
Fault Endpoint Polylines from Attribute Table	I	70 (26%)
	III	197 (74%)
Fault Location Polylines	II	3659 (90%)
	III	422 (10%)

Table 5 shows that using a strict intersection rule (i.e. the polylines must share at least one common point) results in a relatively large number of type I and type II relationships. This is due in part to the relatively low resolution and accuracy of the fault endpoint polylines created from information in the fault attribute table. The small number of vertices in the fault endpoint polylines, and their nature as general geographic locations, reduces the likelihood that they will intersect a polyline fault trace which increases the number of type I and type II relationships.

One method to reduce the number of type I and type II relationships is to relax the strict intersection requirement used in relating the two sets of polyline data. If the requirement for a type III relationship is relaxed so that polylines within 300 m of each other are considered to be spatially related, then the percentage of type I and type II associations drops to 10% and 76% respectively (see Table 6). Figure 12 shows an example of where this process developed a type III association from a set of polylines that do not strictly intersect.

The left plot in Figure 12 shows a fault endpoint polyline (red lines) which does not intersect any fault trace polylines (blue lines). The right plot shows the same area with a 300 m buffer (grey polygon) around the fault endpoint polyline. Associating fault traces within this polygon with the fault endpoint polyline provides a mechanism to transfer attribute information to the nearby fault traces thereby reducing the number of type I and II associations, and increasing the number of type III relationships.

Table 6. Occurrences of fault relationship types with 300 m tolerance at endpoints.

Data Set	Relationship Type	Polyline Count (Percentage of Total)
Fault Endpoint Polylines from Attribute Table	I	26 (10%)
	III	241 (90%)
Fault Location Polylines	II	3092 (76%)
	III	989 (24%)

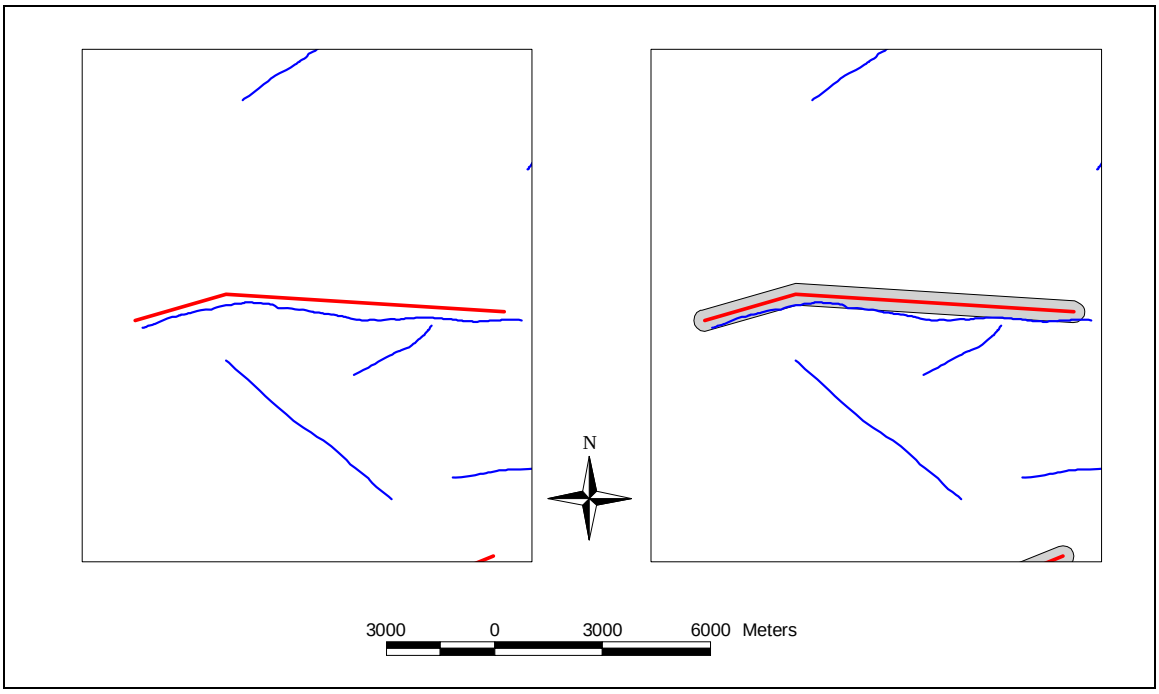

Figure 12. Example of using fault endpoint buffer. Fault endpoint polylines (red) are associated with adjacent fault trace polylines (blue).

Although this process results in improvement, there are still a relatively large number of type II associations remaining. This is primarily due to two circumstances. The first situation is brought about by fault trace polylines which have no fault endpoint polylines in their vicinity (a true type II association). The second circumstance is that what appear to be long continuous polyline fault traces are, in fact, a series of shorter polyline segments which are separated by small gaps. These discontinuities cause the propagation and association of the fault attributes to be interrupted, resulting in many type II relationships.

In order to reduce the number of type II associations a polyline association growing technique was used. This technique increases the number of attributed fault trace polylines by assuming that fault trace polylines which are sufficiently close to one another should have similar attributes. This procedure operates by selecting all fault trace polylines within 300 m of a type III association and transferring the attributes from the attributed fault trace to the newly selected fault traces. This process is repeated until the selected number of fault trace polylines remains stable. Figure 13 shows an example of where this process allowed for the attribute association of a small isolated fault trace. Table 7 shows the reduction in type II associations, and subsequent increase in type III associations as a result of this procedure.

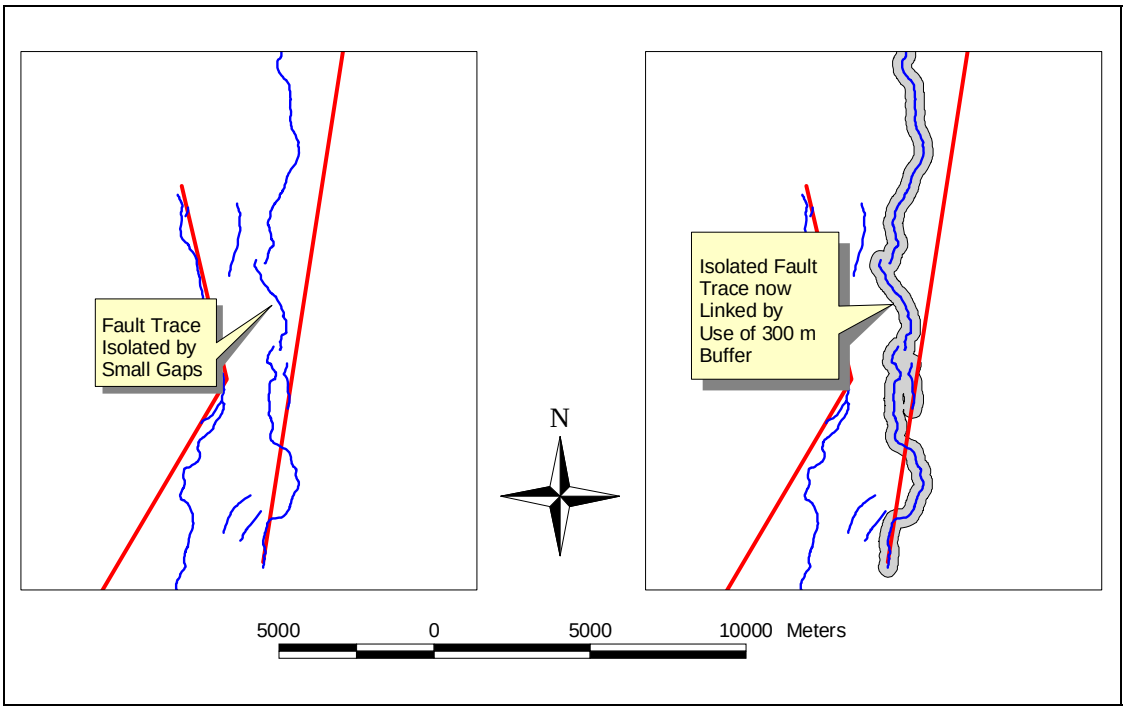

Figure 13. Example of small isolated fault trace. Isolated fault traces (blue lines) are linked to adjacent, attributed fault traces through the use of a 300 m buffer.

The process of growing the associations between separate fault trace segments is designed to group together fault trace polylines which fall within a similar spatial realm. A side effect of this process is that attribute information can be promulgated in a manner that would not match the results from a manual inspection process. This results in a small percentage of fault trace polylines having fault attribute information (fault name, fault system, etc.) which may not match those expected based on the fault attribute table.

Table 7. Fault relationship type counts with processing of all fault trace polylines within 300 m.

Data Set	Relationship Type	Polyline Count (Percentage of Total)
Fault Location Polylines	II	2438 (60%)
	III	1643 (40%)

The two processes described above were applied to the polyline data using a custom ArcView Avenue program. A distance of 300 m was used for both the fault endpoint polyline buffer and the fault trace growing buffer. This value was chosen as optimal for these data sets through a series of experimental efforts. It provides for the association of fault traces which are in close proximity to one another, but does not associate fault traces with gaps larger than 300 m. Although using a larger buffer size would allow for the connection of more fault traces, this has the undesirable side effect of potentially associating fault traces which are not related.

Additional information regarding the Avenue code used for this process can be found in Appendix A.

After the processing of the polylines through these procedures, a subset of the original fault trace location polylines was attributed with the information from the fault attribute table and available for additional processing. To aid in the identification of individual fault traces, a unique identifier (SNL_FID) was added to each attributed fault trace.

Hypocenter Filtering

The post-1982 hypocenter information was spatially filtered to restrict the analyses to the most appropriate hypocenters and reduce the computational burden. Only hypocenters within 20 km of the fault traces and with a depth of less than 20 km were retained for further processing (Figure 14). After filtering of the hypocenter data, a unique identifier (SNL_HID) was added to each remaining hypocenter.

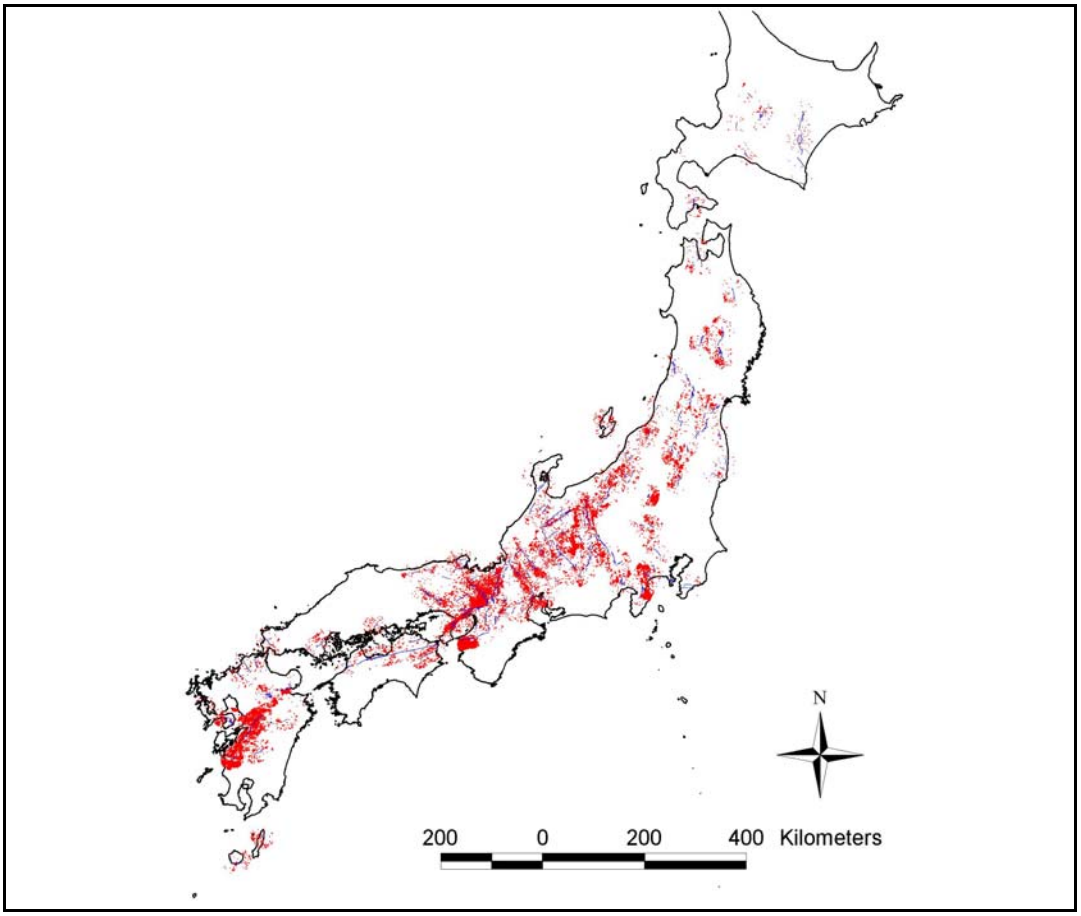

Figure 14. Hypocenter locations (red points) remaining after spatial filtering. Attributed fault traces shown in blue.

Hypocenter Limiting Polygons

In order to avoid the potential for inappropriate associations between hypocenters and fault traces, a spatial filter was constructed to exclude the association of hypocenters that are beyond the end of a given fault trace. This spatial filter consisted of a series of polygon buffers that extended 20 km from the attributed fault traces, but which were truncated perpendicular to the end of the fault trace (Figure 15).

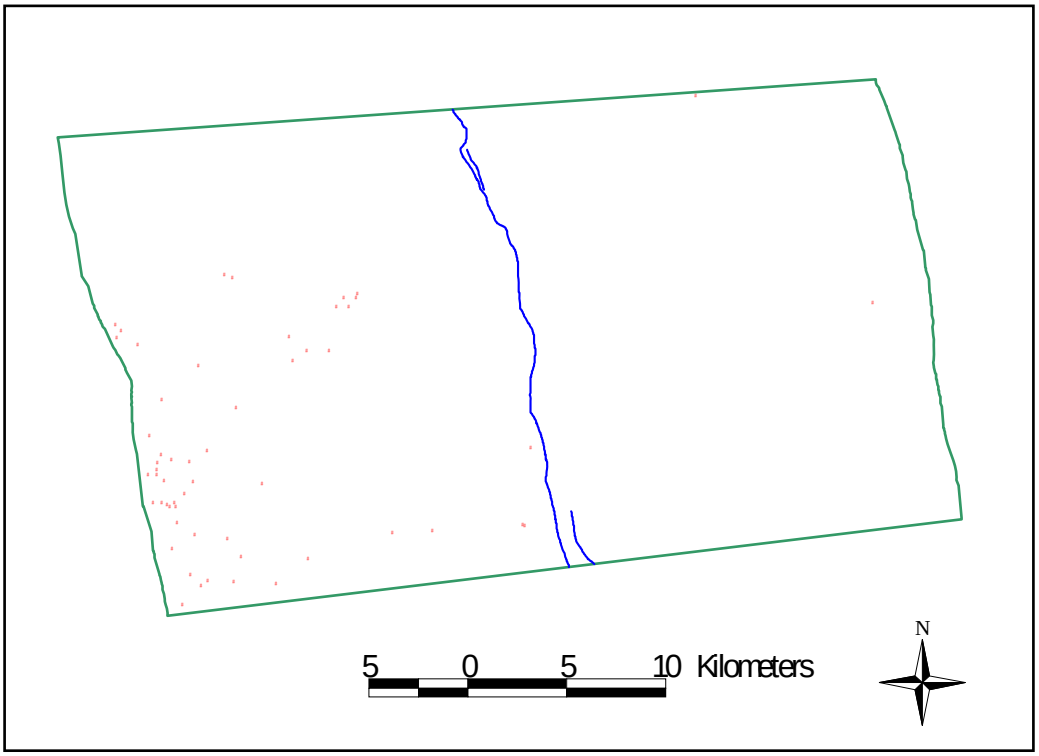

Figure 15. Example hypocenter limiting polygon (green), attributed fault trace (blue lines) and associated hypocenters (red points).

These limiting polygons were used in later processing steps to assure that hypocenters beyond the end of a given fault trace would not be associated with that particular fault.

Distance Computations

The above steps were focused on preparing data sets for the primary objective of providing depth-corrected, normal distance measurements between each hypocenter and its nearest fault trace. This section details the procedures used to compute these measurements.

The calculation of the depth-corrected, normal distance measurements consisted of two major steps. The first step consisted of computing the planimetric distances between each hypocenter and its four nearest fault traces. The second step involved taking the planimetric hypocenter distances, correcting for depth and fault dip, choosing a single nearest fault trace based on this corrected distance, and computing various attributes for each hypocenter.

The original source data files were all supplied using geographic coordinates (latitude and longitude). This type of coordinate system is not suitable for the distance calculations performed here, so all distance calculations were performed using a projected coordinate system. The Universal Transverse Mercator (UTM) projection system was chosen because it produces minimal errors which are relatively consistent for latitude and longitude. In particular, UTM Zone 53, using the 1983 North American Datum and Global Reference System 80 spheroid, projection parameters were used.

The main islands of Japan span at least three UTM zones (Figure 16). Zone 53 was chosen because it is the most central of the Zones and therefore should reduce potential errors introduced by expanding the projection's use beyond its defined zone. A series of test distances were computed to assess the magnitude of the distance errors that would be introduced by using the UTM Zone 53 projection. These tests computed the error, defined as geographic distance (m) minus projected distance (m), for a series of nine locations spread across the area of interest (Figure 16). A suite of four error measurements, each with a nominal distance of 10,000 m, was computed at each of the nine locations, two for latitude and two for longitude, for a total of 36 error measurements. A summary of the results from these measurements is presented in Table 8.

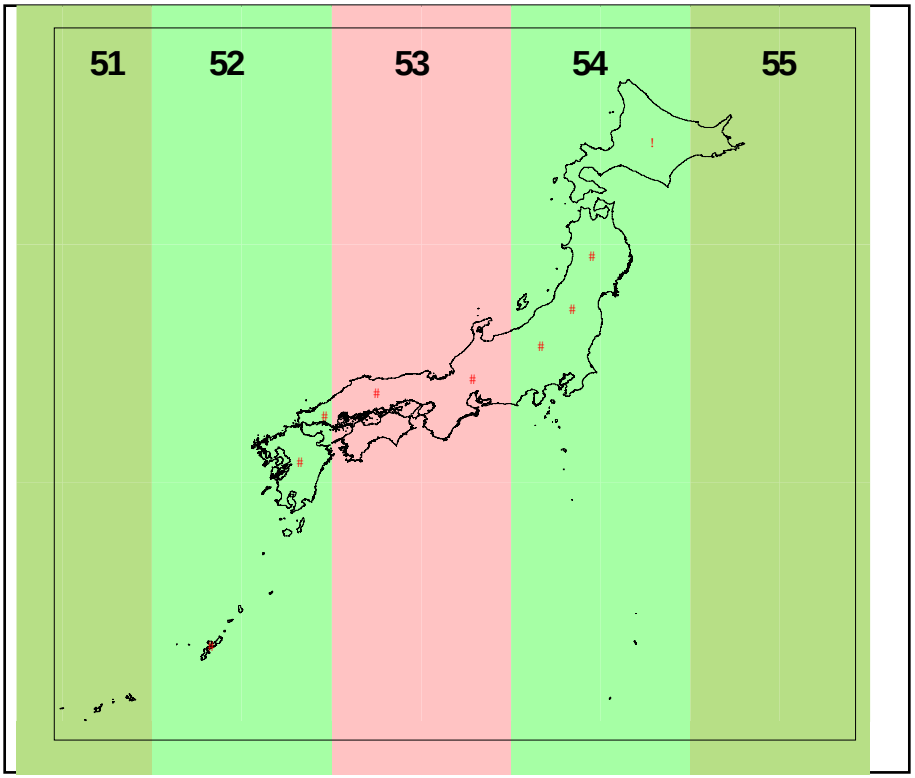

Figure 16. UTM Zones and projection test locations (red points).

Table 8. UTM projection errors.

Measurement	Value
Minimum Absolute Error	0.63 m
Maximum Absolute Error	56.91 m
Mean Error	19.71 m
Standard Deviation of Error	19.02 m
Root Mean Square Error	18.14 m

The results from this analysis show that the maximum error for the test point locations was approximately 57 m for a distance measurement of 10,000 m, and the Root Mean Square Error computed from all the point measurements was approximately 18 m. These values are considered acceptable for the procedures used in this project, and so the UTM Zone 53 projection was adopted for all distance measurements.

The first step in the final calculation of the depth-corrected distances was to compute the planimetric distance from each hypocenter location to the four nearest attributed fault traces. These calculations were only performed on those hypocenters falling within one of the hypocenter limiting polygons discussed above. The four nearest fault features were used for the distance calculations to assure that the nearest fault trace was maintained once the dip and depth-corrections were applied to the distance values. These planimetric distances were used as the basis for computing the depth and dip corrected distances. The planimetric distances were computed within ArcView using the Nearest Features extension (version 3.7a). Details regarding this extension and its use can be found in Appendix A.

Once the planimetric distances were computed they were used to compute the depth- and dip-corrected distances. The first step in this process was to compute the depth-corrected planimetric distance. This represents the horizontal distance to the fault plane after correcting for the dip of the fault and the depth of the hypocenter. This process is illustrated schematically in Figure 17.

As shown in Figure 17, to correctly compute the depth corrected planimetric distance, it is necessary to know if the hypocenter under consideration lies on the foot wall or hanging wall side of the fault plane. This determination can be made by looking at the relationship between the vector connecting the hypocenter to the fault trace and the vector describing the dip direction of the fault plane. If these two vectors have a similar direction, then the hypocenter should be located on the foot wall side of the fault plane. If the two vectors have nearly opposing directions, then the hypocenter may be on the foot wall or hanging wall side of the fault plane depending on the depth of the hypocenter (if the depth is large, then the vertical projection of the hypocenter may penetrate the fault plane and change the location from one fault block to another). The process of determining on which side of the fault plane the hypocenter lies can be easily automated by adding the unit vectors of these two vectors and looking at the value of the resultant vector. If the length of the resultant vector is greater than

the square-root of two, then the hypocenter is on the foot wall side of the fault plane. This is graphically illustrated in Figure 18.

If the length of the resultant vector is less than the square-root of two, then the hypocenter depth has to be considered in the determination. In this case, the vertical depth to the fault plane at the hypocenter location is computed and compared to the hypocenter depth. If the hypocenter depth is less than the fault plane depth, then the hypocenter is on the hanging wall side of the fault plane. Conversely, if the hypocenter depth is greater than the fault plane depth, then it has been projected through the fault plane and is on the foot wall side of the fault. Computation of the depth-corrected planimetric distance in this case is illustrated in Figure 19.

For faults known or assumed to be vertical the hanging wall or foot wall determination is not applicable, yet it is still desirable to treat hypocenters falling on one side of a fault as a single group during the statistical analyses. For these faults, an attribute was added identifying each hypocenter as being on one side of the fault trace or the other. This unique fault-side determination was made by offsetting a midpoint from the fault trace polyline, then connecting each hypocenter associated with this fault to this point. The number of intersections recorded for each connection determined whether a hypocenter was on the same side of the fault trace as the off-set midpoint. If there is an even number of intersections, then the hypocenter is on the same side of the fault trace as the off-set midpoint; an odd number indicates that it is on the opposite side.

Although the depth-corrected planimetric distance is an intermediate value, its value was recorded in the data set for each hypocenter in the event that it would be of interest for future analyses. The primary purpose for computing this value is its use in computing the fault normal distances (N_d). The fault normal distance is the distance from the hypocenter to the nearest fault trace along a vector normal to the fault dip (Figure 20).

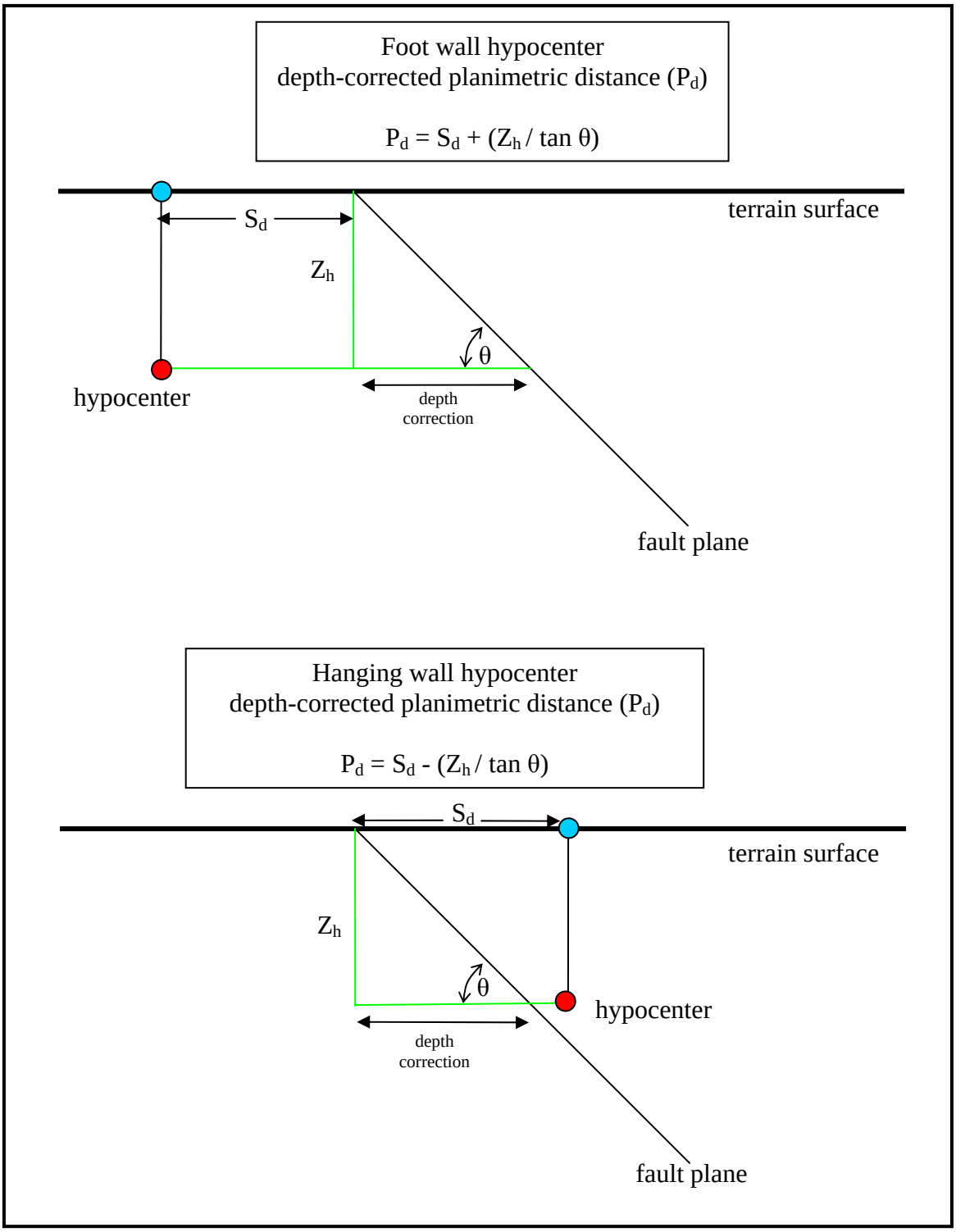

Figure 17. Schematic cross-sections showing depth-corrected planimetric distances. Where θ is the fault dip angle, Sd is the surface planimetric distance, and Zh is the hypocenter depth.

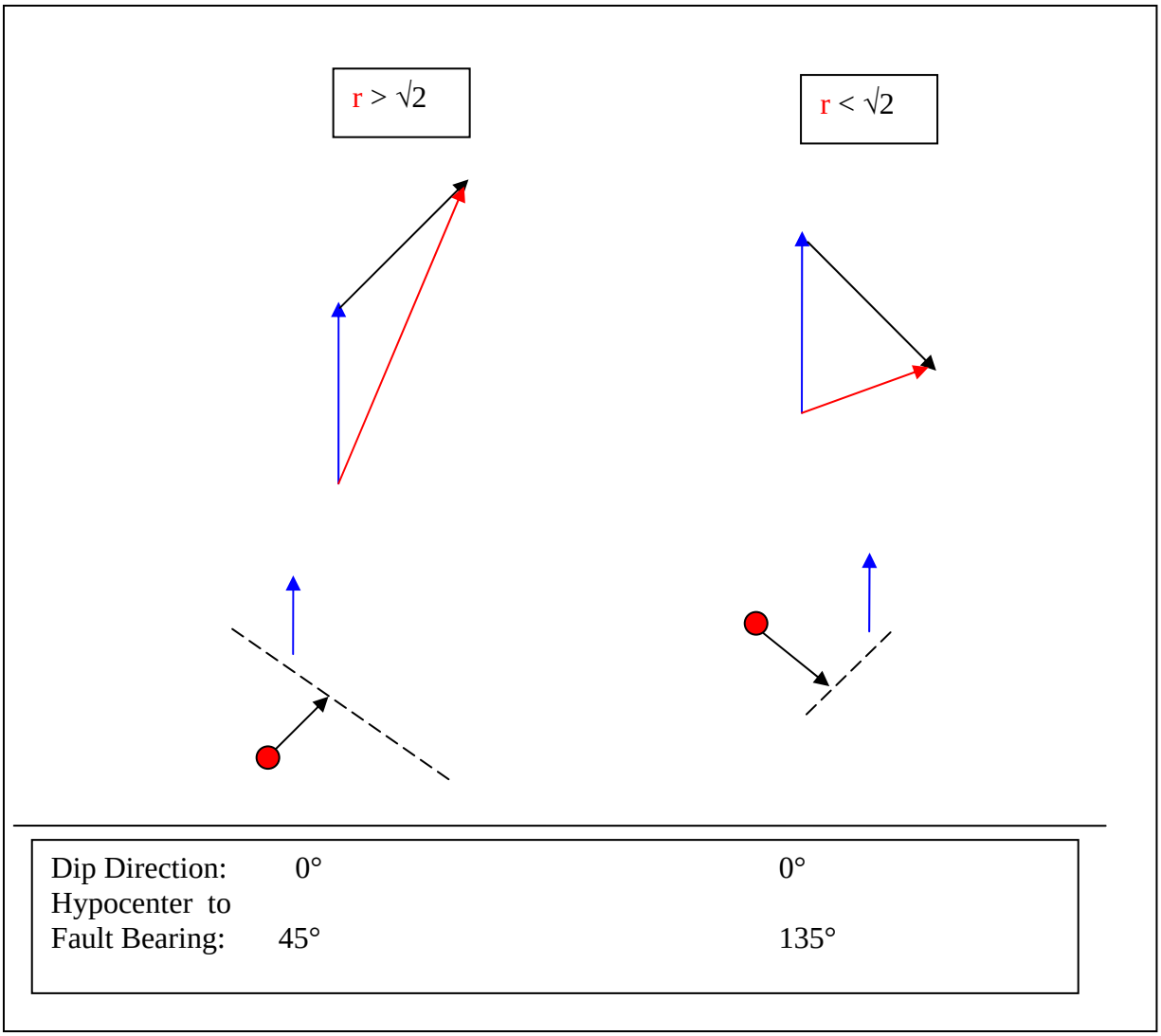

Figure 18. Hypocenter fault block determination. Illustration of determining which fault block a hypocenter (red points) lies within, fault dip vector shown in blue, hypocenter-to-fault connecting vector in black, and resultant vector in red; surface traces of faults shown as dashed black lines.

The calculation of the fault normal distance relies on the depth-corrected planimetric distance. It also assumes that the dip direction is perpendicular to the fault trace. Figure 20 shows the geometry used in calculating the fault normal distances for foot wall and hanging wall hypocenter locations. For these calculations the equations in both cases are the same.

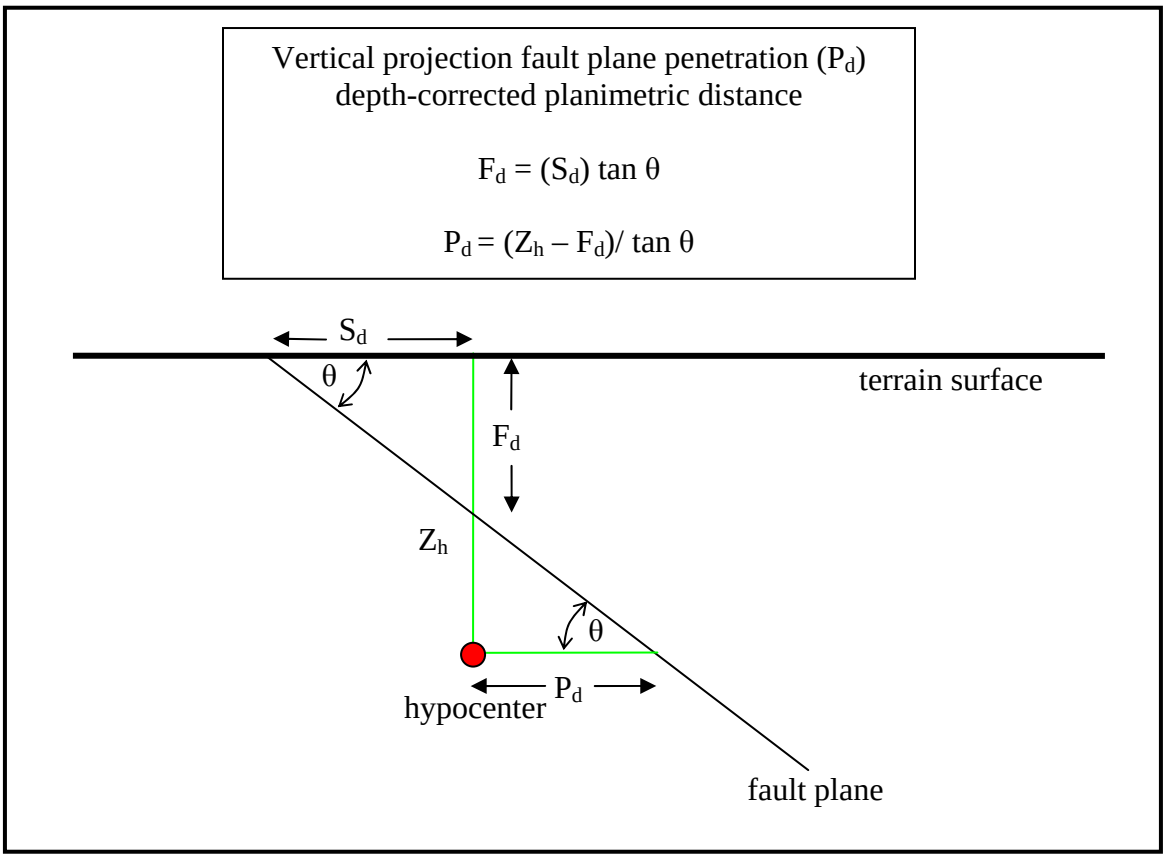

Figure 19. Depth correction where hypocenter projection penetrates fault plane. Schematic showing the geometry used to compute the depth-corrected planimetric distances (P_d) in cases where the vertical projection of the hypocenter penetrates the fault plane, where θ is the fault dip angle, S_d is the surface planimetric distance, F_d is the depth to the fault plane at the hypocenter location, and Z_h is the hypocenter depth.

The process of computing the depth-corrected planimetric distance and the fault normal distance is carried out by a custom-coded ArcView Avenue program. This program uses the hypocenter data, the four nearest fault traces for each hypocenter (computed using the Nearest Features extension described above), and the fault trace polyline data as primary inputs for the computations. In addition, the hypocenter limiting polygons, which are used to filter hypocenters beyond the end of the fault traces, are included in this process.

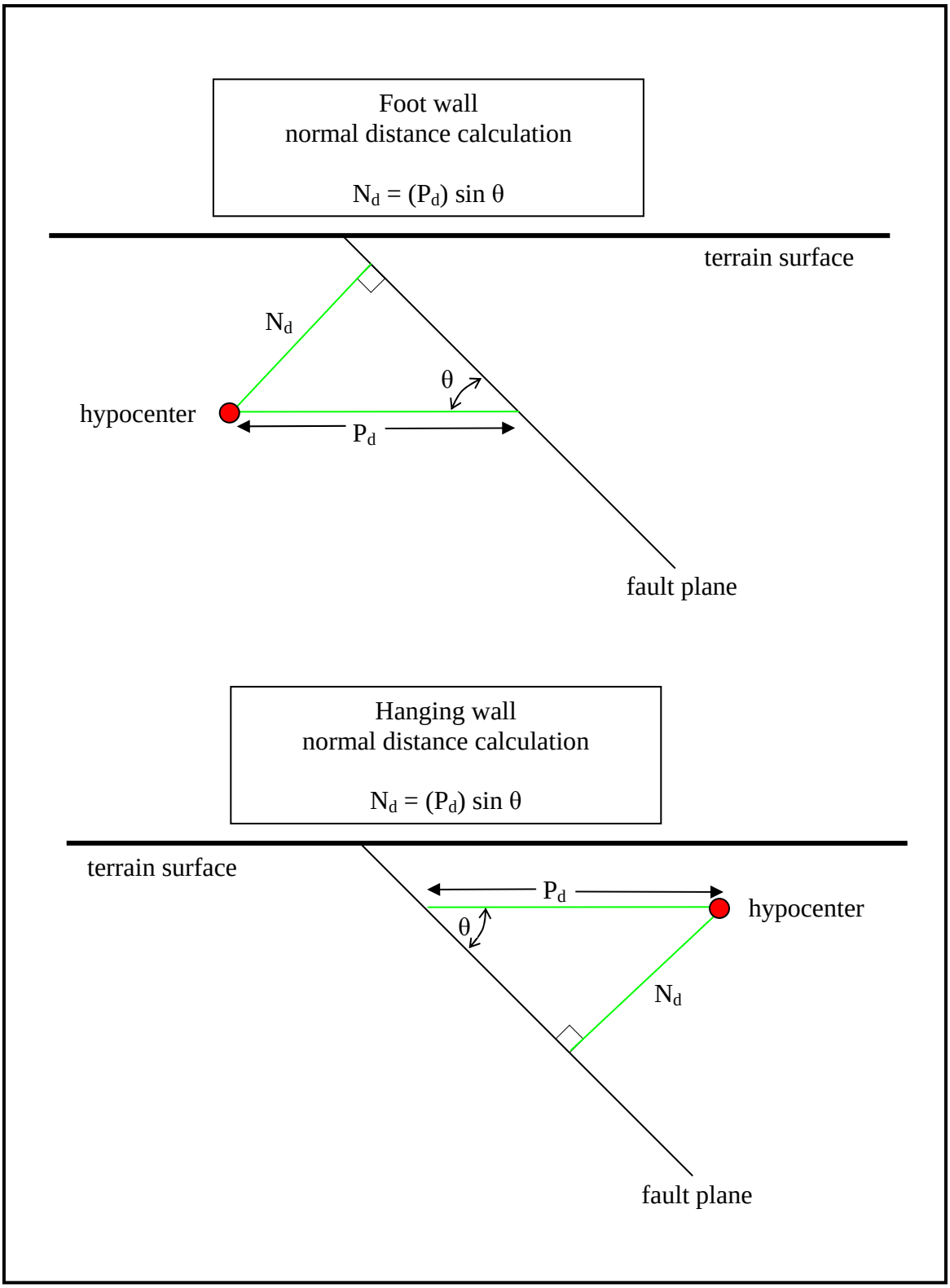

Figure 20. Geometry used to compute the fault normal distances. Fault normal distance (N_d) computed from the depth-corrected planimetric distance (P_d) and fault dip θ.

The program operates by considering each hypocenter and its four nearest fault trace features. If the hypocenter under consideration is not within the limiting polygon for a particular fault trace, then computations for that fault trace are skipped since it is not a valid association. Otherwise, the full series of computations are carried out, including hanging wall / foot wall determination, depth-corrected planimetric distance, and fault normal distance. These computations are performed for each of the four nearest fault traces, and the fault trace with the shortest normal distance is recorded as the final nearest fault trace and its attributes are recorded in the hypocenter data set.

As a final step in the GIS processing the length of each fault trace segment was computed and added to the fault trace attribute table. This length was computed in the projected coordinate space using meters as the units. This length was then available for use in the later statistical analyses.

Limitations and Assumptions

To provide a workable framework for the GIS analyses using the available data sources, a series of assumptions was necessary. The primary assumptions are listed below. These assumptions are considered reasonable and consistent with the goals of this project. Their relative importance is only ascertainable on a case-by-case basis, and so will not be discussed here.

1. Fault records in the fault attribute table which did not have valid dip information were assumed to have a vertical orientation.
2. Fault dip magnitude and direction are constant with depth.
3. Fault dip direction is always normal to the fault trace.
4. Fault trace segments separated by more than 300 m are not related to one another.
5. Hypocenters beyond the end of a fault trace are not related to that fault trace.

In addition to the above assumptions, there is a series of limitations related to these analyses which are listed below. These are, in part due, to limitations in the available data sources and, in part, due to the process assumptions discussed above.

1. The fault normal distances should not be compared against horizontal surface distances since these values are computed normal to a dipping surface. This limitation does not exist for values computed for vertical faults since the fault normal and horizontal distances are equal.
2. Only seismic events (hypocenter data) recorded after 1982 were used in the analyses due to data set anomalies.
3. Only faults in the original fault attribute table were available for analysis.
4. Some mismatch between the original fault attribute table and the final fault trace attribution may be present due to necessary grouping of the fault traces.

Summary of GIS Analysis and Processing

The GIS analyses presented here met the primary objective of providing depth-corrected normal distance measurements between each hypocenter and its nearest fault trace. This objective was met through a series of spatial data procedures performed within the ArcView GIS. These procedures were implemented using a series of custom-coded Avenue programs, third-party software extensions, and native ArcView capabilities.

The final product from this task is a GIS point data set (shapefile) which contains one record for each hypocenter considered in the study. There are a total of 99,787 records. Each hypocenter record contains all the attribute information originally available for that hypocenter and all the available fault attribute information for the nearest fault trace. In addition, each record contains all the computed distances (surface planimetric, depth corrected planimetric, and fault normal) to the nearest fault trace, plus the length of that fault trace polyline segment as computed within the GIS. Additional information such as average fault dip and block wall determination (hanging or foot) is also included. A data dictionary listing all the attributes is provided in Appendix A.

This page intentionally left blank

Statistical Analysis

Having completed the GIS processing, statistical analysis of the resulting data could proceed to investigate trends and relationships among the various attributes. The specific objective was to establish the width of the seismic process zone and investigate its relationship to fault length.

Initial Descriptive Assessment of Hypocenter Distance and Further Screening of Hypocenters

At the end of the GIS analysis and data processing, 99,787 hypocenters were available for study, representing a total of 207 faults (Table B-1 in Appendix B). For all faults, individual histograms of the normal distance from the hypocenters to the associated fault planes were constructed. The distance computations are described in more detail earlier in this report. In the discussion that follows, the distance is sometimes called the hypocenter distance.

As might be expected, an examination of the histograms revealed that the shape and character of the graphs becomes erratic when the number of hypocenters attributed to a fault falls below about 50. Figure 21 (a-d) shows the progressive improvement, (better defined and more symmetric), in the character of the histograms for four faults with an increasing number of attributed hypocenters. However, not all faults to which larger numbers of hypocenters are attributed have associated distributions of hypocenter distance that are symmetric.

Consequently, to ensure reliability of any statistical calculations tied to individual faults, a lower limit of 50 hypocenters was imposed, and all faults having fewer than 50 attributed hypocenters were eliminated from further consideration. This additional screening of the data automatically resulted in a reduction in both the number of faults and hypocenters available for consideration. The remaining data set consisted of 97,272 hypocenters associated with 126 individual faults—a 2.5% reduction in hypocenters but a 40.6% reduction in faults. The number of faults is substantially reduced under the 50 hypocenter restriction because so many of them have very small numbers of associated hypocenters (again see Table B-1 in Appendix B). Decreasing the limit to 40 hypocenters per fault would have added six faults to the database but would not have appreciably altered any subsequent calculations or conclusions.

Further assessment of the histograms of hypocenter distance associated with the remaining faults suggested the existence of four typical shapes: symmetric, bimodal, skewed left, and skewed right. The histograms shown in Figure 22 (a-d) are representative examples of these shapes.

In addition, it was observed that many of the histograms are considerably “off center” relative to the locations of the associated faults; i.e., the middle of the distribution (as represented by the mean or median distance) is rather far from zero. This would imply that, for such situations, the hypocenters are clustered some distance away from their associated faults. It was further observed that, for many faults, the hypocenters tend to lie almost exclusively on one side. Of course, there is no geological reason why such situations could not exist, but the

frequency and consistency with which they are observed, in addition to the disparity in histogram shapes, suggests other factors may be responsible.

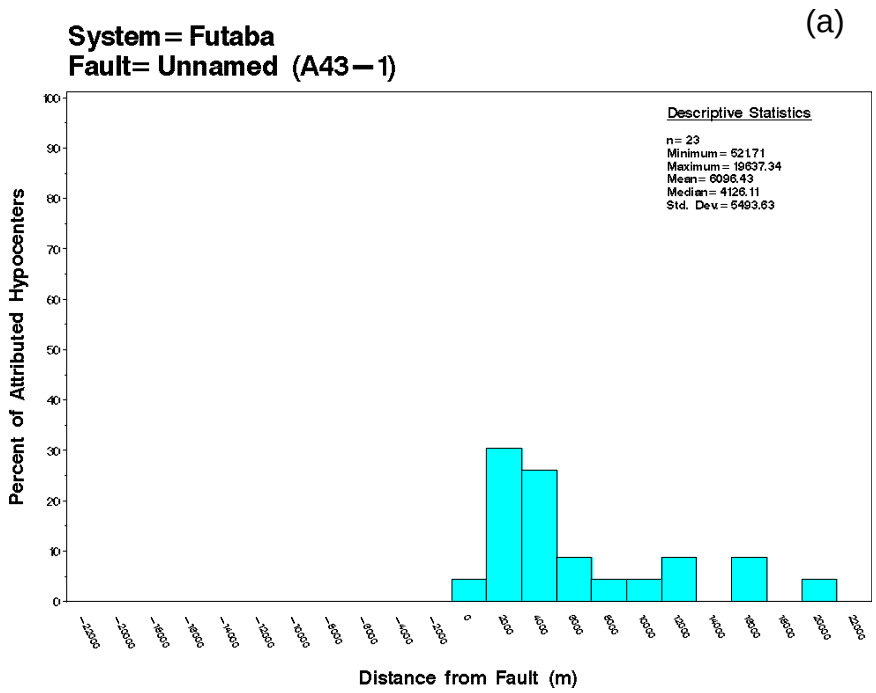

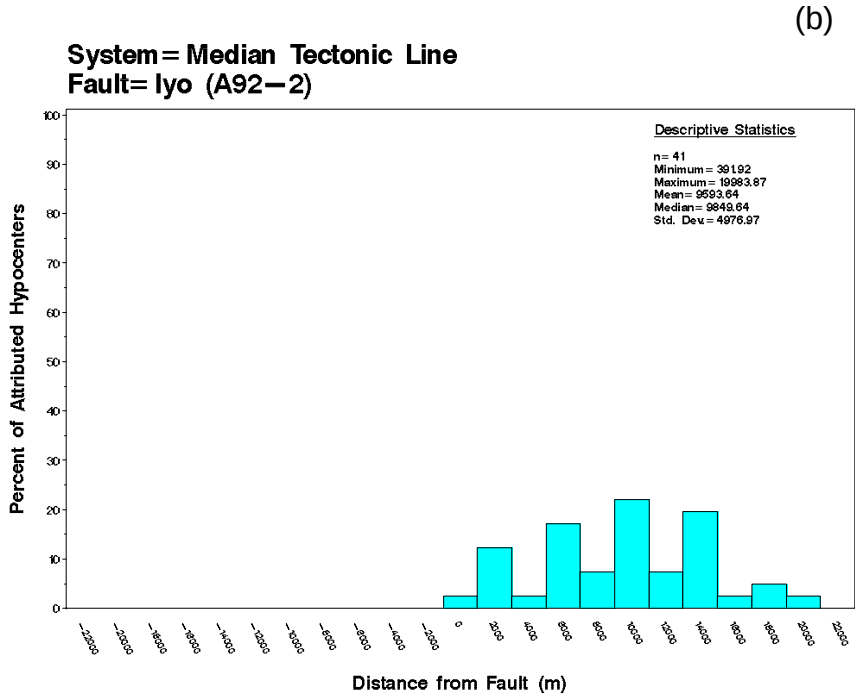

(c)

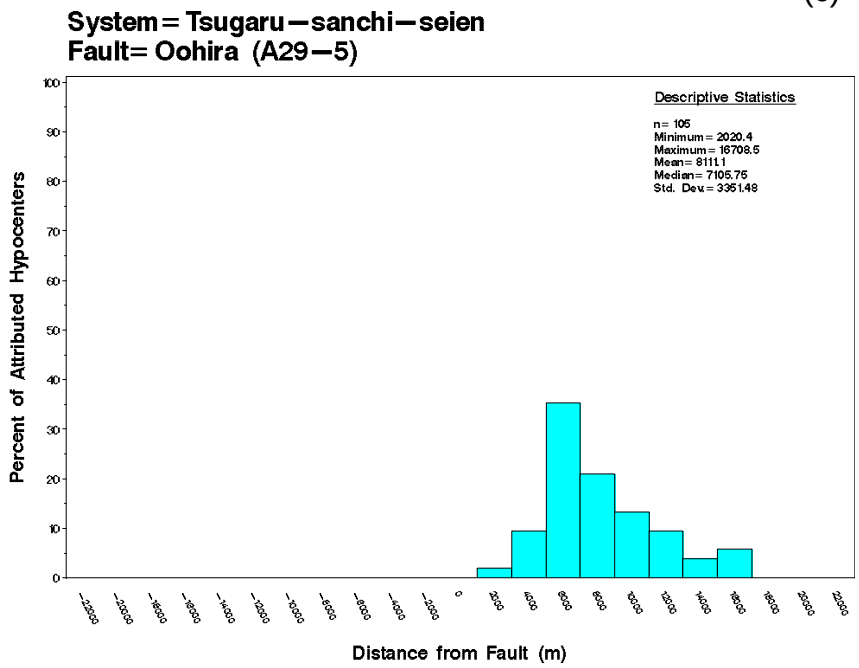
System = Tsugaru−sanchi−seien
Fault= Oohira (A29−5)
Descriptive Statistics
n= 105
Minimum = 2020.4
Maximum = 16708.5
Mean= 8111.1
Median= 7105.75
Std. Dev.= 3351.48
Percent of Attributed Hypocenters
Distance from Fault (m)

(d)

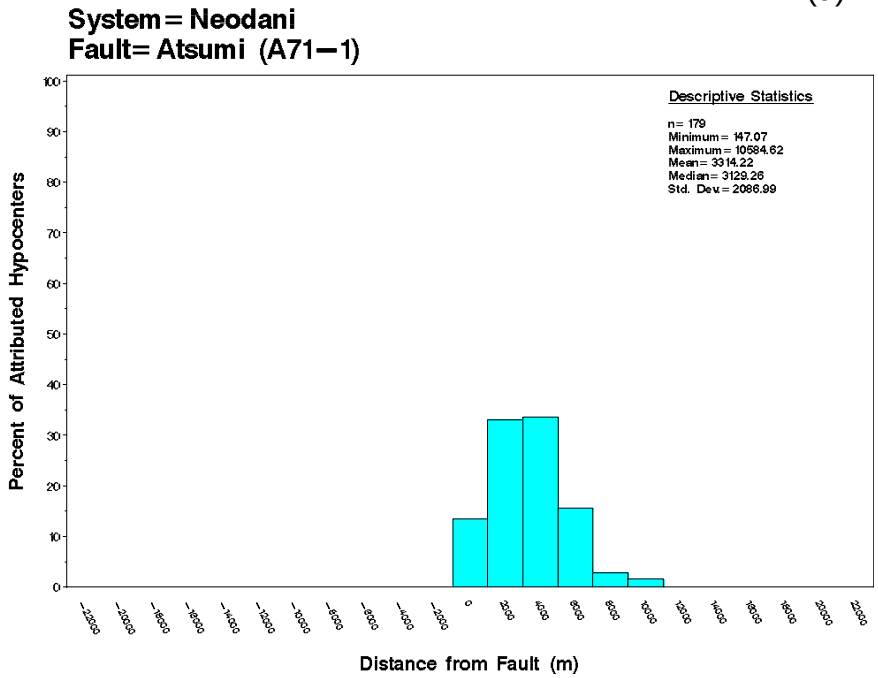
System = Neodani
Fault= Atsumi (A71−1)
Descriptive Statistics
n= 179
Minimum = 147.07
Maximum = 10584.62
Mean= 3314.22
Median= 3129.26
Std. Dev.= 2086.99
Percent of Attributed Hypocenters
Distance from Fault (m)

Figure 21. Percentage histograms of normal distance from hypocenters to fault planes. Four different faults with an increasingly larger number of associated hypocenters: (a) A 43-1 (Unnamed), with n=23; (b) A 92-2 (Iyo), with n=41; (c) A 29-5 (Oohira), with n=105; and (d) A 71-1 (Atsumi), with n=179.

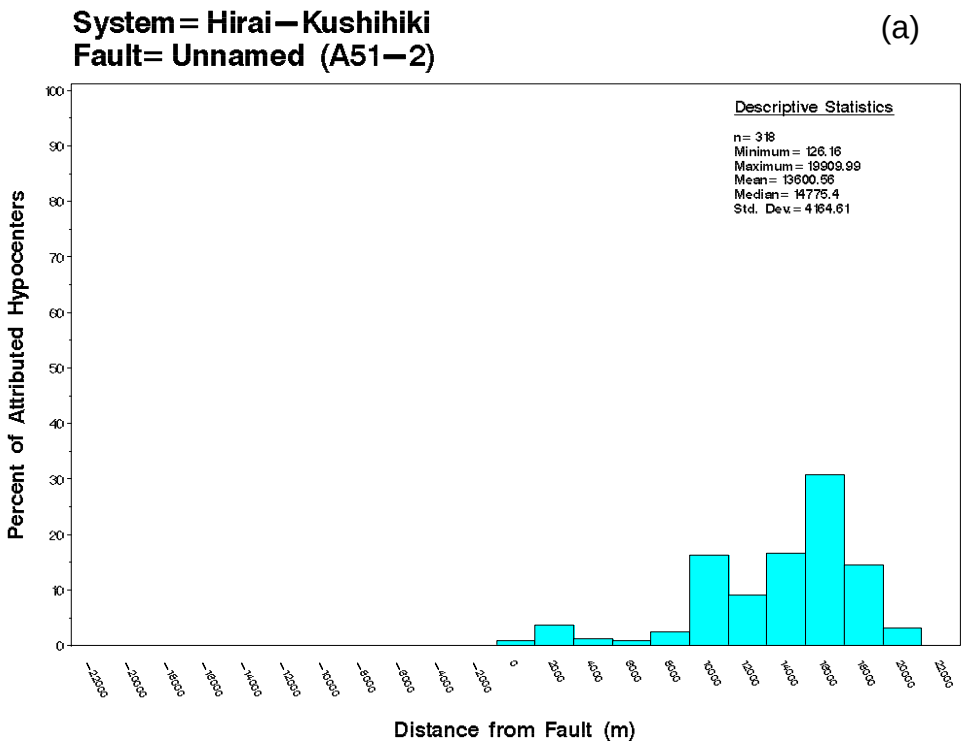

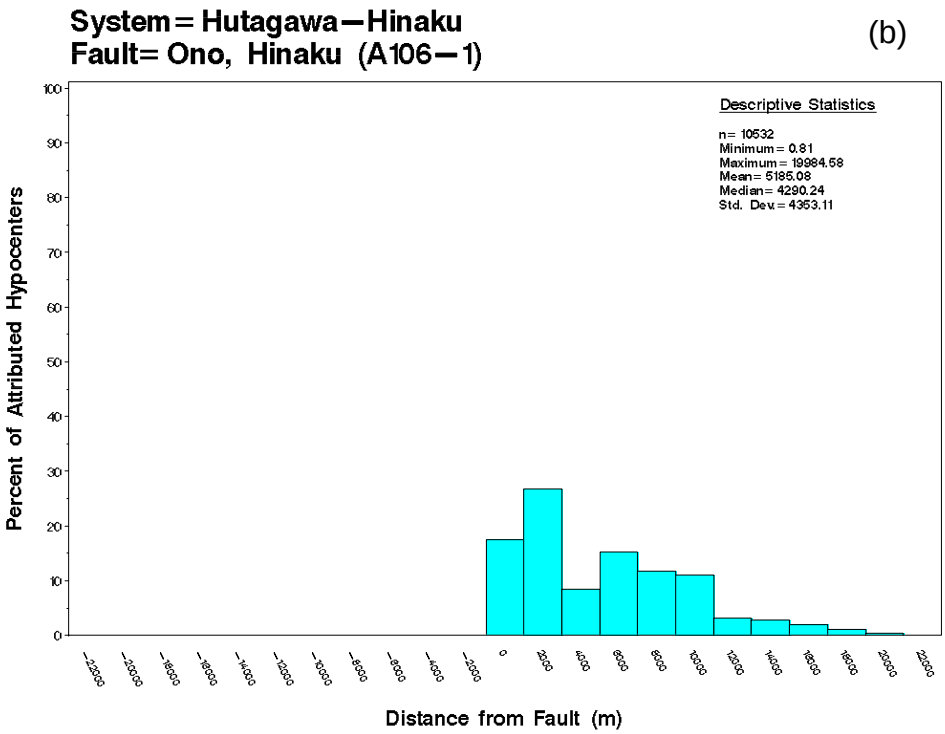
System = Hutagawa—Hinaku
Fault= Ono, Hinaku (A106—1)
(b)
Descriptive Statistics
n= 10532
Minimum= 0.81
Maximum= 19984.58
Mean= 5185.08
Median= 4290.24
Std. Dev.= 4353.11
Percent of Attributed Hypocenters
Distance from Fault (m)

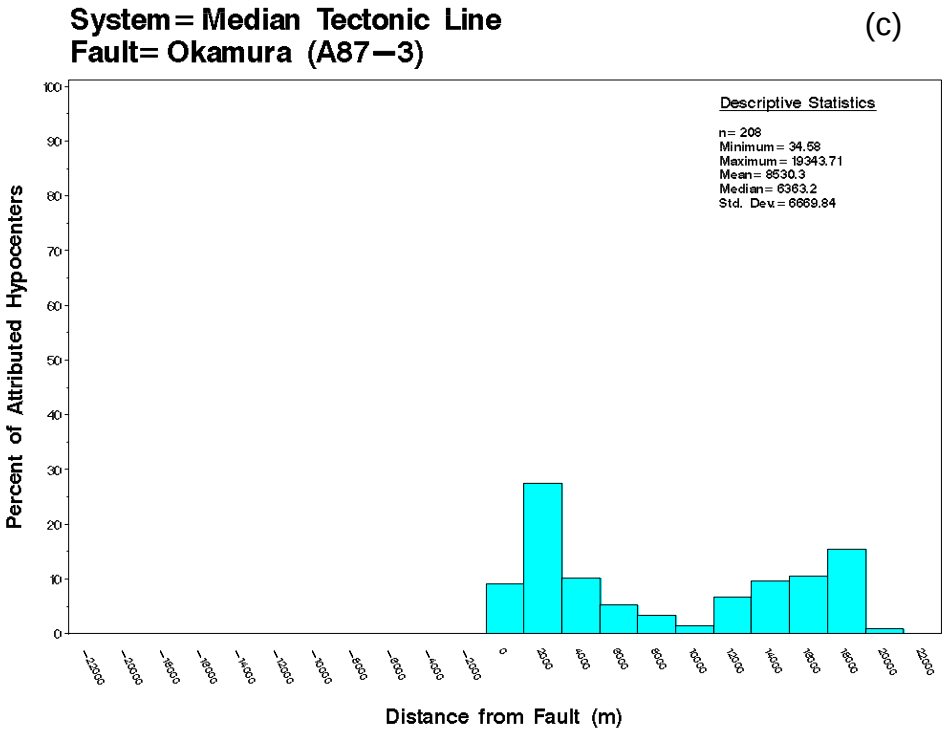
System = Median Tectonic Line
Fault= Okamura (A87—3)
(c)
Descriptive Statistics
n= 208
Minimum= 34.58
Maximum= 19343.71
Mean= 8530.3
Median= 6363.2
Std. Dev.= 6669.84
Percent of Attributed Hypocenters
Distance from Fault (m)

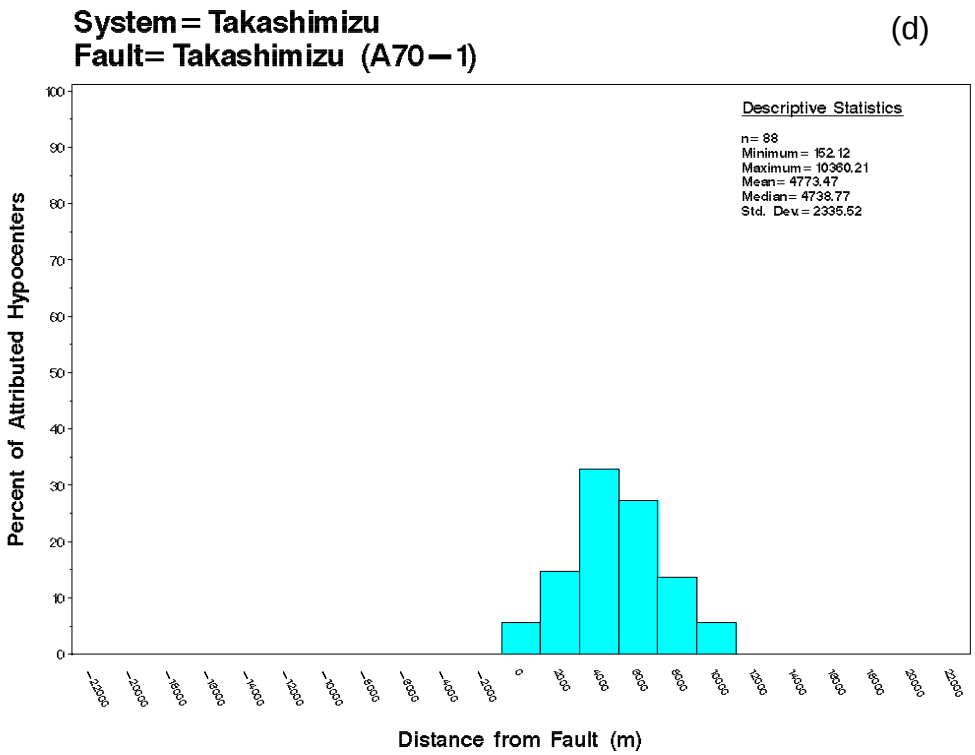

Figure 22. Percentage histograms of normal distance from hypocenters to fault planes. Four different faults for which the associated histograms exhibit one of four recurring patterns: (a) A 51-2 (unknown name), skewed left, with n=318; (b) A 106-1 (Ono, Hinaku), skewed right, with n=10,532; (c) A 87-3 (Okamura), bimodal, with n=208; and (d) A 70-1 (Takashimizu), symmetric, with n=88.

For each of the 126 individual faults, Figure 23 (a-d) presents the distributions of the hypocenter distances as box plots. The box plots are presented in increasing order of fault length; i.e., the box plot of hypocenter distance associated with the shortest fault (B60-1) is presented first and the box plot of hypocenter distance associated with the longest fault (A87-2) is presented last (see the discussion of fault length presented below). Figure 23a contains the box plots associated with the first 32 faults, Figure 23b contains the box plots associated with the next 32 faults, Figure 23c presents the box plots associated with the third group containing 31 faults, and Figure 23d presents the box plots associated with the last 31 faults.

Each box plot summarizes the empirical distribution of hypocenter distance, showing the 25th, 50th, and 75th percentiles, along with any values that would be considered outliers or statistical extremes. The 25th, 50th, and 75th percentiles are often denoted Q_1, Q_2 (the median), and Q_3, and are shown by the lower end of the box, the black horizontal line within the box and the upper end of the box, respectively. The numerical difference between Q_3 and Q_1 is called the interquartile range, denoted by IQR. Fifty percent of the observed values fall between Q_1 and Q_3, and the IQR itself is a measure of dispersion (a proxy for standard deviation) around Q_2, the median value. In the box plots shown in Figure 23 (a-d), outliers and extreme values are identified using the following standard convention: values are designated as *outliers* if they are larger than Q_3 + 1.5*IQR or smaller than Q_1 – 1.5*IQR. These two quantities define the ends

of the whiskers attached to the boxes. Values are designated as *extremes* if they are larger than Q_3 + 3*IQR or smaller than Q_1 – 3*IQR.

Inspection of Figure 23 (a-d) indicates that outliers and extreme values persist in the empirical distributions of hypocenter distance associated with many of the faults. Examination of the histograms themselves confirms this observation (see Figures 24-27 for examples). The decision was made to eliminate the outliers and the extreme values in order to improve the overall character of the histograms before making any other statistical calculations. The elimination of these values reduced the total number of hypocenters to 94,329.

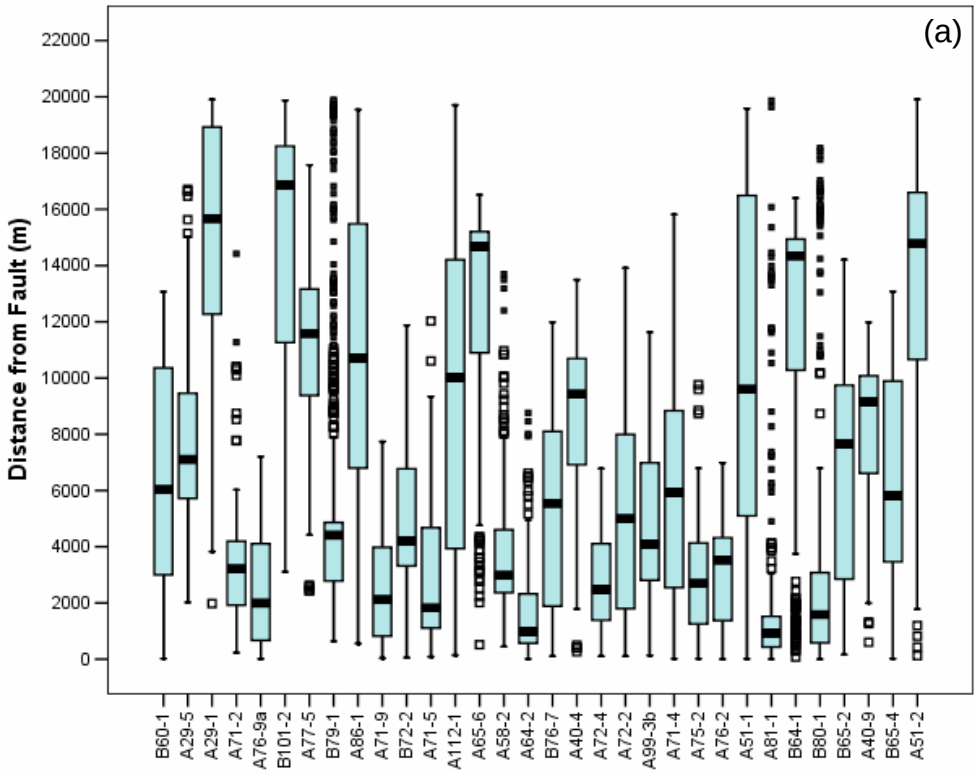
(a)
Distance from Fault (m)
0
2000
4000
6000
8000
10000
12000
14000
16000
18000
20000
22000
B60-1
A29-5
A29-1
A71-2
A76-9a
B101-2
A77-5
B79-1
A86-1
A71-9
B72-2
A71-5
A112-1
A65-6
A58-2
A64-2
B76-7
A40-4
A72-4
A72-2
A99-3b
A71-4
A75-2
A76-2
A51-1
A81-1
B64-1
B80-1
B65-2
A40-9
B65-4
A51-2

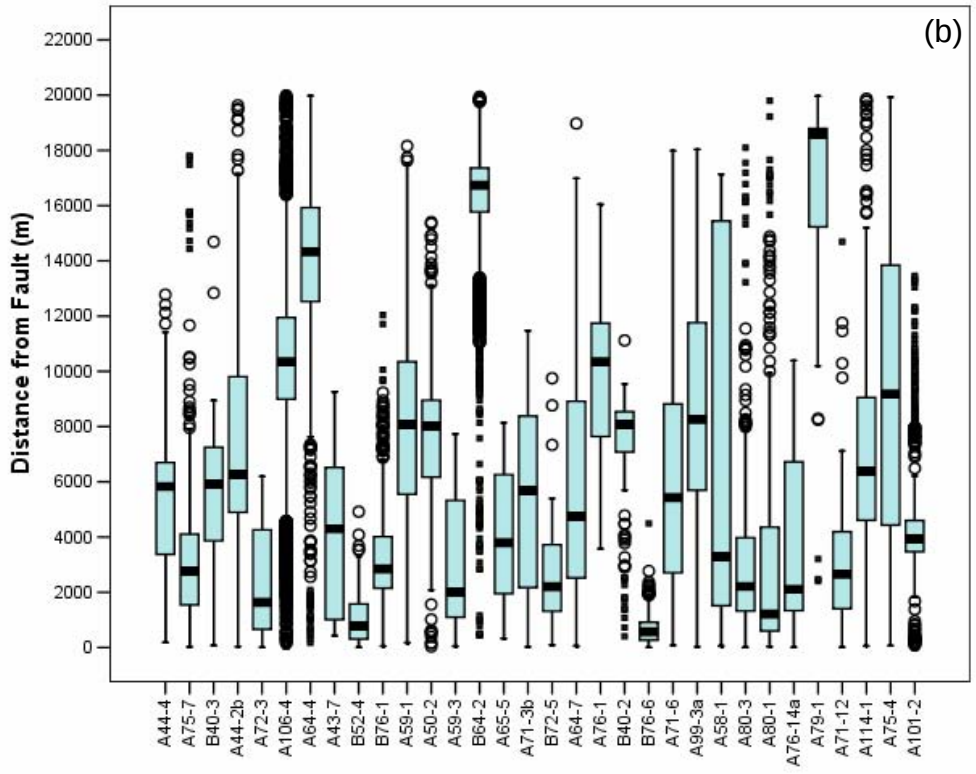
(b)
Distance from Fault (m)
0
2000
4000
6000
8000
10000
12000
14000
16000
18000
20000
22000
A44-4
A75-7
B40-3
A44-2b
A72-3
A106-4
A64-4
A43-7
B52-4
B76-1
A59-1
A50-2
A59-3
B64-2
A65-5
A71-3b
B72-5
A64-7
A76-1
B40-2
B76-6
A71-6
A99-3a
A58-1
A80-3
A80-1
A76-14a
A79-1
A71-12
A114-1
A75-4
A101-2

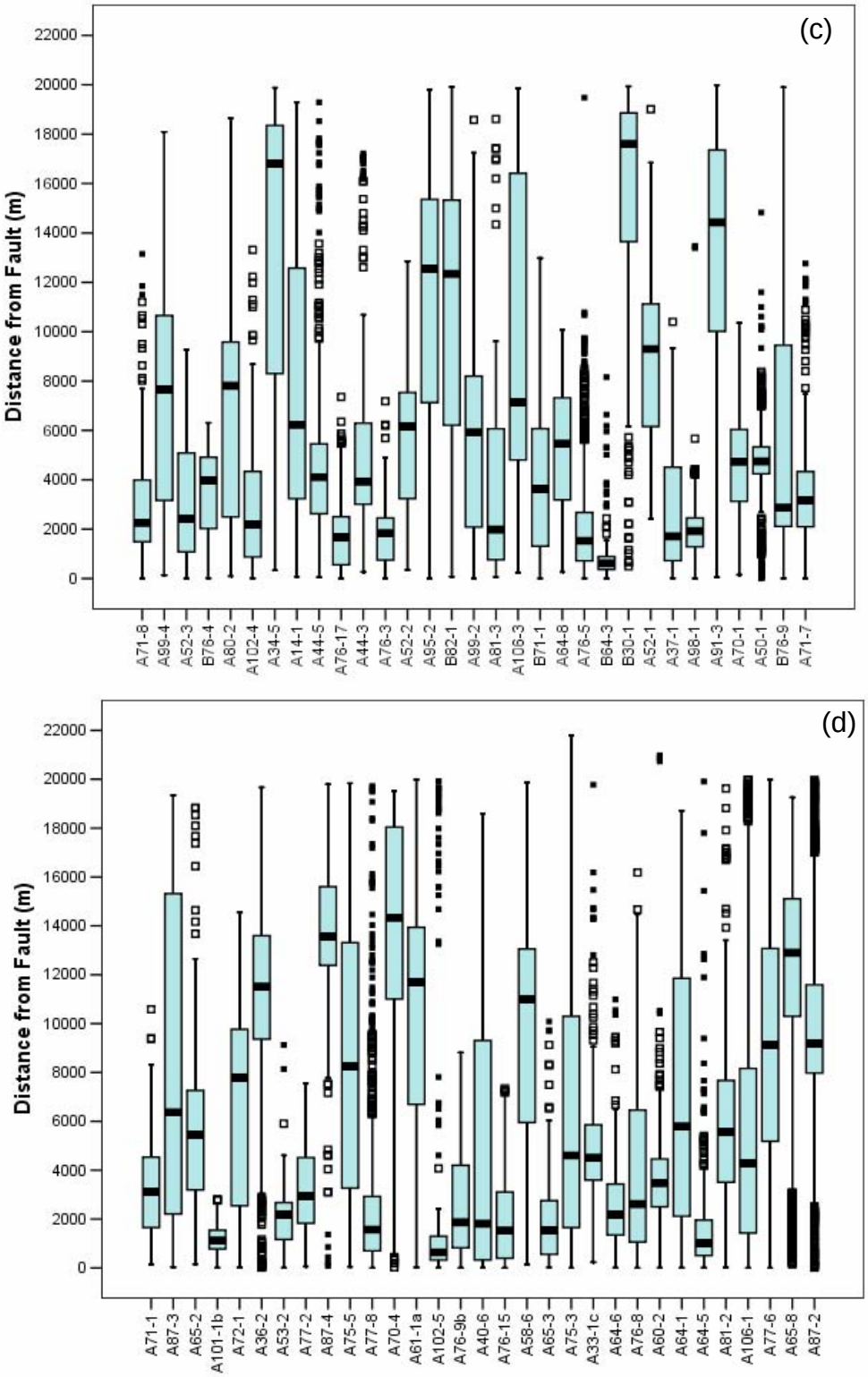

Figure 23. Box plots of normal distance from hypocenters to fault planes (truncated at zero on the lower end). The data set is restricted to faults having 50 or more associated hypocenters. Plots are presented in order of increasing fault length, beginning with B60-1 in (a) having a total length of 6,964.1 m and ending with A87-2 in (d) having a total length of 107,204.8 m. Statistical outliers shown as empty squares; statistical extremes shown as filled squares.

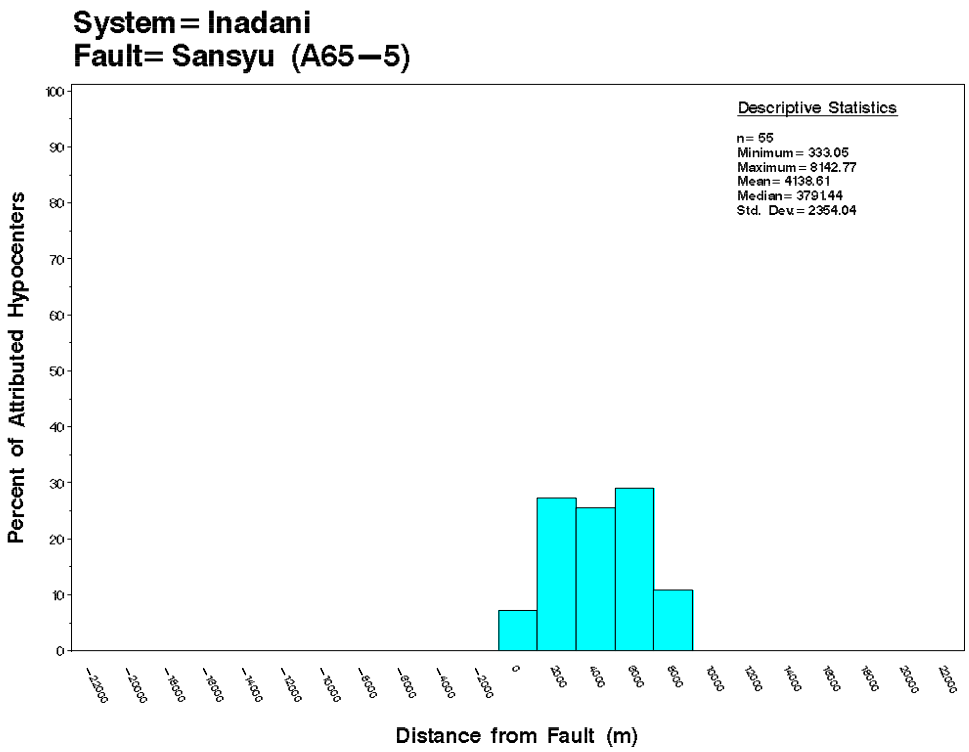

Figure 24. Percentage histogram of hypocenter distance associated with Fault A 65-5 (Sansyu). The distribution encompasses no outliers.

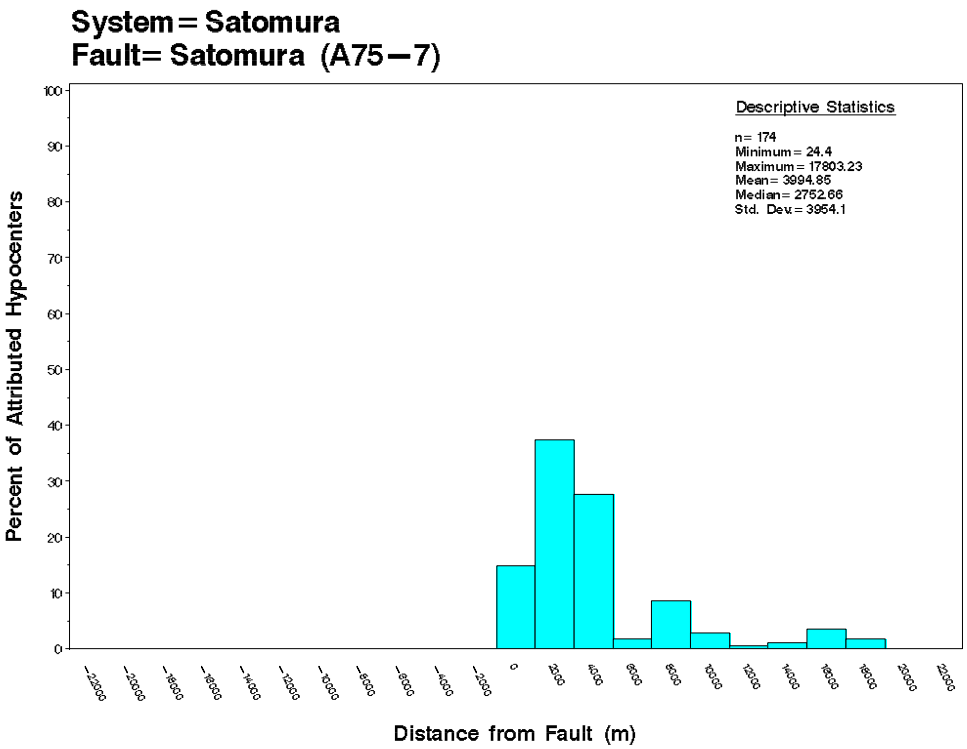

Figure 25. Percentage histogram of hypocenter distance associated with Fault A 75-7 (Satomura). The distribution encompasses outliers on the right side.

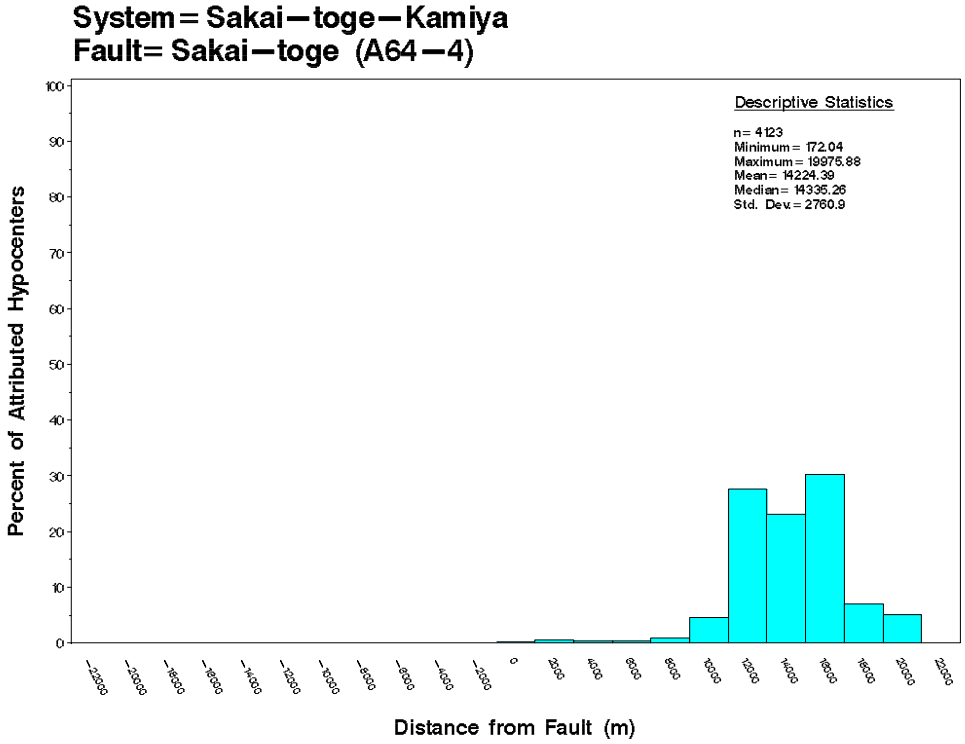

Figure 26. Percentage histogram of hypocenter distance associated with Fault A 64-4 (Sakai-toge). The distribution encompasses outliers and extreme values on the left side.

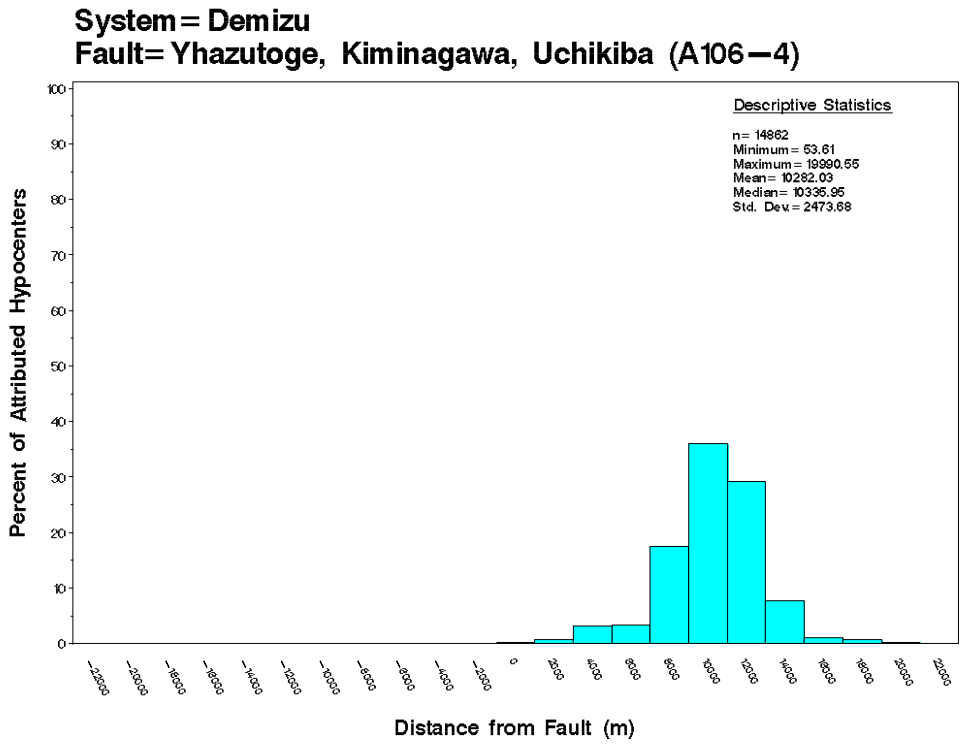

Figure 27. Percentage histogram of hypocenter distance associated with Fault A 106-4 (Yhazutoge, Kiminagawa, Uchikiba). The distribution encompasses outliers and extreme values on both sides.

Figure 28 contains the revised box plots of hypocenter distance after removing the outliers and extreme values. Although the distributions of hypocenter distance associated with most faults are cleaner, the adjustment process did not totally eliminate all outliers (since the values of Q_1 and Q_3 change as values are eliminated from consideration). The outlier identification and elimination process could be repeated, but such additional passes through the database would not be expected to yield substantial improvements.

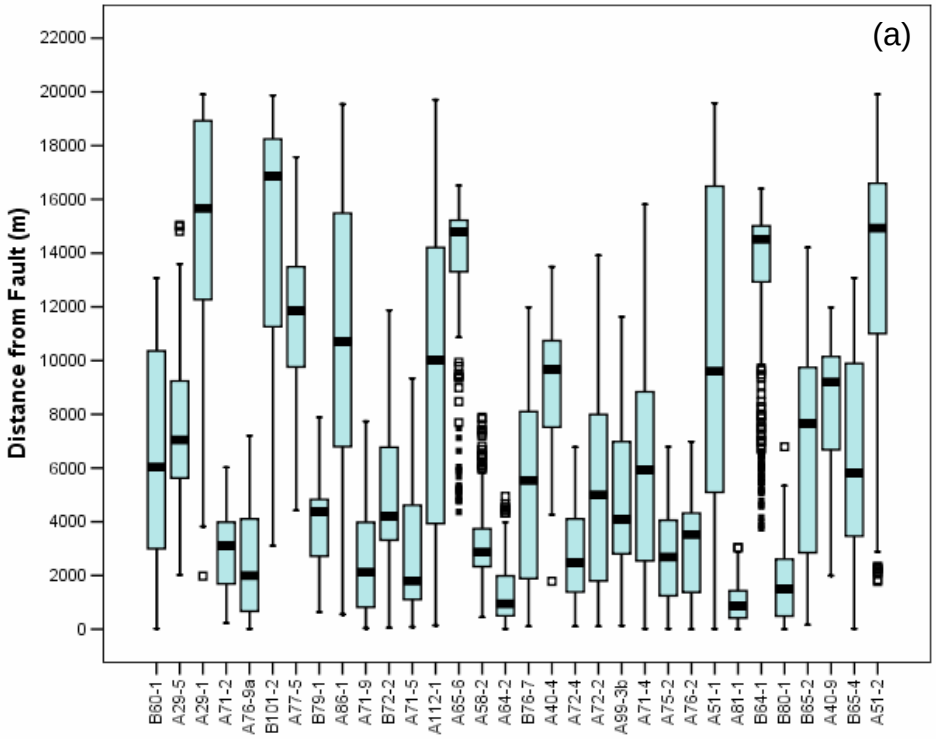
(a)
Distance from Fault (m)
0
2000
4000
6000
8000
10000
12000
14000
16000
18000
20000
22000
B60-1
A29-5
A29-1
A71-2
A76-9a
B101-2
A77-5
B79-1
A86-1
A71-9
B72-2
A71-5
A112-1
A65-6
A58-2
A64-2
B76-7
A40-4
A72-4
A72-2
A99-3b
A71-4
A75-2
A76-2
A51-1
A81-1
B64-1
B60-1
B65-2
A40-9
B65-4
A51-2

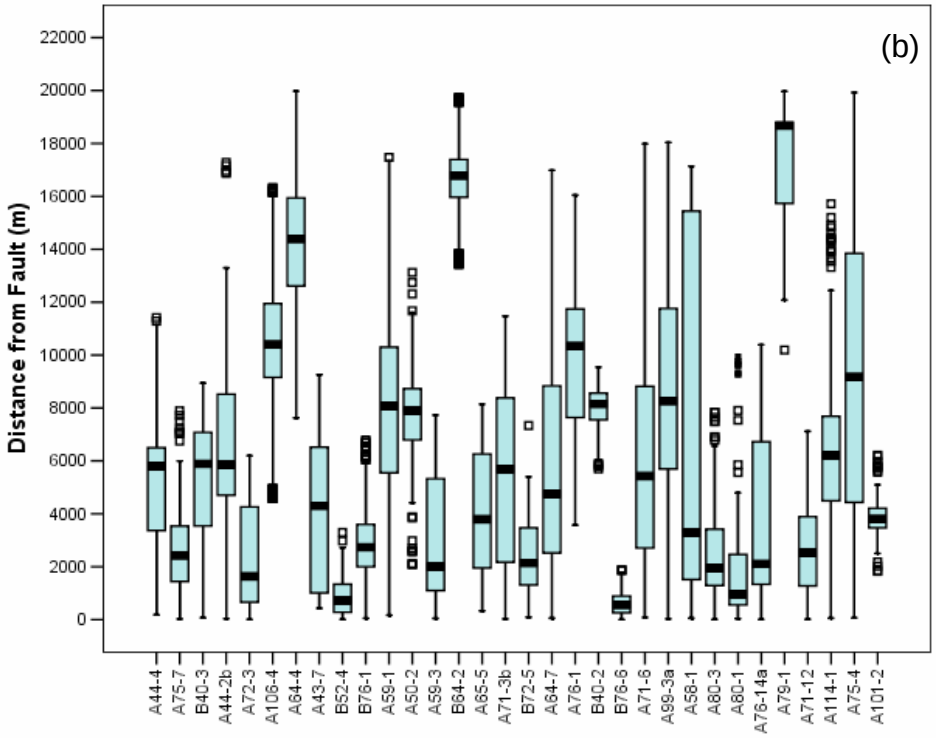
(b)
Distance from Fault (m)
0
2000
4000
6000
8000
10000
12000
14000
16000
18000
20000
22000
A44-4
A75-7
B40-3
A44-2b
A72-3
A106-4
A64-4
A43-7
B52-4
B76-1
A59-1
A50-2
A59-3
B64-2
A65-5
A71-3b
B72-5
A64-7
A76-1
B40-2
B76-6
A71-6
A99-3a
A58-1
A80-3
A80-1
A76-14a
A79-1
A71-12
A114-1
A75-4
A101-2

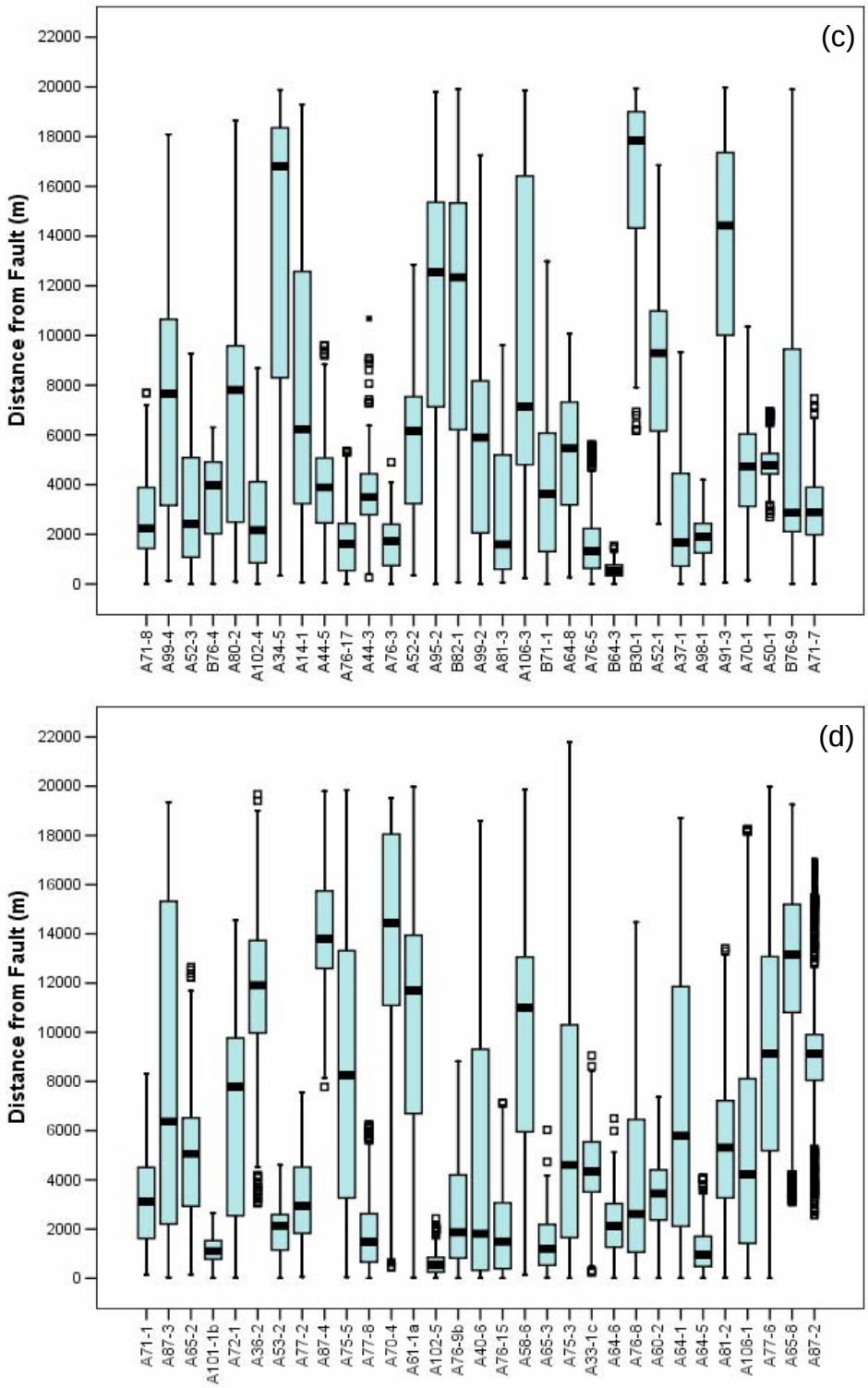

Figure 28. Box plots of normal distance from hypocenters to fault planes, after eliminating outliers and extreme values (e.g., see Figures 29-32). The data set is restricted to faults having 50 or more associated hypocenters. Plots are presented in order of increasing fault length, beginning with B60-1 in (a) having a total length of 6,964.1 m and ending with A87-2 in (d) having a total length of 107,204.8 m. Remaining statistical outliers are shown as empty squares; statistical extremes are shown as filled squares.

Figures 29a, 30a, 31a, and 32a show the revised histograms (after the single pass of outlier elimination) corresponding to those shown in Figures 24-27. These histograms again illustrate the cleansing of the data that has been achieved through the outlier removal process.

Figures 29b, 30b, 31b, and 32b are comparative histograms associated with the same faults except that distances for hypocenters located on one or the other sides of the fault are considered to be positive and negative values, respectively. In this perspective, in which the hypocenter distances are referred to as signed distances, the histograms clearly illustrate how hypocenters are still spatially clustered on one side of the fault plane. The procedure for determining the side of the fault on which a hypocenter is located is described in more detail above (see "Distance Computations). For faults with known dip, the hanging wall and foot wall are identified as the two sides. Appendix C contains a complete catalog of all these histograms.

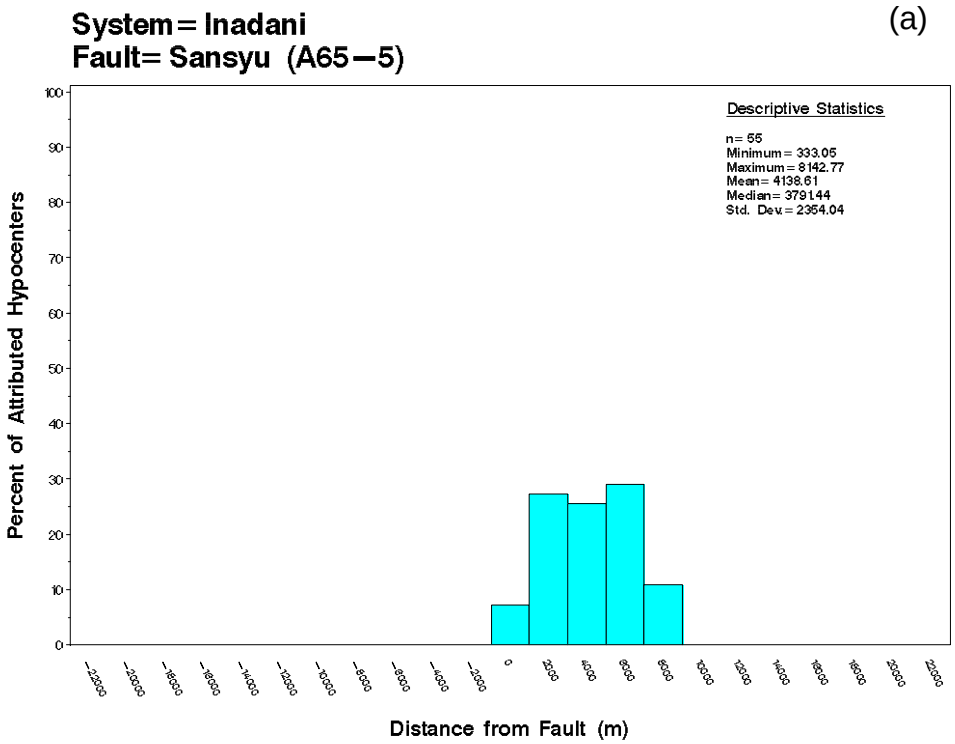

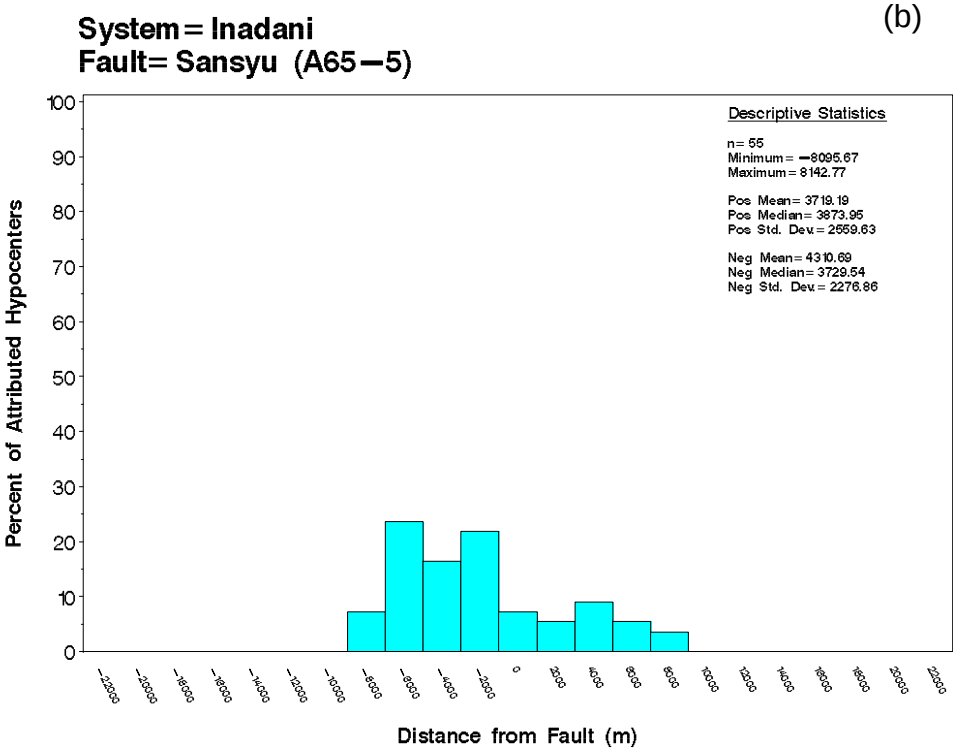

Figure 29. Percentage histogram of normal distances from hypocenters to Fault A65-5 (Sansyu): (a) unsigned distances and (b) signed distances. Statistical outliers are omitted.

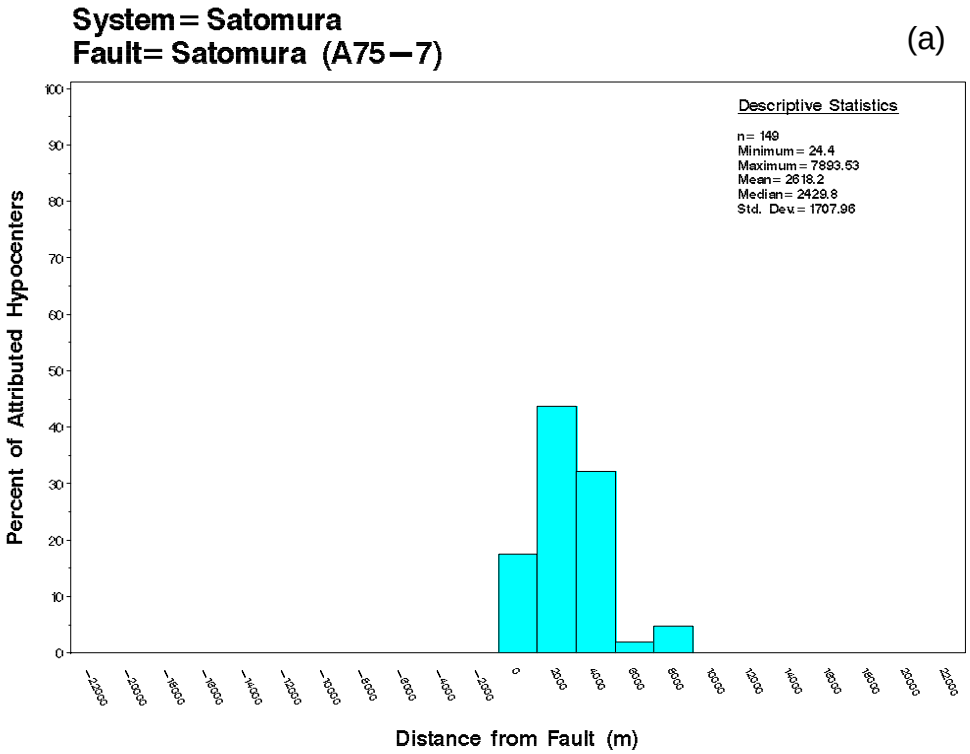

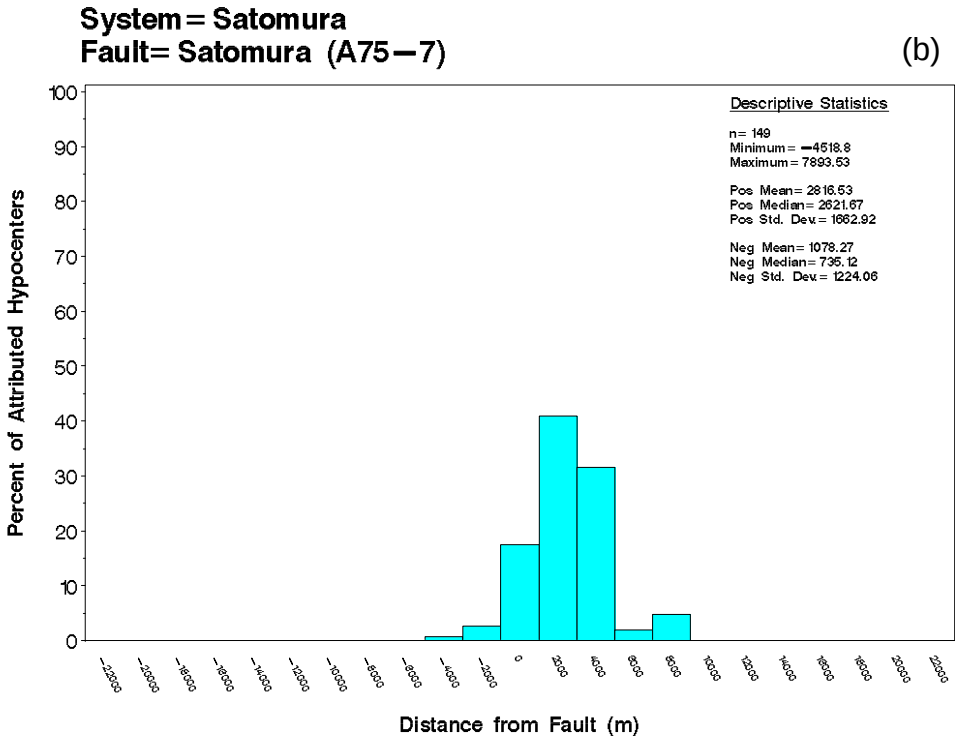

Figure 30. Percentage histogram of normal distances from hypocenters to Fault A75-7 (Satomura): (a) unsigned distances and (b) signed distances. Statistical outliers are omitted.

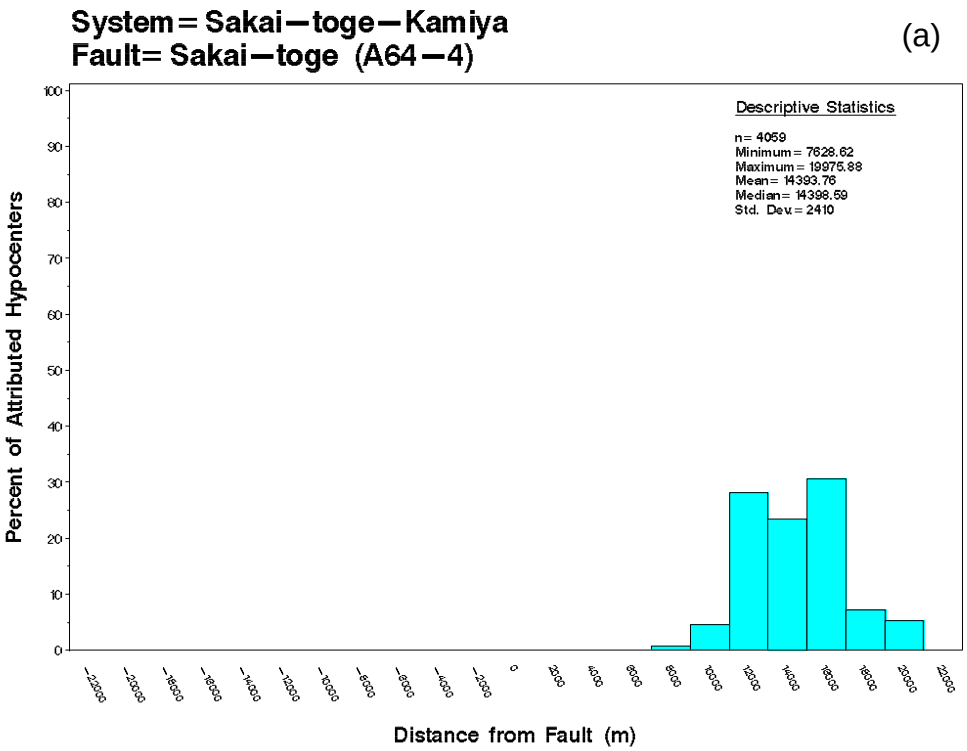

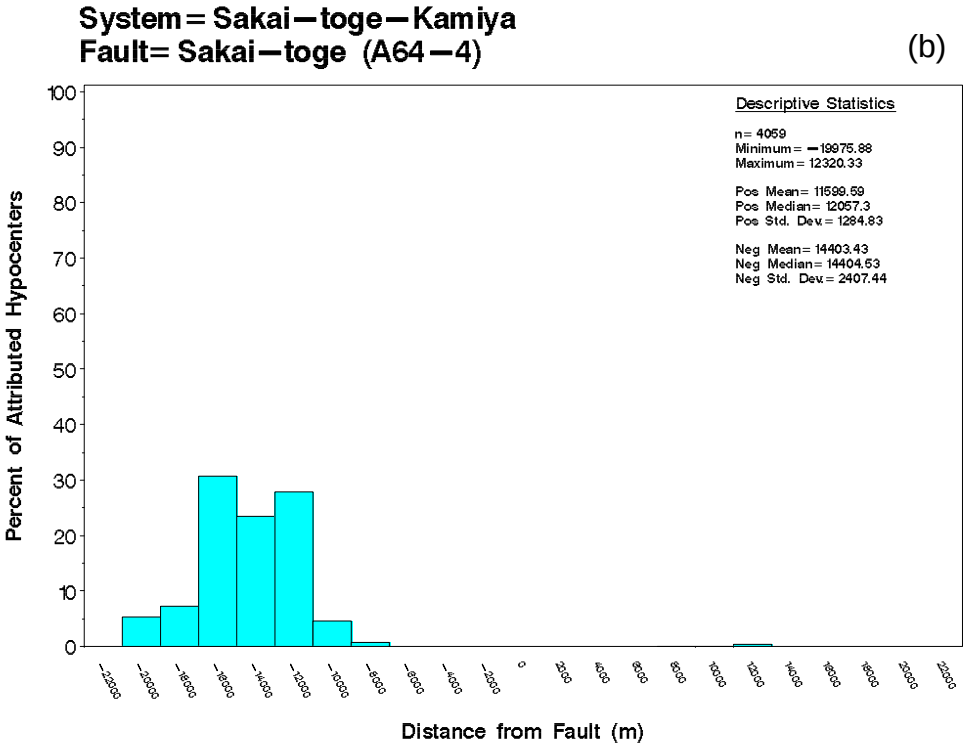

Figure 31**. Percentage histogram of normal distances from hypocenters to Fault A64-4 (Sakai-toge):** (a) unsigned distances and (b) signed distances. Statistical outliers are omitted.

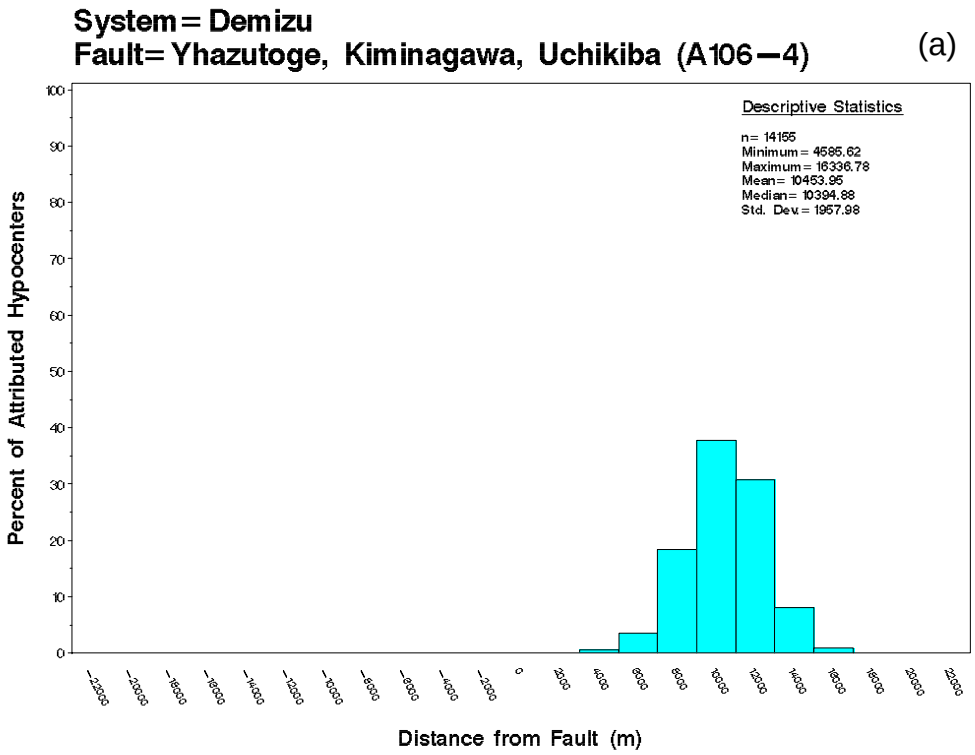

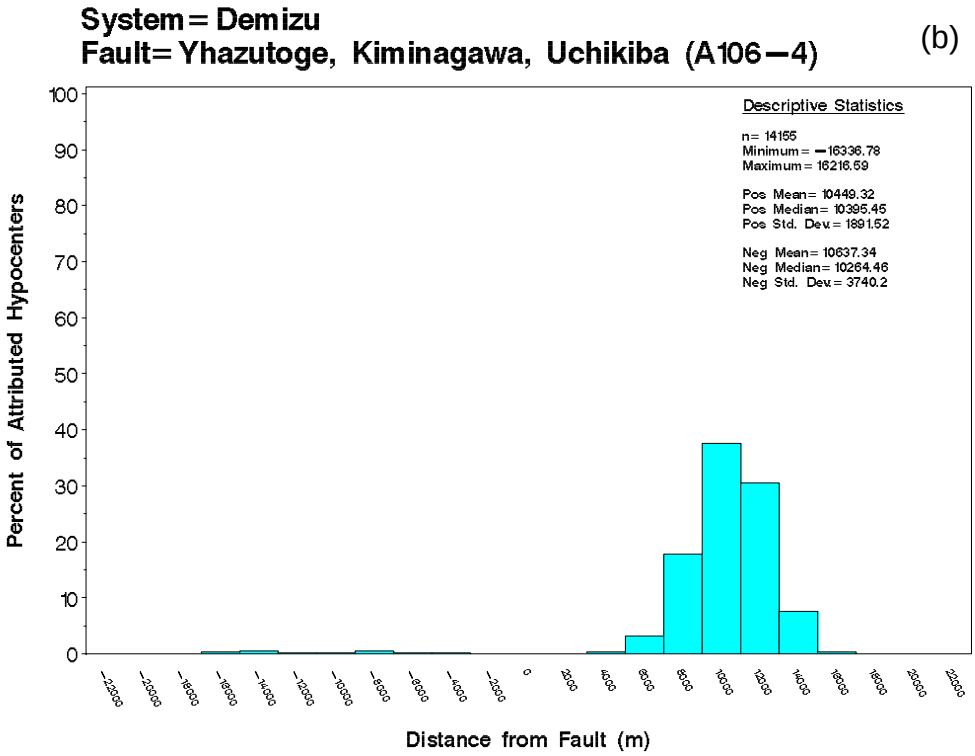

Figure 32. Percentage histogram of normal distances from hypocenters to Fault A106-4 (Yhazutoge, Kiminagawa, Uchikiba): (a) unsigned distances and (b) signed distances. Statistical outliers are omitted.

The final database for purposes of statistical analysis consists of 94,329 hypocenters associated with 126 individual faults. A histogram of hypocenter distance encompassing the entire database is presented in Figure 33. This histogram is trimodal in character, reflecting the multiple shapes of histograms associated with the individual faults. The shape of this distribution is considerably different from the shape of the one depicted in Figure 3 which was based on preliminary analysis.

(a)

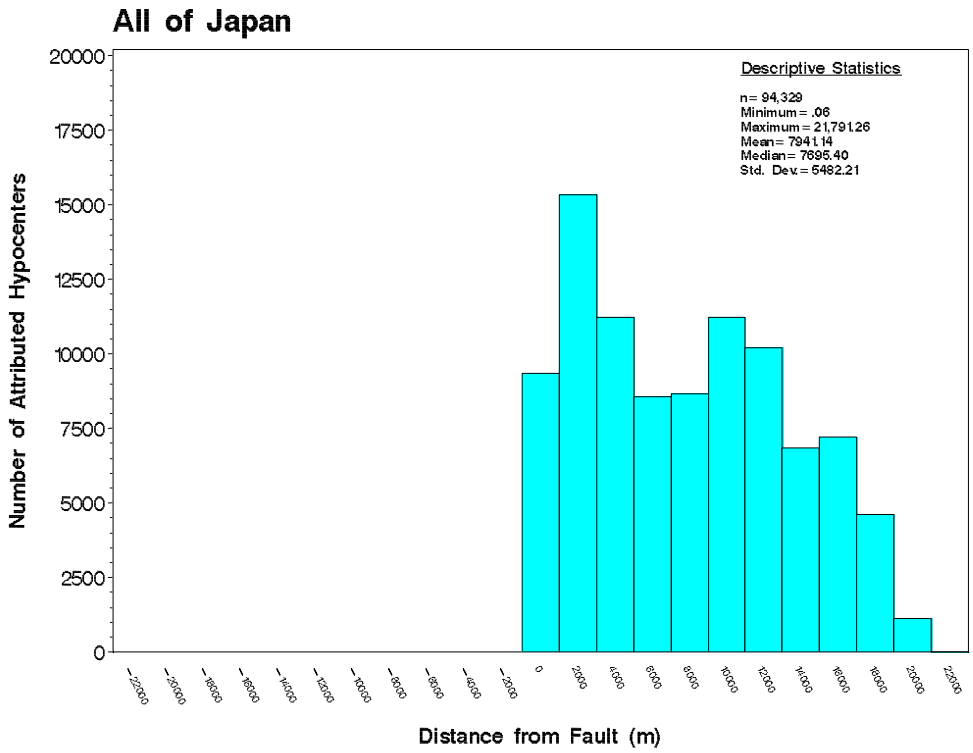

(b)

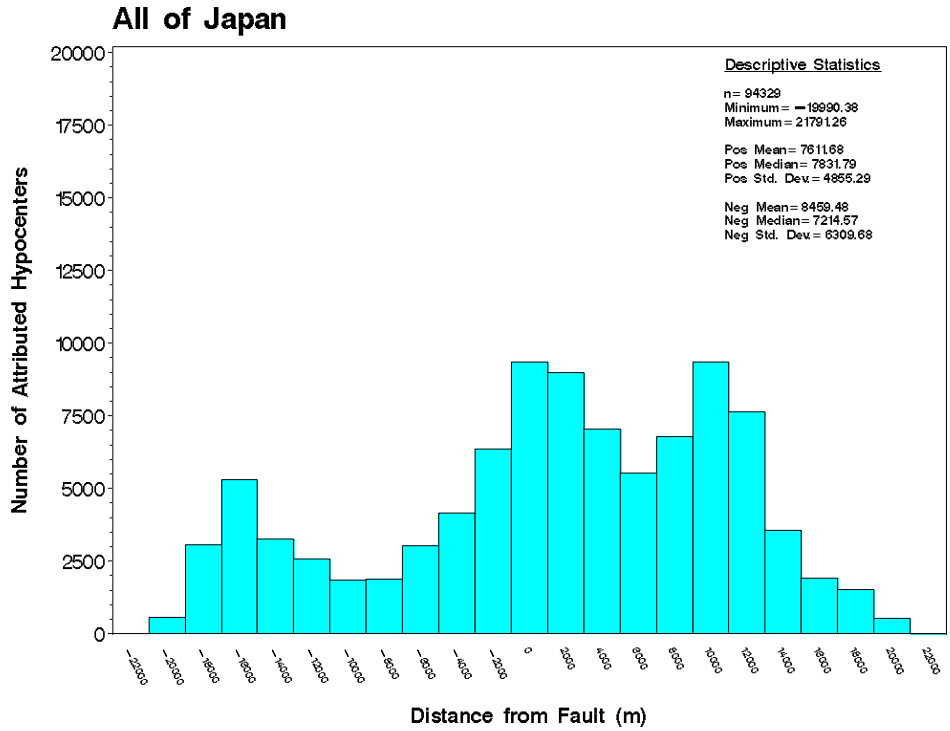

Figure 33. Frequency histogram of (a) unsigned distance and (b) signed distance from hypocenters to fault planes, all of Japan. Statistical outliers are omitted, as are those distances associated with faults to which fewer than 50 hypocenters are attributed.

Descriptive Characteristics of Hypocenters

Before pursuing further statistical analysis of hypocenter distance, it is instructive to consider some of the descriptive characteristics associated with the hypocenters themselves. Two such characteristics of interest are hypocenter depth and earthquake magnitude.

Table B-2 (Appendix B) contains counts and corresponding percentages of hypocenters associated with each fault within each of five different depth intervals (as discussed previously, the original database was restricted to hypocenters located 20 or less km deep). Figure 34 presents a histogram of all hypocenters in the database, by depth category, along with a cumulative percentage curve. The modal class is 5 – 9.99 km, suggesting that for all of Japan, most hypocenters are in this depth range.

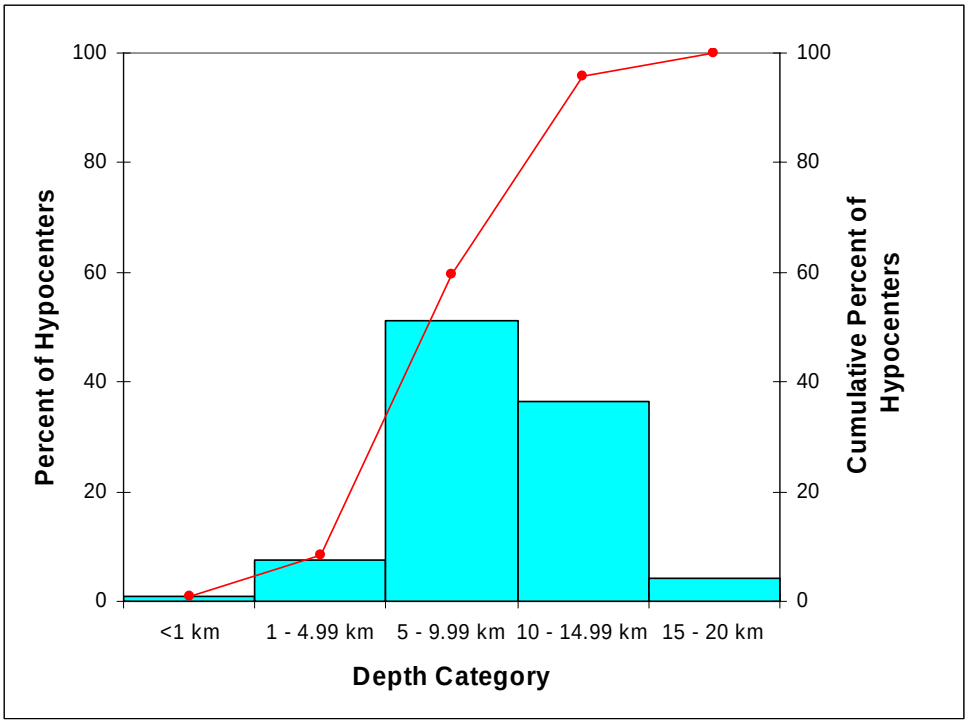

Figure 34. Histogram of the percentage of all hypocenter distances (all Japan), by depth category, with corresponding cumulative percentage histogram. Statistical outliers are omitted, as are those distances associated with faults to which fewer than 50 hypocenters are attributed.

Figure 35 (a-d) presents stacked histograms of the percentages of hypocenters within the various depth intervals for each of the individual faults. The histograms are presented in increasing order of fault length; i.e., the stacked percentage histogram associated with the shortest fault (B60-1) is presented first in Figure 35a and the stacked percentage histogram associated with the longest fault (A87-2) is presented last in Figure 35d (see the discussion of fault length presented below). Figure 35a contains the stacked histograms associated with the first 32 faults, Figure 35b contains the stacked histograms associated with the next 32 faults, Figure 35c presents the stacked histograms associated with the next 31 faults, and Figure 35d presents the stacked histograms for the final 31 faults.

These stacked histograms visually illustrate that almost all the faults have attributed hypocenters in each of the five depth ranges. They also illustrate that a majority of the hypocenters attributed to many of the faults are located 5-15 km deep (a combination of the 5 – 9.99 km and 10 – 14.99 km in Table B-2). Figure 35 (a-d) further suggests that length of the fault is not a significant factor in determining the depth of hypocenters (see the discussion of length presented below). This observation is discussed in more detail below.

(a)

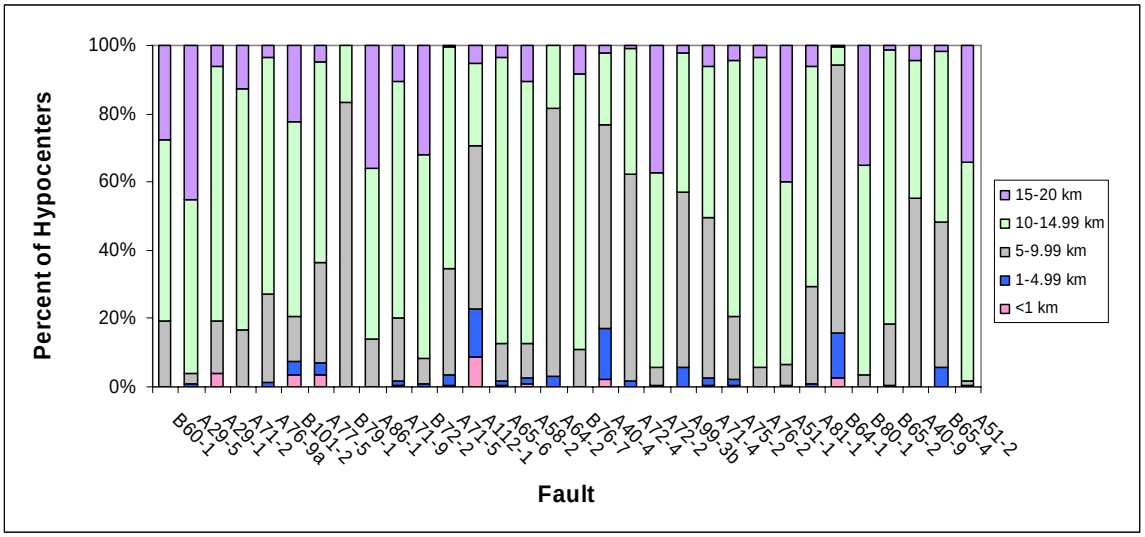
100%
80%
60%
40%
20%
0%
Percent of Hypocenters
15-20 km
10-14.99 km
5-9.99 km
1-4.99 km
<1 km
B60-1
A29-5
A29-1
A71-2
A76-9a
B101-2
A77-5
B79-1
A86-1
A71-9
B72-2
A71-5
A112-1
A65-6
A58-2
A64-2
B76-7
A40-4
A72-4
A72-2
A99-3b
A71-4
A75-2
A76-2
A51-1
A81-1
B64-1
B80-1
B65-2
A40-9
B65-4
A51-2
Fault

(b)

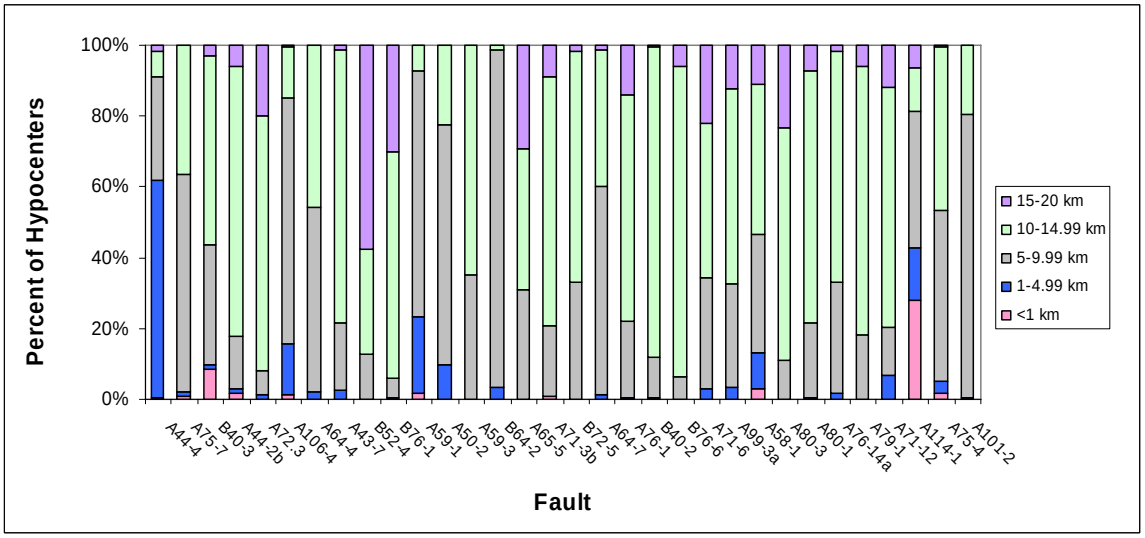
100%
80%
60%
40%
20%
0%
Percent of Hypocenters
15-20 km
10-14.99 km
5-9.99 km
1-4.99 km
<1 km
A44-4
A75-7
B40-3
A44-2b
A72-3
A106-4
A64-4
A43-7
B52-4
B76-1
A59-1
A50-2
A59-3
B64-2
A65-5
A71-3b
B72-5
A64-7
A76-1
B40-2
B76-6
A71-6
A99-3a
A58-1
A80-3
A80-1
A76-14a
A79-1
A71-12
A114-1
A75-4
A101-2
Fault

(c)

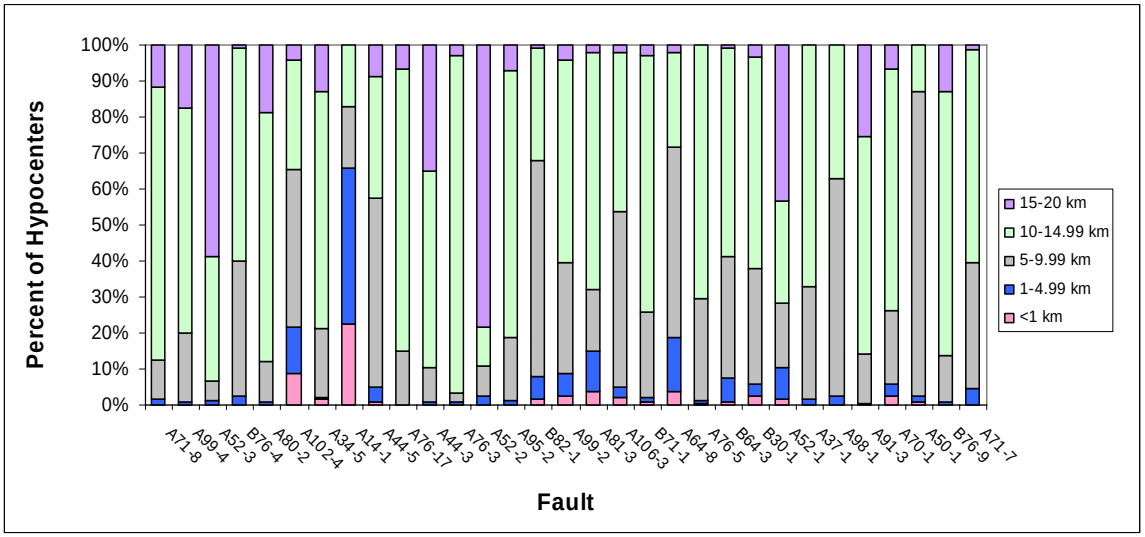

(d)

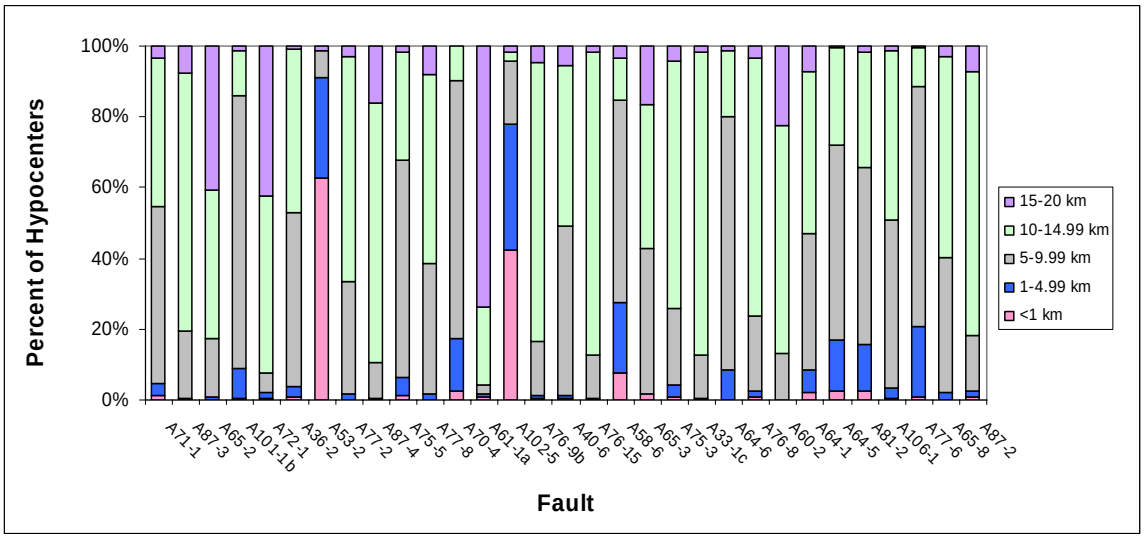

Figure 35. Stacked histograms of the percentage of the hypocenters associated with each fault, by depth category. Histograms are presented in order of increasing fault length, beginning with B60-1 in (a) having a total length of 6,964.1 m and ending with A87-2 in (d) having a total length of 107,204.8 m. Hypocenters associated with statistical outliers of distance are omitted, as are those linked to faults having fewer than 50 attributed hypocenters.

Table B-3 (Appendix B) contains counts and corresponding percentages of hypocenters associated with each fault within 13 earthquake magnitude categories (original magnitudes provided by NUMO). Magnitude is either missing or negative for 10,919 (11.6%) hypocenters, and negative values are not considered further. Figure 36 contains a percentage histogram of the number of hypocenters in each magnitude category, along with a cumulative percentage curve. The modal magnitude class is 1.01 – 1.5, which represents approximately 24% of the hypocenters. About 43.9% fall in the 1.01 – 2 range, and about 92% of the magnitudes are less than 2.5.

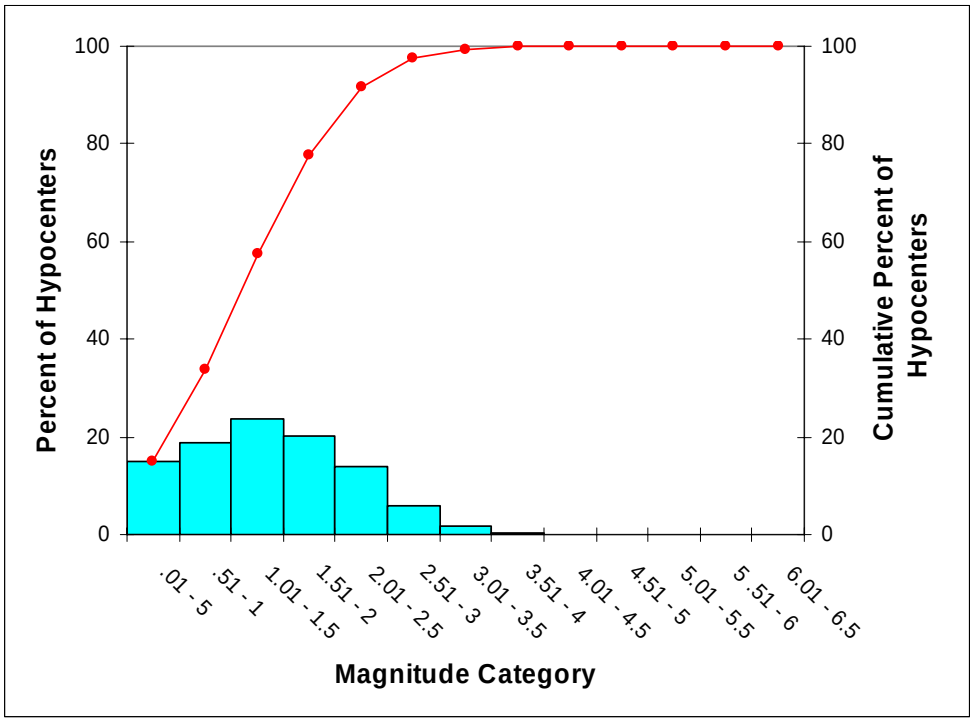

Figure 36. Histogram of the percentage of all hypocenters (all Japan), by magnitude category, with corresponding cumulative percentage histogram. Hypocenters associated with statistical outliers of distance are omitted, as are those linked to faults having fewer than 50 attributed hypocenters.

Many faults have attributed hypocenters at multiple magnitude values. Figure 37 (a-d) presents stacked histograms of the percentages of hypocenters within the various magnitude categories for each of the individual faults. As in Figure 35 (a-d), the histograms are presented in order of increasing fault length. Figure 37a contains the stacked histograms associated with the first 32 faults, Figure 37b contains the stacked histograms associated with the next 32 faults, Figure 37c presents the stacked histograms associated with the next 31 faults, and Figure 37d presents the stacked histograms for the final 31 faults. The relatively high percentage of hypocenters within the 1.01 – 1.5 and 1.51 – 2 magnitude categories is apparent. In this data set (not counting the hypocenters with missing or negative magnitudes), fault length does not appear to be a significant factor in controlling earthquake magnitude.

(a)

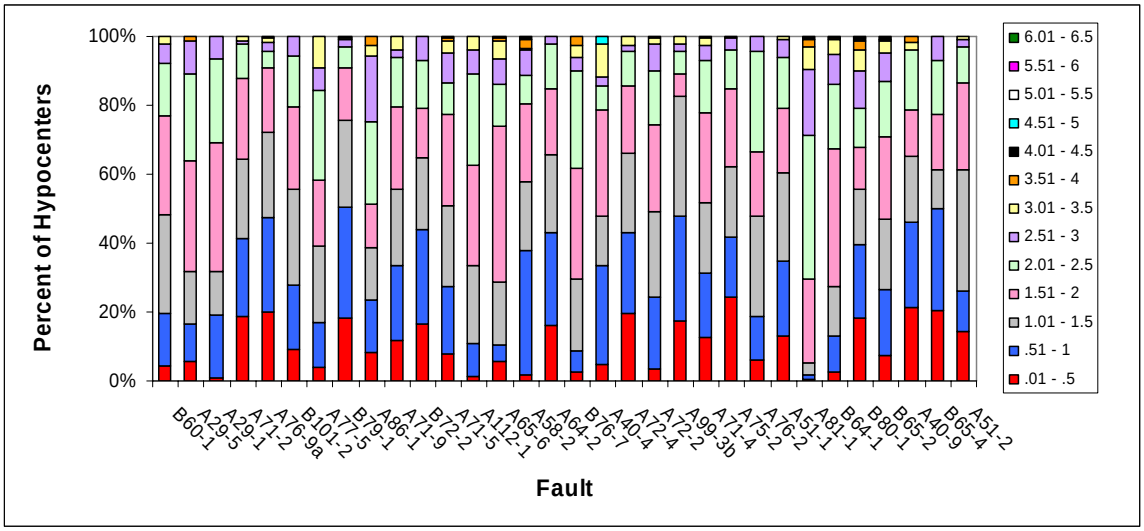
Percent of Hypocenters
100%
80%
60%
40%
20%
0%
B60-1
A29-5
A29-1
A71-2
A76-9a
B101-2
A77-5
B79-1
A86-1
A71-9
B72-2
A71-5
A112-1
A65-6
A58-2
A64-2
B76-7
A40-4
A72-4
A72-2
A99-3b
A71-4
A75-2
A76-2
A51-1
A81-1
B64-1
B80-1
B65-2
A40-9
B65-4
A51-2
Fault
6.01 - 6.5
5.51 - 6
5.01 - 5.5
4.51 - 5
4.01 - 4.5
3.51 - 4
3.01 - 3.5
2.51 - 3
2.01 - 2.5
1.51 - 2
1.01 - 1.5
.51 - 1
.01 - .5

(b)

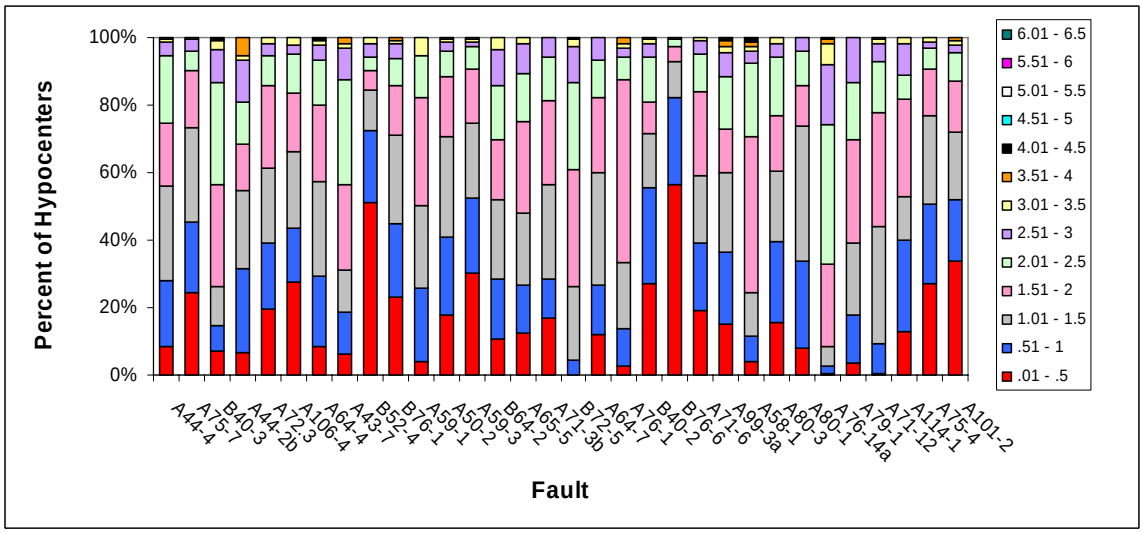
Percent of Hypocenters
100%
80%
60%
40%
20%
0%
A44-4
A75-7
B40-3
A44-2b
A72-3
A106-4
A64-4
A43-7
B52-4
B76-1
A59-1
A50-2
A59-3
B64-2
A65-5
A71-3b
B72-5
A64-7
A76-1
B40-2
B76-6
A71-6
A99-3a
A58-1
A80-3
A80-1
A76-14a
A79-1
A71-12
A114-1
A75-4
A101-2
Fault
6.01 - 6.5
5.51 - 6
5.01 - 5.5
4.51 - 5
4.01 - 4.5
3.51 - 4
3.01 - 3.5
2.51 - 3
2.01 - 2.5
1.51 - 2
1.01 - 1.5
.51 - 1
.01 - .5

(c)

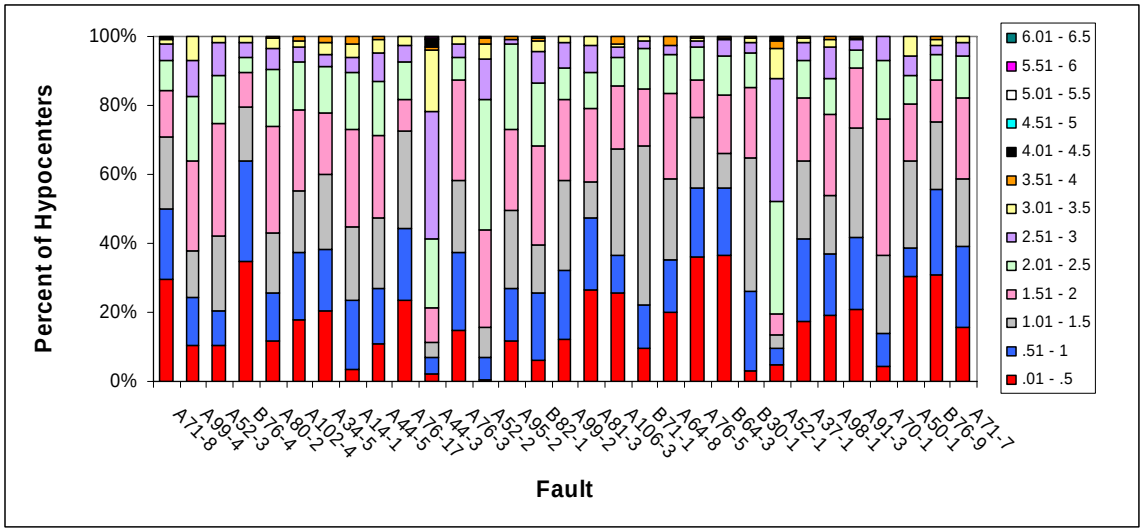

(d)

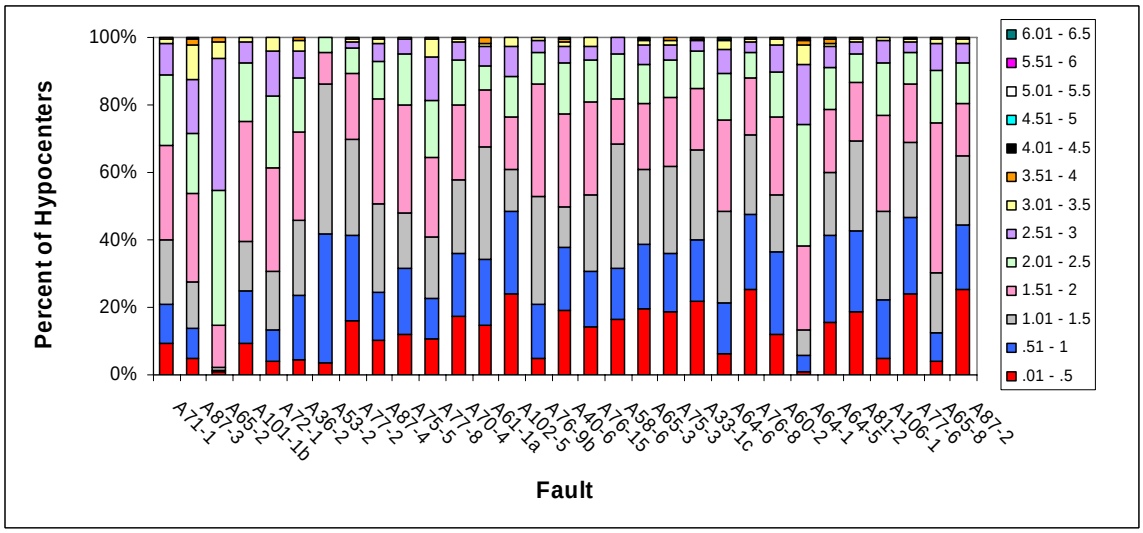

Figure 37. Stacked histograms of the percentage of the hypocenters associated with each fault, by magnitude category. Histograms are presented in order of increasing fault length, beginning with B60-1 in (a) having a total length of 6,964.1 m and ending with A87-2 in (d) having a total length of 107,204.8 m. Hypocenters associated with statistical outliers of distance are omitted, as are those linked to faults having fewer than 50 attributed hypocenters and those with missing or negative magnitudes.

Figure 38 consists of side-by-side comparative histograms of the number of hypocenters within magnitude categories by depth interval (hypocenters with missing or negative magnitudes are omitted). The figure again suggests that the majority of hypocenters are located about 5 – 15 km deep. Within the 5 – 9.99 km depth interval, the majority of hypocenters have associated earthquake magnitudes of .5 to 1.5; and within the 10 – 14.99 km depth interval, the majority of hypocenters have associated earthquake magnitude values in the range of 1.01 – 2. Somewhat different patterns regarding earthquake magnitude are present among the hypocenters in both the shallower and deeper depth intervals. Table B-4 (Appendix B) provides a full accounting of the numbers and percentages of hypocenters associated with each combination of the depth and magnitude categories.

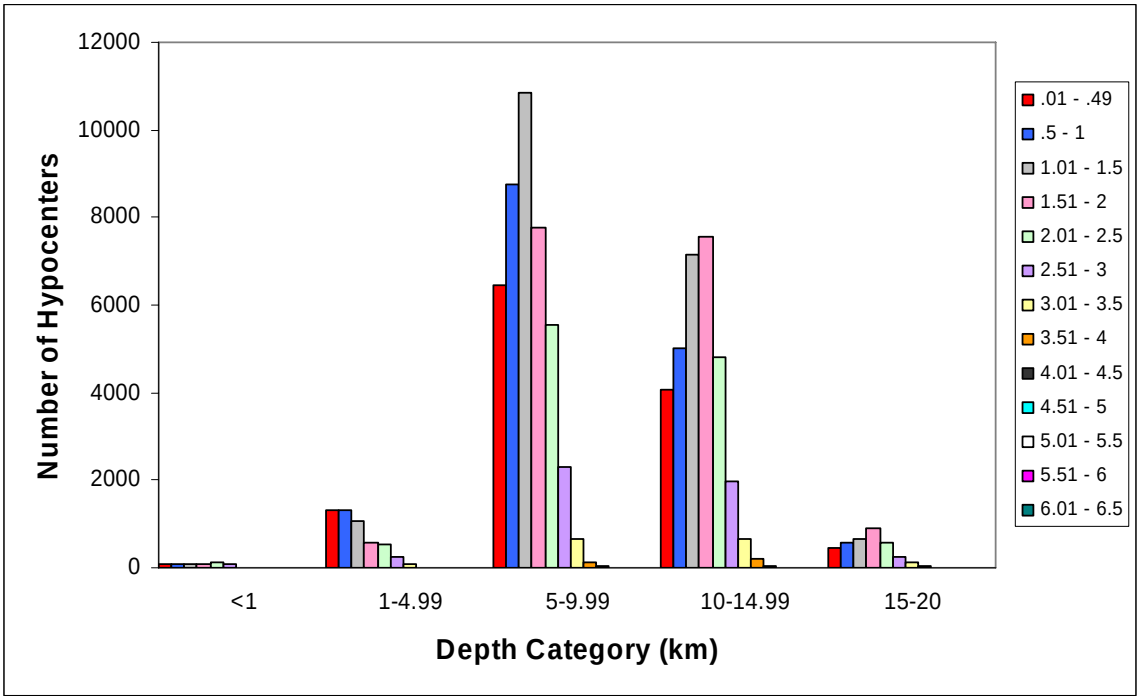

Figure 38. Side-by-side frequency histograms showing the number of hypocenters in magnitude categories within depth categories. Hypocenters associated with statistical outliers of distance are omitted, as are those linked to faults having fewer than 50 associated hypocenters and those with missing or negative magnitudes.

Fault Length Considerations

In order to investigate the relationship between fault length and process zone width, as estimated from the normal distance of hypocenters to fault planes, a total length must first be computed for each fault. As previously described, GIS processing yields the length of each fault trace polyline segment. These segments can then be summed to obtain the total length of each fault. However, as a result of applying the various filters to the hypocenters, some segments of the faults are left without any associated hypocenters. A question arises, then, as to whether such segments should be included in the calculation of total length for purposes of investigating the relationship between total length and hypocenter distance. This situation is illustrated in Figure 39. Also note that, in the case of *en echelon* fault segments, the calculation of total fault length is compounded by adding the lengths of overlapping fragments. Consequently, for purposes of the statistical analysis, total fault length is calculated by summing the lengths of the individual fault segments in two ways: (1) Type I, in which fault segments having no associated hypocenters are omitted; and (2) Type II, in which all fault segments are included. No correction for overlapping fault segments is made in either calculation. Type III length is the "fault trace length" as defined in the fault database.

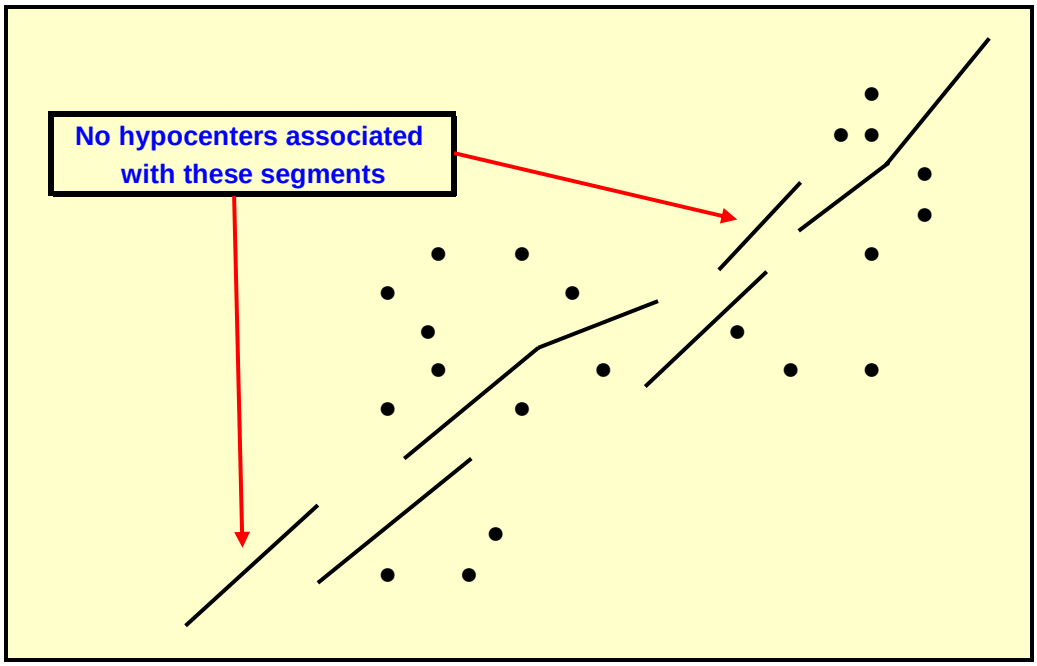

Figure 39. Illustration of the situation in which some fault segments have no associated hypocenters after hypocenter filtering.

Relationship of Fault Length to Number of Hypocenters

Figure 40 (a-d) consists of bar charts of the number of hypocenters associated with each fault in the statistical database. The bars are presented in order of increasing fault length. The figures suggest there is no statistical relationship between the length of a fault and the number of hypocenters that are attributed to it. This indicates that seismic activity is not uniformly distributed across the study area. In particular, there are a few faults that have many more hypocenters than the others, indicating regions of increased seismicity along those faults.

This situation is further depicted in Figure 41, which is a scatter diagram of Type I fault length and the number of hypocenters attributed to each fault. In this figure there are six faults (A64-4, A77-6, A106-1, A106-4, B64-2, and B79-1) with more than 4,000 attributed hypocenters. However, inspection of the associated percentage distributions of hypocenter distance (see Appendix C) suggests that these faults are really no more different than any of the others, and so there is no need to exclude them from further analysis.

(a)

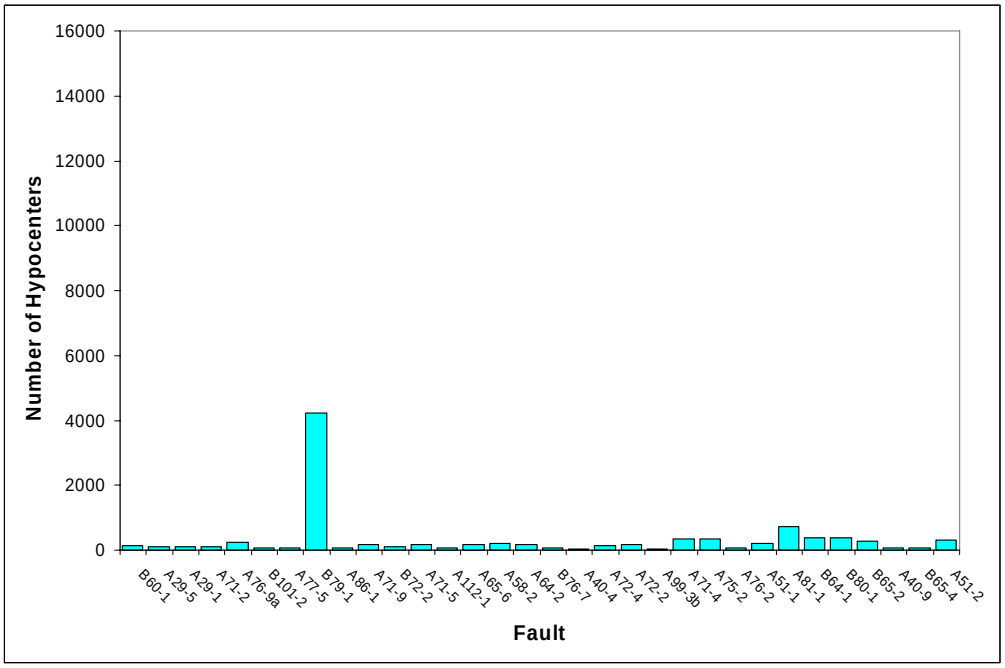
Number of Hypocenters
16000
14000
12000
10000
8000
6000
4000
2000
0
B60-1
A29-5
A29-1
A71-2
A76-9a
B101-2
A72-5
B79-1
A86-1
A71-9
B72-2
A71-5
A112-1
A65-6
A58-2
A64-2
B76-7
A40-4
A72-4
A72-2
A99-3b
A71-4
A75-2
A76-2
A51-1
A81-1
B64-1
B80-1
B65-2
A40-9
B65-4
A51-2
Fault

(b)

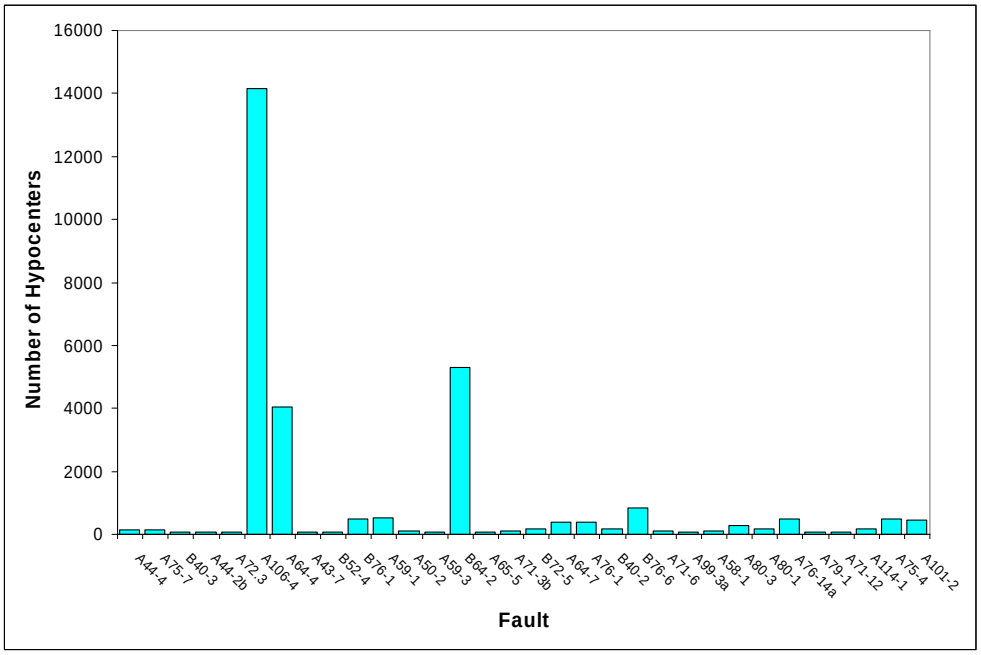
Number of Hypocenters
16000
14000
12000
10000
8000
6000
4000
2000
0
A44-4
A75-7
B40-3
A44-2b
A72-3
A106-4
A64-4
A43-7
B52-4
B76-1
A59-1
A50-2
A59-3
B64-2
A65-5
A71-3b
B72-5
A64-7
A76-1
B40-2
B76-6
A71-6
A99-3a
A58-1
A80-3
A80-1
A76-14a
A79-1
A71-12
A114-1
A75-4
A101-2
Fault

(c)

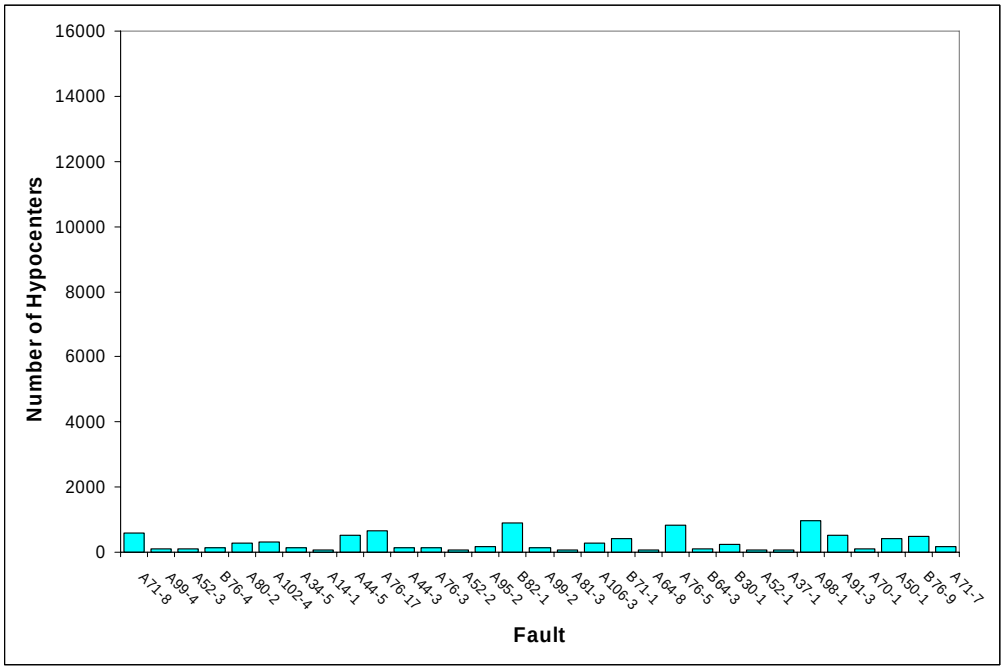

(d)

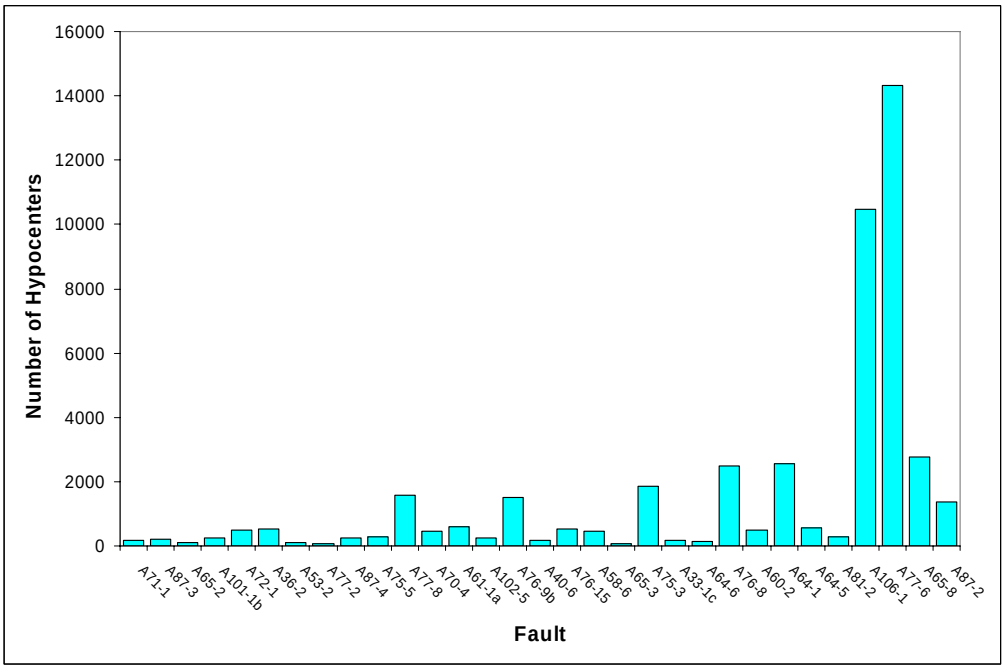

Figure 40. Bar chart of the number of hypocenters attributed to each of the 68 faults. The bars are presented in order of increasing fault length (Type I), beginning with B60-1 in (a) having a total length of 6,964.1 m and ending with A87-2 in (d) having a total length of 107,204.8 m. Hypocenters associated with statistical outliers of distance are omitted, as are those linked to faults having fewer than 50 associated hypocenters.

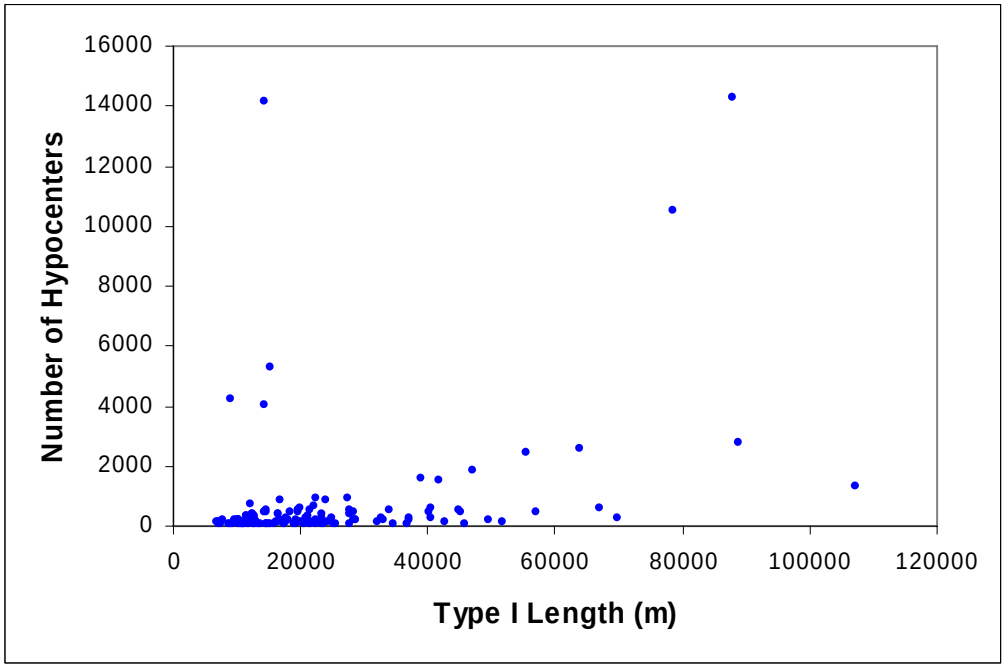

Figure 41. Relationship of Type I fault length (m) to number of attributed hypocenters.

Relationship of Fault Length to Depth of Hypocenters and Earthquake Magnitude

As indicated above, Figures 35 (a-d) and 37 (a-d), respectively, suggest there is no a statistical relationship or trend in this data set between fault length and hypocenter depth or between fault length and earthquake magnitude. In other words, the length of a fault does not appear to have a specific impact on the distribution of earthquakes associated with the fault originating at different depths and occurring at different magnitudes.

This observation is also corroborated in Figures 42 and 43. Figure 42 is a scatter diagram of fault length and the median depth of the hypocenters attributed to faults. The graph shows there is little to no correlation (r=-.14) between fault length and median hypocenter depth. Similarly, Figure 43 is a scatter diagram of fault length and the median earthquake magnitude of the hypocenters attributed to faults. This graph shows there is little to no correlation (r=-.03) between fault length and median earthquake magnitude.

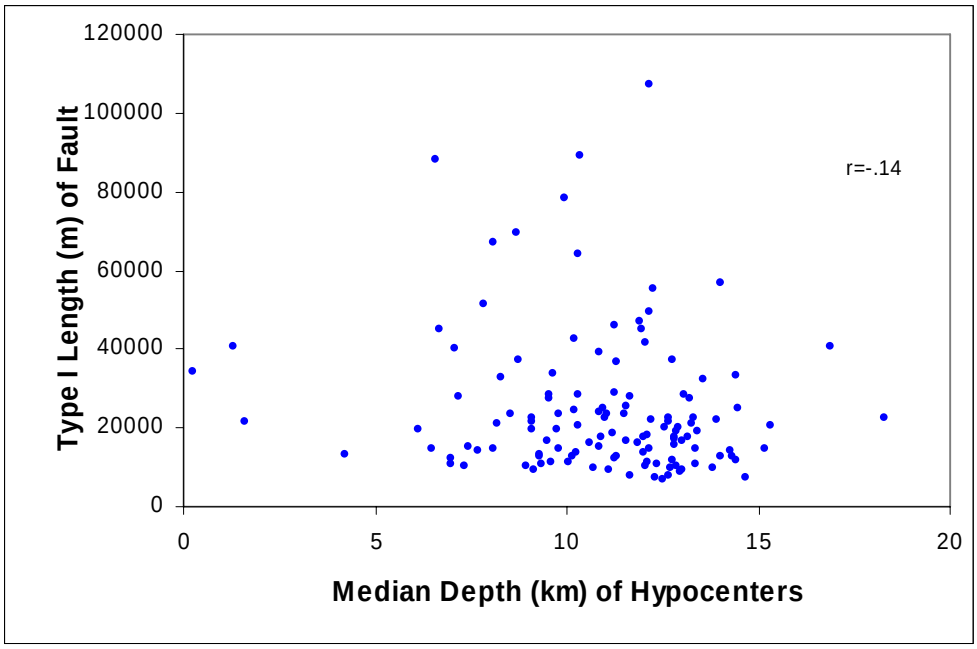

Figure 42. Relationship of fault length (Type I) to median depth (km) of hypocenters attributed to faults.

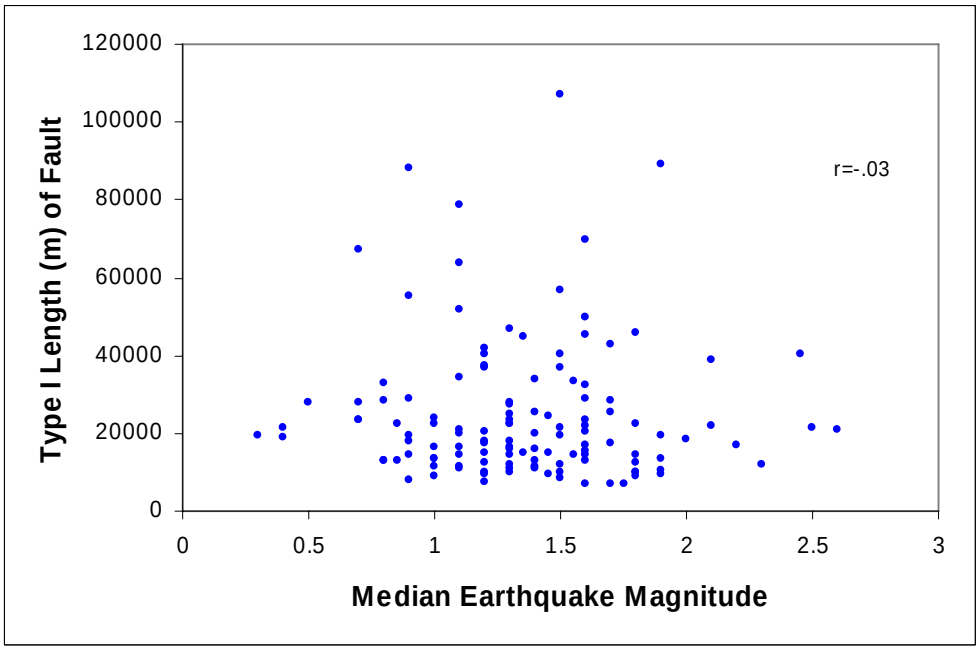

Figure 43. Relationship of fault length (Type I) to median earthquake magnitude associated with the hypocenters attributed to the faults. Missing or negative magnitudes are omitted in the median calculation.

Relationship of Hypocenter Distance to Hypocenter Depth and Earthquake Magnitude

As in the case of fault length, it is instructive to consider the relationship between hypocenter to fault normal distance, and hypocenter depth, as well as the relationship between hypocenter distance and earthquake magnitude. Figure 44 presents box plots of hypocenter distance for each of the five depth categories. In this figure, distances associated with all hypocenters in the statistical database are considered without regard to the faults to which they are attributed. The figure suggests that the range of values of hypocenter distance is essentially equivalent for all five depth categories. For the 1-4.99 km and 5-9.99 km depth categories, the distribution of hypocenter distances is fairly symmetric. On the other hand, for the shallowest depth category (<1 m) and the two deepest depth categories, the distribution of hypocenter distance is somewhat skewed towards higher values. The median distance for the1-4.99 km and 5-9.99 km categories is also higher than for the other three depth categories, suggesting that, as a general rule, hypocenters at the middle depths are found further from the faults to which they are attributed than their shallower or deeper counterparts.

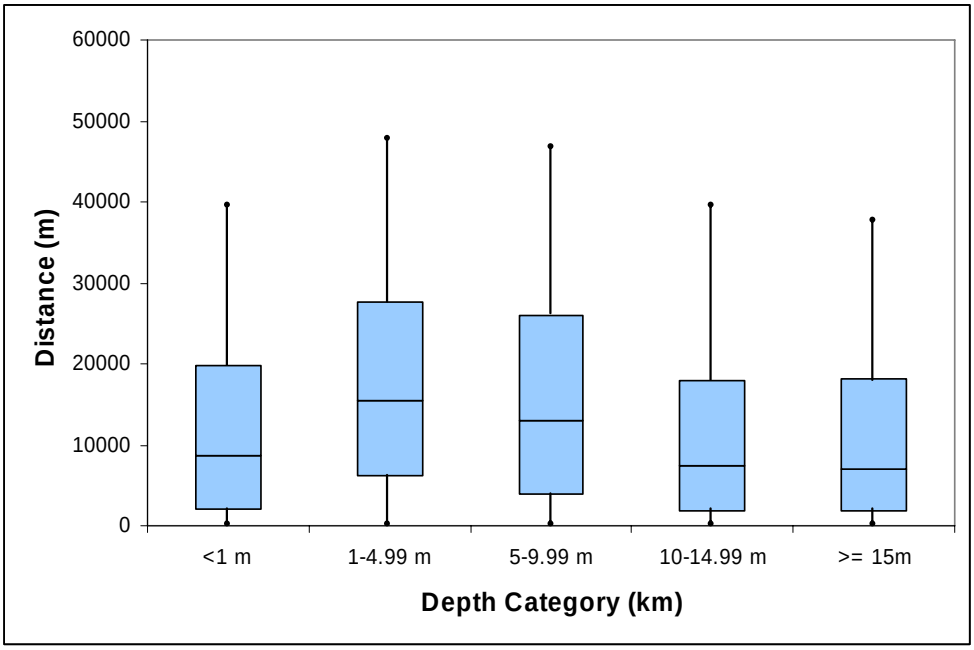

Figure 44. Box plots of normal distance from hypocenters to fault planes, by depth category, after one pass of eliminating distance outliers. Hypocenters attributed to faults having fewer than 50 associated hypocenters are also omitted.

Figure 45 presents box plots of hypocenter distance for each of the 13 earthquake magnitude categories. Again, in this figure, distances associated with all hypocenters in the statistical database are considered without regard to the faults to which they are attributed. Except for the three highest magnitude categories, the figure suggests that the range of values of hypocenter

distance is essentially equivalent and that the distributions are somewhat skewed toward higher values. Note that there are very few observations is each of the four magnitude categories above 4.5 (30 observations in the 4.51-5 category, six in the 5.01-5.5 category, six in the 5.51-6 category, and one in the 6.01-6.5 category). On the other hand, as the magnitude category increases from 1.01-1.5 to 4.01-4.5 (seven categories), the median value of distance decreases. The distribution of distance is very similar for the two categories associated with the lowest magnitudes (.01-.5 and .51-1). The medians are 6,749.2 and 6,488.4, respectively, and the ranges are 20,635.8 and 20,678.5, respectively. Together, these two low-magnitude categories contain about 34% of all the observations (13.1% for the .01-.5 category, and 16.7% for the .51-1 category), and they may represent background seismicity. For the three largest magnitude categories, the distribution of hypocenter distance is much more inconsistent. The faults to which these hypocenters are attributed have lengths (Type I) ranging from about 9,200 m to about 88,900 m, so fault length does not appear to be an additional causal factor.

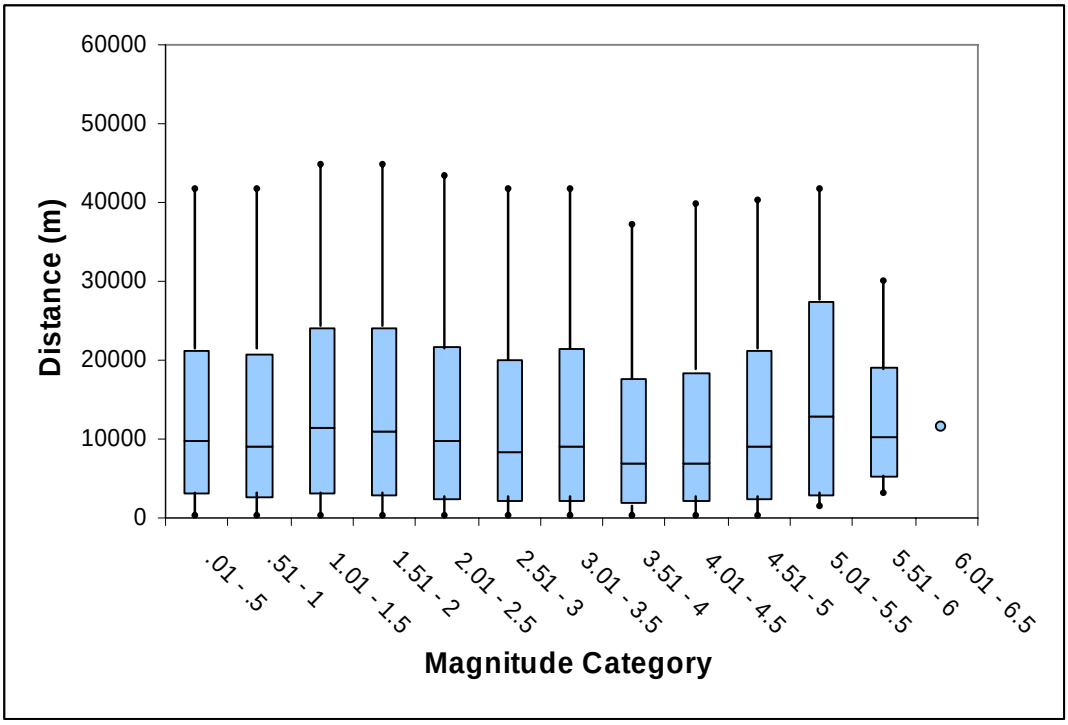

Figure 45. Box plots of normal distance from hypocenters to fault planes, by magnitude category, after one pass of eliminating distance outliers. Hypocenters attributed to faults having fewer than 50 associated hypocenters are also omitted.

Figures 46 (a,b) – 48(a,b) provide additional information about the relationship between hypocenter depth, earthquake magnitude, and the distance between hypocenters and the faults to which they are attributed. Figure 46a is a three-dimensional scatter diagram for Fault A71-9 showing the simultaneous relationships among these three quantities (n=168). Figure 46b is a corresponding two-dimensional matrix scatter diagram for all pairs of relationships among the three quantities. For this fault, which has a symmetric percentage distribution of signed

hypocenter distances centered on zero (see Appendix C), the correlation between depth and magnitude is .102, the correlation between depth and distance is .01, and the correlation between magnitude and distance is .035. All of these correlations suggest a lack of relationship between the three quantities. Figures 47a and 47b are similar plots for Fault A29-5 (n=100). For this fault, whose percentage distribution of signed hypocenter distances is skewed left, the correlation between depth and magnitude is .1, the correlation between depth and distance is -.295, and the correlation between magnitude and distance is .054. Again, the correlations suggest little of no correlation among the three quantities. Finally, Figures 48a and 48b show similar relationships for Fault 58-2 (n=219), whose percentage distribution of signed hypocenter distances is bimodal. The correlation between depth and magnitude is -.095, the correlation between depth and distance is -.433, and the correlation between magnitude and distance is .179.

(a)

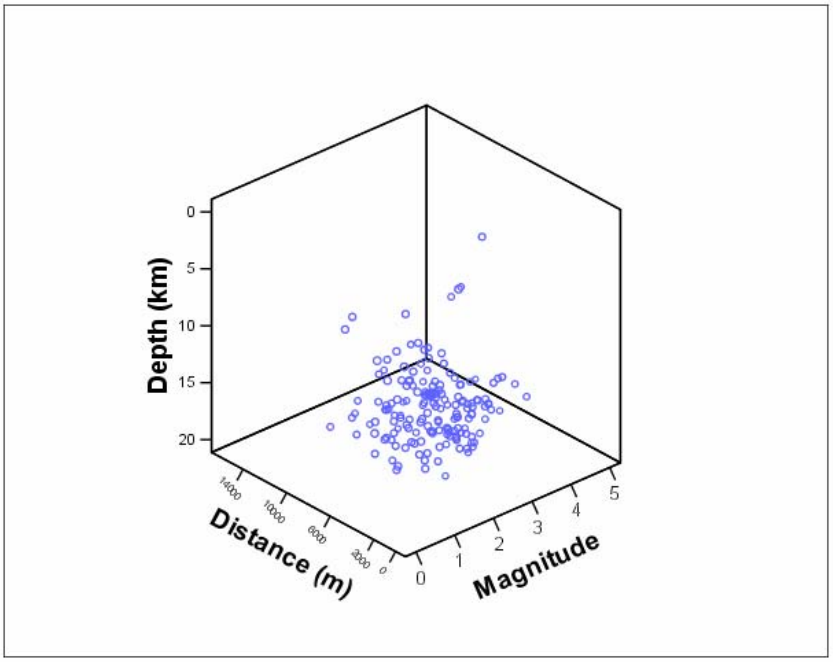

(b)

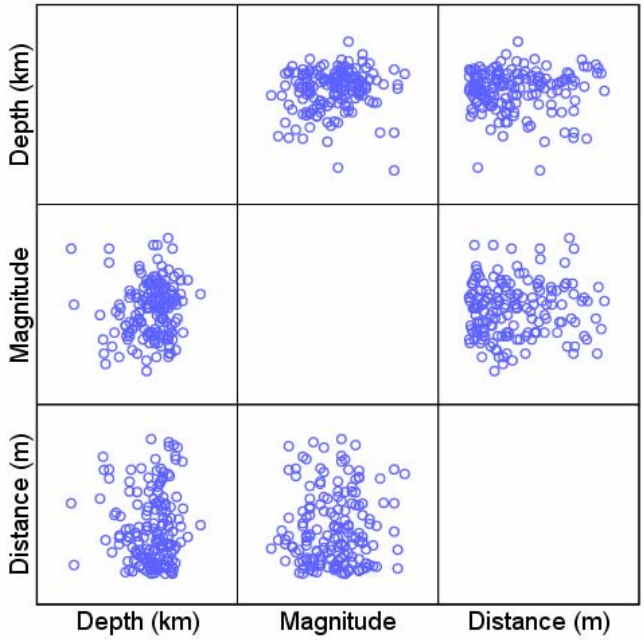

Figure 46. The relationship between hypocenter depth, earthquake magnitude, and distance to the fault plane for A71-9 (n=168): (a) three-dimensional scatter diagram and (b) two-dimensional matrix scatter diagram. Where applicable, hypocenters are omitted for which magnitude is missing or negative.

(a)

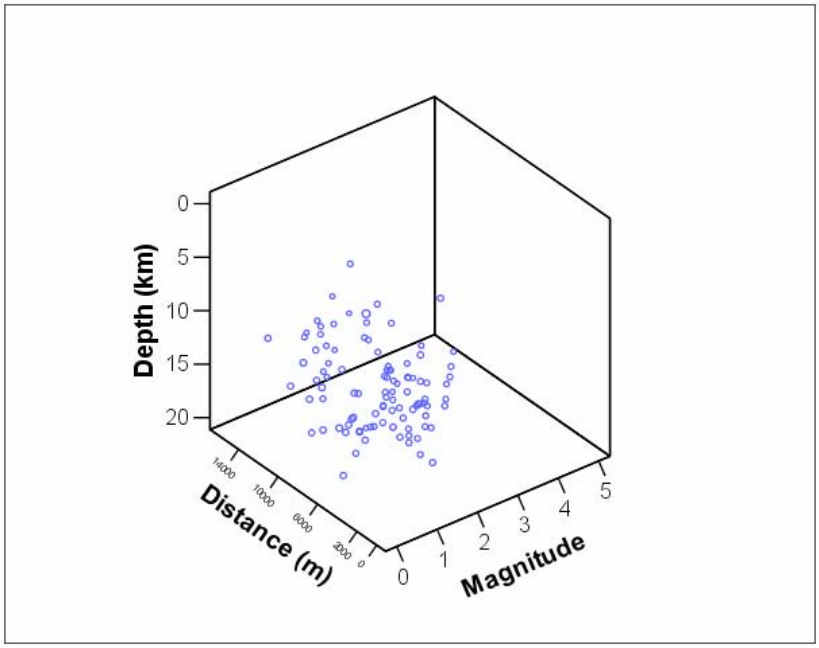

(b)

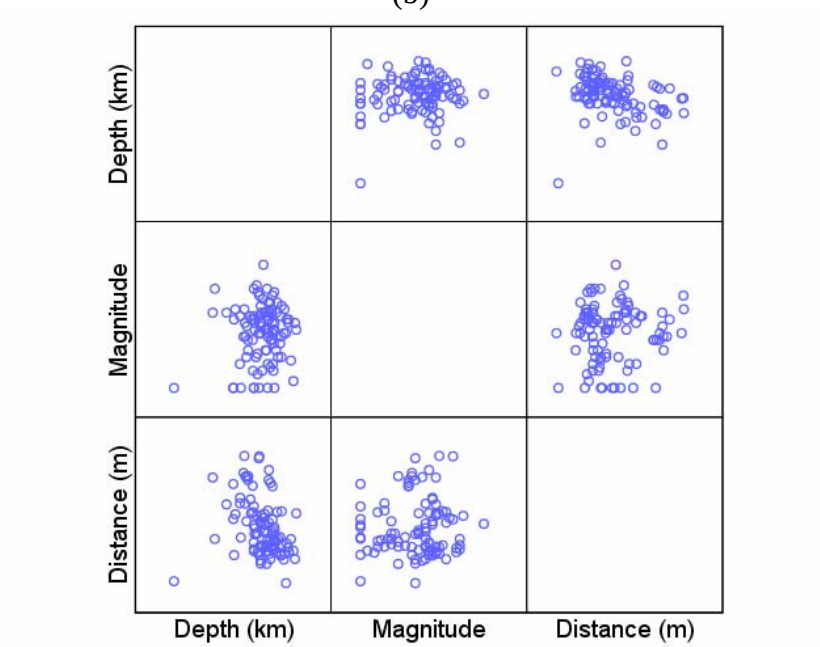

Figure 47. The relationship between hypocenter depth, earthquake magnitude, and distance to the fault plane for A29-5 (n=100): (a) three-dimensional scatter diagram and (b) two-dimensional matrix scatter diagram. Where applicable, hypocenters are omitted for which magnitude is missing or negative.

(a)

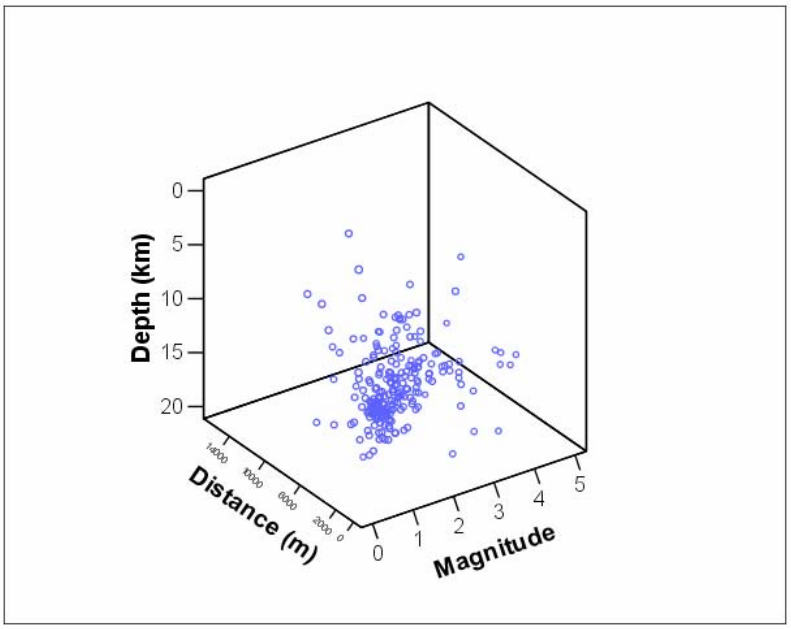

(b)

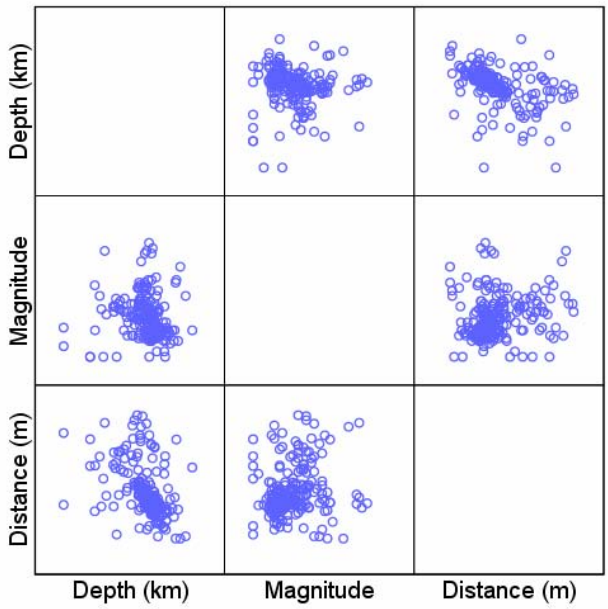

Figure 48. The relationship between hypocenter depth, earthquake magnitude, and distance to the fault plane for A58-2 (n=219): (a) three-dimensional scatter diagram and (b) two-dimensional matrix scatter diagram. Where applicable, hypocenters are omitted for which magnitude is missing or negative.

The relationships between hypocenter depth, earthquake magnitude, and hypocenter distance described above for Faults A71-9, A29-5, and A58-2 are representative of those observed for all the faults. Table B-5 in Appendix B reports the pairwise correlations for all faults, very few of which exceed .5. This further evidence suggests that there is no consistent relationship among these quantities that might have a carry-over effect on the relationship between hypocenter distance and fault length.

Estimating the Width of the Process Zone

In terms of the revised concept for analysis described above, hypocenter distance is used to define the width of the seismic process zone. Descriptive statistics, including the mean, median, Q_1, Q_3, and IQR of hypocenter distance, were computed for the hypocenters associated with each of the 126 faults in the statistical database. These values are contained in Table B-6 (Appendix B). Figure 49 presents a frequency histogram of mean hypocenter distance for the 126 faults, along with a cumulative percentage distribution curve. Under the assumption that an equal number of hypocenters is associated with each of the faults, the well-known Central Limit Theorem would suggest this distribution should be approximately Gaussian and that its mean should be approximate the true mean of the population of hypocenter distances. In reality, a different number of hypocenters are associated with each fault, and the distribution is clearly skewed to the right. The skewness may be due partly to disparity among the numbers of hypocenters associated with each fault, but is also partly due to the spatial arrangement of the hypocenters.

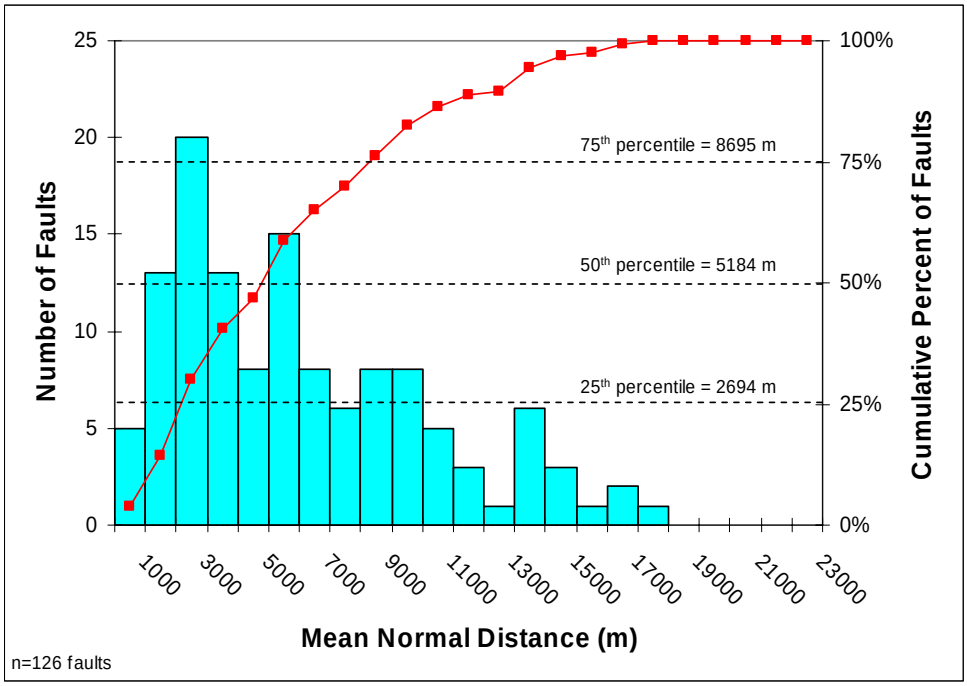

Figure 49. Frequency histogram and cumulative percentage histogram of mean normal distance of hypocenters to fault planes. Faults having fewer than 50 attributed hypocenters are omitted. Statistical outliers of hypocenter distance are omitted from the mean distance calculation.

The initial model of the spatial relationship of hypocenters to faults assumed that hypocenters, like fracture intensity, are uniformly located within an ellipse around the fault, as illustrated in Figure 50, and that hypocenter distance has an approximately Gaussian distribution around a mean corresponding to the center of the fault path or trajectory. Figure 33, along with Figures 29b, 30b, 31b, and 32b (which are representative of the empirical histograms associated with all 126 faults), suggests this is not the case. In fact, as noted above, the distributions associated with many of the 126 faults are off-center relative to the corresponding faults, and they tend to remain somewhat skewed, even after applying the single pass outlier screen (see the two example cases provided in Figure 51. There are multiple possible explanations for this situation, including (1) incomplete information on fault dip (discussed earlier), (2) the true attribution of some hypocenters to faults that are still unknown or unmapped, and (3) preferential strain release and seismicity in the hanging wall or foot wall of the fault.

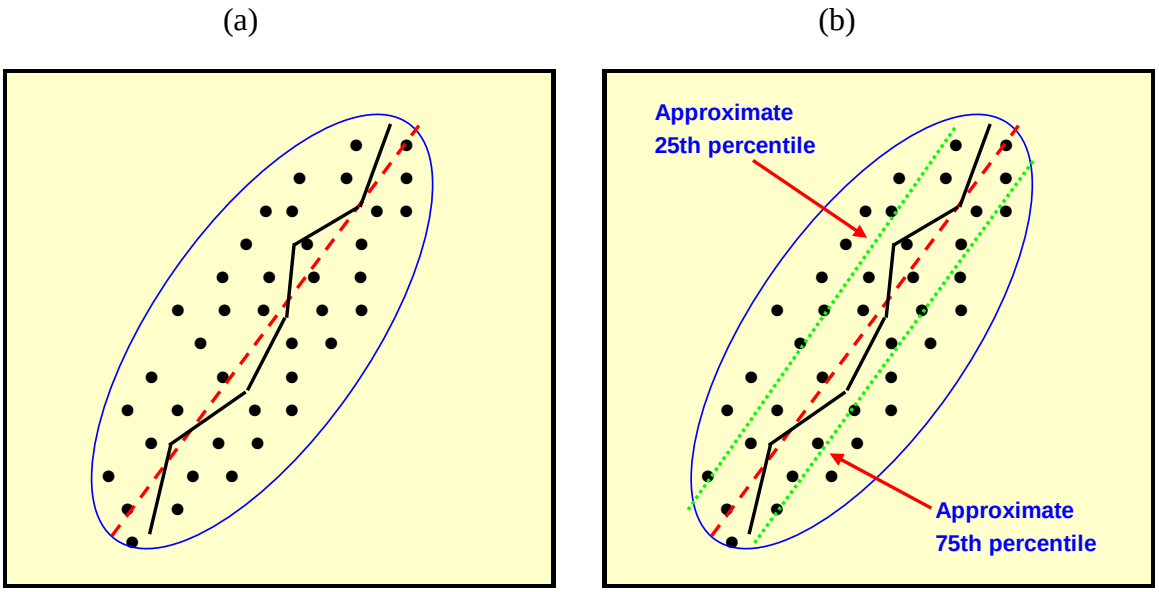

Figure 50. Illustration of (a) the initial concept of the spatial distribution of hypocenters around a fault, and (b) how the IQR would be used to estimate the width of the process zone. The lines in (b) indicating the locations of the spatial 25th and 75th percentiles are proxies for the boundaries of an ellipse around the fault that would encompass 50% of the hypocenters.

Under the initial model, the IQR would provide an appropriate measure of the width of the process zone associated with each fault, the IQR corresponding to the middle 50% of the hypocenter distances, with 25% lying on either side of the fault (Figure 50b). However, when the spatial distribution of hypocenters is off-center and the corresponding distribution of hypocenter distances is possibly skewed, as illustrated in Figure 52 (a,b), the IQR is no longer a valid measure of the width of the process zone. Algebraically adjusting the locations of the hypocenters to center them on the fault trace by subtracting the mean distance from all the individual distances is an undesirable remedy because it (1) effectively changes the physical locations of the hypocenters, (2) forces the adjusted distances associated with half the hypocenters attributed to each fault to become negative which, without further treatment, adversely impacts the statistical calculations, (3) is inconsistent in that, for some faults, the

adjustment would be too large or too small due to the variation in skewness of the distributions, and (4) is not geologically justifiable based on current knowledge of the data.

(a)

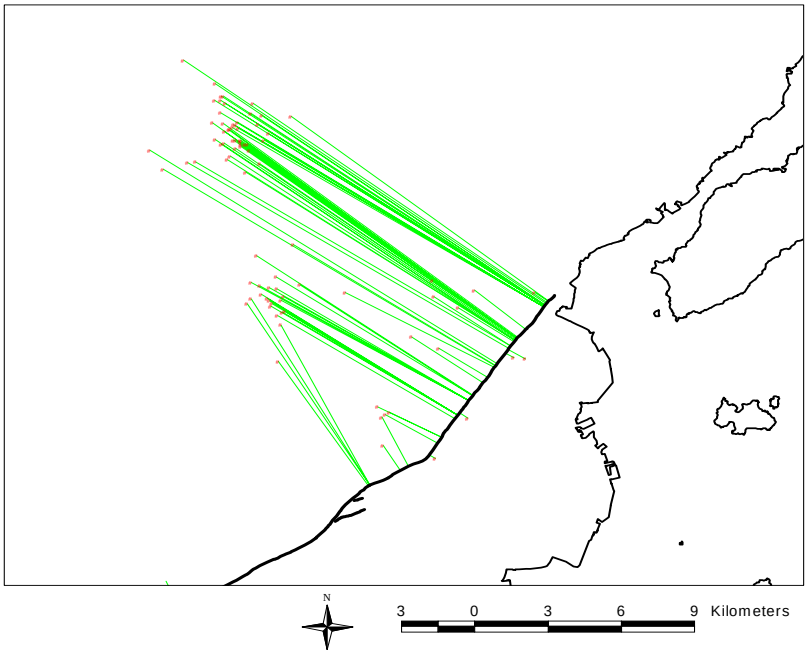

(b)

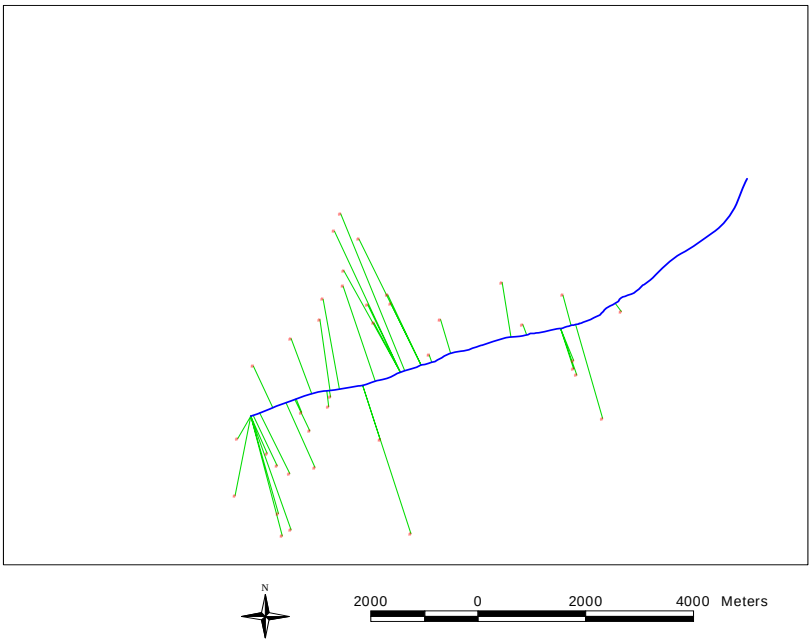

Figure 51. Spatial arrangement of hypocenters around two faults for which: A) all attributed hypocenters are on the same side, and B) attributed hypocenters are located on both sides, approximating spatial symmetry.

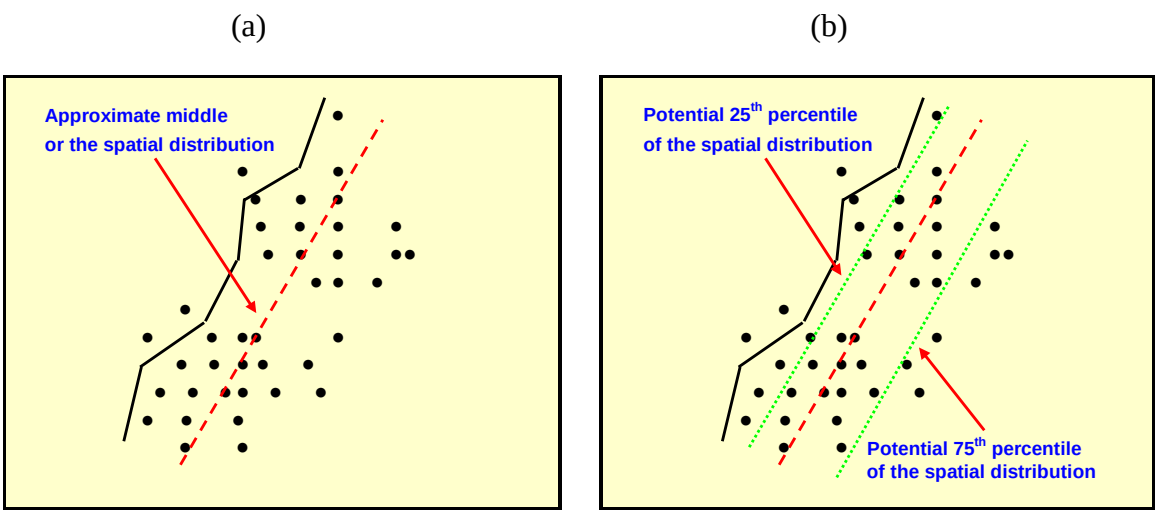

Figure 52. Illustration of (a) the actual spatial distribution of hypocenters relative to the nearest fault, and (b) potential spatial locations of the 25th and 75th percentiles. The distance between the line representing the 25th percentile and the line representing the middle of the distribution is not necessarily equal to the distance between the line representing the 75th percentile and the line representing the middle of the distribution.

Figure 52 suggests that, in this situation, twice the mean, median, or some other middle value associated with the distribution of hypocenter distances is a more appropriate measure of the width of the process zone. However, such a measure is likely to be conservative in the sense that it is too large, particularly with regard to the side of the fault that is least populated with hypocenters. An alternative, intermediate measure of the width of the process zone can be developed by considering hypocenters on each side of the fault separately and calculating the median hypocenter distance for each side and then summing the two medians. As noted above, the assignment of hypocenters to one or the other of the two sides of a fault is accomplished for essentially vertical faults using the technique described in the section titled "Distance Computations;" and for faults with known dip, the hanging wall and foot wall are identified as the two sides.

Similar to Figure 49, Figure 53 (a-c) presents histograms for the 126 faults of twice the mean of hypocenter distance, twice the median of hypocenter distance, and the sum of median hypocenter distance associated with the two sides of each fault, respectively, along with corresponding cumulative percentage distribution curves. Of these three graphs, the sum of the median normal distance associated with the two sides of each fault appears to be the most reasonable in terms of shape. The distribution of this quantity taken over the 126 faults also has the lowest variability of the three quantities, as indicated by the difference in the 75th and 25th percentiles (about 10,700 m), and the range of the distribution (maximum – minimum) is slightly larger than the range of the distribution for twice the mean, which has the smallest range (about 33,200 m). Further, the middle value, or 50th percentile (about 7,800 m), of the distribution of sum of the medians for the two sides of the faults is intermediate between the corresponding values for the distributions of twice the mean (about 10,300 m) and twice the median (about 9,500 m). Table 9 contains the descriptive statistics for all three distributions.

(a)

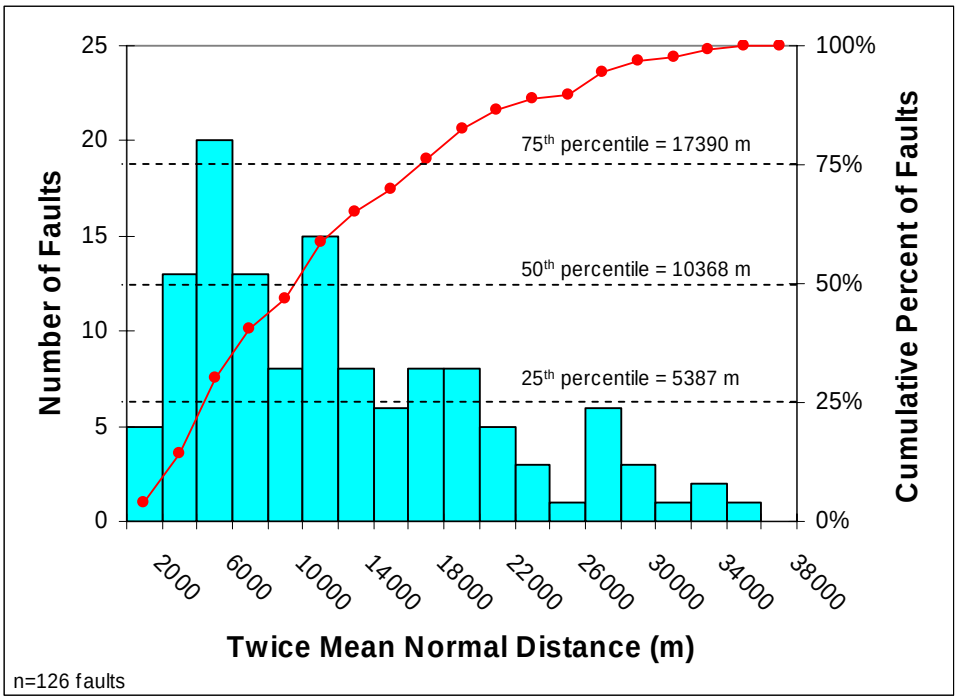
25
20
15
10
5
0
100%
75%
50%
25%
0%
75th percentile = 17390 m
50th percentile = 10368 m
25th percentile = 5387 m
Number of Faults
Cumulative Percent of Faults
2000
6000
10000
14000
18000
22000
26000
30000
34000
38000
Twice Mean Normal Distance (m)
n=126 faults

(b)

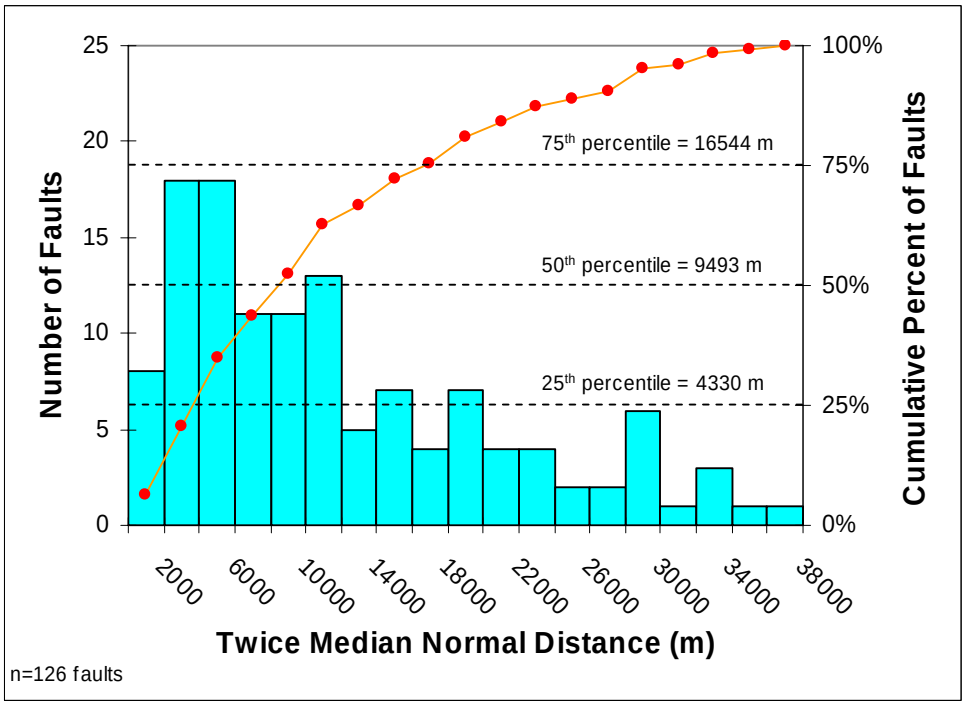
25
20
15
10
5
0
100%
75%
50%
25%
0%
75th percentile = 16544 m
50th percentile = 9493 m
25th percentile = 4330 m
Number of Faults
Cumulative Percent of Faults
2000
6000
10000
14000
18000
22000
26000
30000
34000
38000
Twice Median Normal Distance (m)
n=126 faults

(c)

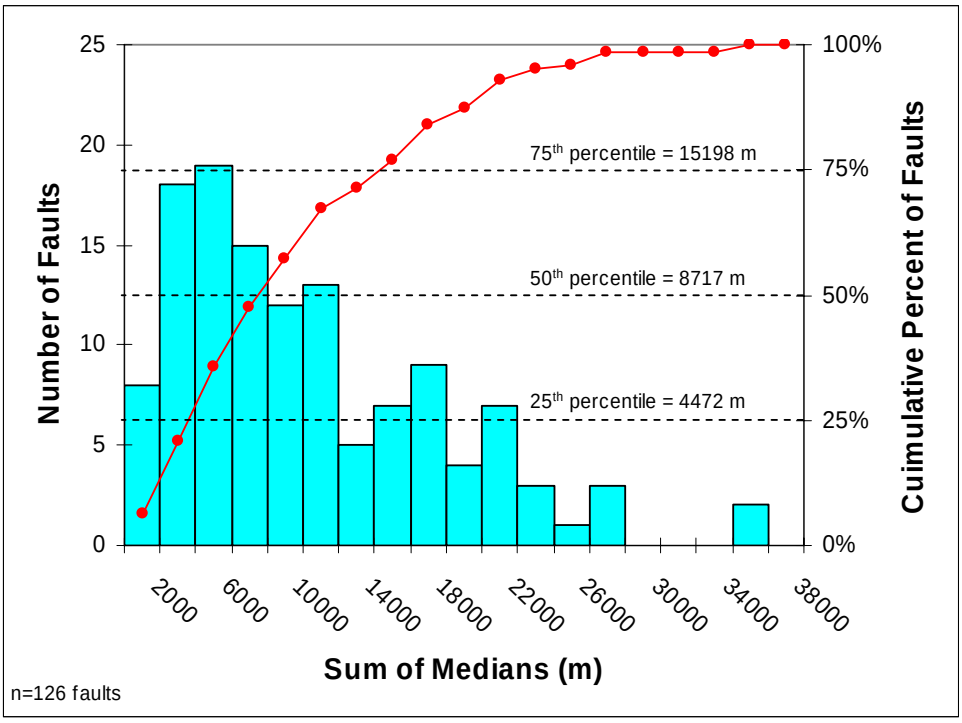

Figure 53. Histograms of three different measures of the width of the seismic process zone, with corresponding cumulative distribution curves: (a) twice the mean of all the hypocenter distances associated with a fault; (b) twice the median of all hypocenter distances associated with a fault; and (c) sum of the medians of the hypocenter distances associated with the two sides of a fault. Statistical outliers of hypocenter distance are omitted from the calculations, as are all hypocenters attributed to faults having fewer than 50 associated hypocenters.

Based on the foregoing assessment, the sum of the medians of hypocenter distance associated with the two different sides of faults is taken to be the most reasonable measure of the width of the seismic process zone for this study. This zone encapsulates the smallest 50% of hypocenter distances on either side of a fault, with values ranging from 820.40 m to 34,797.83 m. The mean and median of these values are 10,332.29 m and 8,717.37 m, respectively.

Table 9. Comparative Descriptive Statistics for the Distributions of Three Different Measures of the Width of the Seismic Process Zone.

Measure of Width of Seismic Process Zone	25th Percentile of Distribution	50th Percentile of Distribution	75th Percentile of Distribution	Difference in 25th and 75th Percentiles	Range of the Distribution	Mean* of the Distribution
Mean Normal Distance x 2	5,388	10,368	17,390	12,002	33,186	12,215
Median Normal Distance x 2	4,330	9,493	16,544	12,214	36,290	11,970
Sum of Median Normal Distance, Both Fault Sides	4,472	8,717	15,188	10,716	33,860	10,332

* The mean is an unreliable measure of the central value because of the skewness of the distributions.

Relationship between Fault Length and Width of the Seismic Process Zone

Finally, it is possible to examine the relationship between fault length and the width of the seismic process zone. Figure 54 (a,b) presents scatter diagrams of fault length (X) versus the sum of the medians of hypocenter distance for the two sides of the faults (Y), the preferred measure of the width of the seismic process zone) for Type I and Type II length, (see the discussion of fault length calculations in the "Fault Length Considerations" section). Figure 54 (c) is a similar scatter diagram using the original fault trace length (Type III) provided by NUMO in the fault database.

All three graphs suggest there is very little statistical relationship between the two quantities. In fact, the straight line fit to the data in each graph is essentially horizontal at the average value of the Y-axis with an R^2 value of no more than .02. The graphs also show that the maximum width of the process zone (sum of median distance, both sides of the fault) is roughly 35,000 meters and that for some of the shorter faults, this width is actually larger than the fault length. These findings are somewhat counterintuitive based on current understanding of the relationship between fault length (or cumulative fault displacement) and the width of the fault crushed zone.

(a)

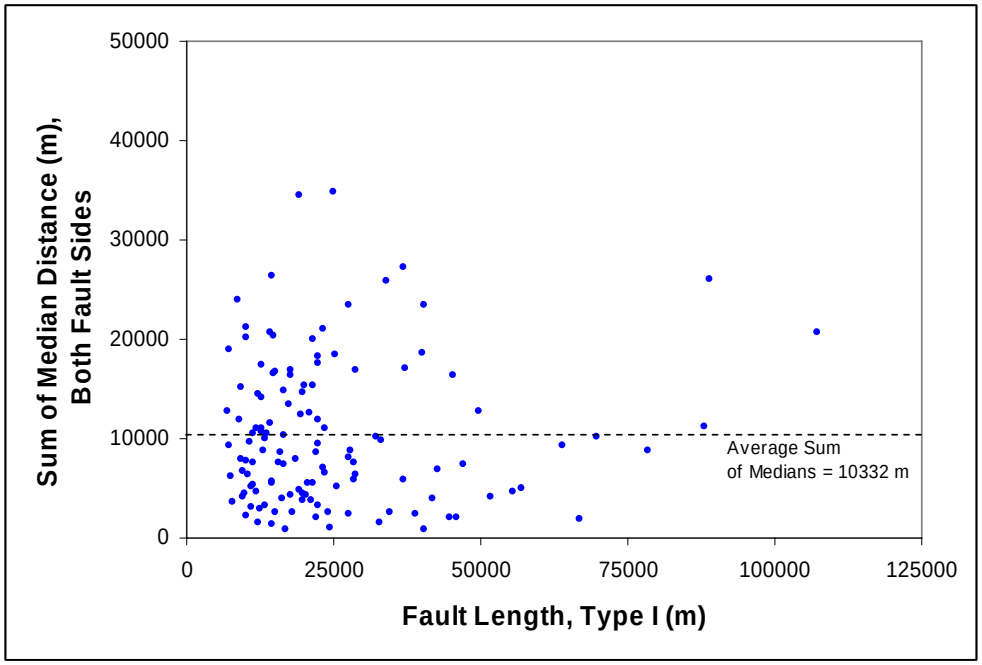
Sum of Median Distance (m), Both Fault Sides
50000
40000
30000
20000
10000
0
0
25000
50000
75000
100000
125000
Fault Length, Type I (m)
Average Sum of Medians = 10332 m

(b)

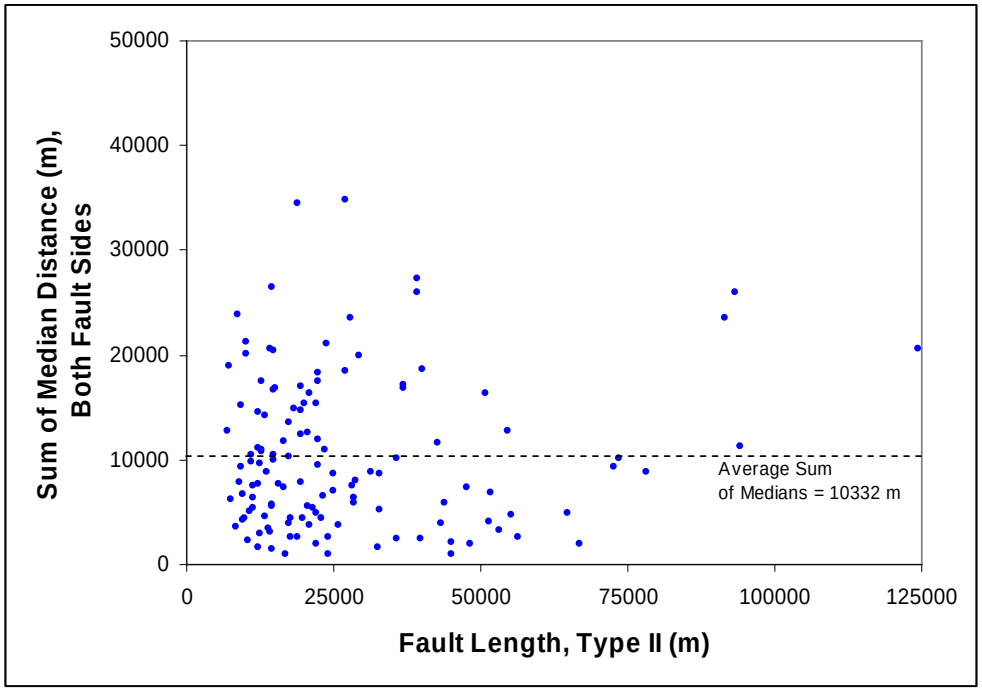
Sum of Median Distance (m), Both Fault Sides
50000
40000
30000
20000
10000
0
0
25000
50000
75000
100000
125000
Fault Length, Type II (m)
Average Sum of Medians = 10332 m

(c)

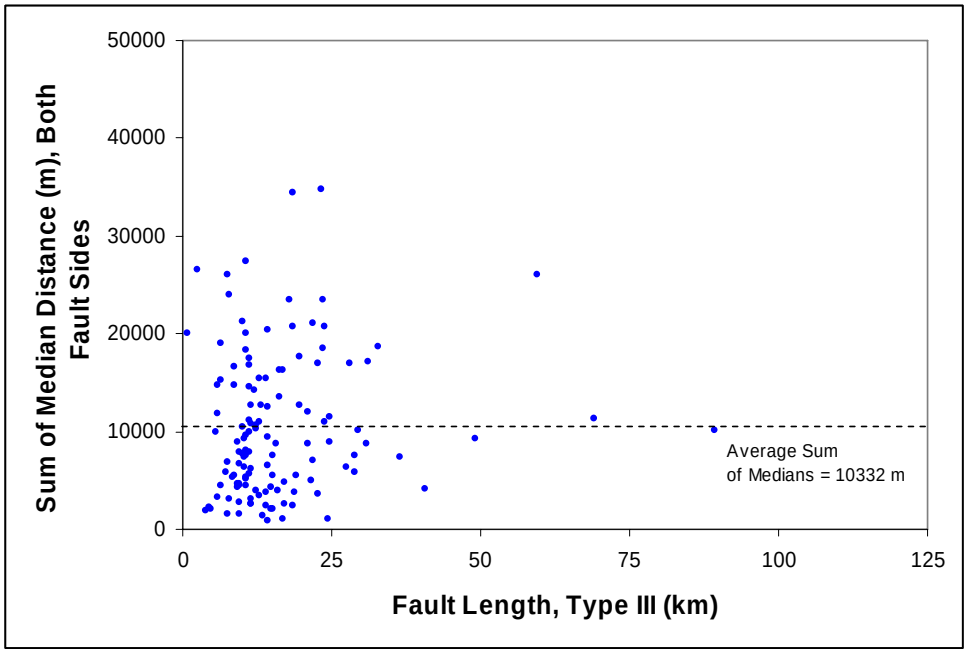

Figure 54. Scatter diagrams of fault length (X) versus the sum of the medians of hypocenter distance associated with the two sides of faults (Y): (a) Type I fault length; (b) Type II fault length; and (c) Type III fault length. Statistical outliers of hypocenter distance are omitted from the median distance calculation, as are all hypocenters attributed to faults having fewer than 50 associated hypocenters.

To insure that the lack of a relationship is not due to the quantity chosen to represent the width of the seismic process zone, Figure 55 (a,b,c) presents similar scatter diagrams substituting twice the usual median of all the hypocenters attributed to a fault as the width of the seismic process zone. Again, the statistical relationship between this quantity and fault length is weak, at best.

(a)

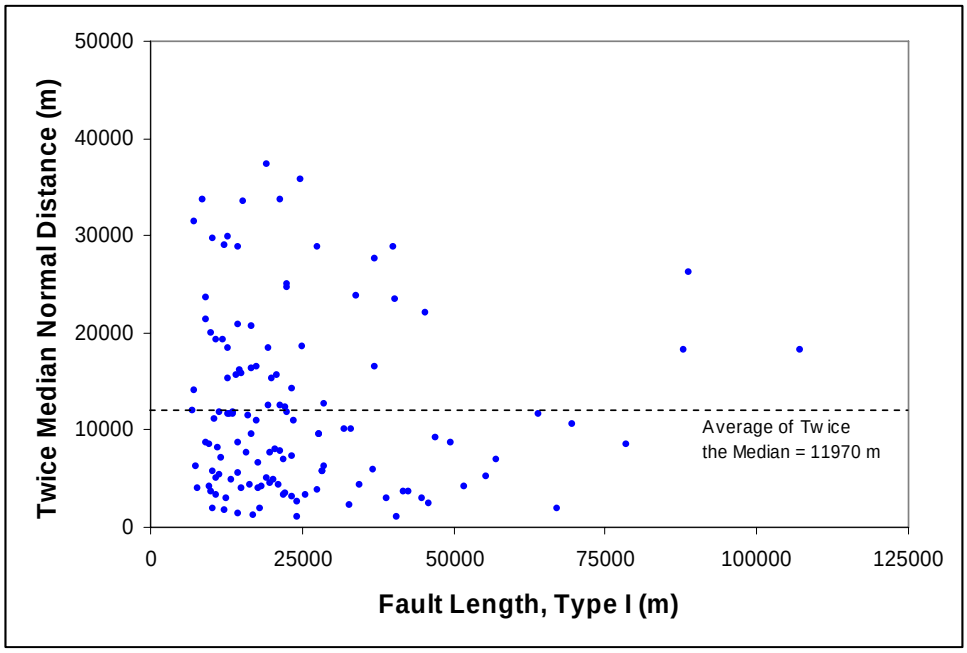
Twice Median Normal Distance (m)
50000
40000
30000
20000
10000
0
0
25000
50000
75000
100000
125000
Fault Length, Type I (m)
Average of Twice
the Median = 11970 m

(b)

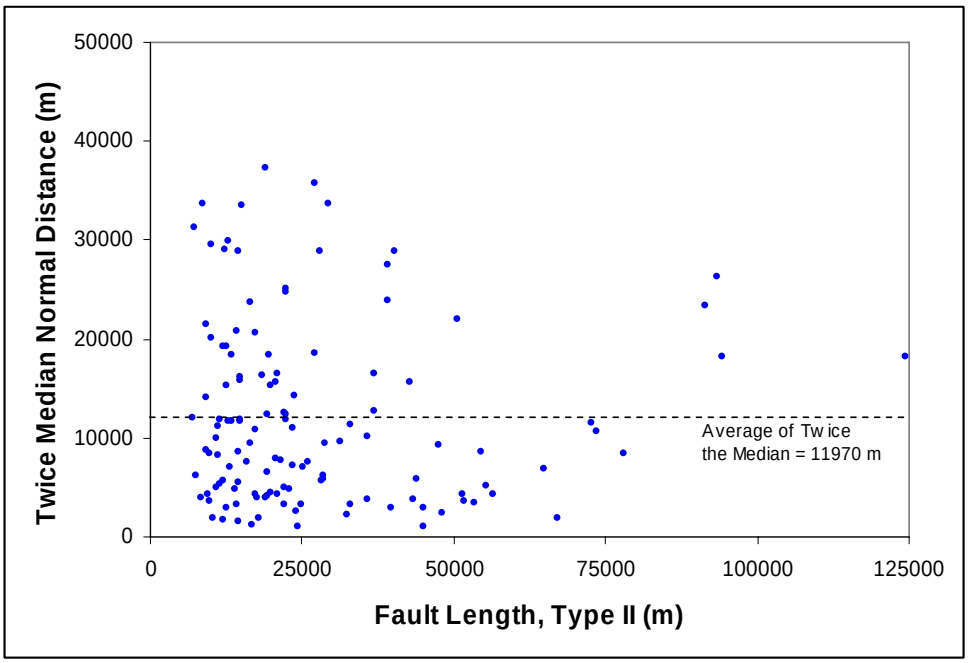
Twice Median Normal Distance (m)
50000
40000
30000
20000
10000
0
0
25000
50000
75000
100000
125000
Fault Length, Type II (m)
Average of Twice
the Median = 11970 m

(c)

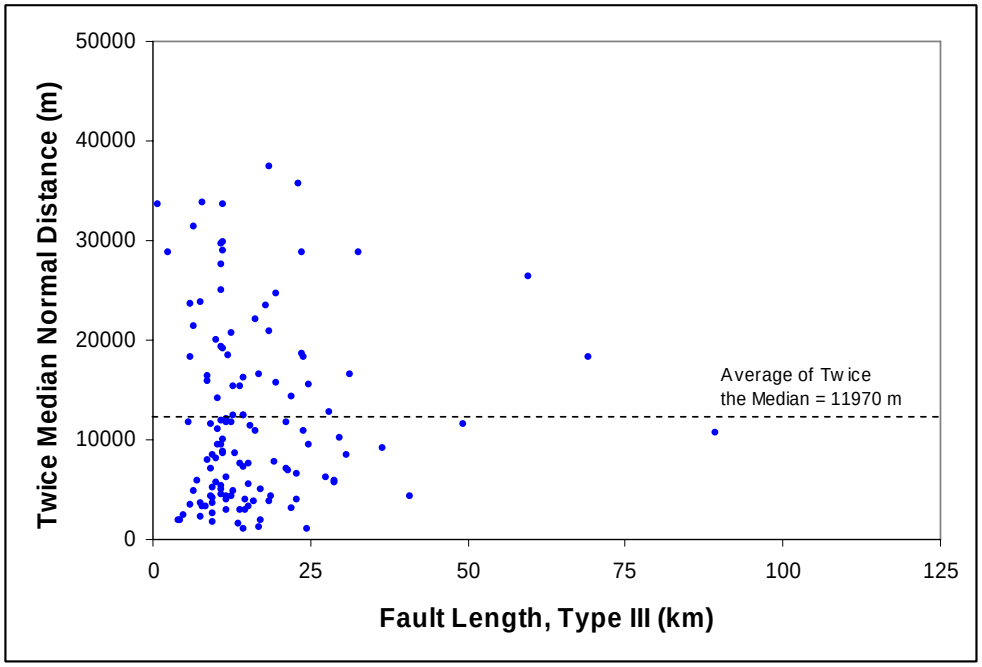

Figure 55. Scatter diagrams of fault length (X) versus twice the median of all hypocenter distances associated with a fault (Y): (a) Type I fault length; (b) Type II fault length; and (c) Type III fault length. Statistical outliers of hypocenter distance are omitted from the median distance calculation, as are all hypocenters attributed to faults having fewer than 50 associated hypocenters.

None of the statistical measures of the width of the seismic process zone considered here show promise in their relationship to fault length. Such measures simply may not be appropriate proxies for the width of the fault crush zone. Further, even though the data set is extensive, questions remain about data quality. From an alternative perspective, it may simply be the case that the width of the seismic process zone is relatively invariant to fault length.

Other Considerations

For completeness, it is instructive to consider whether the relationship between fault length and width of the seismic process zone can be improved by grouping similar faults together on the basis of various criteria. The data on fault characteristics is not complete for all faults, and so the extent to which such analysis can be pursued is somewhat limited.

One factor to consider is fault shape. Each fault in the database is characterized by one of five basic shapes (straight, curved, kinked, wavy, en echelon) or a combination of any two, and so groups of similarly shaped faults can be formed. Figure 56 (a-d) depicts the relationship between fault length (Type I) and width of the seismic process zone (as defined above) for four of the five basic shapes. Unfortunately, as the graphs suggest, consideration of fault shape does not lead to any apparent improvement in the relationship between fault length and width of the seismic process zone depicted in Figure 54 (a-c).

Grouping faults according to their designated fault systems is also a logical approach to consider. However, the linkage between individual faults and fault systems is also incomplete, which restricts its usefulness. Figure 57 (a,b) shows the histograms of signed hypocenter distance for two faults (A44-3, A44-4) in the same fault system: Aizu-bonchi-seisn. Note the considerable difference in the shapes of the two histograms, a common situation for faults identified with the same fault system. Hence, this approach would appear to not yield any potentially meaningful improvement in the relationship between fault length and width of the seismic process zone.

Geographic location is another obvious consideration; yet the connection between fault geography and fault geology is also not well established in the database, which precludes the use of geographic location as a fault grouping criteria. Grouping faults together on the basis of their geographic locations on a surface map would have limited value and might lead to incorrect conclusions.

On whole, the information on fault characteristics that is available in the database does not yield any additional explanations about the weak relationship between fault length and width of the seismic process zone depicted in Figure 54 (a-c). The most likely scenario is that, even though extensive, the database still does not contain all the information necessary, particularly with respect to faults, to establish a strong trend between these quantities.

(a)

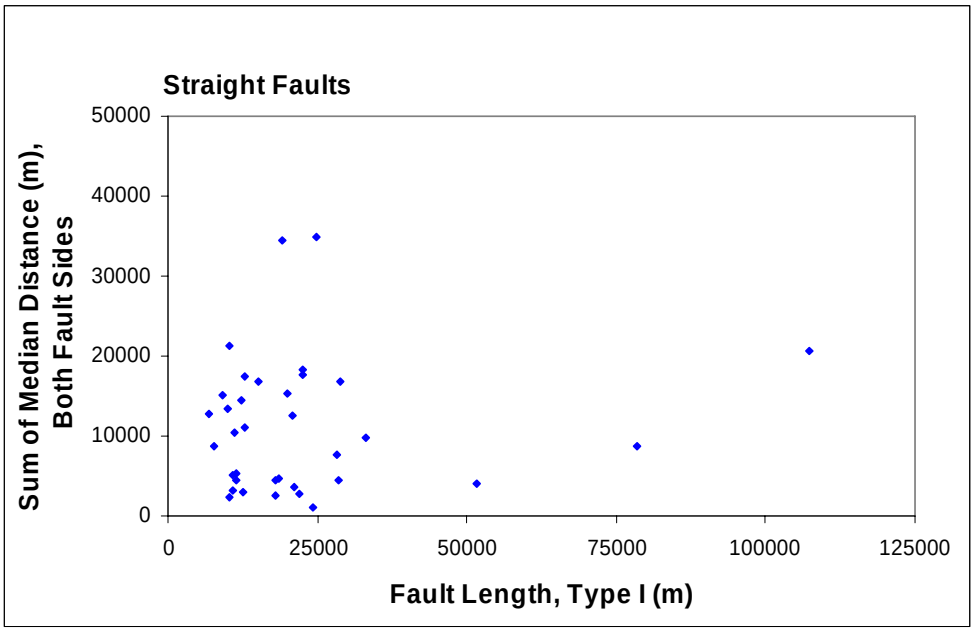
Straight Faults
Sum of Median Distance (m), Both Fault Sides
50000
40000
30000
20000
10000
0
0
25000
50000
75000
100000
125000
Fault Length, Type I (m)

(b)

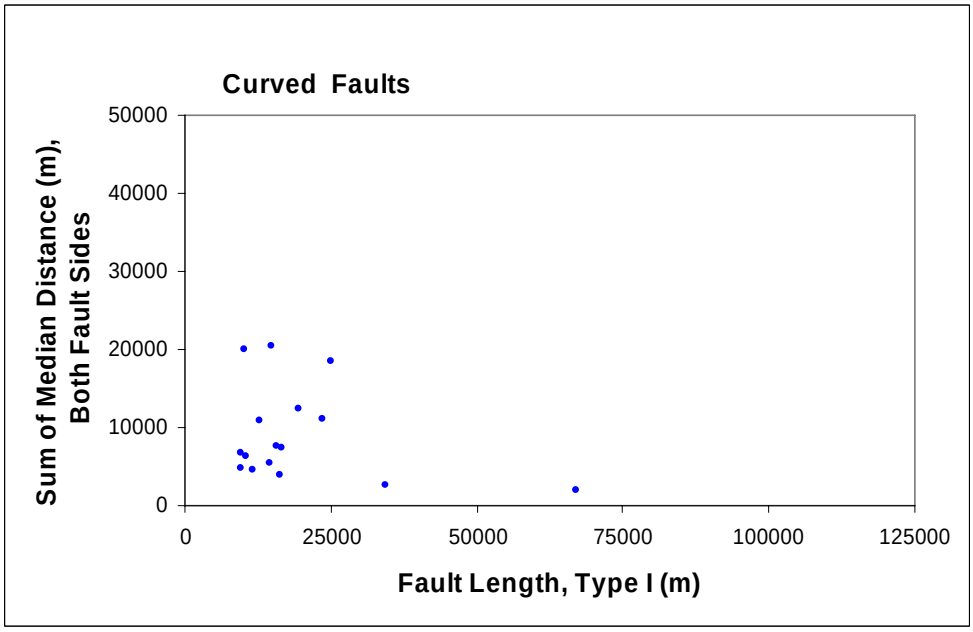
Curved Faults
Sum of Median Distance (m), Both Fault Sides
50000
40000
30000
20000
10000
0
0
25000
50000
75000
100000
125000
Fault Length, Type I (m)

(c)

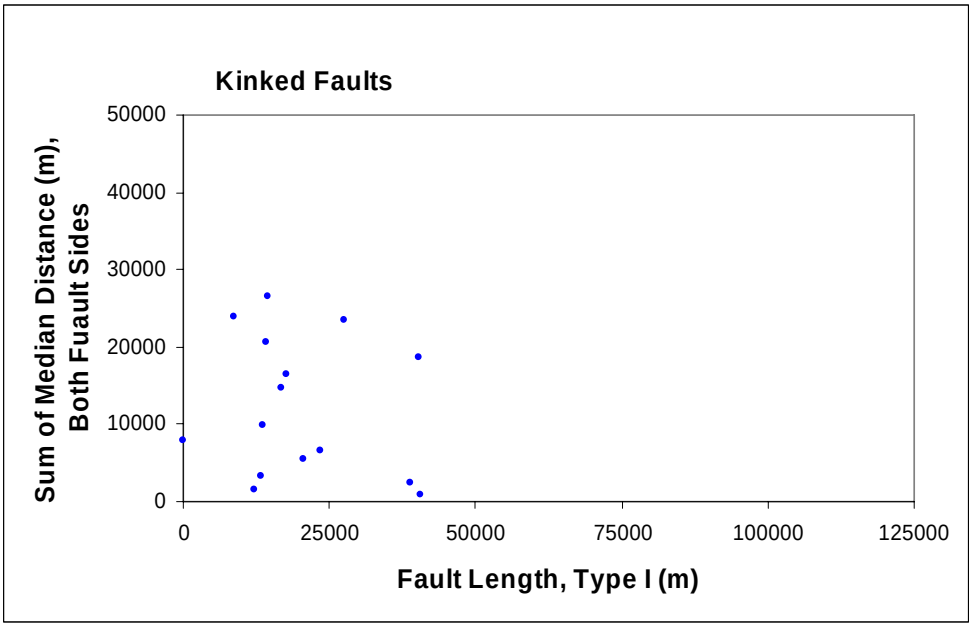

(d)

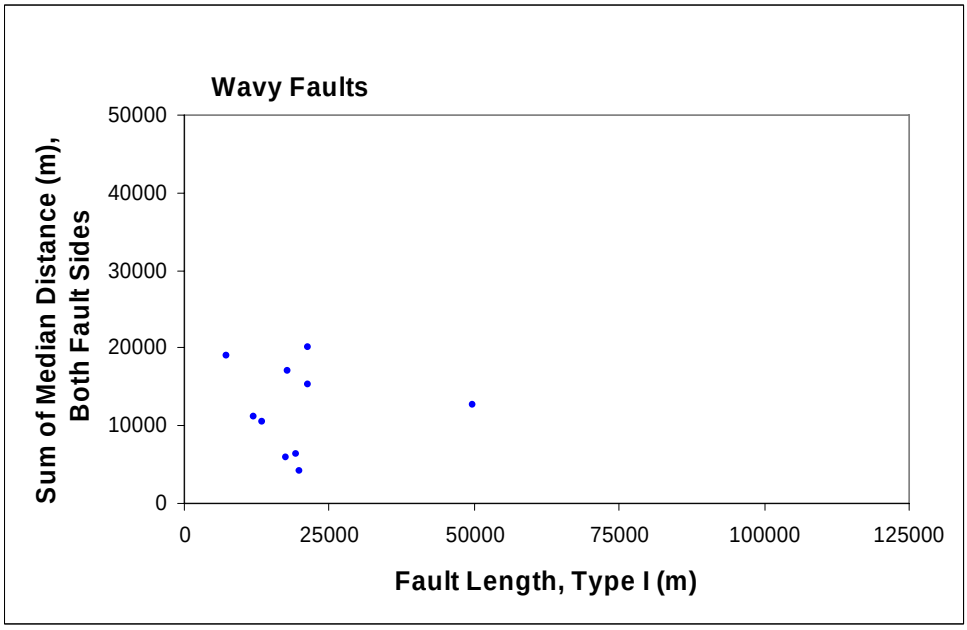

Figure 56. Scatter diagrams of fault length (X) versus the sum of the medians of hypocenter distance associated with the two sides of faults (Y) for four shapes of faults: (a) straight faults; (b) curved faults; (c) kinked faults; and (d) wavy faults. Statistical outliers of hypocenter distance are omitted from the median distance calculation, as are all hypocenters attributed to faults having fewer than 50 associated hypocenters.

(a)

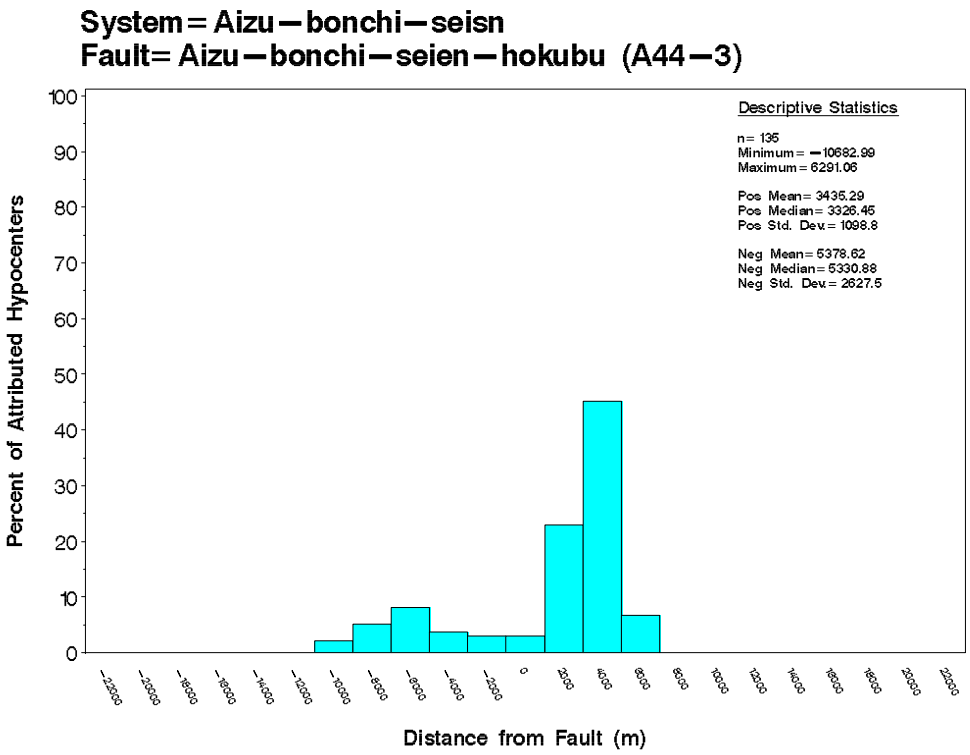

(b)

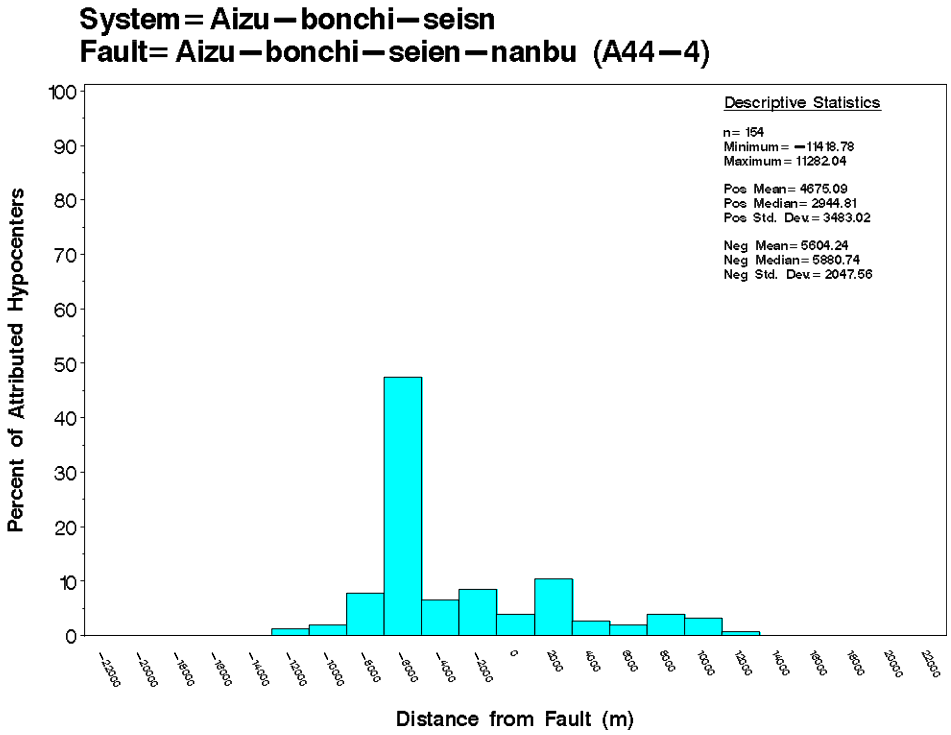

Figure 57. Percentage histograms of hypocenter distance for two faults in the same fault system: (a) A44-3 and (b) A44-4.

This page intentionally left blank

Summary and Conclusions

Preliminary investigation areas (PIA) for a potential repository of high-level radioactive waste must be evaluated by NUMO with regard to a number of qualifying factors. One of these factors is related to earthquakes and fault activity. The overall objective of this study was to develop a spatial statistical assessment method that can be applied to the active faults in Japan to perform such screening evaluations. In particular, this method should provide confidence that fault crushed zones and surrounding deformation zones (or process zones) are excluded in a nationwide survey of PIAs.

The spatial statistical assessment method should define a buffer around active faults in Japan, preferably varying in width as a function of fault characteristics. In the absence of widespread geological data on fracture frequency adjacent to active faults, the concept for this analysis is to use the distribution of seismicity near faults to define the width of the associated process zone. This concept is based on previous observations of aftershock earthquakes clustered near active faults and on the assumption that such seismic activity is indicative of fracturing and associated impacts on bedrock integrity. Preliminary analyses of aggregate data for all of Japan confirmed that the frequency of earthquakes is higher near active faults.

Several potential sources of error associated with this method of analysis were identified, including uncertainty in the locations of earthquake hypocenters, uncertainties in fault orientation, uncertainty in the association of seismic events with individual active faults, and the relatively short period of record for high-resolution seismic data. These sources of error and uncertainty may result in a broader distribution of the hypocenter-fault distances and consequently lead to an overestimate of the width of the associated process zone.

Data used in the analysis were obtained from NUMO and consisted of three primary sources: 1) active fault attributes compiled in a spreadsheet, 2) earthquake hypocenter data, and 3) active fault locations. Examination of these data revealed several limitations with regard to the ability to associate fault attributes from the spreadsheet to locations of individual fault trace segments.

GIS processing of the data was used to compute the distances from earthquake hypocenters to the nearest active fault. This geographical processing involved developing automated methods to associate fault polylines with specific faults in the fault attribute data set. The processing involved several steps and approximations, but it was visually checked to ensure it was adequate for the intended use. The earthquake hypocenter data were filtered with regard to distance from active faults, depth, and approximately perpendicular offset from active faults. For dipping faults it was necessary to make a geometric correction for the dip of the fault and the depth of the earthquake in the calculation of the distance to the nearest active fault. Only those earthquake hypocenters that could be attributed to nearby faults were retained in the analysis. There were numerous faults identified by location in the GIS-based active fault location data set that were not among the active faults in the fault attribute spreadsheet.

In addition, faults which branch at depth or have other complex subsurface geometries may have active zones that are not well represented by the mapped fault traces. Some deeper faults may

not exhibit any surface expression and therefore are completely unrepresented in the GIS fault database. For some hypocenters it is probable that the fault they are truly associated with is not represented by the available GIS fault traces. Considering these issues it is expected that some portion of the computed fault-hypocenter associations are not accurately representing the desired relationships.

The first step of the statistical analysis involved data exploration in which histograms of normal distances from hypocenters to active faults were plotted for constructed. This task revealed several types of the distributions, including symmetric, bimodal, and skewed. In addition, it was observed that many of the distributions were not centered on the fault plane. Some of these characteristics suggested that additional processing and filtering of the data were warranted. In particular, hypocenters that qualified as statistical outliers were filtered out of the data set. Additional processing of the hypocenter data was also used to assign positive or negative distance values corresponding to location on one or the other side of the associated active fault.

Examination of the earthquake characteristics of depth and magnitude was conducted, revealing that most of the earthquakes in the filtered data set were from 5 to 15 km depth and the highest frequency of occurrence was for magnitudes of 1 to 1.5. No consistent relationship was observed among the distance of hypocenters to fault traces, depth of hypocenters, or associated earthquake magnitudes. Similarly, no consistent relationship was observed between associated active fault length and depth or magnitude.

Even with the additional processing and filtering of the earthquake hypocenter data, many of the active faults show distributions of normal distance from associated hypocenter locations that are off center, skewed, or multimodal. Use of the interquartile range as a measure of variability in hypocenter distances around the active fault was considered, but rejected because it would be misleading for the observed distributions in the histograms for many faults. Three alternative statistical measures considered to be potentially representative of the width of the seismic process zone around active faults were evaluated: 1) twice the mean of all hypocenter distances, 2) twice the median of all hypocenter distances, and 3) sum of the medians of the hypocenter distances on the two sides of the fault. Based on the distributions of these three alternative measures among the faults, the sum of the medians of the hypocenter distances on the two sides of the fault was determined to be the most reasonable measure of the width of the seismic process zone. The 50th percentile value of this measure among the active faults evaluated is about 8700 m.

Based on the relationship between the width of the fault crushed zone and fault length or cumulative fault displacement (e.g., Otsuki, 1978), it was expected that a similar relationship exists for the process zone and that the width of the seismic process zone would be greater for longer faults. However, cross-plots of the sum of the medians of the hypocenter distances on the two sides of the fault and the fault length showed no correlation between these two variables. This lack of positive correlation could be due to lack of validity of this measure of the width of the seismic process zone or remaining data inaccuracy. It is possible that the width of the process zone is relatively invariant with fault length.

The statistical analyses conducted in this study are partially successful in meeting the objectives of developing a spatial statistical assessment method for application to active faults in Japan.

The conceptual model of identifying the width of the process zone around active faults using seismic data is supported when applied in an aggregate sense to all active faults. A suite of GIS processes and tools has been developed to filter the earthquake hypocenter data and to calculate normal distances to nearby active faults, successfully accounting for fault dip and some potential biases. However, when these data on distances from hypocenters to faults are analyzed statistically for individual active faults, the analysis is confounded by non-ideal distributions for many faults. It is probable that these non-ideal distributions of distance are primarily due to sources of the uncertainties/limitations mentioned above. Clusters of earthquakes that occur along faults that are not formally identified as active faults in the data set are probably particularly important sources of error that result in "off center" distributions noted in the text. More complete and improved data sets, particularly for fault locations, would help in improving the analyses.

References

Guilbert, J.M. and C.F. Park, 1986, *The Geology of Ore Deposits*, W.H. Freeman and Company, New York.

Japan Nuclear Cycle Development Institute (JNC), 2000, *H12: Project to Establish the Scientific and Technical Basis for HLW Disposal in Japan*, Japan Nuclear Cycle Development Institute, Tokai-Mura, Japan.

Jenness, J. 2004. Nearest features (nearfeat.avx) extension for ArcView 3.x, v. 3.7a. Jenness Enterprises. At: http://www.jennessent.com/arcview/nearest_features.htm.

Nuclear Waste Management Organization of Japan (NUMO), 2002, *Siting Factors for the Selection of Preliminary Investigation Areas*, Nuclear Waste Management Organization of Japan, Tokyo, Japan.

Otsuki, K., 1978, On the relationship between the width of shear zone and the displacement along fault, *Journal of the Geological Society of Japan*, 84, pp. 601-619.

Yoshida, S., 2003, *The Range of Damage Zones of Faults in Terms of Impact on the Repository*, presentation at the NUMO 2nd International Tectonics Meeting, March 12-13, 2003, Tokyo, Japan.

Appendix A

ArcView GIS Processing Codes

This section of Appendix A describes the computational codes used during the GIS analyses. Copies of these codes and extensions are included on the digital data media accompanying this report.

Endpoints2polylines.ave

This Avenue program reads the fault endpoint locations (latitude and longitude) from the fault attribute table, and then creates polylines using those endpoint locations as vertices.
A majority of the fault records in the fault attribute table have only two latitude-longitude pairs for fault endpoint locations. In these cases a single-segment polyline is created connecting the pair of endpoints.

In some other cases, more than two points are listed in the table for that fault record. In these cases, a multi-segment polyline is created. The complexity in these cases, is that there is not a unique order for the vertices, and so different polyline configurations are possible for a given fault record. In this situation, the Avenue code connects the points in two different orders, and chooses the shortest polyline as the final configuration. This reduces the production of polylines which contain many acute angles which are not expected in natural fault traces.

Although this automated process is successful for a majority of the fault records, there are some records with multiple endpoints whose final endpoint polyline required some manual editing to more closely resemble the associated fault trace. In addition, in cases where a fault swarm was being associated to a single multi-segment polyline, the polyline was manually edited to increase the number of intersections between the fault traces and the fault endpoint polyline. This increased the potential for the transfer of attributes from the fault endpoint polyline to the fault traces.

After creation of the new polyline features, all the information from the original fault attribute table was transferred to the new fault endpoint polyline file for use in later processing. Table A-1 summarizes the input and output files used in this process. Figure 14 in the main text shows an example of the output from this procedure.

Table A-1. Data and Processing Files Used During the Fault Endpoint to Polyline Conversion Process

Input Files	snl_reduced_fault_data_snl20040616.txt
Processing Code	endpoints2polylines.ave
Output Files	snl20040616_fault_endpoints.shp

Associate_attributes.ave

The associate_attributes Avenue code is responsible for relating the fault endpoint polylines created from the endpoints2polylines code to the original fault trace polylines. Once a relationship has been established between a fault endpoint polyline and the nearby fault trace polylines, the attributes for the fault endpoint polyline (see Table A-2) are transferred to the fault trace. It is through this process that attributes are added to the fault trace polyline shapefile. The input and output files used in this process are summarized in Table A-2.

Table A-2. Data and Processing Files Used During the Attribute Association Process

Input Files	snl20040616_fault_endpoints.shp
	300m_endpoint_all_faults_consolid.shp
Processing Code	associate_attributes.ave
Output Files	300m_endpoint_all_faults_consolid.shp

For the processing performed for this report, the fault endpoint file *snl20040616_fault_endpoints.shp* and fault trace file *300m_endpoint_all_faults_consolid.shp* were used as input files.

The fault endpoint file *snl20040616_fault_endpoints.shp* was created with the endpoints2polylines Avenue code. The fault trace file *300m_endpoint_all_faults_consolid.shp* represents a processed subset of the original fault trace polylines. This subset was created by first grouping the individual fault trace location files listed in Table 1 of the main text. Then a polyline consolidation routine (third party ArcView extension Point and Polyline Tools v1.2) was applied to the polylines. Some manual editing of the shapefile was also needed to remove duplicate polylines and digitizing artifacts. Finally, all fault trace polylines within 300 m of a fault endpoint polyline were selected and written to 300m_endpoint_all_faults_consolid.shp for use as input for the associate_attributes Avenue script.

To increase the number of fault traces which receive attributes from the fault endpoint polylines, all fault traces within 300 m of a fault endpoint polyline are considered to be associated with that endpoint polyline, and so, is attributed appropriately. In addition, after the fault traces selected in this manner are attributed, a check is performed to search for any additional fault traces within 300 m of the current fault trace. This procedure extends the coverage of the attributed fault traces and avoids problems induced by small gaps in the fault trace polylines. The code repeats this procedure until no additional fault trace polyline segments fall within the selection radius. Figures 16 and 17 in the main text show examples of these procedures. While this automated procedure works well for maintaining continuity for the attributed fault traces, it can extend attributes to fault traces which would have been attributed differently if the attribution were performed manually.

The output file from this script is the attributed *300m_endpoint_all_faults_consolid.shp* fault trace location shapefile.

Limit_polygons.ave

The limit_polygons Avenue code was written to address the need to restrict the associations between fault traces and hypocenters beyond the end of the fault trace. This code reads in the fault trace polylines and then creates a buffer around the polyline at a specified distance. The special requirement for these buffer polygons, which necessitated writing this code, is the need for the polygons to be truncated at the end of the polyline.

The code operates by first creating full polygon buffers around the fault trace polylines, then computing polylines normal to the ends of the fault traces and using these normal polylines to split the buffer polygon into three segments. The middle segment of these, which contains the fault trace polyline, is then retained as the limiting polygon. Figure 19 in the main text shows example output from this procedure. A summary of the files used in this process are provided in Table A-3.

Table A-3. Data and Processing Files Used During the Limiting Polygon Creation Process

Input Files	300m_endpoint_all_faults_consolid.shp
Processing Code	limit_polygons.ave
Output Files	limit_polygons.shp

Depth_correction.ave

This Avenue code is responsible for computing the depth corrected distances using the surface planimetric distances, and choosing the closest fault trace for each hypocenter. In addition, this code determines within which fault block the hypocenter is located (hanging or foot).

The input files consist of the filtered hypocenter data, the attributed fault trace polylines, the fault end limiting polygons, and the distance to nearest feature data table. The files used here for this process are listed in Table A-4 in their respective order. The output file from this process is the same hypocenter file used for input, but augmented with additional fields to contain the processing results.

Table A-4. Data and Processing Files Used During the Distance Depth Correction Process

Input Files	UTM53_post1994_20km_buff_20km_hypocenters.shp
	300m_endpoint_all_faults_consolid.shp
	limit_polygons.shp
	utm53_distance_7_29_04.dbf
Processing Code	depth_correction.ave
Output Files	UTM53_post1994_20km_buff_20km_hypocenters.shp

The code operates by reading in all the input data files, and then processing each selected hypocenter record. The code then loops through the four nearest fault trace distance records for that hypocenter. These are contained in the nearest feature data table which holds the distance and bearing to the four nearest fault trace polylines. These surface planimetric distances are then used in the computation of the depth-corrected planimetric and fault normal distances. During this process a check is performed to assure that the hypocenter under consideration is contained in the limiting polygon for the associated fault trace. The fault block (hanging or foot) for hypocenters associated with dipping faults is also determined during this processing. At the completion of processing for each hypocenter, the shortest fault normal distance is selected as the final value and its associated distances and fault ID, along with additional attribute data are added to the input hypocenter data file.

The original surface planimetric distance values used in this procedure were computed using a third-party ArcView extension as described in the Nearest Feature Extension section provided below.

Projected_length.ave

The projected_length Avenue code is a utility code that computes the projected length (in meters) of each segment of a polyline file and writes this value to a new field in that file. It was written to provide the length of each of the individual fault trace segments. This code should only be applied to polyline shapefiles with original location values in geographic coordinates. Table A-5 summarizes the files used for this process.

Table A-5. Data and Processing Files Used for Computing GIS Polyline Segment Lengths

Input Files	300m_endpoint_all_faults_consolid.shp
Processing Code	Projected_length.ave
Output Files	300m_endpoint_all_faults_consolid.shp

Nearest Feature Extension

A critical element to the GIS analyses were the calculation of distances from the hypocenters to the nearest fault traces. The basis for the calculation of all the different distance values was the planimetric distance. The planimetric distance represents the distance between the hypocenter and the fault trace treating both as being contained in the same horizontal plane.

A third-party ArcView extension, the Nearest Features extension version 3.7a (Jenness, 2004) was used for this process. This extension was obtained from the ESRI web site (www.esri.com). The extension computes the nearest features for a set of selected features. The code provides many options to record different attributes during this process including the length and bearing of the line connecting the nearest features. In addition, this extension has the capability of finding the n nearest neighbors to the selected features. This capability was used for this project to record the four nearest fault traces for each hypocenter. Table A-6 summarizes the files used during this process.

Table A-6. Data and Processing Files Used to Identify the Four Nearest Fault Traces for Each Hypocenter Location

Input Files	UTM53_post1994_20km_buff_20km_hypocenters.shp
	300m_endpoint_all_faults_consolid.shp
Processing Code	nearfeat.avx
Output Files	utm53_distance_7_29_04.dbf
	Utm53_connect_7_29_04.shp

The extension operates through a series of menus where the input and output files are specified and the desired options selected. The options and operating parameters used for this project were:

1. record comparison feature id
2. record closest edge X coordinate
3. record closest edge Y coordinate
4. record distance to closest edge
5. record bearing to closest edge
6. generate a polyline shape file of nearest feature connections
7. use edge of feature to define nearest
8. record four nearest features for each input feature
9. use UTM Zone 53 view projection for distance calculations

Once the options and input and output files are specified, the code begins the nearest feature computations. During this, each selected feature in the base theme is examined and the n nearest neighbors to that feature are identified. Once the nearest features are established, a unique identifier for these features, and any additional requested information (distance, bearing, etc.) are recorded in the output data table. Optionally, the extension can also create a polyline shapefile showing how the base and comparison features are related.

Data dictionary

Table A-7 in Appendix A contains a listing of the information contained in the final data product produced from the GIS analysis. The information in the final data product was used in the statistical analyses performed for this project. In the table below, "Column Name" is the field name used in the final data product, "Original Column Name" is the original data source field name for those fields acquired from preexisting tables, "Explanation" provides additional details regarding that field, and "Source" provides the origin of the information contained in that field.

Table A-7. Data Dictionary

		NUMO Distance Calculation Data Dictionary	
Column Name	**Original Column Name**	**Explanation**	**Source**
			Original hypocenter shapefiles
Shape	Shape	ArcView shape field	Original hypocenter shapefiles
X	X		Original hypocenter shapefiles
Y	Y		Original hypocenter shapefiles
Header	Header	Header (source of record); J: JMA, I: ISC, U: USGS	Original hypocenter shapefiles
Years	Years	Years of origin time	Original hypocenter shapefiles
Months	Months	Months of origin time	Original hypocenter shapefiles
Days	Days	Days of origin time	Original hypocenter shapefiles
Hours	Hours	Hours of origin time	Original hypocenter shapefiles
Minutes	Minutes	Minutes of origin time	Original hypocenter shapefiles
Seconds	Seconds	Seconds of origin time	Original hypocenter shapefiles
Time	Time	Standard error of origin time	Original hypocenter shapefiles
Latitude	Latitude	Latitude of epicenter (degrees)	Original hypocenter shapefiles
Minutes0	Minutes0	Latitude of epicenter (minutes)	Original hypocenter shapefiles
Error_lat	Error_lat	Standard error of latitude	Original hypocenter shapefiles
Longitude	Longitude	Longitude of epicenter (degrees)	Original hypocenter shapefiles
Minutes1	Minutes1	Longitude of epicenter (minutes)	Original hypocenter shapefiles
Error_lon	Error_lon	Standard error of longitude	Original hypocenter shapefiles
Depth	Depth	Depth	Original hypocenter shapefiles
Error_dep	Error_depth	Standard error of depth	Original hypocenter shapefiles
Magnitude1	Magnitude1	Magnitude 1; bodily wave by JMA or ISC, etc.	Original hypocenter shapefiles
Magnitud0	magnitud0	Type of magnitude 1; J: JMA, B: MB, S: MS	Original hypocenter shapefiles
Magnitude2	Magnitude 2	Magnitude 2; surface wave by ISC, etc.	Original hypocenter shapefiles
Magnitud1	Magnitud1	Type of magnitude 2	Original hypocenter shapefiles
Traveltime	Traveltime	Type of travel time table; 1: standard, 2: for Sanriku offshore, 3: for Hokkaido Eastern offshore, 4: for Kurile Islands	Original hypocenter shapefiles

Precisiono	Precisiono	Premises for hypocenter estimation; 1: depth free, 2: depth interval at 1km, 3: fixed depth (by expert judgment), 4: using Depth Phase, 5: for reference only, 6: not for use	Original hypocenter shapefiles
Subsidiary	Subsidiary	Subsidiary information of the event; 1: normal earthquake, 2: dependent on other institutes, 3: artificial earthquakes, 4: noise	Original hypocenter shapefiles
Intensity	Intensity	Maximum intensity (JMA scale)	Original hypocenter shapefiles
Class	Class	Damage class (after Utsu)	Original hypocenter shapefiles
Class0	Class0	Tsunami class (after Imamura and Iida)	Original hypocenter shapefiles
Epicenter	Epicenter	District number of epicenter	Original hypocenter shapefiles
Number	Number	Geographical region number of epicenter	Original hypocenter shapefiles
Name	Name	Geographical region name of epicenter	Original hypocenter shapefiles
Observatio	Observation	Number of observations contributing to hypocenter determination	Original hypocenter shapefiles
Flag	Flag	Hypocenter determination flag depends on JMA computer system	Original hypocenter shapefiles
Snl_HID		Unique ID for hypocenter	SNL Assigned
SurfDist		Planimetric distance from epicenter to selected nearest fault* at ground surface (m)	Computed
DepthDist		Planimetric distance from hypocenter to selected nearest fault* at hypocenter depth (m)	Computed
NormDist		Distance from hypocenter to fault plane, computed normal to fault plane (m)	Computed
Wall		Hypocenter location indicator (0=vertical, 1=hanging wall, 2=foot wall, -1=footwall with penetration, -99=beyond end of fault trace)	Computed
Snl_FID		Unique ID of polyline segment representing nearest fault trace	SNL Assigned
Line_id		Intermediate ID code	SNL generated
Descriptio		General fault type (text description)	Original fault trace shapefiles
Sec_code		General fault type (numeric code)	Original fault trace shapefiles
Fault_id	Fault ID	ID numbers of fault zones used in the "Digital Active Fault Map of Japan". A fault zone comprise several faults which are close to each other and have similar characteristics.	SNL 20040616.xls
No_		Original sequential number	SNL 20040616.xls
Fault_type	Fault Type	A: active faults longer than 10km in the "Digital Active Fault Map of Japan*". B: estimated active faults longer than 10km in the "Digital Active Fault Map of Japan".	SNL 20040616.xls

Fault_numb	Fault Number	The first (left) numbers show the map numbers in the NUMO's fault compilation report. The second numbers show the fault numbers in each specific map, which are given in the order from east to west and from north to south. Note that these numbers are given to each fault type, thus A5-1, B5-1 and 5-1 are all different faults. For the subsidiary faults, alphabets are given after the numbers.	SNL 20040616.xls
Fault_name	Fault Name	Name of the faults.	SNL 20040616.xls
Fault_syst	Fault System Name	Name of the fault systems to which the faults belong.	SNL 20040616.xls
North_lat	Northern End (Latitude)		SNL 20040616.xls
North_long	Northern End (Longitude)		SNL 20040616.xls
South_lat	Southern End (Latitude)		SNL 20040616.xls
South_long	Southern End (Longitude)		SNL 20040616.xls
East_lat	Eastern End (Latitude)		SNL 20040616.xls
East_long	Eastern End (Longitude)		SNL 20040616.xls
West_lat	Western End (Latitude)		SNL 20040616.xls
West_long	Western End (Longitude)		SNL 20040616.xls
Length__km	Length (km)	Trace length of the faults. In case of shallowly dipping faults, distances between both ends are given.	SNL 20040616.xls
Net_length	Net Length (km)	If the fault is branched or strands between two maps, the accumulated length is given.	SNL 20040616.xls
Strike	Strike	If the fault is not straight, the first strike shows representative strike, and the rest (after "//") show each measurement data.	SNL 20040616.xls
Dip	Dip	Plural values are given if the dip changes in places.	SNL 20040616.xls
MeanDip		Mean dip angle computed from "dip" field; value of -1 indicates no dip value was available (degrees)	Computed

MeanDir		Mean dip direction computed from "dip" field; value of -1 indicates no dip value was available (degrees from north)	Computed
Fshape	Shape	S: straight ("/ "means combination), C: curved, W: wavy, K: kinked, E: en echelon configuration	SNL 20040616.xls
Maximum_zo	Maximum Zone Width (m)	Maximum width of the zone shown below.	SNL 20040616.xls
Type_of_zo	Type of Zone	crushed: crushed zone. clay: fault clay (gouge). (blanc): not specified, only described as "width of the fault".	SNL 20040616.xls
Net_displa	Net Displacement (m)	Accumulated displacement of the fault since its formation.	SNL 20040616.xls
Maxlatdisp	Maximum Lateral Displacement (m)	Maximum value of the estimated lateral displacement.	SNL 20040616.xls
Maxverdisp	Maximum Vertical Displacement (m)	Maximum value of the estimated vertical displacement.	SNL 20040616.xls
Maxavrate	Maximum Average Displacement Rate (m/103 years)	Maximum value of the estimated displacement rate (displacement per 1000 years).	SNL 20040616.xls
GIS_Length		Length of polyline segment representing nearest fault trace (m)	Computed
Snl_FID		Unique ID of polyline segment representing nearest fault trace	SNL Assigned

*Nearest fault trace is defined using normal distance to fault plane from hypocenter.

Appendix B

Statistics on Earthquake Hypocenters Associated with Individual Faults

Table B-1. Number of Hypocenters* Attributed to Individual Faults, Listed in Increasing Count Size

Fault Type** & Number	Count
A10-1	23
A10-2	6
A14-1	53
A20-2	2
A24-1	36
A24-2	36
A29-1	99
A29-2	10
A29-3	3
A29-5	105
A33-1a	11
A33-1b	25
A33-1c	210
A34-2	18
A34-5	137
A36-2	574
A37-1	62
A37-2	17
A37-4	24
A38-1	8
A38-2	26
A38-3	11
A40-10	29
A40-2	8
A40-3a	31
A40-4	51
A40-5	9
A40-6	165
A40-8	11
A40-9	68
A41-1	38
A42-1	16
A43-1	23
A43-2	32
A43-3	8
A43-4	42
A43-7	84
A44-2b	75
A44-3	165

Fault Type & Number	Count
A44-4	158
A44-5	578
A45-2	45
A45-3	35
A45-4	34
A49-1	9
A50-1	536
A50-2	118
A51-1	196
A51-2	318
A52-1	68
A52-2	74
A52-3	87
A53-1	1
A53-2	92
A58-1	107
A58-2	239
A58-3	33
A58-6	454
A59-1	517
A59-2	16
A59-3	60
A60-1	1
A60-2	494
A60-3	23
A61-1a	600
A64-1	2,569
A64-2	200
A64-3	15
A64-4	4,123
A64-5	604
A64-6	150
A64-7	371
A64-8	53
A65-1	44
A65-2	113
A65-3	63
A65-5	55
A65-6	199
A65-8	2,914
A66-2a	14
A69-2	44
A70-1	88
A70-2	20
A70-3	14
A70-4	447

Fault Type & Number	Count
A71-1	179
A71-2	105
A71-3b	102
A71-4	339
A71-5	173
A71-6	96
A71-7	201
A71-8	612
A71-9	168
A71-10	34
A71-11	16
A71-12	64
A72-1	475
A72-2	172
A72-3	75
A72-4	125
A75-2	334
A75-3	1,858
A75-4	503
A75-5	291
A75-6	28
A75-7	174
A76-1	391
A76-13	33
A76-14a	475
A76-14b	21
A76-15	536
A76-16	27
A76-17	676
A76-2	55
A76-3	131
A76-5	940
A76-8	2,473
A76-9a	230
A76-9b	1,502
A77-2	66
A77-5	90
A77-6	14,306
A77-8	1,675
A79-1	71
A79-2	30
A80-1	220
A80-2	277
A80-3	321
A81-1	749
A81-2	289

Fault Type & Number	Count
A81-3	61
A81-4	2
A86-1	72
A87-1	24
A87-2	1,548
A87-3	208
A87-4	243
A9-1	4
A91-3	508
A9-2	23
A92-2	41
A9-3	3
A9-4	2
A9-5	2
A95-2	166
A98-1	967
A99-2	127
A99-3a	58
A99-3b	51
A99-4	120
A101-1b	246
A101-2	629
A101-3	8
A101-4	3
A101-5	13
A102-4	328
A102-5	275
A106-1	10,532
A106-3	269
A106-4	14,862
A112-1	79
A114-1	191
B13-1	9
B14-1	4
B20-3	16
B22-1	9
B30-1	256
B40-2	208
B40-3	73
B41-1	23
B46-1	3
B46-2	38
B46-3	35
B49-1	14

Fault Type & Number	Count
B51-1	28
B52-4	83
B53-2	1
B60-1	141
B64-1	437
B64-2	5,555
B64-3	123
B65-2	292
B65-3	30
B65-4	54
B66-1	10
B69-1	10
B71-1	413
B71-3	28
B72-2	119
B72-3	21
B72-4	4
B72-5	159
B76-1	521
B76-4	127
B76-6	860
B76-7	82
B76-9	494
B77-1	12
B79-1	4,333
B80-1	422
B82-1	914
B101-1	3
B101-2	54
B101-3	9
B10-2	1
B103-1	46
Total	**98,791**

*The counts represent the number of hypocenters attributed to individual faults prior to imposing the 50-fault minimum and prior to the identification of outliers.

**Fault Type A = active faults longer than 10km and Fault Type B = estimated active faults longer than 10km

Table B-2. Number of Hypocenters* Associated with Faults, by Depth

Fault Type & Number		Depth Interval (km)					
		<1	1-4.99	5-9.99	10-14.99	≥15	Total
A14-1	Count	12	23	9	9	0	53
	Percent	22.6	43.4	17.0	17.0	0.0	100
A29-1	Count	4	0	15	74	6	99
	Percent	4.0	0.0	15.2	74.7	6.1	100
A29-5	Count	0	1	3	51	45	100
	Percent	0.0	1.0	3.0	51.0	45.0	100
A33-1c	Count	1	0	23	161	3	188
	Percent	0.5	0.0	12.2	85.6	1.6	100
A34-5	Count	2	1	26	90	18	137
	Percent	1.5	0.7	19.0	65.7	13.1	100
A36-2	Count	5	14	258	243	4	524
	Percent	1.0	2.7	49.2	46.4	0.8	100
A37-1	Count	0	1	19	41	0	61
	Percent	0.0	1.6	31.1	67.2	0.0	100
A40-4	Count	1	7	28	10	1	47
	Percent	2.1	14.9	59.6	21.3	2.1	100
A40-6	Count	1	1	79	75	9	165
	Percent	0.6	0.6	47.9	45.5	5.5	100
A40-9	Count	0	0	36	26	3	65
	Percent	0.0	0.0	55.4	40.0	4.6	100
A43-7	Count	0	2	16	65	1	84
	Percent	0.0	2.4	19.0	77.4	1.2	100
A44-2b	Count	1	1	10	51	4	67
	Percent	1.5	1.5	14.9	76.1	6.0	100
A44-3	Count	0	1	13	74	47	135
	Percent	0.0	0.7	9.6	54.8	34.8	100
A44-4	Count	1	94	45	11	3	154
	Percent	0.6	61.0	29.2	7.1	1.9	100
A44-5	Count	4	22	281	182	46	535
	Percent	0.7	4.1	52.5	34.0	8.6	100

Fault Type & Number		Depth Interval (km)					
		<1	1-4.99	5-9.99	10-14.99	≥15	Total
A50-1	Count	3	7	347	52	1	410
	Percent	0.7	1.7	84.6	12.7	0.2	100
A50-2	Count	0	9	64	21	0	94
	Percent	0.0	9.6	68.1	22.3	0.0	100
A51-1	Count	0	1	12	105	78	196
	Percent	0.0	0.5	6.1	53.6	39.8	100
A51-2	Count	0	1	4	202	107	314
	Percent	0.0	0.3	1.3	64.3	34.1	100
A52-1	Count	1	6	12	19	29	67
	Percent	1.5	9.0	17.9	28.4	43.3	100
A52-2	Count	0	2	6	8	58	74
	Percent	0.0	2.7	8.1	10.8	78.4	100
A52-3	Count	0	1	5	30	51	87
	Percent	0.0	1.1	5.7	34.5	58.6	100
A53-2	Count	56	25	7	0	1	89
	Percent	62.9	28.1	7.9	0.0	1.1	100
A58-1	Count	3	11	36	45	12	107
	Percent	2.8	10.3	33.6	42.1	11.2	100
A58-2	Count	2	4	22	168	23	219
	Percent	0.9	1.8	10.0	76.7	10.5	100
A58-6	Count	34	91	259	55	15	454
	Percent	7.5	20.0	57.0	12.1	3.3	100
A59-1	Count	9	111	357	36	1	514
	Percent	1.8	21.6	69.5	7.0	0.2	100
A59-3	Count	0	0	21	39	0	60
	Percent	0.0	0.0	35.0	65.0	0.0	100
A60-2	Count	0	1	61	308	107	477
	Percent	0.0	0.2	12.8	64.6	22.4	100
A61-1a	Count	4	6	15	133	442	600
	Percent	0.7	1.0	2.5	22.2	73.7	100

Fault Type & Number		Depth Interval (km)					
		<1	1-4.99	5-9.99	10-14.99	≥15	Total
A64-1	Count	58	160	987	1,181	183	2,569
	Percent	2.3	6.2	38.4	46.0	7.1	100
A64-2	Count	0	6	147	35	0	188
	Percent	0.0	3.2	78.2	18.6	0.0	100
A64-4	Count	3	79	2,122	1,846	9	4,059
	Percent	0.1	1.9	52.3	45.5	0.2	100
A64-5	Count	14	83	314	157	2	570
	Percent	2.5	14.6	55.1	27.5	0.4	100
A64-6	Count	0	12	99	26	2	139
	Percent	0.0	8.6	71.2	18.7	1.4	100
A64-7	Count	0	5	217	144	4	370
	Percent	0.0	1.4	58.6	38.9	1.1	100
A64-8	Count	2	8	28	14	1	53
	Percent	3.8	15.1	52.8	26.4	1.9	100
A65-2	Count	0	1	17	43	42	103
	Percent	0.0	1.0	16.5	41.7	40.8	100
A65-3	Count	1	0	22	22	9	54
	Percent	1.9	0.0	40.7	40.7	16.7	100
A65-5	Count	0	0	17	22	16	55
	Percent	0.0	0.0	30.9	40.0	29.1	100
A65-6	Count	1	2	20	150	6	179
	Percent	0.6	1.1	11.2	83.8	3.4	100
A65-8	Count	5	52	1,061	1,568	85	2,771
	Percent	0.2	1.9	38.3	56.6	3.1	100
A70-1	Count	2	3	18	59	6	88
	Percent	2.3	3.4	20.5	67.0	6.8	100
A70-4	Count	12	65	322	43	0	442
	Percent	2.7	14.7	72.9	9.7	0.0	100
A71-1	Count	2	6	88	74	6	176
	Percent	1.1	3.4	50.0	42.0	3.4	100

Fault Type & Number		Depth Interval (km)					
		<1	1-4.99	5-9.99	10-14.99	≥15	Total
A71-2	Count	0	0	16	67	12	95
	Percent	0.0	0.0	16.8	70.5	12.6	100
A71-3b	Count	1	0	20	72	9	102
	Percent	1.0	0.0	19.6	70.6	8.8	100
A71-4	Count	2	7	159	150	21	339
	Percent	0.6	2.1	46.9	44.2	6.2	100
A71-5	Count	1	5	53	111	1	171
	Percent	0.6	2.9	31.0	64.9	0.6	100
A71-6	Count	0	3	30	42	21	96
	Percent	0.0	3.1	31.3	43.8	21.9	100
A71-7	Count	0	8	62	104	2	176
	Percent	0.0	4.5	35.2	59.1	1.1	100
A71-8	Count	1	8	65	456	70	600
	Percent	0.2	1.3	10.8	76.0	11.7	100
A71-9	Count	1	2	31	116	18	168
	Percent	0.6	1.2	18.5	69.0	10.7	100
A71-12	Count	0	4	8	40	7	59
	Percent	0.0	6.8	13.6	67.8	11.9	100
A72-1	Count	2	8	27	237	201	475
	Percent	0.4	1.7	5.7	49.9	42.3	100
A72-2	Count	0	1	9	98	64	172
	Percent	0.0	0.6	5.2	57.0	37.2	100
A72-3	Count	0	1	5	54	15	75
	Percent	0.0	1.3	6.7	72.0	20.0	100
A72-4	Count	0	2	76	46	1	125
	Percent	0.0	1.6	60.8	36.8	0.8	100
A75-2	Count	2	5	61	248	14	330
	Percent	0.6	1.5	18.5	75.2	4.2	100
A75-3	Count	14	65	399	1,300	80	1,858
	Percent	0.8	3.5	21.5	70.0	4.3	100

Fault Type & Number		Depth Interval (km)					
		<1	1-4.99	5-9.99	10-14.99	≥15	Total
A75-4	Count	9	17	242	233	2	503
	Percent	1.8	3.4	48.1	46.3	0.4	100
A75-5	Count	4	14	179	89	5	291
	Percent	1.4	4.8	61.5	30.6	1.7	100
A75-7	Count	1	2	92	54	0	149
	Percent	0.7	1.3	61.7	36.2	0.0	100
A76-1	Count	0	2	84	251	54	391
	Percent	0.0	0.5	21.5	64.2	13.8	100
A76-2	Count	0	0	3	50	2	55
	Percent	0.0	0.0	5.5	90.9	3.6	100
A76-3	Count	0	1	3	119	4	127
	Percent	0.0	0.8	2.4	93.7	3.1	100
A76-5	Count	5	7	236	590	1	839
	Percent	0.6	0.8	28.1	70.3	0.1	100
A76-8	Count	18	44	530	1,800	79	2,471
	Percent	0.7	1.8	21.4	72.8	3.2	100
A76-9a	Count	0	3	60	159	8	230
	Percent	0.0	1.3	26.1	69.1	3.5	100
A76-9b	Count	7	10	231	1,184	70	1,502
	Percent	0.5	0.7	15.4	78.8	4.7	100
A76-14a	Count	1	7	149	311	7	475
	Percent	0.2	1.5	31.4	65.5	1.5	100
A76-15	Count	0	3	65	454	10	532
	Percent	0.0	0.6	12.2	85.3	1.9	100
A76-17	Count	0	1	97	522	43	663
	Percent	0.0	0.2	14.6	78.7	6.5	100
A77-2	Count	0	1	21	42	2	66
	Percent	0.0	1.5	31.8	63.6	3.0	100
A77-5	Count	3	3	25	50	4	85
	Percent	3.5	3.5	29.4	58.8	4.7	100

Fault Type & Number		Depth Interval (km)					
		<1	1-4.99	5-9.99	10-14.99	≥15	Total
A77-6	Count	97	2854	9,734	1,540	81	14,306
	Percent	0.7	19.9	68.0	10.8	0.6	100
A77-8	Count	2	25	582	838	125	1,572
	Percent	0.1	1.6	37.0	53.3	8.0	100
A79-1	Count	0	0	12	50	4	66
	Percent	0.0	0.0	18.2	75.8	6.1	100
A80-1	Count	0	1	39	130	13	183
	Percent	0.0	0.5	21.3	71.0	7.1	100
A80-2	Count	0	2	32	191	52	277
	Percent	0.0	0.7	11.6	69.0	18.8	100
A80-3	Count	0	0	32	188	67	287
	Percent	0.0	0.0	11.1	65.5	23.3	100
A81-1	Count	0	7	202	461	43	713
	Percent	0.0	1.0	28.3	64.7	6.0	100
A81-2	Count	7	36	137	90	4	274
	Percent	2.6	13.1	50.0	32.8	1.5	100
A81-3	Count	2	6	9	35	1	53
	Percent	3.8	11.3	17.0	66.0	1.9	100
A86-1	Count	0	0	10	36	26	72
	Percent	0.0	0.0	13.9	50.0	36.1	100
A87-2	Count	11	21	216	1,007	95	1,350
	Percent	0.8	1.6	16.0	74.6	7.0	100
A87-3	Count	1	0	39	152	16	208
	Percent	0.5	0.0	18.8	73.1	7.7	100
A87-4	Count	0	1	23	168	37	229
	Percent	0.0	0.4	10.0	73.4	16.2	100
A91-3	Count	0	2	70	306	130	508
	Percent	0.0	0.4	13.8	60.2	25.6	100

Fault Type & Number		Depth Interval (km)					
		<1	1-4.99	5-9.99	10-14.99	≥15	Total
A95-2	Count	0	2	29	123	12	166
	Percent	0.0	1.2	17.5	74.1	7.2	100
A98-1	Count	1	23	577	349	2	952
	Percent	0.1	2.4	60.6	36.7	0.2	100
A99-2	Count	3	8	39	71	5	126
	Percent	2.4	6.3	31.0	56.3	3.968254	100
A99-3a	Count	0	2	17	32	7	58
	Percent	0.0	3.4	29.3	55.2	12.1	100
A99-3b	Count	0	3	26	21	1	51
	Percent	0.0	5.9	51.0	41.2	2.0	100
A99-4	Count	0	1	23	75	21	120
	Percent	0.0	0.8	19.2	62.5	17.5	100
A101-1b	Count	1	21	187	31	3	243
	Percent	0.4	8.6	77.0	12.8	1.2	100
A101-2	Count	1	1	369	89	0	460
	Percent	0.2	0.2	80.2	19.3	0.0	100
A102-4	Count	28	41	139	98	13	319
	Percent	8.8	12.9	43.6	30.7	4.1	100
A102-5	Count	98	83	41	6	4	232
	Percent	42.2	35.8	17.7	2.6	1.7	100
A106-1	Count	38	304	5,010	5,008	124	10,484
	Percent	0.4	2.9	47.8	47.8	1.2	100
A106-3	Count	5	9	131	119	5	269
	Percent	1.9	3.3	48.7	44.2	1.9	100
A106-4	Count	199	2,014	9,839	2,039	64	14,155
	Percent	1.4	14.2	69.5	14.4	0.5	100
A112-1	Count	7	11	38	19	4	79
	Percent	8.9	13.9	48.1	24.1	5.1	100

Fault Type & Number		Depth Interval (km)					
		<1	1-4.99	5-9.99	10-14.99	≥15	Total
A114-1	Count	48	26	66	21	11	172
	Percent	27.9	15.1	38.4	12.2	6.4	100
B30-1	Count	6	8	76	138	8	236
	Percent	2.5	3.4	32.2	58.5	3.4	100
B40-2	Count	0	1	21	160	1	183
	Percent	0.0	0.5	11.5	87.4	0.5	100
B40-3	Count	6	1	24	38	2	71
	Percent	8.5	1.4	33.8	53.5	2.8	100
B52-4	Count	0	0	10	23	45	78
	Percent	0.0	0.0	12.8	29.5	57.7	100
B60-1	Count	0	0	27	75	39	141
	Percent	0.0	0.0	19.1	53.2	27.7	100
B64-1	Count	11	51	308	21	1	392
	Percent	2.8	13.0	78.6	5.4	0.3	100
B64-2	Count	5	181	5,047	75	0	5,308
	Percent	0.1	3.4	95.1	1.4	0.0	100
B64-3	Count	1	7	35	60	1	104
	Percent	1.0	6.7	33.7	57.7	1.0	100
B65-2	Count	0	1	53	234	4	292
	Percent	0.0	0.3	18.2	80.1	1.4	100
B65-4	Count	0	3	23	27	1	54
	Percent	0.0	5.6	42.6	50.0	1.9	100
B71-1	Count	3	6	97	294	13	413
	Percent	0.7	1.5	23.5	71.2	3.1	100
B72-2	Count	0	1	9	71	38	119
	Percent	0.0	0.8	7.6	59.7	31.9	100
B72-5	Count	0	0	52	102	3	157
	Percent	0.0	0.0	33.1	65.0	1.9	100

Fault Type & Number		Depth Interval (km)					
		<1	1-4.99	5-9.99	10-14.99	≥15	Total
B76-1	Count	0	2	26	302	141	471
	Percent	0.0	0.4	5.5	64.1	29.9	100
B76-4	Count	0	3	48	75	1	127
	Percent	0.0	2.4	37.8	59.1	0.8	100
B76-6	Count	1	0	52	738	51	842
	Percent	0.1	0.0	6.2	87.6	6.1	100
B76-7	Count	0	0	9	66	7	82
	Percent	0.0	0.0	11.0	80.5	8.5	100
B76-9	Count	1	3	64	362	64	494
	Percent	0.2	0.6	13.0	73.3	13.0	100
B79-1	Count	2	10	3,512	698	0	4,222
	Percent	0.0	0.2	83.2	16.5	0.0	100
B80-1	Count	0	0	14	232	133	379
	Percent	0.0	0.0	3.7	61.2	35.1	100
B82-1	Count	14	58	549	285	8	914
	Percent	1.5	6.3	60.1	31.2	0.9	100
B101-2	Count	2	2	7	31	12	54
	Percent	3.7	3.7	13.0	57.4	22.2	100
All	**Count**	**917**	**7,002**	**48,337**	**34,217**	**3,856**	**94,329**
	Percent	**1.0**	**7.4**	**51.2**	**36.3**	**4.1**	

*After imposing the 50-hypocenter minimum limit and omitting outliers

Table B-3. Number of Hypocenters* Associated with Faults, by Magnitude

Fault Type & Number		Magnitude Category													
		≤.5	.51-1	1.01-1.5	1.51-2	2.01-2.5	2.51-3	3.01-3.5	3.51-4	4.01-4.5	4.51-5	5.01-5.5	5.51-6	≥6	Total
A14-1	Count	11	3	9	6	3	2	2	0	0	0	0	0	0	36
	Percent	30.6	8.3	25.0	16.7	8.3	5.6	5.6	0.0	0.0	0.0	0.0	0.0	0.0	100.0
A29-1	Count	1	17	12	35	23	6	0	0	0	0	0	0	0	94
	Percent	1.1	18.1	12.8	37.2	24.5	6.4	0.0	0.0	0.0	0.0	0.0	0.0	0.0	100.0
A29-5	Count	5	10	14	29	23	9	0	1	0	0	0	0	0	91
	Percent	5.5	11.0	15.4	31.9	25.3	9.9	0.0	1.1	0.0	0.0	0.0	0.0	0.0	100.0
A33-1c	Count	22	36	30	58	28	8	1	0	0	0	0	0	0	183
	Percent	12.0	19.7	16.4	31.7	15.3	4.4	0.5	0.0	0.0	0.0	0.0	0.0	0.0	100.0
A34-5	Count	14	21	26	31	20	11	5	1	0	0	0	0	0	129
	Percent	10.9	16.3	20.2	24.0	15.5	8.5	3.9	0.8	0.0	0.0	0.0	0.0	0.0	100.0
A36-2	Count	92	90	58	131	73	25	6	4	0	2	0	0	0	481
	Percent	19.1	18.7	12.1	27.2	15.2	5.2	1.2	0.8	0.0	0.4	0.0	0.0	0.0	100.0
A37-1	Count	6	8	8	15	11	6	4	0	0	0	0	0	0	58
	Percent	10.3	13.8	13.8	25.9	19.0	10.3	6.9	0.0	0.0	0.0	0.0	0.0	0.0	100.0
A40-4	Count	2	12	6	13	3	1	4	0	0	1	0	0	0	42
	Percent	4.8	28.6	14.3	31.0	7.1	2.4	9.5	0.0	0.0	2.4	0.0	0.0	0.0	100.0
A40-6	Count	6	13	28	69	24	12	2	1	0	0	0	0	0	155
	Percent	3.9	8.4	18.1	44.5	15.5	7.7	1.3	0.6	0.0	0.0	0.0	0.0	0.0	100.0
A40-9	Count	11	13	10	7	9	0	1	1	0	0	0	0	0	52
	Percent	21.2	25.0	19.2	13.5	17.3	0.0	1.9	1.9	0.0	0.0	0.0	0.0	0.0	100.0
A43-7	Count	3	6	10	36	17	3	1	1	1	0	0	0	0	78
	Percent	3.8	7.7	12.8	46.2	21.8	3.8	1.3	1.3	1.3	0.0	0.0	0.0	0.0	100.0
A44-2b	Count	4	8	8	16	20	6	1	1	0	0	0	0	0	64
	Percent	6.3	12.5	12.5	25.0	31.3	9.4	1.6	1.6	0.0	0.0	0.0	0.0	0.0	100.0
A44-3	Count	13	12	27	40	17	12	2	0	0	0	0	0	0	123
	Percent	10.6	9.8	22.0	32.5	13.8	9.8	1.6	0.0	0.0	0.0	0.0	0.0	0.0	100.0

Fault Type & Number		Magnitude Category													
		≤.5	.51-1	1.01-1.5	1.51-2	2.01-2.5	2.51-3	3.01-3.5	3.51-4	4.01-4.5	4.51-5	5.01-5.5	5.51-6	≥6	Total
A44-4	Count	45	24	27	20	11	3	2	1	0	0	0	0	0	133
	Percent	33.8	18.0	20.3	15.0	8.3	2.3	1.5	0.8	0.0	0.0	0.0	0.0	0.0	100.0
A44-5	Count	24	25	22	31	170	187	44	13	5	0	1	0	0	522
	Percent	4.6	4.8	4.2	5.9	32.6	35.8	8.4	2.5	1.0	0.0	0.2	0.0	0.0	100.0
A50-1	Count	135	113	61	38	17	18	6	0	0	0	0	0	0	388
	Percent	34.8	29.1	15.7	9.8	4.4	4.6	1.5	0.0	0.0	0.0	0.0	0.0	0.0	100.0
A50-2	Count	11	13	30	20	10	6	0	0	0	0	0	0	0	90
	Percent	12.2	14.4	33.3	22.2	11.1	6.7	0.0	0.0	0.0	0.0	0.0	0.0	0.0	100.0
A51-1	Count	25	42	49	36	28	10	2	0	0	0	0	0	0	192
	Percent	13.0	21.9	25.5	18.8	14.6	5.2	1.0	0.0	0.0	0.0	0.0	0.0	0.0	100.0
A51-2	Count	42	34	103	74	31	7	2	0	0	0	0	0	0	293
	Percent	14.3	11.6	35.2	25.3	10.6	2.4	0.7	0.0	0.0	0.0	0.0	0.0	0.0	100.0
A52-1	Count	8	13	17	15	6	5	1	0	0	0	0	0	0	65
	Percent	12.3	20.0	26.2	23.1	9.2	7.7	1.5	0.0	0.0	0.0	0.0	0.0	0.0	100.0
A52-2	Count	3	7	16	28	12	5	0	0	0	0	0	0	0	71
	Percent	4.2	9.9	22.5	39.4	16.9	7.0	0.0	0.0	0.0	0.0	0.0	0.0	0.0	100.0
A52-3	Count	3	17	18	24	14	4	3	2	0	0	0	0	0	85
	Percent	3.5	20.0	21.2	28.2	16.5	4.7	3.5	2.4	0.0	0.0	0.0	0.0	0.0	100.0
A53-2	Count	3	33	38	8	4	0	0	0	0	0	0	0	0	86
	Percent	3.5	38.4	44.2	9.3	4.7	0.0	0.0	0.0	0.0	0.0	0.0	0.0	0.0	100.0
A58-1	Count	16	25	22	17	18	4	2	0	0	0	0	0	0	104
	Percent	15.4	24.0	21.2	16.3	17.3	3.8	1.9	0.0	0.0	0.0	0.0	0.0	0.0	100.0
A58-2	Count	4	77	42	48	18	16	1	5	2	0	0	0	0	213
	Percent	1.9	36.2	19.7	22.5	8.5	7.5	0.5	2.3	0.9	0.0	0.0	0.0	0.0	100.0
A58-6	Count	38	46	76	111	84	37	5	2	0	0	0	0	0	399
	Percent	9.5	11.5	19.0	27.8	21.1	9.3	1.3	0.5	0.0	0.0	0.0	0.0	0.0	100.0
A59-1	Count	37	89	122	97	58	20	6	1	2	0	0	0	0	432
	Percent	8.6	20.6	28.2	22.5	13.4	4.6	1.4	0.2	0.5	0.0	0.0	0.0	0.0	100.0

Fault Type & Number		Magnitude Category													
		≤.5	.51-1	1.01-1.5	1.51-2	2.01-2.5	2.51-3	3.01-3.5	3.51-4	4.01-4.5	4.51-5	5.01-5.5	5.51-6	≥6	Total
A59-3	Count	7	8	12	15	8	5	1	0	0	0	0	0	0	56
	Percent	12.5	14.3	21.4	26.8	14.3	8.9	1.8	0.0	0.0	0.0	0.0	0.0	0.0	100.0
A60-2	Count	22	74	148	154	44	15	4	1	0	0	0	0	0	462
	Percent	4.8	16.0	32.0	33.3	9.5	3.2	0.9	0.2	0.0	0.0	0.0	0.0	0.0	100.0
A61-1a	Count	35	85	152	155	76	41	15	3	0	2	0	0	0	564
	Percent	6.2	15.1	27.0	27.5	13.5	7.3	2.7	0.5	0.0	0.4	0.0	0.0	0.0	100.0
A64-1	Count	371	581	657	457	171	47	16	7	0	2	0	1	0	2,310
	Percent	16.1	25.2	28.4	19.8	7.4	2.0	0.7	0.3	0.0	0.1	0.0	0.0	0.0	100.0
A64-2	Count	29	48	40	34	23	4	0	0	0	0	0	0	0	178
	Percent	16.3	27.0	22.5	19.1	12.9	2.2	0.0	0.0	0.0	0.0	0.0	0.0	0.0	100.0
A64-4	Count	640	815	1,060	634	259	108	33	5	4	0	0	0	0	3,558
	Percent	18.0	22.9	29.8	17.8	7.3	3.0	0.9	0.1	0.1	0.0	0.0	0.0	0.0	100.0
A64-2	Count	29	48	40	34	23	4	0	0	0	0	0	0	0	178
		16.3	27.0	22.5	19.1	12.9	2.2	0.0	0.0	0.0	0.0	0.0	0.0	0.0	100.0
A64-5	Count	99	92	91	71	39	13	3	1	1	0	0	0	0	A64-5
	Percent	24.1	22.4	22.2	17.3	9.5	3.2	0.7	0.2	0.2	0.0	0.0	0.0	0.0	100.0
A64-6	Count	15	17	24	29	13	4	3	0	0	0	0	0	0	105
	Percent	14.3	16.2	22.9	27.6	12.4	3.8	2.9	0.0	0.0	0.0	0.0	0.0	0.0	100.0
A64-7	Count	84	73	82	43	20	5	4	0	0	0	0	0	0	311
	Percent	27.0	23.5	26.4	13.8	6.4	1.6	1.3	0.0	0.0	0.0	0.0	0.0	0.0	100.0
A64-8	Count	10	8	4	8	4	3	1	0	0	0	0	0	0	38
	Percent	26.3	21.1	10.5	21.1	10.5	7.9	2.6	0.0	0.0	0.0	0.0	0.0	0.0	100.0
A65-2	Count	5	18	27	29	16	7	1	0	0	0	0	0	0	103
	Percent	4.9	17.5	26.2	28.2	15.5	6.8	1.0	0.0	0.0	0.0	0.0	0.0	0.0	100.0
A65-3	Count	2	5	9	16	11	7	2	0	0	0	0	0	0	52
	Percent	3.8	9.6	17.3	30.8	21.2	13.5	3.8	0.0	0.0	0.0	0.0	0.0	0.0	100.0
A65-5	Count	9	6	15	13	7	3	0	0	0	0	0	0	0	53
	Percent	17.0	11.3	28.3	24.5	13.2	5.7	0.0	0.0	0.0	0.0	0.0	0.0	0.0	100.0

Fault Type & Number		Magnitude Category													
		≤.5	.51-1	1.01-1.5	1.51-2	2.01-2.5	2.51-3	3.01-3.5	3.51-4	4.01-4.5	4.51-5	5.01-5.5	5.51-6	≥6	Total
A65-6	Count	9	8	30	75	20	12	9	1	0	0	1	0	0	165
	Percent	5.5	4.8	18.2	45.5	12.1	7.3	5.5	0.6	0.0	0.0	0.6	0.0	0.0	100.0
A65-8	Count	119	226	349	651	450	401	252	39	10	1	2	1	1	2,502
	Percent	4.8	9.0	13.9	26.0	18.0	16.0	10.1	1.6	0.4	0.0	0.1	0.0	0.0	100.0
A70-1	Count	8	11	39	14	10	2	1	0	0	0	0	0	0	85
	Percent	9.4	12.9	45.9	16.5	11.8	2.4	1.2	0.0	0.0	0.0	0.0	0.0	0.0	100.0
A70-4	Count	65	105	77	78	52	25	4	5	1	1	0	0	0	413
	Percent	15.7	25.4	18.6	18.9	12.6	6.1	1.0	1.2	0.2	0.2	0.0	0.0	0.0	100.0
A71-1	Count	15	25	23	57	28	10	2	0	0	0	0	0	0	160
	Percent	9.4	15.6	14.4	35.6	17.5	6.3	1.3	0.0	0.0	0.0	0.0	0.0	0.0	100.0
A71-2	Count	17	20	21	21	9	1	1	0	0	0	0	0	0	90
	Percent	18.9	22.2	23.3	23.3	10.0	1.1	1.1	0.0	0.0	0.0	0.0	0.0	0.0	100.0
A71-3b	Count	19	20	20	25	11	4	1	0	0	0	0	0	0	100
	Percent	19.0	20.0	20.0	25.0	11.0	4.0	1.0	0.0	0.0	0.0	0.0	0.0	0.0	100.0
A71-4	Count	41	60	65	85	49	13	8	1	0	0	0	0	0	322
	Percent	12.7	18.6	20.2	26.4	15.2	4.0	2.5	0.3	0.0	0.0	0.0	0.0	0.0	100.0
A71-5	Count	13	33	40	45	15	15	6	1	1	0	0	0	0	169
	Percent	7.7	19.5	23.7	26.6	8.9	8.9	3.6	0.6	0.6	0.0	0.0	0.0	0.0	100.0
A71-6	Count	3	13	19	27	15	12	0	0	0	0	0	0	0	89
	Percent	3.4	14.6	21.3	30.3	16.9	13.5	0.0	0.0	0.0	0.0	0.0	0.0	0.0	100.0
A71-7	Count	10	33	24	48	31	16	5	1	0	1	0	0	0	169
	Percent	5.9	19.5	14.2	28.4	18.3	9.5	3.0	0.6	0.0	0.6	0.0	0.0	0.0	100.0
A71-8	Count	98	111	98	130	77	25	10	7	0	0	0	0	0	556
	Percent	17.6	20.0	17.6	23.4	13.8	4.5	1.8	1.3	0.0	0.0	0.0	0.0	0.0	100.0
A71-9	Count	19	35	36	39	23	4	6	0	0	0	0	0	0	162
	Percent	11.7	21.6	22.2	24.1	14.2	2.5	3.7	0.0	0.0	0.0	0.0	0.0	0.0	100.0
A71-12	Count	6	10	13	10	9	6	2	0	0	0	0	0	0	56
	Percent	10.7	17.9	23.2	17.9	16.1	10.7	3.6	0.0	0.0	0.0	0.0	0.0	0.0	100.0

Fault Type & Number		Magnitude Category													
		≤.5	.51-1	1.01-1.5	1.51-2	2.01-2.5	2.51-3	3.01-3.5	3.51-4	4.01-4.5	4.51-5	5.01-5.5	5.51-6	≥6	Total
A72-1	Count	20	90	104	123	74	37	14	5	0	0	0	0	0	467
	Percent	4.3	19.3	22.3	26.3	15.8	7.9	3.0	1.1	0.0	0.0	0.0	0.0	0.0	100.0
A72-2	Count	6	35	42	43	26	13	3	1	0	0	0	0	0	169
	Percent	3.6	20.7	24.9	25.4	15.4	7.7	1.8	0.6	0.0	0.0	0.0	0.0	0.0	100.0
A72-3	Count	5	18	17	10	9	9	1	4	0	0	0	0	0	73
	Percent	6.8	24.7	23.3	13.7	12.3	12.3	1.4	5.5	0.0	0.0	0.0	0.0	0.0	100.0
A72-4	Count	22	26	26	22	11	2	3	0	0	0	0	0	0	112
	Percent	19.6	23.2	23.2	19.6	9.8	1.8	2.7	0.0	0.0	0.0	0.0	0.0	0.0	100.0
A75-2	Count	72	52	61	67	34	10	0	0	1	0	0	0	0	297
	Percent	24.2	17.5	20.5	22.6	11.4	3.4	0.0	0.0	0.3	0.0	0.0	0.0	0.0	100.0
A75-3	Count	319	300	447	356	189	78	27	10	2	1	0	0	0	1,729
	Percent	18.4	17.4	25.9	20.6	10.9	4.5	1.6	0.6	0.1	0.1	0.0	0.0	0.0	100.0
A75-4	Count	97	93	111	62	34	18	5	3	0	0	0	0	0	423
	Percent	22.9	22.0	26.2	14.7	8.0	4.3	1.2	0.7	0.0	0.0	0.0	0.0	0.0	100.0
A75-5	Count	38	51	87	43	19	15	2	5	0	0	0	0	0	260
	Percent	14.6	19.6	33.5	16.5	7.3	5.8	0.8	1.9	0.0	0.0	0.0	0.0	0.0	100.0
A75-7	Count	35	21	29	22	15	3	3	0	0	0	0	0	0	128
	Percent	27.3	16.4	22.7	17.2	11.7	2.3	2.3	0.0	0.0	0.0	0.0	0.0	0.0	100.0
A76-1	Count	88	76	100	61	21	13	1	0	0	1	0	0	0	361
	Percent	24.4	21.1	27.7	16.9	5.8	3.6	0.3	0.0	0.0	0.3	0.0	0.0	0.0	100.0
A76-2	Count	3	6	14	9	14	2	0	0	0	0	0	0	0	48
	Percent	6.3	12.5	29.2	18.8	29.2	4.2	0.0	0.0	0.0	0.0	0.0	0.0	0.0	100.0
A76-3	Count	23	18	27	29	13	3	0	3	0	0	0	0	0	116
	Percent	19.8	15.5	23.3	25.0	11.2	2.6	0.0	2.6	0.0	0.0	0.0	0.0	0.0	100.0
A76-5	Count	152	150	227	126	37	23	4	2	0	0	0	0	0	721
	Percent	21.1	20.8	31.5	17.5	5.1	3.2	0.6	0.3	0.0	0.0	0.0	0.0	0.0	100.0
A76-8	Count	520	464	480	350	154	65	19	7	1	0	0	0	0	2,060
	Percent	25.2	22.5	23.3	17.0	7.5	3.2	0.9	0.3	0.0	0.0	0.0	0.0	0.0	100.0

Fault Type & Number		Magnitude Category													
		≤.5	.51-1	1.01-1.5	1.51-2	2.01-2.5	2.51-3	3.01-3.5	3.51-4	4.01-4.5	4.51-5	5.01-5.5	5.51-6	≥6	Total
A76-9a	Count	37	51	46	35	9	5	2	0	1	0	0	0	0	186
	Percent	19.9	27.4	24.7	18.8	4.8	2.7	1.1	0.0	0.5	0.0	0.0	0.0	0.0	100.0
A76-9b	Count	253	252	289	254	155	73	19	8	2	1	0	0	0	1,306
	Percent	19.4	19.3	22.1	19.4	11.9	5.6	1.5	0.6	0.2	0.1	0.0	0.0	0.0	100.0
A76-14a	Count	32	36	54	140	140	46	11	3	1	0	1	0	0	464
	Percent	6.9	7.8	11.6	30.2	30.2	9.9	2.4	0.6	0.2	0.0	0.2	0.0	0.0	100.0
A76-15	Count	89	95	109	114	68	27	5	1	1	0	0	0	0	509
	Percent	17.5	18.7	21.4	22.4	13.4	5.3	1.0	0.2	0.2	0.0	0.0	0.0	0.0	100.0
A76-17	Count	4	40	57	184	247	78	27	12	3	0	0	0	0	652
	Percent	0.6	6.1	8.7	28.2	37.9	12.0	4.1	1.8	0.5	0.0	0.0	0.0	0.0	100.0
A77-2	Count	10	9	22	8	8	3	0	0	0	0	0	0	0	60
	Percent	16.7	15.0	36.7	13.3	13.3	5.0	0.0	0.0	0.0	0.0	0.0	0.0	0.0	100.0
A77-5	Count	3	10	17	15	20	5	7	0	0	0	0	0	0	77
	Percent	3.9	13.0	22.1	19.5	26.0	6.5	9.1	0.0	0.0	0.0	0.0	0.0	0.0	100.0
A77-6	Count	2,892	2,158	2,326	1,740	1,370	647	160	32	9	1	0	0	0	11,335
	Percent	25.5	19.0	20.5	15.4	12.1	5.7	1.4	0.3	0.1	0.0	0.0	0.0	0.0	100.0
A77-8	Count	14	72	113	368	529	262	83	26	9	1	0	0	0	1,477
	Percent	0.9	4.9	7.7	24.9	35.8	17.7	5.6	1.8	0.6	0.1	0.0	0.0	0.0	100.0
A79-1	Count	26	11	6	3	2	2	1	0	0	0	0	0	0	51
	Percent	51.0	21.6	11.8	5.9	3.9	3.9	2.0	0.0	0.0	0.0	0.0	0.0	0.0	100.0
A80-1	Count	46	49	27	16	23	7	2	1	0	0	0	0	0	171
	Percent	26.9	28.7	15.8	9.4	13.5	4.1	1.2	0.6	0.0	0.0	0.0	0.0	0.0	100.0
A80-2	Count	45	62	58	47	28	13	4	1	0	0	0	0	0	258
	Percent	17.4	24.0	22.5	18.2	10.9	5.0	1.6	0.4	0.0	0.0	0.0	0.0	0.0	100.0
A80-3	Count	38	53	60	32	39	18	4	5	1	0	0	1	0	251
	Percent	15.1	21.1	23.9	12.7	15.5	7.2	1.6	2.0	0.4	0.0	0.0	0.4	0.0	100.0

Fault Type & Number		Magnitude Category													
		≤.5	.51-1	1.01-1.5	1.51-2	2.01-2.5	2.51-3	3.01-3.5	3.51-4	4.01-4.5	4.51-5	5.01-5.5	5.51-6	≥6	Total
A81-1	Count	3	9	25	169	291	132	46	14	7	0	0	0	0	696
	Percent	0.4	1.3	3.6	24.3	41.8	19.0	6.6	2.0	1.0	0.0	0.0	0.0	0.0	100.0
A81-2	Count	26	29	45	57	41	32	13	1	0	0	0	0	0	244
	Percent	10.7	11.9	18.4	23.4	16.8	13.1	5.3	0.4	0.0	0.0	0.0	0.0	0.0	100.0
A81-3	Count	7	11	10	14	3	2	1	0	0	0	0	0	0	48
	Percent	14.6	22.9	20.8	29.2	6.3	4.2	2.1	0.0	0.0	0.0	0.0	0.0	0.0	100.0
A86-1	Count	6	11	11	9	17	14	2	2	0	0	0	0	0	72
	Percent	8.3	15.3	15.3	12.5	23.6	19.4	2.8	2.8	0.0	0.0	0.0	0.0	0.0	100.0
A87-2	Count	132	178	335	395	138	68	18	5	1	0	0	0	0	1,270
	Percent	10.4	14.0	26.4	31.1	10.9	5.4	1.4	0.4	0.1	0.0	0.0	0.0	0.0	100.0
A87-3	Count	43	44	22	28	21	16	5	0	0	0	0	0	0	179
	Percent	24.0	24.6	12.3	15.6	11.7	8.9	2.8	0.0	0.0	0.0	0.0	0.0	0.0	100.0
A87-4	Count	27	54	37	51	29	18	4	1	0	0	0	0	0	221
	Percent	12.2	24.4	16.7	23.1	13.1	8.1	1.8	0.5	0.0	0.0	0.0	0.0	0.0	100.0
A91-3	Count	141	77	38	66	44	18	3	1	0	0	0	0	0	388
	Percent	36.3	19.8	9.8	17.0	11.3	4.6	0.8	0.3	0.0	0.0	0.0	0.0	0.0	100.0
A95-2	Count	25	37	31	38	19	6	3	0	0	0	0	0	0	159
	Percent	15.7	23.3	19.5	23.9	11.9	3.8	1.9	0.0	0.0	0.0	0.0	0.0	0.0	100.0
A98-1	Count	24	195	329	174	82	26	13	2	0	1	0	0	0	846
	Percent	2.8	23.0	38.9	20.6	9.7	3.1	1.5	0.2	0.0	0.1	0.0	0.0	0.0	100.0
A99-2	Count	26	23	31	10	12	5	3	0	0	0	0	0	0	110
	Percent	23.6	20.9	28.2	9.1	10.9	4.5	2.7	0.0	0.0	0.0	0.0	0.0	0.0	100.0
A99-3a	Count	4	13	20	6	5	2	0	0	0	0	0	0	0	50
	Percent	8.0	26.0	40.0	12.0	10.0	4.0	0.0	0.0	0.0	0.0	0.0	0.0	0.0	100.0
A99-3b	Count	8	14	16	3	3	1	1	0	0	0	0	0	0	46
	Percent	17.4	30.4	34.8	6.5	6.5	2.2	2.2	0.0	0.0	0.0	0.0	0.0	0.0	100.0
A99-4	Count	25	11	30	18	8	3	1	2	0	0	0	0	0	98
	Percent	25.5	11.2	30.6	18.4	8.2	3.1	1.0	2.0	0.0	0.0	0.0	0.0	0.0	100.0

Fault Type & Number		Magnitude Category													
		≤.5	.51-1	1.01-1.5	1.51-2	2.01-2.5	2.51-3	3.01-3.5	3.51-4	4.01-4.5	4.51-5	5.01-5.5	5.51-6	≥6	Total
A101-1b	Count	40	34	49	34	21	5	1	1	0	0	0	0	0	185
	Percent	21.6	18.4	26.5	18.4	11.4	2.7	0.5	0.5	0.0	0.0	0.0	0.0	0.0	100.0
A101-2	Count	179	82	33	14	8	1	0	0	0	0	0	0	0	317
	Percent	56.5	25.9	10.4	4.4	2.5	0.3	0.0	0.0	0.0	0.0	0.0	0.0	0.0	100.0
A102-4	Count	7	13	13	29	59	109	52	3	6	2	0	1	0	294
	Percent	2.4	4.4	4.4	9.9	20.1	37.1	17.7	1.0	2.0	0.7	0.0	0.3	0.0	100.0
A102-5	Count	2	1	2	27	88	86	11	3	0	0	0	0	0	220
	Percent	0.9	0.5	0.9	12.3	40.0	39.1	5.0	1.4	0.0	0.0	0.0	0.0	0.0	100.0
A106-1	Count	1754	2261	2480	1619	794	322	88	39	3	2	0	0	0	9,362
	Percent	18.7	24.2	26.5	17.3	8.5	3.4	0.9	0.4	0.0	0.0	0.0	0.0	0.0	100.0
A106-3	Count	86	48	49	26	23	4	2	1	0	0	0	0	0	239
	Percent	36.0	20.1	20.5	10.9	9.6	1.7	0.8	0.4	0.0	0.0	0.0	0.0	0.0	100.0
A106-4	Count	994	2359	3396	2211	2397	517	110	19	6	3	0	1	0	12,013
	Percent	8.3	19.6	28.3	18.4	20.0	4.3	0.9	0.2	0.0	0.0	0.0	0.0	0.0	100.0
A112-1	Count	1	7	17	22	20	5	3	0	0	0	0	0	0	75
	Percent	1.3	9.3	22.7	29.3	26.7	6.7	4.0	0.0	0.0	0.0	0.0	0.0	0.0	100.0
A114-1	Count	0	7	36	56	42	18	3	0	1	0	0	0	0	163
	Percent	0.0	4.3	22.1	34.4	25.8	11.0	1.8	0.0	0.6	0.0	0.0	0.0	0.0	100.0
B30-1	Count	41	37	36	50	22	20	4	2	0	0	0	0	0	212
	Percent	19.3	17.5	17.0	23.6	10.4	9.4	1.9	0.9	0.0	0.0	0.0	0.0	0.0	100.0
B40-2	Count	4	18	31	87	11	4	2	3	0	0	0	0	0	160
	Percent	2.5	11.3	19.4	54.4	6.9	2.5	1.3	1.9	0.0	0.0	0.0	0.0	0.0	100.0
B40-3	Count	7	15	7	16	4	5	1	0	0	0	0	0	0	55
	Percent	12.7	27.3	12.7	29.1	7.3	9.1	1.8	0.0	0.0	0.0	0.0	0.0	0.0	100.0
B52-4	Count	3	17	19	25	10	0	4	0	0	0	0	0	0	78
	Percent	3.8	21.8	24.4	32.1	12.8	0.0	5.1	0.0	0.0	0.0	0.0	0.0	0.0	100.0

Fault Type & Number		Magnitude Category													
		≤.5	.51-1	1.01-1.5	1.51-2	2.01-2.5	2.51-3	3.01-3.5	3.51-4	4.01-4.5	4.51-5	5.01-5.5	5.51-6	≥6	Total
B60-1	Count	6	21	40	40	21	8	3	0	0	0	0	0	0	139
	Percent	4.3	15.1	28.8	28.8	15.1	5.8	2.2	0.0	0.0	0.0	0.0	0.0	0.0	100.0
B64-1	Count	9	39	54	148	71	32	15	3	1	0	0	0	0	372
	Percent	2.4	10.5	14.5	39.8	19.1	8.6	4.0	0.8	0.3	0.0	0.0	0.0	0.0	100.0
B64-2	Count	23	461	1,833	1,771	785	276	73	14	5	1	0	0	0	5,242
	Percent	0.4	8.8	35.0	33.8	15.0	5.3	1.4	0.3	0.1	0.0	0.0	0.0	0.0	100.0
B64-3	Count	11	14	21	22	23	1	0	1	0	0	0	0	0	93
	Percent	11.8	15.1	22.6	23.7	24.7	1.1	0.0	1.1	0.0	0.0	0.0	0.0	0.0	100.0
B65-2	Count	21	52	57	66	45	23	9	1	3	0	0	0	0	277
	Percent	7.6	18.8	20.6	23.8	16.2	8.3	3.2	0.4	1.1	0.0	0.0	0.0	0.0	100.0
B65-4	Count	9	13	5	7	7	3	0	0	0	0	0	0	0	44
	Percent	20.5	29.5	11.4	15.9	15.9	6.8	0.0	0.0	0.0	0.0	0.0	0.0	0.0	100.0
B71-1	Count	45	54	69	119	65	23	12	2	0	0	0	0	0	389
	Percent	11.6	13.9	17.7	30.6	16.7	5.9	3.1	0.5	0.0	0.0	0.0	0.0	0.0	100.0
B72-2	Count	19	32	24	17	16	8	0	0	0	0	0	0	0	116
	Percent	16.4	27.6	20.7	14.7	13.8	6.9	0.0	0.0	0.0	0.0	0.0	0.0	0.0	100.0
B72-5	Count	30	30	34	37	14	5	3	0	0	0	0	0	0	153
	Percent	19.6	19.6	22.2	24.2	9.2	3.3	2.0	0.0	0.0	0.0	0.0	0.0	0.0	100.0
B76-1	Count	135	99	99	70	31	5	4	1	0	0	1	0	0	445
	Percent	30.3	22.2	22.2	15.7	7.0	1.1	0.9	0.2	0.0	0.0	0.2	0.0	0.0	100.0
B76-4	Count	23	20	25	20	15	4	4	2	0	0	0	0	0	113
	Percent	20.4	17.7	22.1	17.7	13.3	3.5	3.5	1.8	0.0	0.0	0.0	0.0	0.0	100.0
B76-6	Count	3	20	47	202	343	149	51	13	1	1	0	0	0	830
	Percent	0.4	2.4	5.7	24.3	41.3	18.0	6.1	1.6	0.1	0.1	0.0	0.0	0.0	100.0
B76-7	Count	2	5	17	26	23	3	3	2	0	0	0	0	0	81
	Percent	2.5	6.2	21.0	32.1	28.4	3.7	3.7	2.5	0.0	0.0	0.0	0.0	0.0	100.0
B76-9	Count	137	109	87	54	31	13	8	3	0	0	0	0	0	442
	Percent	31.0	24.7	19.7	12.2	7.0	2.9	1.8	0.7	0.0	0.0	0.0	0.0	0.0	100.0

Fault Type & Number		Magnitude Category													
		≤.5	.51-1	1.01-1.5	1.51-2	2.01-2.5	2.51-3	3.01-3.5	3.51-4	4.01-4.5	4.51-5	5.01-5.5	5.51-6	≥6	Total
B79-1	Count	733	1304	1,011	602	260	74	19	10	7	3	0	1	0	4,024
	Percent	18.2	32.4	25.1	15.0	6.5	1.8	0.5	0.2	0.2	0.1	0.0	0.0	0.0	100.0
B80-1	Count	64	73	56	42	39	38	21	10	2	2	0	0	0	347
	Percent	18.4	21.0	16.1	12.1	11.2	11.0	6.1	2.9	0.6	0.6	0.0	0.0	0.0	100.0
B82-1	Count	233	161	167	106	69	37	12	4	2	0	0	0	0	791
	Percent	29.5	20.4	21.1	13.4	8.7	4.7	1.5	0.5	0.3	0.0	0.0	0.0	0.0	100.0
B101-2	Count	5	10	15	13	8	3	0	0	0	0	0	0	0	54
	Percent	9.3	18.5	27.8	24.1	14.8	5.6	0.0	0.0	0.0	0.0	0.0	0.0	0.0	100.0
All	**Count**	**12,366**	**15,767**	**19,829**	**16,911**	**11,608**	**4,852**	**1,531**	**400**	**103**	**30**	**6**	**6**	**1**	**83,410**
	Percent	**14.8**	**18.9**	**23.8**	**20.3**	**13.9**	**5.8**	**1.8**	**0.5**	**0.1**	**0.0**	**0.0**	**0.0**	**0.0**	**100.0**

*After imposing the 50-hypocenter minimum limit and omitting outliers.

Table B-4. Number of Hypocenters* Associated with Faults, by Magnitude and Depth

Magnitude Category		Depth Category (km)					
		<1	1-4.99	5-9.99	10-14.99	≥15	Total
.01 - .49	Count	88	1,328	6,439	4,068	443	12,366
	Row %	0.7	10.7	52.1	32.9	3.6	100.0
	Column %	15.3	25.7	15.1	12.9	12.2	14.8
	% of Total	0.1	1.6	7.7	4.9	0.5	14.8
.5 - 1	Count	96	1,316	8,768	5,023	564	15,767
	Row %	0.6	8.3	55.6	31.9	3.6	100.0
	Column %	16.7	25.5	20.6	15.9	15.5	18.9
	% of Total	0.1	1.6	10.5	6.0	0.7	18.9
1.01 - 1.5	Count	98	1,056	10,856	7,150	669	19,829
	Row %	0.5	5.3	54.7	36.1	3.4	100.0
	Column %	17.1	20.5	25.5	22.7	18.4	23.8
	% of Total	0.1	1.3	13.0	8.6	0.8	23.8
1.51 - 2	Count	87	585	7,773	7,554	912	16,911
	Row %	0.5	3.5	46.0	44.7	5.4	100.0
	Column %	15.2	11.3	18.3	24.0	25.1	20.3
	% of Total	0.1	0.7	9.3	9.1	1.1	20.3
2.01 - 2.5	Count	108	546	5,567	4,793	594	11,608
	Row %	0.9	4.7	48.0	41.3	5.1	100.0
	Column %	18.8	10.6	13.1	15.2	16.3	13.9
	% of Total	0.1	0.7	6.7	5.7	0.7	13.9
2.51 - 3	Count	85	242	2,281	1,977	267	4,852
	Row %	1.8	5.0	47.0	40.7	5.5	100.0
	Column %	14.8	4.7	5.4	6.3	7.3	5.8
	% of Total	0.1	0.3	2.7	2.4	0.3	5.8
3.01 - 3.5	Count	9	67	668	678	109	1,531
	Row %	0.6	4.4	43.6	44.3	7.1	100.0
	Column %	1.6	1.3	1.6	2.2	3.0	1.8
	% of Total	0.0	0.1	0.8	0.8	0.1	1.8
4.01 - 4.5	Count	3	14	133	193	57	400
	Row %	0.8	3.5	33.3	48.3	14.3	100.0
	Column %	0.5	0.3	0.3	0.6	1.6	0.5
	% of Total	0.0	0.0	0.2	0.2	0.1	0.5
4.51 - 5	Count	0	4	39	45	15	103
	Row %	0.0	3.9	37.9	43.7	14.6	100.0
	Column %	0.0	0.1	0.1	0.1	0.4	0.1
	% of Total	0.0	0.0	0.0	0.1	0.0	0.1

Magnitude Category		Depth Category (km)					
		<1	1-4.99	5-9.99	10-14.99	≥15	Total
5.01 - 5.5	Count	0	0	2	3	1	6
	Row %	0.0	0.0	33.3	50.0	16.7	100.0
	Column %	0.0	0.0	0.0	0.0	0.0	0.0
	% of Total	0.0	0.0	0.0	0.0	0.0	0.0
5.51 - 6	Count	0	1	3	1	1	6
	Row %	0.0	16.7	50.0	16.7	16.7	100.0
	Column %	0.0	0.0	0.0	0.0	0.0	0.0
	% of Total	0.0	0.0	0.0	0.0	0.0	0.0
6.01 - 6.5	Count	0	0	1	0	0	1
	Row %	0.0	0.0	100.0	0.0	0.0	100.0
	Column %	0.0	0.0	0.0	0.0	0.0	0.0
	% of Total	0.0	0.0	0.0	0.0	0.0	0.0
All	**Count**	**574**	**5,161**	**42,536**	**31,504**	**3,635**	**83,410**
	Column %	**0.7**	**6.2**	**51.0**	**37.8**	**4.4**	**100.0**
	% of Total	**100.0**	**100.0**	**100.0**	**100.0**	**100.0**	**100.0**

*After imposing the 50-hypocenter minimum limit and omitting outliers.

Table B-5. Pairwise Correlation between Hypocenter Depth, Earthquake Magnitude, and Normal Distance between Hypocenter and Fault Plane, by Fault.

Fault Type & Number	Number of Hypocenters	Correlation*		
		Depth vs Magnitude**	Depth vs Distance	Magnitude** vs Distance
A14-1	53	-0.055	-0.098	0.131
A29-1	99	0.454	-0.142	0.074
A29-5	100	0.100	-0.295	0.054
A33-1c	188	-0.147	0.124	-0.128
A34-5	137	0.046	0.246	0.204
A36-2	524	0.447	0.182	0.047
A37-1	61	0.070	0.304	-0.111
A40-4	47	0.419	-0.091	-0.072
A40-6	165	0.022	0.364	-0.085
A40-9	65	0.391	0.118	-0.099
A43-7	84	0.282	-0.329	-0.231
A44-2b	67	-0.007	0.248	-0.073
A44-3	135	0.430	-0.133	0.186
A44-4	154	0.457	-0.006	-0.128
A44-5	535	-0.030	0.167	0.131
A50-1	410	0.406	0.307	0.240
A50-2	94	0.567	-0.125	0.164
A51-1	196	0.287	-0.356	-0.180
A51-2	314	0.264	-0.319	-0.039
A52-1	67	0.164	0.008	-0.351
A52-2	74	-0.195	-0.050	-0.313
A52-3	87	0.023	-0.331	0.123
A53-2	89	0.101	-0.227	-0.054
A58-1	107	0.263	-0.559	-0.106
A58-2	219	-0.095	-0.433	0.179
A58-6	454	0.062	-0.351	0.069
A59-1	514	0.105	-0.287	-0.003
A59-3	60	0.210	0.131	0.263
A60-2	477	0.044	-0.047	-0.044
A61-1a	600	-0.093	0.325	-0.181
A64-1	2569	-0.197	-0.329	0.063
A64-2	188	0.203	0.458	0.219
A64-4	4059	0.154	-0.176	0.087
A64-5	570	-0.004	-0.322	-0.128
A64-6	139	-0.129	0.222	-0.046
A64-7	370	-0.140	0.057	0.199
A64-8	53	-0.142	0.189	-0.156
A65-2	103	0.131	0.063	-0.255
A65-3	54	0.187	0.292	-0.109
A65-5	55	-0.108	0.132	0.104
A65-6	179	0.420	0.293	0.282
A65-8	2771	0.129	0.014	0.151
A70-1	88	-0.347	-0.123	0.058
A70-4	442	-0.016	-0.180	-0.133
A71-1	176	0.066	0.062	0.022
A71-2	95	0.043	-0.032	-0.021
A71-3b	102	0.227	0.319	-0.033

Fault Type & Number	Number of Hypocenters	Correlation*		
		Depth vs Magnitude**	Depth vs Distance	Magnitude** vs Distance
A71-4	339	0.409	-0.039	0.044
A71-5	171	-0.008	-0.145	0.169
A71-6	96	0.065	-0.339	-0.035
A71-7	176	-0.030	0.243	-0.035
A71-8	600	-0.061	-0.092	0.068
A71-9	168	0.102	0.010	0.035
A71-12	59	-0.256	-0.099	-0.007
A72-1	475	-0.118	0.150	0.014
A72-2	172	-0.044	0.299	-0.037
A72-3	75	0.034	0.214	0.297
A72-4	125	0.309	-0.239	-0.070
A75-2	330	0.059	0.199	0.014
A75-3	1,858	-0.005	-0.228	0.003
A75-4	503	0.250	-0.063	0.164
A75-5	291	0.194	0.222	0.008
A75-7	149	0.032	0.255	0.164
A76-1	391	0.098	0.815	0.148
A76-2	55	0.035	-0.185	0.056
A76-3	127	0.049	-0.257	-0.382
A76-5	839	0.250	0.053	0.009
A76-8	2,471	0.180	-0.048	-0.036
A76-9a	230	0.318	0.424	-0.096
A76-9b	1,502	0.216	0.028	0.095
A76-14a	475	0.379	-0.352	-0.277
A76-15	532	0.182	-0.058	-0.011
A76-17	663	0.342	0.316	-0.053
A77-2	66	0.248	0.154	0.099
A77-5	85	0.626	-0.277	-0.254
A77-6	14,306	0.504	-0.097	-0.152
A77-8	1,572	0.140	-0.164	0.072
A79-1	66	-0.232	0.447	-0.169
A80-1	183	0.041	-0.219	0.110
A80-2	277	-0.073	0.218	-0.208
A80-3	287	0.403	0.228	0.118
A81-1	713	0.070	0.075	-0.024
A81-2	274	0.323	0.099	-0.210
A81-3	53	-0.125	-0.660	0.231
A86-1	72	-0.063	0.138	0.175
A87-2	1,350	0.127	0.109	-0.131
A87-3	208	0.168	0.142	0.012
A87-4	229	-0.213	-0.019	0.328
A91-3	508	0.164	0.219	-0.078
A95-2	166	-0.040	0.306	-0.105
A98-1	952	-0.065	-0.317	-0.164
A99-2	126	0.032	-0.242	-0.032
A99-3a	58	-0.012	0.001	-0.150
A99-3b	51	0.302	-0.356	-0.260
A99-4	120	0.199	-0.302	-0.200
A101-1b	243	0.145	-0.316	-0.324
A101-2	460	0.423	0.130	0.271

Fault Type & Number	Number of Hypocenters	Correlation*		
		Depth vs Magnitude**	Depth vs Distance	Magnitude** vs Distance
A102-4	319	-0.248	0.468	-0.097
A102-5	232	-0.187	0.220	-0.296
A106-1	10,484	0.058	0.319	-0.055
A106-3	269	-0.081	0.016	-0.019
A106-4	14,155	0.237	0.116	-0.011
A112-1	79	-0.063	-0.001	0.121
A114-1	172	0.490	0.122	0.077
B30-1	236	0.095	0.035	-0.082
B40-2	183	0.289	0.099	0.131
B40-3	71	0.447	0.134	0.171
B52-4	78	-0.231	-0.092	0.018
B60-1	141	0.206	0.507	0.092
B64-1	392	-0.054	0.070	0.159
B64-2	5,308	0.019	-0.231	0.118
B64-3	104	-0.310	-0.131	-0.164
B65-2	292	0.023	-0.087	0.255
B65-4	54	0.057	0.204	-0.238
B71-1	413	0.236	0.000	0.044
B72-2	119	0.193	-0.054	0.154
B72-5	157	0.453	-0.117	-0.101
B76-1	471	-0.156	0.071	-0.046
B76-4	127	0.481	-0.281	-0.126
B76-6	842	0.267	-0.066	-0.047
B76-7	82	0.342	0.259	-0.059
B76-9	494	0.080	0.136	0.136
B79-1	4,222	0.198	0.111	-0.077
B80-1	379	0.415	-0.380	-0.223
B82-1	914	0.264	0.317	-0.040
B101-2	54	-0.159	0.637	-0.090

*Pearson product-moment correlation, r.
**For these calculations of correlation, hypocenters are omitted for which magnitude is missing or negative.

Table B-6. Descriptive Statistics on Hypocenter Distance, by Fault

Fault Type & Number	Fault Name	Fault System	Fault Length (Type I, m)	Fault Length (Type II, m)	Fault Trace Length (Type III, km)	Number* of Attributed Hypocenters			Mean Distance to Fault Plane		
						Side A	Side B	Total	Side A	Side B	Overall
A14-1	Asahikawa-Hurano-sen	Unknown	21468.50	21985	12.9	30	23	53	10315.38	5238.01	8112.00
A29-1	Negishi-seihou	Unknown	7189.16	7171	6.4	97	2	99	15392.10	2903.69	15139.81
A29-5	Oohira	Tsugaru-sanchi-seien	7158.34	9240	10.4	1	99	100	2212.05	7766.18	7710.64
A33-1c	Aratani-shimomura	Kitakami-teichi-seien	49671.89	54644	13.2	5	183	188	5412.90	4283.19	4313.24
A34-5	Yokote, Sugisawa	Yokote-bonchi-seien	21394.22	29298	0.8	16	121	137	3067.01	15168.85	13755.50
A36-2	Nozaki, Urusawa, ?hikizawa	Kitakami-teichi-seien	33890.82	39241	7.6	47	477	524	11925.52	11518.27	11554.79
A37-1	Horuno-Urasawa, Hachimoriyama-higashi	Kitakami-teichi-seien	25603.77	32877	8.4	30	31	61	1035.66	4155.58	2621.19
A40-4	Unnamed	Tookarita	10790.02	12606	10.8	0	47	47	-	9088.62	9088.62
A40-6	Unnamed	Yamagata-bonchi	42598.49	51710	7.6	69	96	165	3154.22	6096.51	4866.10
A40-9	Unnamed	Nagai-bonchi-seien	12825.16	13334	12.0	8	57	65	4401.08	8904.19	8349.96
A43-7	Unnamed	Kawaketayama	14514.60	14479	11.2	34	50	84	2660.95	5250.69	4202.47
A44-2b	Kamimiyori	Unknown	13592.59	14807	12.4	64	3	67	7199.97	3549.64	7036.53
A44-3	Aizu-bonchi-seien-hokubu	Aizu-bonchi-seisn	22128.66	25129	21.2	103	32	135	3435.29	5378.62	3895.93
A44-4	Aizu-bonchi-seien-nanbu	Aizu-bonchi-seisn	13175.67	13531	9.2	39	115	154	4675.09	5604.24	5368.93
A44-5	Tsukioka	Tsukioka	21478.76	21441	19.2	48	487	535	2118.49	4030.01	3858.51
A50-1	Sekiya	Sekiya	27837.07	31342	24.8	13	397	410	4250.97	4885.97	4865.83
A50-2	Unnamed	Unknown	14931.20	14891	8.8	78	16	94	7663.01	7173.37	7579.67
A51-1	Unnamed	Kanto-heiya-hokuseien	11965.11	12084	11.2	191	5	196	10746.75	2048.78	10524.86

Fault Type & Number	Fault Name	Fault System	Fault Length (Type I, m)	Fault Length (Type II, m)	Fault Trace Length (Type III, km)	Number* of Attributed Hypocenters			Mean Distance to Fault Plane		
						Side A	Side B	Total	Side A	Side B	Overall
A51-2	Unnamed	Hirai-Kushihiki	12901.19	12804	11.2	298	16	314	14348.21	2914.36	13765.60
A52-1	Unnamed	Tachikawa	25175.31	27080	23.6	12	55	67	9655.78	8646.86	8827.56
A52-2	Isehara	Isehara	22394.97	22318	14.4	54	20	74	6501.74	3622.85	5723.66
A52-3	Kouzu-Matsuda	Kannawa/Kouzu-Matsuda	20459.43	22919	6.4	15	72	87	1204.69	3784.86	3340.00
A53-2	Unnamed	Tanna	34451.69	56459	11.6	78	11	89	2058.91	988.48	1926.61
A58-1	Ishiuchi	Muikamachi-bonchi-hokuen Tectonic Line	17711.77	19367	22.8	68	39	107	9537.52	2350.90	6918.10
A58-2	Tokamachi	Tokamachi	10189.62	12148	10.0	156	63	219	2577.72	4981.63	3269.25
A58-6	Asano, Sansai, Nagaoka, Toyono, Iriishi, Minamigo	Shinanogawa	45267.35	50753	16.4	357	97	454	10944.37	4905.86	9654.21
A59-1	Shiroyama, Zenkoji, Komoatsubara, Amori	Shinanogawa, Nagano-bonchi-seien Tectonic Line	14734.59	14685	14.4	470	44	514	7971.31	10608.10	8197.03
A59-3	Suwako-minami	Itoigawa-Shizuoka Tectonic Line	15142.07	18906	11.6	3	57	60	448.78	2955.19	2829.87
A60-2	Simotsugi, Hakusyu	Itoigawa-Shizuoka Tectonic Line	56970.26	64946	21.6	46	431	477	2227.19	3591.77	3460.18
A61-1a	Ankyoyama	Fujigawa-kako	40465.34	91430	18.0	112	488	600	10400.60	10948.76	10846.44
A64-1	Shinsiro, Matsumoto-bonchi-touen	Itoigawa-Shizuoka Tectonic Line	63950.96	72688	49.2	2111	458	2569	7235.99	4618.96	6769.43
A64-2	Ushifuseji	Itoigawa-Shizuoka Tectonic Line	10204.2	10389	4.4	162	26	188	1373.41	1567.47	1400.24
A64-4	Sakai-toge	Sakai-toge-Kamiya	14466.26	14640	2.4	14	4045	4059	11599.59	14403.43	14393.76
A64-5	Atotsugawa	Enago	66977.11	66994	4.0	224	346	570	1314.59	1119.83	1196.37
A64-6	Ushikubi	Ushikubi	51670.41	51424	40.8	89	50	139	2159.90	2278.21	2202.45
A64-7	Enago	Enago	16611.83	16501	10.4	334	36	370	6195.90	2031.98	5790.76
A64-8	Makigabura	Takayama-Ohara	23566.29	23455	24.0	27	26	53	5412.46	5110.28	5264.22
A65-2	Ogurogawa, Tagiri	Inadani	32145.04	35808	29.6	78	25	103	5428.97	4237.91	5139.88
A65-3	Tagiri	Inadani	45808.20	48151	4.8	12	42	54	1068.42	1603.05	1484.24
A65-5	Sansyu	Inadani	15839.19	15811	15.2	16	39	55	3719.19	4310.69	4138.61

Fault Type & Number	Fault Name	Fault System	Fault Length (Type I, m)	Fault Length (Type II, m)	Fault Trace Length (Type III, km)	Number* of Attributed Hypocenters			Mean Distance to Fault Plane		
						Side A	Side B	Total	Side A	Side B	Overall
A65-6	Seinaiji-toge	Kisogawa	10188.1	10179	10.8	18	161	179	5659.44	14355.75	13481.26
A65-8	Atera, Ogiwara-higashi, Gero, Ogiwara-nishi	Atera	88907.43	93393	59.6	106	2665	2771	10786.36	12426.90	12364.15
A70-1	Takashimizu	Takashimizu	27761.05	28917	10.8	74	14	88	4981.42	3674.29	4773.47
A70-4	Kzura, Shirakawa, Miogawa	Shokawa	40196.07	40154	32.8	26	416	442	3212.28	13851.81	13225.96
A71-1	Atsumi	Neodani	28641.81	28524	27.6	48	128	176	3262.65	3181.88	3203.91
A71-2	Mugigawa	Neodani	7595.8	7556	11.6	21	74	95	2920.51	2821.57	2843.44
A71-3b	Neodani	Neodani	16101.48	32989	15.6	90	12	102	6152.98	1842.65	5645.88
A71-4	Umehara	Neodani	11435.86	11394	10.8	51	288	339	1418.80	6693.32	5899.81
A71-5	Kinsoudake	Kinsoudake	9921.29	9890	9.6	109	62	171	3671.37	1406.79	2850.30
A71-6	Ikedayama	Yoro-Kuwana-Yokkaichi	17449.67	17427	16.4	50	46	96	7917.69	4159.57	6116.92
A71-7	Yanagase	Yanagase	28478.02	28461	28.8	110	66	176	3067.72	2700.95	2930.18
A71-8	Kajiya	Sekigahara	19905.14	19825	10.8	190	410	600	2546.66	2632.47	2605.29
A71-9	Sekigahara	Sekigahara	9634.56	9594	9.2	74	94	168	2633.15	2558.20	2591.21
A71-12	Sakanami, Enbano, Kamitera	Biwako-seigan	19322.05	22027	17.2	34	25	59	2672.79	2703.93	2685.98
A72-1	Kuwana-Yokkaichi,?Tarusaka	Yoro-Kuwana-Yokkaichi	14309.98	42710	24.8	364	111	475	7853.99	2891.98	6694.44
A72-2	Yokkaichi	Yoro-Kuwana-Yokkaichi	33125.68	10922	11.2	142	30	172	5257.20	4397.83	5107.31
A72-3	Suzuka-Sakamoto	Suzuka-Sakashita	10923.73	14220	8.0	54	21	75	2613.01	1757.06	2373.34
A72-4	Kizugawa-seibu	Kizugawa	10917.44	10858	10.8	53	72	125	2559.25	2762.31	2676.21
A75-2	Kumagawa	Kumagawa	11471.79	11399	10.8	217	113	330	2585.92	2900.75	2693.73
A75-3	Hanaore	Mikata-Hanaore	46951.31	47654	36.4	1664	194	1858	6919.72	1053.97	6307.25
A75-4	Joringawa	Joringawa	19625.84	19525	6.0	426	77	503	9817.05	5737.68	9192.57
A75-5	Yamada, Yasukeyakma-nishi	Yamada	37127.68	36973	31.2	186	105	291	10715.31	4853.35	8600.17
A75-7	Satomura	Satomura	13234.98	13868	12.8	132	17	149	2816.53	1078.27	2618.20
A76-1	kasida	Biwako-seigan	16664.46	17402	12.4	391	0	391	9868.83	-	9868.83
A76-2	Hiei	Biwako-seigan	11781.82	13256	9.2	52	3	55	3123.74	945.51	3004.93
A76-3	Kouheki	Mikata-Hanaore	22330.37	53283	6.0	83	44	127	1473.05	2149.39	1707.37

Fault Type & Number	Fault Name	Fault System	Fault Length (Type I, m)	Fault Length (Type II, m)	Fault Trace Length (Type III, km)	Number* of Attributed Hypocenters			Mean Distance to Fault Plane		
						Side A	Side B	Total	Side A	Side B	Overall
A76-5	Mitouge	Mitouge-Kyoto-Nishiyama	24135.21	23987	9.6	561	278	839	1601.29	1571.99	1591.58
A76-8	Kashihara	Mitouge-Kyoto-Nishiyama	55426.66	55277	9.6	1805	666	2471	4523.51	1452.85	3695.88
A76-9a	Kameoka	Kameoka	7894.08	8443	22.8	170	60	230	3070.64	504.30	2401.16
A76-9b	Koumyoji, Taguchi	Kameoka	41835.77	43416	16.0	384	1118	1502	951.93	3150.85	2588.68
A76-14a	Arima-Takatsuki	Arima-Takatsuki	18486.06	19421	9.6	236	239	475	1866.38	5110.71	3498.79
A76-15	Onohara	Arima-Takatsuki	44910.68	45120	14.8	104	428	532	731.77	2201.94	1914.54
A76-17	Gosukebashi, Suwayama	Rokko, Awaji-shima	22040.19	22096	15.2	592	71	663	1819.68	347.17	1661.99
A77-2	Ikoma, Tamateyama	Ikoma	36777.64	43928	7.2	32	34	66	3027.69	3151.39	3091.42
A77-5	Sakamoto	Uemachi	9142.63	16539	6.0	0	85	85	-	11519.50	11519.50
A77-6	Kougo, Gojodani, Negoro	Median Tectonic Line	88002.27	94296	69.2	13621	685	14306	9705.16	2726.90	9371.03
A77-8	Kusumoto, Higashiura, Nodao	Rokko-Awaji	38957.02	39718	14.0	385	1187	1572	1283.23	1927.74	1769.90
A79-1	Youhu	Unknown	19140.18	19014	18.4	19	47	66	14997.89	18037.05	17162.14
A80-1	Ohara	Yamasaki	17961.91	17861	17.2	38	145	183	3464.86	1437.35	1858.36
A80-2	Doman-Yasutomi	Yamasaki	20882.16	20768	19.6	68	209	277	4600.37	8098.19	7239.52
A80-3	Yasutomi	Yamasaki	17857.98	17748	14.8	197	90	287	2338.59	2638.47	2432.63
A81-1	Nojima	Rokko-Awaji	12191.3	12157	9.6	513	200	713	1004.12	832.66	956.02
A81-2	Unnamed	Median Tectonic Line	69705.78	73545	89.2	209	65	274	5692.24	4997.89	5527.53
A81-3	Unnamed	Nagao	23273.54	24890	22.0	37	16	53	1841.00	4888.49	2761.00
A86-1	Chyojagahara	Unknown	9272.37	9258	6.4	66	6	72	10980.13	5001.68	10481.93
A87-2	Ishizuchi	Median Tectonic Line	107204.84	124462	24.0	249	1101	1350	11138.46	9244.13	9593.53
A87-3	Okamura	Median Tectonic Line	28702.22	37038	28.0	129	79	208	6133.50	12444.05	8530.30
A87-4	Kawakami, Kitagata	Median Tectonic Line	37060.20	39222	10.8	7	222	229	12804.22	14156.11	14114.79
A91-3	Ogata-Oze	Iwakuni	27646.82	27931	23.6	39	469	508	9577.32	13501.74	13200.45
A95-2	Kikugawa	Kikugawa	22484.08	22376	10.8	27	139	166	6796.79	11812.51	10996.70
A98-1	Unnamed	Beppu-Mannenyama	27484.51	35806	18.4	857	95	952	1990.85	677.83	1859.82
A99-2	Hukuchiyama	Hukuchiyama	22490.46	22430	21.2	103	23	126	6022.19	5508.59	5928.44

Fault Type & Number	Fault Name	Fault System	Fault Length (Type I, m)	Fault Length (Type II, m)	Fault Trace Length (Type III, km)	Number* of Attributed Hypocenters			Mean Distance to Fault Plane		
						Side A	Side B	Total	Side A	Side B	Overall
A99-3a	Hukuyama-Wakamiya	Nishiyama	17599.01	21033	16.8	11	47	58	8778.65	8675.39	8694.97
A99-3b	Iizuka-nishi	Nishiyama	11228.17	11177	10.0	30	21	51	5448.48	4451.16	5037.82
A99-4	Keiko	Kwiko	20086.84	19979	14.0	99	21	120	7691.74	6181.73	7427.48
A101-1b	Kurotake	Beppu-Mannenyama	32781.78	32536	7.6	222	21	243	1269.13	761.36	1225.25
A101-2	Hanaka	Beppu-Mannenyama	19635.63	25888	14.0	0	460	460	-	3830.15	3830.15
A102-4	Chijiishi	Unzen	21081.64	20902	18.8	231	88	319	2962.32	1891.62	2666.96
A102-5	Nunotsu	Unzen	40545.75	45043	14.4	136	96	232	709.46	533.53	636.66
A106-1	Ono, Hinaku	Hutagawa-Hinaku	78491.23	78134	30.8	5054	5430	10484	6238.13	4081.63	5121.21
A106-3	Touhou-Tabata, Motobeppu	Hitoyoshi-bonchi	23308.13	23768	22.0	154	115	269	12823.27	5774.52	9809.87
A106-4	Yhazutoge, Kiminagawa, Uchikiba	Demizu	14354.27	14286	18.4	13807	348	14155	10449.32	10637.34	10453.95
A112-1	Hnasatozaki-Tanosaki	Tanegashima	10158.81	10126	10.0	10	69	79	9341.09	9341.57	9341.51
A114-1	Onoma	Yakushima-nangann	19467.60	19362	14.4	165	7	172	6537.94	7390.47	6572.64
B30-1	Oritsume	Oritsume	24905.87	27021	23.2	8	228	236	17120.85	16433.43	16456.73
B40-2	Murata	Unknown	16709.12	18431	8.8	1	182	183	6634.94	8036.13	8028.48
B40-3	Unnamed	Unknown	13515.76	14924	5.6	48	23	71	5769.58	4177.54	5253.85
B52-4	Kannawa Thrust, Fujisawa	Unknown	14517.91	14402	13.6	32	46	78	813.71	1006.44	927.37
B60-1	Unnamed	Median Tectonic Line	6964.11	6959	11.6	89	52	141	8731.65	2742.44	6522.86
B64-1	Jonendake, Kashimamanganji	Unknown	12354.27	12346	11.2	0	392	392	-	13135.18	13135.18
B64-2	Shinanozaka	Unknown	15187.86	15166	11.2	0	5308	5308	-	16669.60	16669.60
B64-3	Mozumi-Hironobe	Unknown	24358.87	24213	24.4	82	22	104	545.16	658.59	569.15
B65-2	Kunogawa	Unknown	12725.35	12666	12.8	56	236	292	2315.39	8214.42	7083.10
B65-4	Ohara	Ohara	12879.21	12854	11.6	45	9	54	7242.57	2788.72	6500.26
B71-1	Hachiman	Nagaragawa-jouryu	23460.30	23399	14.4	205	208	413	4107.64	4003.10	4054.99
B72-2	Kakiya, Nawa-Kaki	Unknown	9689.63	9685	9.6	9	110	119	1967.33	4930.38	4706.29

Fault Type & Number	Fault Name	Fault System	Fault Length (Type I, m)	Fault Length (Type II, m)	Fault Trace Length (Type III, km)	Number* of Attributed Hypocenters			Mean Distance to Fault Plane		
						Side A	Side B	Total	Side A	Side B	Overall
B72-5	Ootorii	Unknown	16401.57	17364	12.4	118	39	157	2736.04	1740.19	2488.66
B76-1	Hira	Biwako-seigan	14578.29	14530	15.2	290	181	471	3042.40	2501.67	2834.60
B76-4	Tahara	Unknown	20624.78	20593	8.8	114	13	127	3731.78	1498.67	3503.20
B76-6	Otsuki, Numobiki	Rokko-Awaji	16935.40	16869	16.8	634	208	842	691.52	419.80	624.39
B76-7	Arino-Dango	Arima-Takatsuki	10598.64	11218	10.4	74	8	82	5747.51	418.69	5227.63
B76-9	Furuichi	Unknown	28373.87	28227	28.8	44	450	494	4469.10	5828.54	5707.46
B79-1	Ametaki-Kamado	Unknown	9187.42	9149	11.2	4204	18	4222	3967.03	3602.31	3965.47
B80-1	Gobantoge	Yamasaki	12534.83	12478	11.6	152	227	379	1127.01	1964.22	1628.46
B82-1	Miyamae, Nanzan	Ayukuigawa	22488.38	22359	19.6	674	240	914	13399.12	4495.55	11061.20
B101-2	Mitate	Unknown	8708.25	8651	8.0	52	2	54	14887.31	6934.59	14592.76

*After imposing the 50-hypocenter minimum limit and omitting outliers.

Table B-6, Part 2**,** Descriptive Statistics on Hypocenter Distance, by Fault

Fault Type & Number	25th Percentile of Distance to Fault Plane	Median Distance to Fault Plane			75th Percentile of Distance to Fault Plane	Interquartile Range of Distance to Fault Plane	Sum of Median Distances for Two Sides of the Fault Plane	Twice Mean Distance to Fault Plane	Twice Median Distance to Fault Plane
		Side A	Side B	Overall					
1	A14-1	3234.97	10832.56	4525.38	6239.34	12573.27	9338.30	15357.94	16224.00
2	A29-1	12148.41	16019.17	2903.69	15670.43	18939.14	6790.73	18922.86	30279.62
3	A29-5	5626.43	2212.05	7058.92	7049.78	9240.83	3614.40	9270.97	15421.28
4	A33-1c	3510.34	8427.28	4321.06	4334.85	5542.83	2032.49	12748.34	8626.48
5	A34-5	8303.80	2640.41	17364.60	16811.39	18353.09	10049.29	20005.01	27511.00
6	A36-2	9969.19	14057.52	11884.91	11904.31	13725.75	3756.56	25942.43	23109.58
7	A37-1	723.33	777.54	4449.09	1661.79	4449.09	3725.76	5226.63	5242.38
8	A40-4	7264.51	-	9664.50	9664.50	10743.60	3479.09	9664.50	18177.24
9	A40-6	323.98	475.36	6396.28	1806.82	9304.79	8980.81	6871.64	9732.20
10	A40-9	6684.72	4844.34	9306.91	9193.07	10146.92	3462.20	14151.25	16699.92
11	A43-7	1013.16	982.38	4705.75	4303.95	6519.26	5506.10	5688.13	8404.94
12	A44-2b	4687.95	6025.71	4506.11	5847.86	8643.95	3956.00	10531.82	14073.06
13	A44-3	2788.27	3326.45	5330.88	3494.55	4479.46	1691.19	8657.33	7791.86
14	A44-4	3368.92	2944.81	5880.74	5810.98	6498.02	3129.10	8825.55	10737.86
15	A44-5	2457.44	1395.52	4045.81	3890.33	5072.80	2615.36	5441.33	7717.02
16	A50-1	4429.88	4046.23	4793.58	4777.28	5250.28	820.40	8839.81	9731.66
17	A50-2	6793.96	7794.47	8800.87	7899.28	8729.06	1935.10	16595.34	15159.34
18	A51-1	5098.13	9913.69	1194.42	9599.70	16489.22	11391.09	11108.11	21049.72
19	A51-2	11004.86	15151.01	2283.22	14933.25	16598.31	5593.45	17434.23	27531.20
20	A52-1	6133.87	9216.81	9295.34	9295.34	11055.73	4921.86	18512.15	17655.12
21	A52-2	3236.56	7016.41	2391.16	6174.04	7535.21	4298.65	9407.57	11447.32
22	A52-3	1062.57	823.25	3549.84	2431.98	5100.34	4037.77	4373.09	6680.00
23	A53-2	1145.34	2230.85	351.85	2139.22	2587.36	1442.02	2582.70	3853.22
24	A58-1	1496.86	14363.15	2573.33	3289.65	15451.87	13955.01	16936.48	13836.20
25	A58-2	2330.70	2597.57	5084.12	2866.76	3761.41	1430.71	7681.69	6538.50
26	A58-6	5950.29	11895.12	4398.01	11006.31	13055.70	7105.41	16293.13	19308.42
27	A59-1	5550.82	7810.05	12563.85	8066.03	10298.89	4748.07	20373.90	16394.06

Fault Type & Number	25th Percentile of Distance to Fault Plane	Median Distance to Fault Plane			75th Percentile of Distance to Fault Plane	Interquartile Range of Distance to Fault Plane	Sum of Median Distances for Two Sides of the Fault Plane	Twice Mean Distance to Fault Plane	Twice Median Distance to Fault Plane
		Side A	Side B	Overall					
A59-3	1097.77	472.58	2092.29	1999.62	5325.82	4228.05	2564.87	5659.74	3999.24
A60-2	2370.36	1419.87	3507.98	3442.90	4405.92	2035.56	4927.85	6920.36	6885.80
A61-1a	6694.48	11842.62	11614.62	11696.17	13939.78	7245.3	23457.24	21692.88	23392.33
A64-1	2116.56	6658.13	2587.30	5783.34	11852.05	9735.49	9245.43	13538.86	11566.68
A64-2	502.47	930.88	1313.51	949.60	1986.41	1483.94	2244.39	2800.48	1899.21
A64-4	12612.19	12057.30	14404.53	14398.59	15942.26	3330.07	26461.83	28787.52	28797.18
A64-5	478.18	1078.34	850.90	947.20	1705.83	1227.65	1929.24	2392.74	1894.41
A64-6	1257.80	2149.70	1921.58	2112.23	3048.77	1790.97	4071.28	4404.90	4224.47
A64-7	2520.02	5165.50	2201.07	4753.82	8836.59	6316.57	7366.57	11581.52	9507.65
A64-8	3187.83	5456.09	5536.87	5456.09	7319.52	4131.69	10992.96	10528.44	10912.17
A65-2	2902.49	5092.24	5010.95	5064.66	6597.96	3695.47	10103.19	10279.76	10129.32
A65-3	532.40	564.78	1427.09	1206.91	2184.36	1651.96	1991.87	2968.48	2413.82
A65-5	1943.38	3873.95	3729.54	3791.44	6262.03	4318.65	7603.49	8277.22	7582.88
A65-6	13015.91	5194.92	14894.99	14803.34	15227.09	2211.18	20089.91	26962.52	29606.69
A65-8	10797.81	12856.74	13158.16	13150.31	15193.23	4395.42	26014.90	24728.30	26300.63
A70-1	3125.95	5046.73	3025.75	4738.77	6040.19	2914.24	8072.48	9546.94	9477.53
A70-4	11088.82	3042.96	15594.93	14431.73	18049.24	6960.42	18637.89	26451.92	28863.46
A71-1	1619.09	3396.52	3001.20	3114.51	4503.94	2884.85	6397.72	6407.82	6229.02
A71-2	1658.01	3212.13	3019.68	3108.92	3992.27	2334.26	6231.81	5686.88	6217.84
A71-3b	2169.44	7331.99	1316.01	5691.50	8379.50	6210.06	8648.00	11291.76	11383.00
A71-4	2536.50	1109.11	6469.79	5939.86	8870.59	6334.09	7578.90	11799.62	11879.71
A71-5	1108.79	3277.48	1128.03	1807.84	4634.96	3526.17	4405.51	5700.60	3615.67
A71-6	2707.03	8625.70	4856.23	5426.25	8818.76	6111.73	13481.93	12233.84	10852.49
A71-7	1986.33	2815.86	3013.05	2898.16	3895.39	1909.06	5828.91	5860.36	5796.33
A71-8	1435.23	2234.74	2236.91	2234.97	3884.59	2449.36	4471.65	5210.58	4469.95
A71-9	820.47	2096.64	2115.74	2115.74	3980.18	3159.71	4212.38	5182.42	4231.48
A71-12	1254.55	2304.19	2536.48	2521.77	3890.34	2635.79	4840.67	5371.96	5043.54
A72-1	2506.86	8912.72	2634.30	7790.48	9774.35	7267.49	11547.02	13388.88	15580.95
A72-2	1799.22	5047.15	4828.07	4992.72	7991.76	6192.54	9875.22	10214.62	9985.44

Fault Type & Number	25th Percentile of Distance to Fault Plane	Median Distance to Fault Plane			75th Percentile of Distance to Fault Plane	Interquartile Range of Distance to Fault Plane	Sum of Median Distances for Two Sides of the Fault Plane	Twice Mean Distance to Fault Plane	Twice Median Distance to Fault Plane
		Side A	Side B	Overall					
A72-3	642.23	2012.15	1078.02	1630.35	4263.59	3621.36	3090.17	4746.68	3260.71
A72-4	1385.37	2242.00	2891.27	2487.54	4109.34	2723.97	5133.27	5352.42	4975.09
A75-2	1248.02	2688.85	2677.87	2685.28	4056.51	2808.49	5366.72	5387.46	5370.55
A75-3	1655.41	6336.85	997.29	4603.87	10300.51	8645.1	7334.14	12614.50	9207.73
A75-4	4415.08	9806.80	4918.41	9172.49	13849.75	9434.67	14725.21	18385.14	18344.98
A75-5	3260.66	12929.90	4189.57	8253.87	13311.22	10050.56	17119.47	17200.34	16507.74
A75-7	1439.96	2621.67	735.12	2429.80	3533.64	2093.68	3356.79	5236.40	4859.60
A76-1	7638.49	10339.43	-	10339.43	11756.48	4117.99	10339.43	19737.66	20678.87
A76-2	1337.54	3623.78	1010.43	3532.17	4321.15	2983.61	4634.21	6009.86	7064.33
A76-3	741.43	1092.19	2099.69	1722.94	2416.65	1675.22	3191.88	3414.74	3445.89
A76-5	632.65	1195.70	1465.77	1321.42	2236.02	1603.37	2661.47	3183.16	2642.85
A76-8	1061.70	3493.25	1171.98	2615.04	6452.51	5390.81	4665.23	7391.76	5230.09
A76-9a	671.31	3264.22	411.65	1994.25	4109.93	3438.62	3675.87	4802.32	3988.50
A76-9b	826.33	847.83	3087.22	1865.68	4201.45	3375.12	3935.05	5177.36	3731.36
A76-14a	1330.79	1577.85	6312.19	2102.47	6740.24	5409.45	7890.04	6997.58	4204.94
A76-15	389.36	257.03	1816.74	1496.37	3065.82	2676.46	2073.77	3829.08	2992.75
A76-17	537.29	1833.02	176.03	1623.73	2437.65	1900.36	2009.05	3323.98	3247.45
A77-2	1829.09	2887.76	2993.61	2951.04	4516.16	2687.07	5881.37	6182.84	5902.07
A77-5	9763.47	-	11845.27	11845.27	13491.47	3728	11845.27	23039.00	23690.54
A77-6	5183.82	9476.65	1791.49	9127.77	13074.59	7890.77	11268.14	18742.06	18255.54
A77-8	660.13	772.00	1653.36	1470.30	2624.57	1964.44	2425.36	3539.80	2940.60
A79-1	15734.67	15653.29	18763.88	18669.47	18795.45	3060.78	34417.17	34324.28	37338.94
A80-1	554.18	1652.31	936.40	962.16	2486.04	1931.86	2588.71	3716.72	1924.32
A80-2	2494.04	3619.32	8993.99	7807.24	9581.01	7086.97	12613.31	14479.04	15614.48
A80-3	1281.65	1736.67	2628.02	1959.86	3424.33	2142.68	4364.69	4865.26	3919.73
A81-1	417.51	966.27	642.97	877.01	1431.26	1013.75	1609.24	1912.04	1754.01
A81-2	3269.61	5640.67	4477.97	5308.54	7221.47	3951.86	10118.64	11055.06	10617.08
A81-3	601.01	1223.21	5776.19	1590.07	5192.90	4591.89	6999.40	5522.00	3180.14
A86-1	6799.28	10881.13	4307.38	10716.25	15484.22	8684.94	15188.51	20963.86	21432.49

Fault Type & Number	25th Percentile of Distance to Fault Plane	Median Distance to Fault Plane			75th Percentile of Distance to Fault Plane	Interquartile Range of Distance to Fault Plane	Sum of Median Distances for Two Sides of the Fault Plane	Twice Mean Distance to Fault Plane	Twice Median Distance to Fault Plane
		Side A	Side B	Overall					
A87-2	8045.62	11607.80	9060.95	9123.69	9902.35	1856.73	20668.75	19187.06	18247.38
A87-3	2208.94	2817.12	14088.89	6363.20	15319.09	13110.15	16906.01	17060.60	12726.40
A87-4	12598.57	13525.54	13792.68	13787.48	15736.10	3137.53	27318.22	28229.58	27574.95
A91-3	10011.58	9035.25	14497.70	14424.47	17356.10	7344.52	23532.95	26400.90	28848.94
A95-2	7128.63	3205.18	15069.68	12538.66	15361.52	8232.89	18274.86	21993.40	25077.32
A98-1	1254.33	1989.71	403.02	1913.28	2436.27	1181.94	2392.73	3719.64	3826.55
A99-2	2056.39	5879.79	6028.81	5897.30	8171.75	6115.36	11908.60	11856.88	11794.61
A99-3a	5695.12	7541.02	8811.18	8271.92	11760.48	6065.36	16352.20	17389.94	16543.84
A99-3b	2766.89	6394.53	4062.80	4090.96	7069.91	4303.02	10457.33	10075.64	8181.92
A99-4	3164.22	7665.27	7672.67	7668.97	10652.51	7488.29	15337.94	14854.96	15337.94
A101-1b	776.66	1129.23	479.79	1101.53	1533.24	756.58	1609.02	2450.50	2203.06
A101-2	3469.75	-	3799.00	3799.00	4211.26	741.51	3799.00	7660.30	7598.00
A102-4	841.43	2662.95	1046.22	2164.75	4143.70	3302.27	3709.17	5333.92	4329.50
A102-5	254.58	569.57	368.76	545.27	850.05	595.47	938.33	1273.32	1090.53
A106-1	1420.19	6592.85	2184.55	4235.45	8109.47	6689.28	8777.40	10242.42	8470.90
A106-3	4801.70	16077.06	4960.89	7145.63	16416.71	11615.01	21037.95	19619.74	14291.26
A106-4	9156.30	10395.45	10264.46	10394.88	11948.02	2791.72	20659.91	20907.90	20789.76
A112-1	3724.97	11208.62	10016.89	10016.89	14285.25	10560.28	21225.51	18683.02	20033.78
A114-1	4490.82	6209.84	6206.69	6208.27	7688.05	3197.23	12416.53	13145.28	12416.54
B30-1	14321.73	16908.21	17889.62	17851.20	18999.63	4677.9	34797.83	32913.46	35702.40
B40-2	7552.75	6634.94	8157.71	8156.68	8568.99	1016.24	14792.65	16056.96	16313.37
B40-3	3210.90	6058.17	3867.26	5889.29	7178.45	3967.55	9925.43	10507.70	11778.58
B52-4	279.08	626.94	776.64	734.18	1337.44	1058.36	1403.58	1854.74	1468.36
B60-1	3000.84	9868.09	2845.84	6032.84	10359.74	7358.9	12713.93	13045.72	12065.67
B64-1	12929.86	-	14522.68	14522.68	15010.31	2080.45	14522.68	26270.36	29045.36
B64-2	15966.07	-	16791.84	16791.84	17392.85	1426.78	16791.84	33339.20	33583.68
B64-3	338.18	525.43	498.87	524.69	764.13	425.95	1024.30	1138.30	1049.38
B65-2	2849.85	2508.61	8477.65	7660.37	9743.45	6893.6	10986.26	14166.20	15320.74
B65-4	3463.68	7451.78	3318.95	5826.01	9891.94	6428.26	10770.73	13000.52	11652.01

Fault Type & Number	25th Percentile of Distance to Fault Plane	Median Distance to Fault Plane			75th Percentile of Distance to Fault Plane	Interquartile Range of Distance to Fault Plane	Sum of Median Distances for Two Sides of the Fault Plane	Twice Mean Distance to Fault Plane	Twice Median Distance to Fault Plane
		Side A	Side B	Overall					
B71-1	1310.68	3948.80	2617.67	3628.79	6074.16	4763.48	6566.47	8109.98	7257.57
B72-2	3313.31	2417.03	4328.00	4215.10	6838.56	3525.25	6745.03	9412.58	8430.21
B72-5	1308.42	2530.39	1430.67	2146.86	3468.70	2160.28	3961.06	4977.32	4293.73
B76-1	1998.42	2844.28	2656.82	2736.94	3602.94	1604.52	5501.10	5669.20	5473.88
B76-4	2004.12	4224.22	1306.17	3967.45	4916.10	2911.98	5530.39	7006.40	7934.90
B76-6	258.37	657.86	290.36	564.30	891.70	633.33	948.22	1248.78	1128.59
B76-7	1887.06	5981.75	355.03	5546.04	8098.51	6211.45	6336.78	10455.26	11092.08
B76-9	2112.18	4751.90	2837.06	2866.34	9447.65	7335.47	7588.96	11414.92	5732.68
B79-1	2719.45	4372.29	3536.00	4369.69	4830.24	2110.79	7908.29	7930.94	8739.39
B80-1	482.33	1020.96	1979.45	1502.09	2625.08	2142.75	3000.41	3256.92	3004.18
B82-1	6211.27	12858.91	4703.00	12343.87	15328.63	9117.36	17561.91	22122.40	24687.74
B101-2	11262.14	16973.44	6934.59	16854.18	18244.36	6982.22	23908.03	29185.52	33708.37

Appendix C

Percentage Histograms of "Signed" Normal Distance from Hypocenters to Fault Planes

This catalog contains a complete set of empirical percentage histograms of the "signed" normal distance from hypocenters to fault planes, specifically considering the sides of the faults on which the hypocenters are located. A separate histogram is presented for each fault, and descriptive statistics accompany each histogram. Zero represents the fault location, and positive and negative values are associated with distances to hypocenters located on either side of a fault. Faults having fewer than 50 attributed hypocenters are omitted, and a single pass filter to remove outlier distances has been applied to the remaining hypocenters associated with each fault.

System = Unknown
Fault= Asahikawa−Hurano−sen (A14−1)

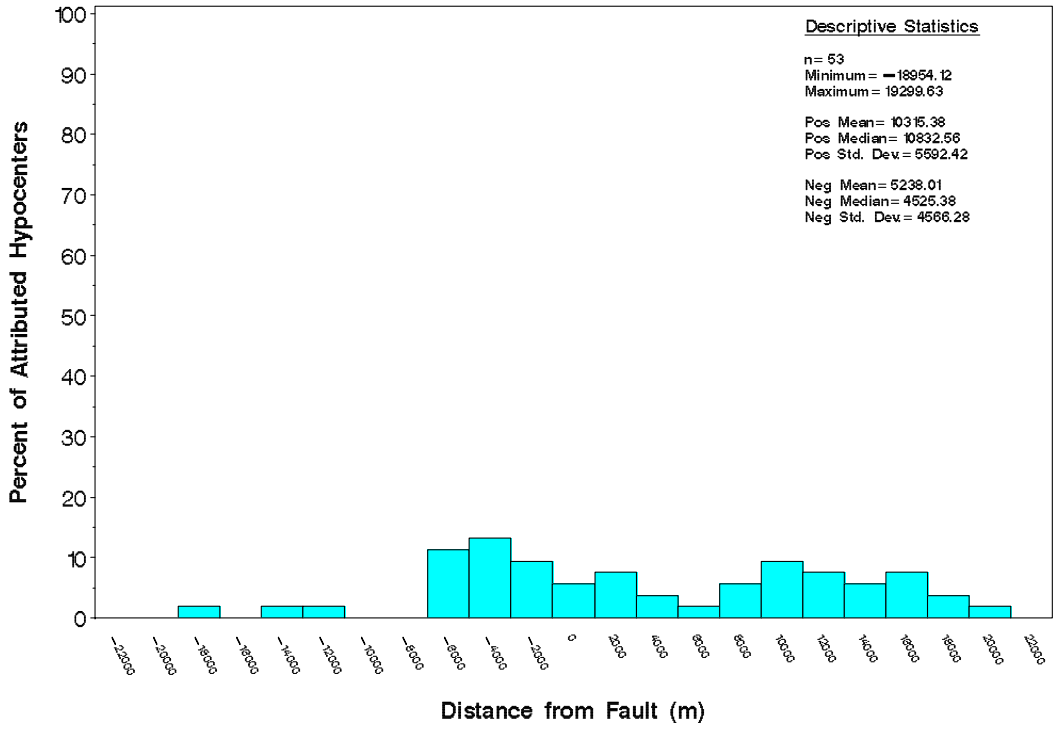

System = Unknown
Fault= Negishi−seihou (A29−1)

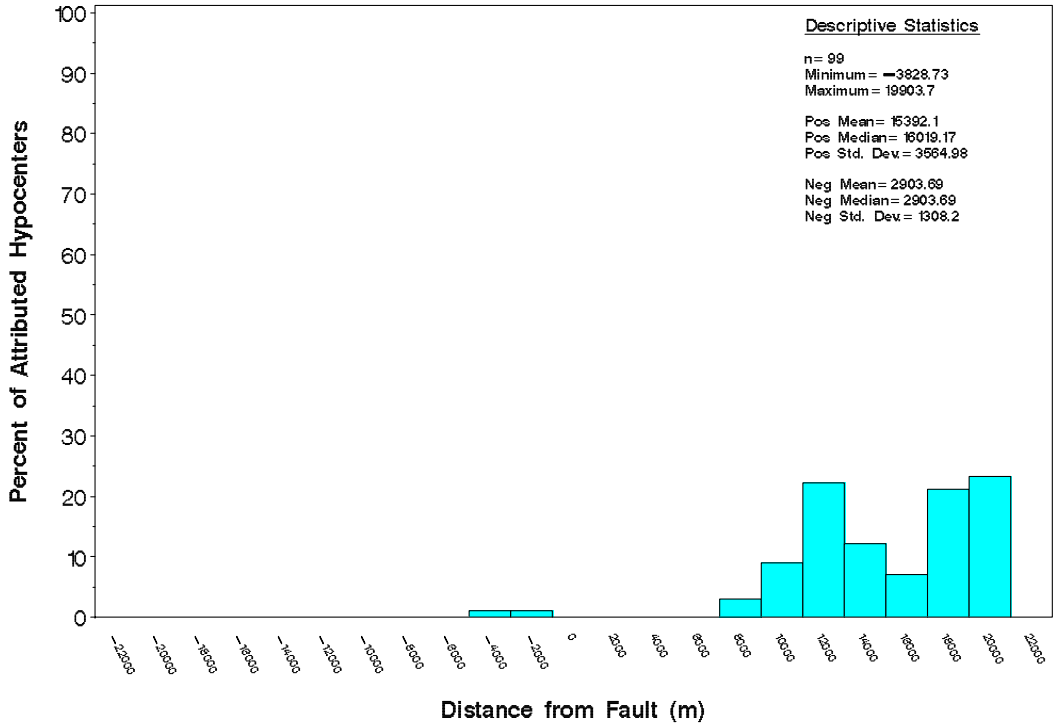

System = Tsugaru−sanchi−seien
Fault= Oohira (A29−5)

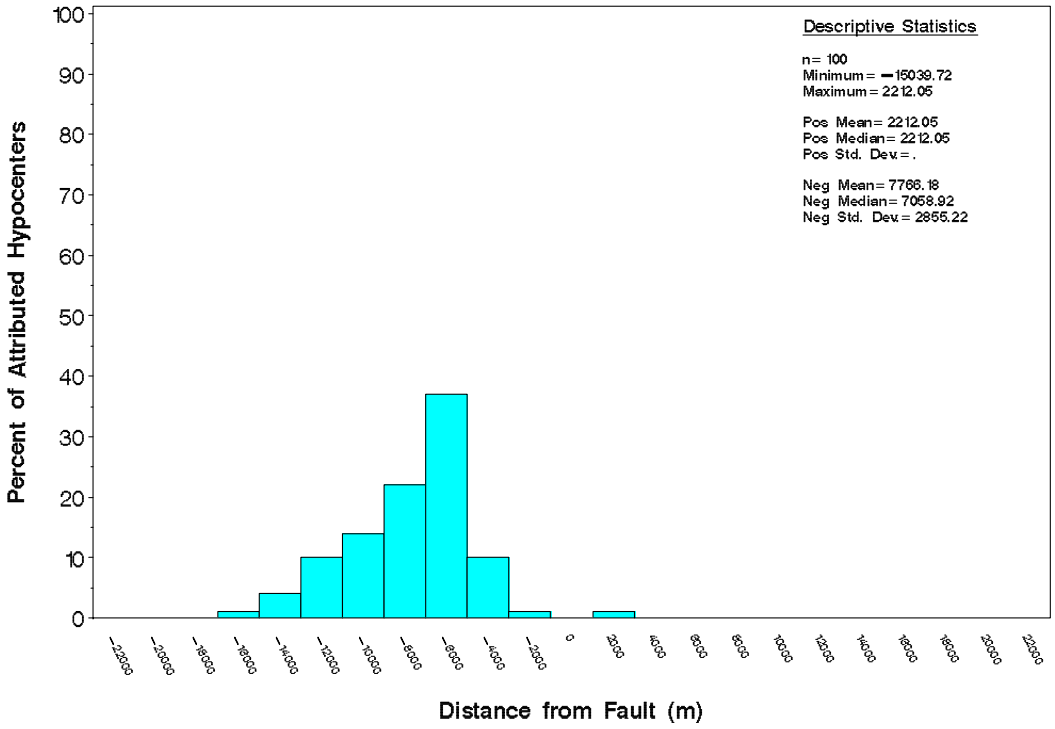

System = Kitakami−teichi−seien
Fault= Aratani−shimomura (A33−1c)

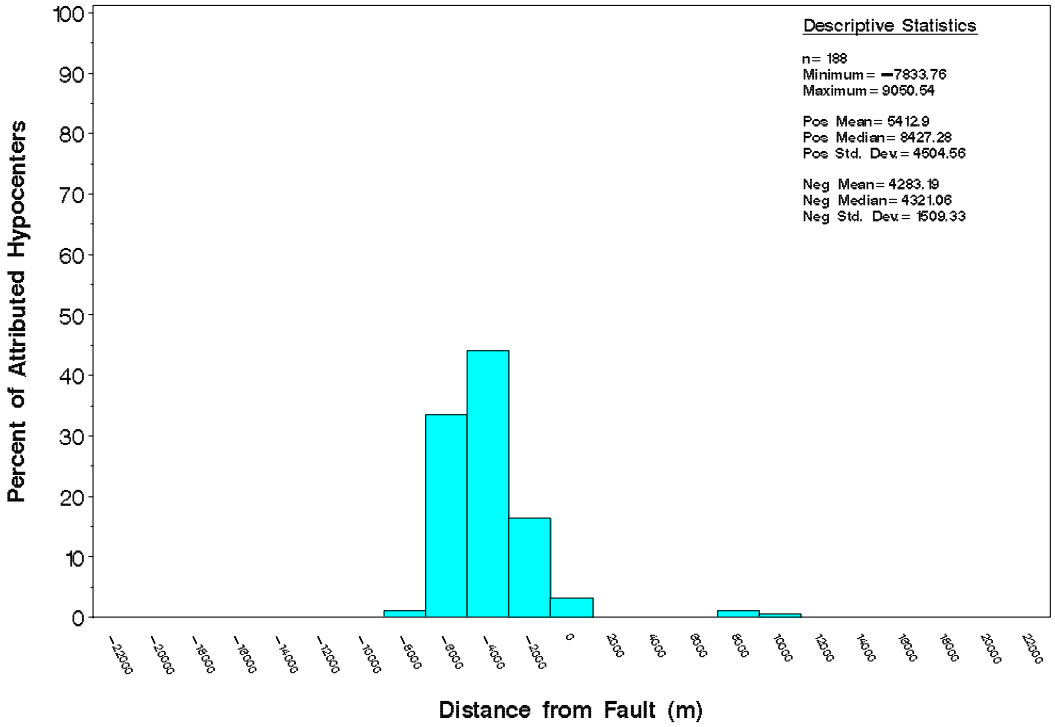

System = Yokote−bonchi−seien
Fault= Yokote, Sugisawa (A34−5)

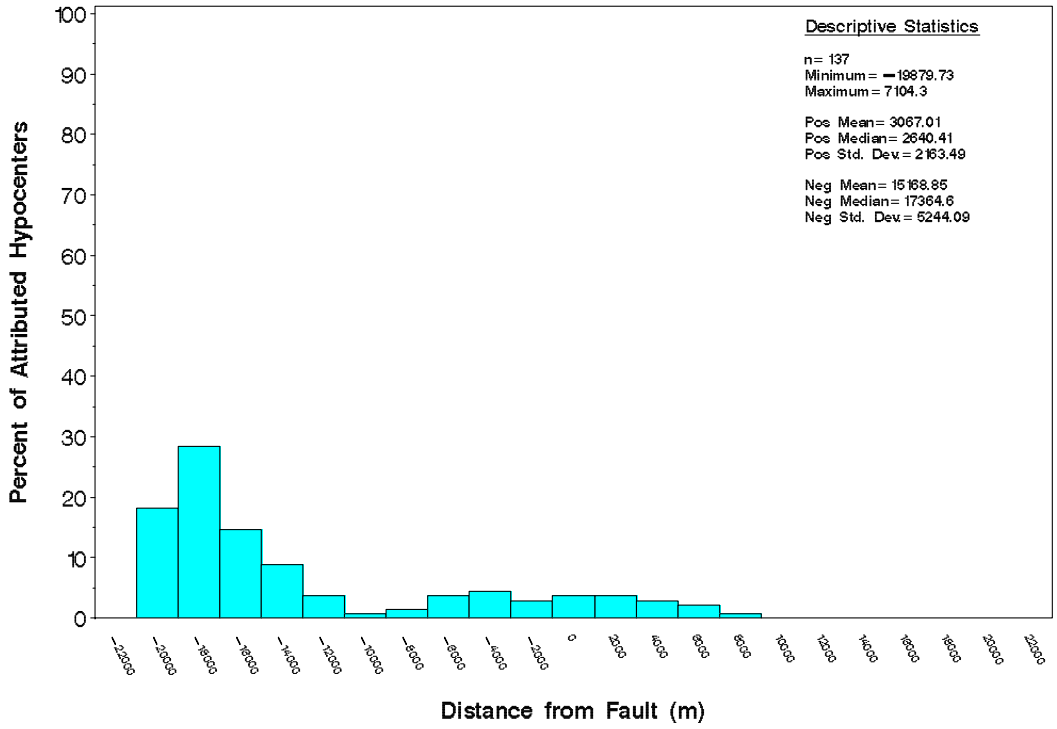

System = Kitakami−teichi−seien
Fault= Nozaki, Urusawa, ?hikizawa (A36−2)

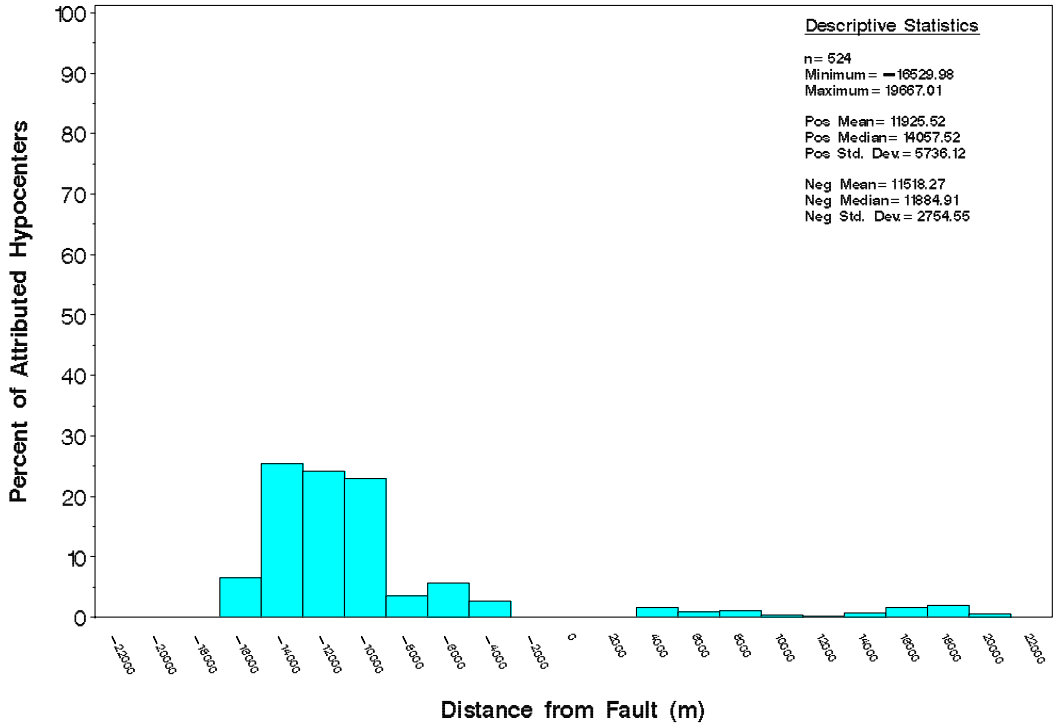

System = Kitakami−teichi−seien
Fault= Horuno−Urasawa, Hachimoriyama−higashi (A37−1)

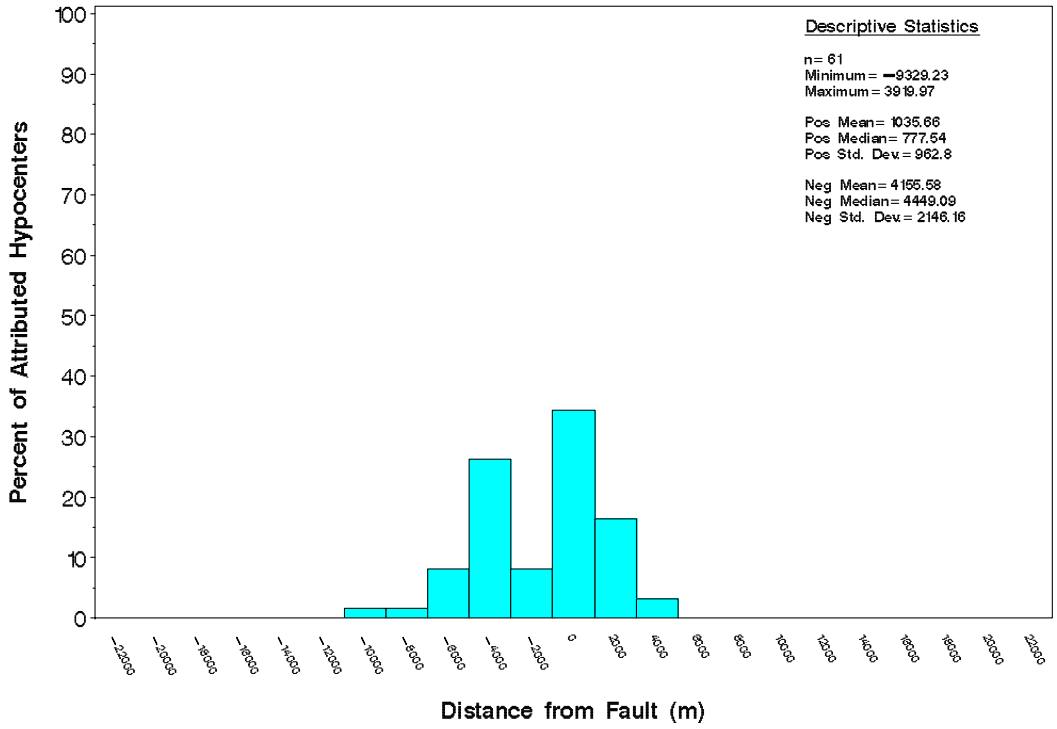

System = Tookarita
Fault= Unnamed (A40−4)

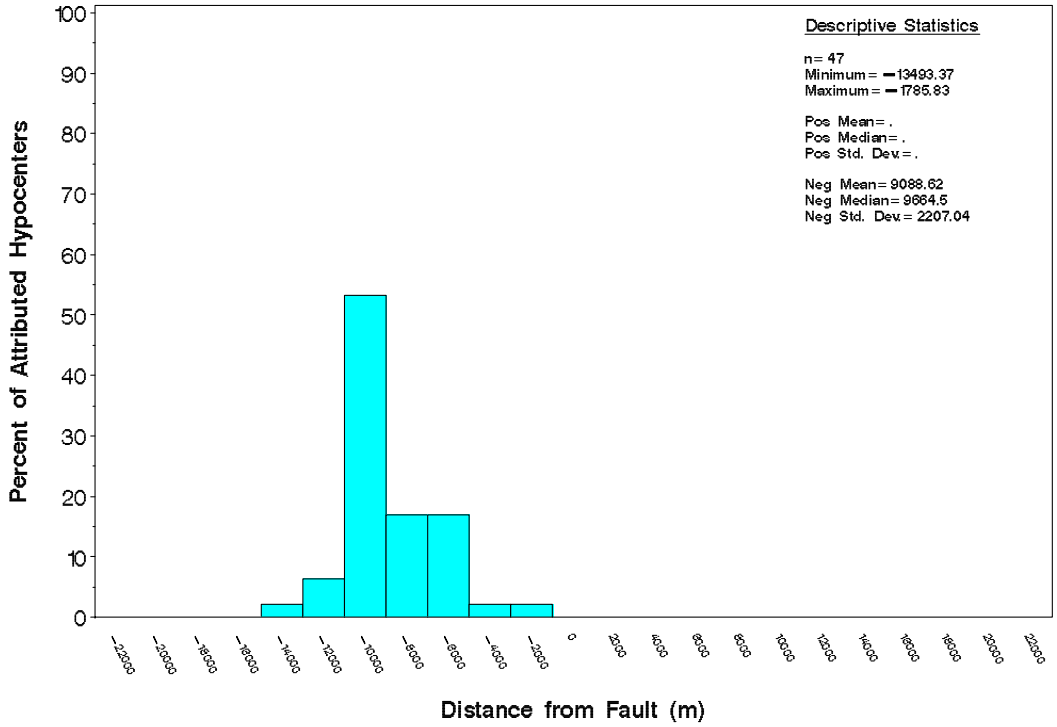

System = Yamagata−bonchi
Fault= Unnamed (A40−6)

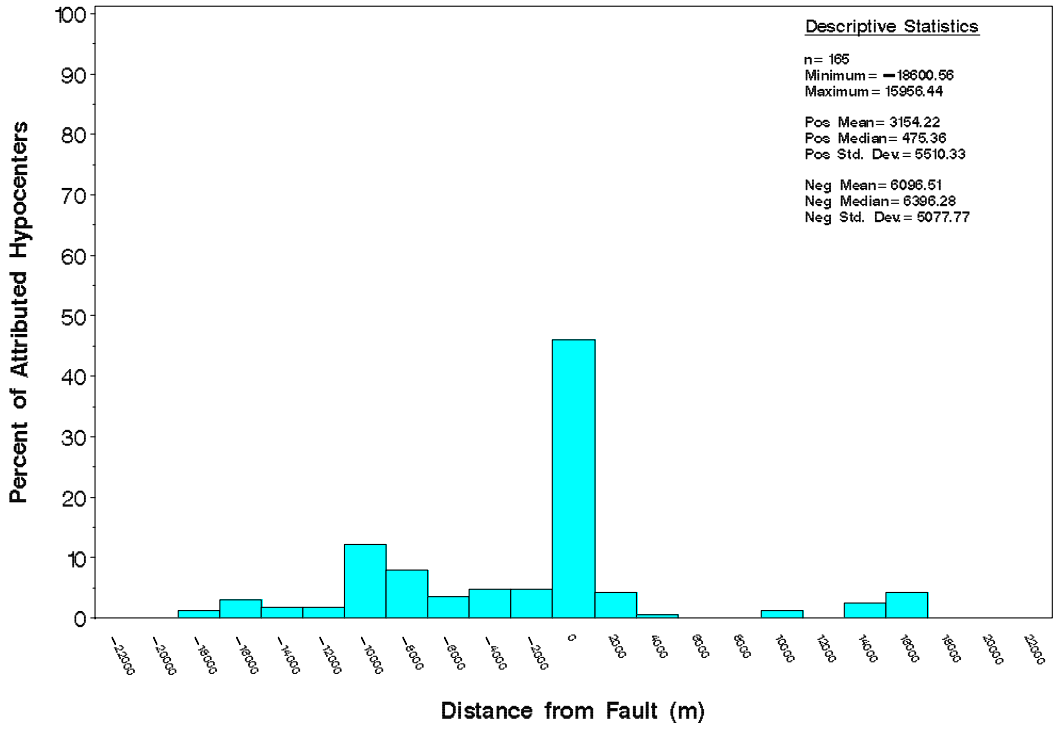

System = Nagai−bonchi−seien
Fault= Unnamed (A40−9)

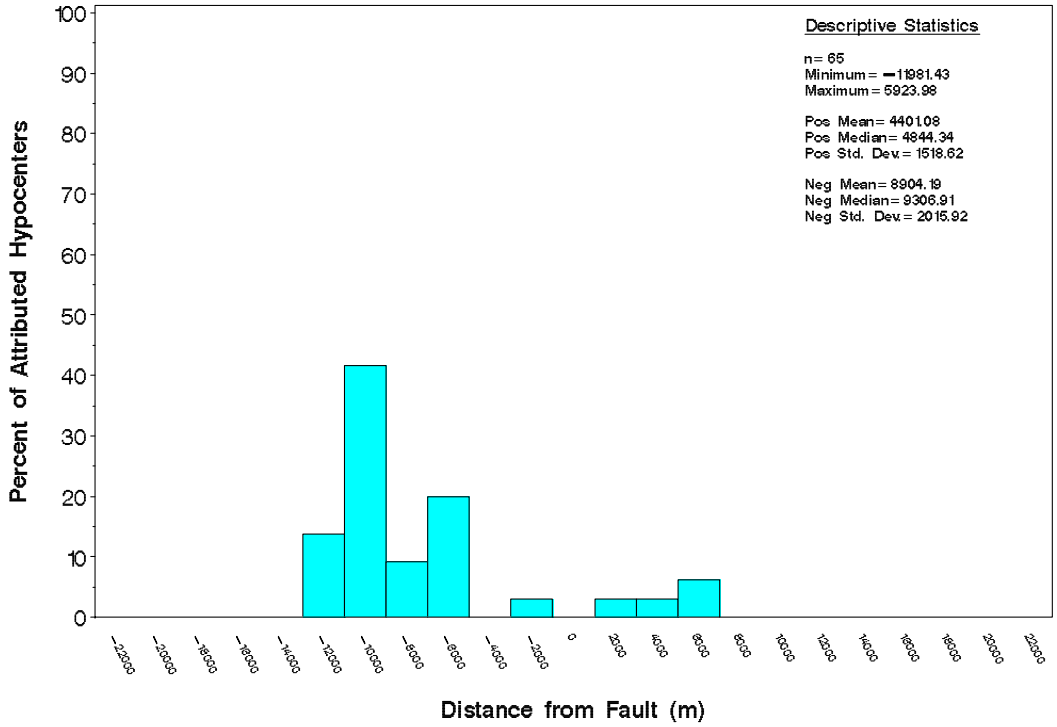

System = Kawaketayama
Fault= Unnamed (A43—7)

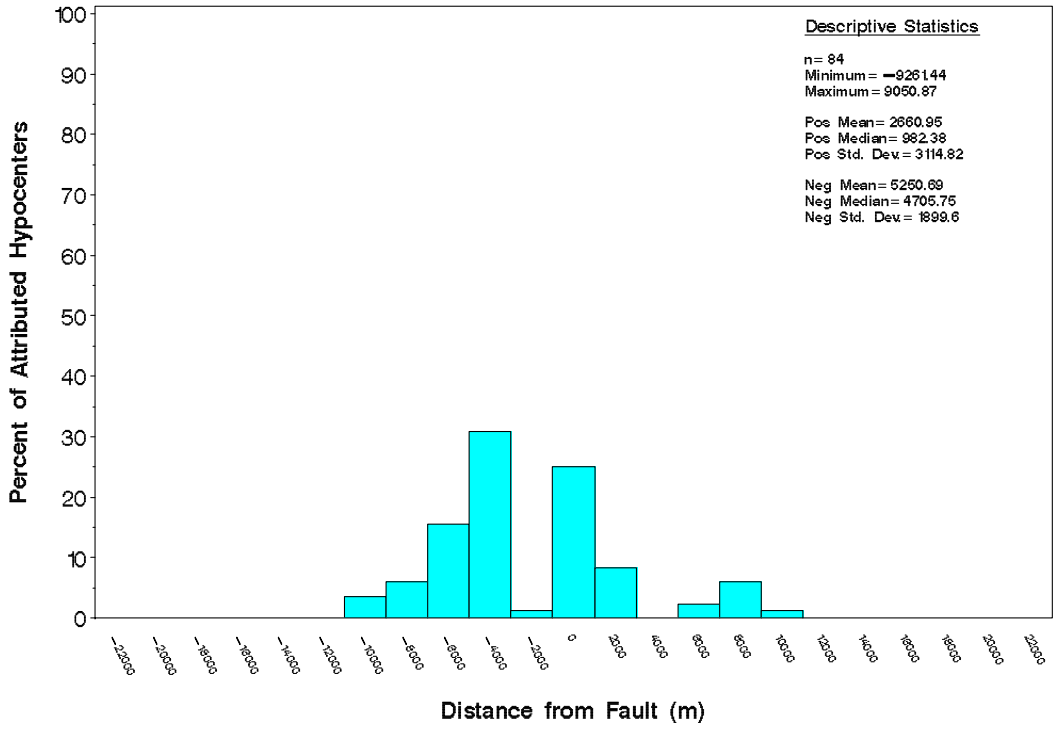

System = Unknown
Fault= Kamimiyori (A44—2b)

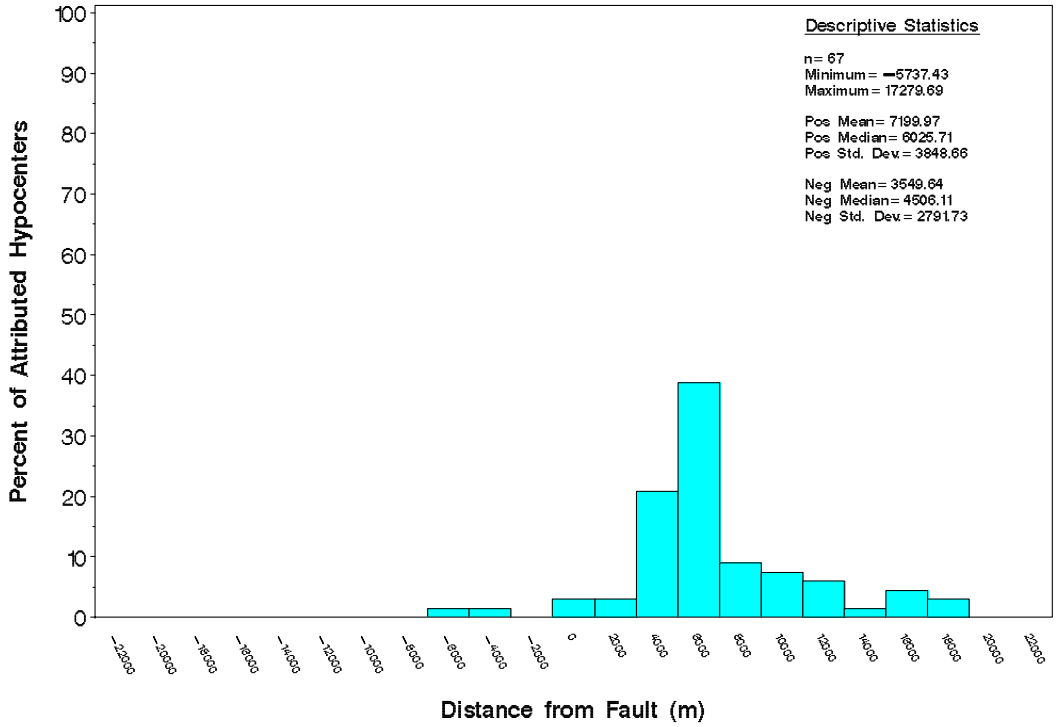

System = Aizu−bonchi−seisn
Fault= Aizu−bonchi−seien−hokubu (A44−3)

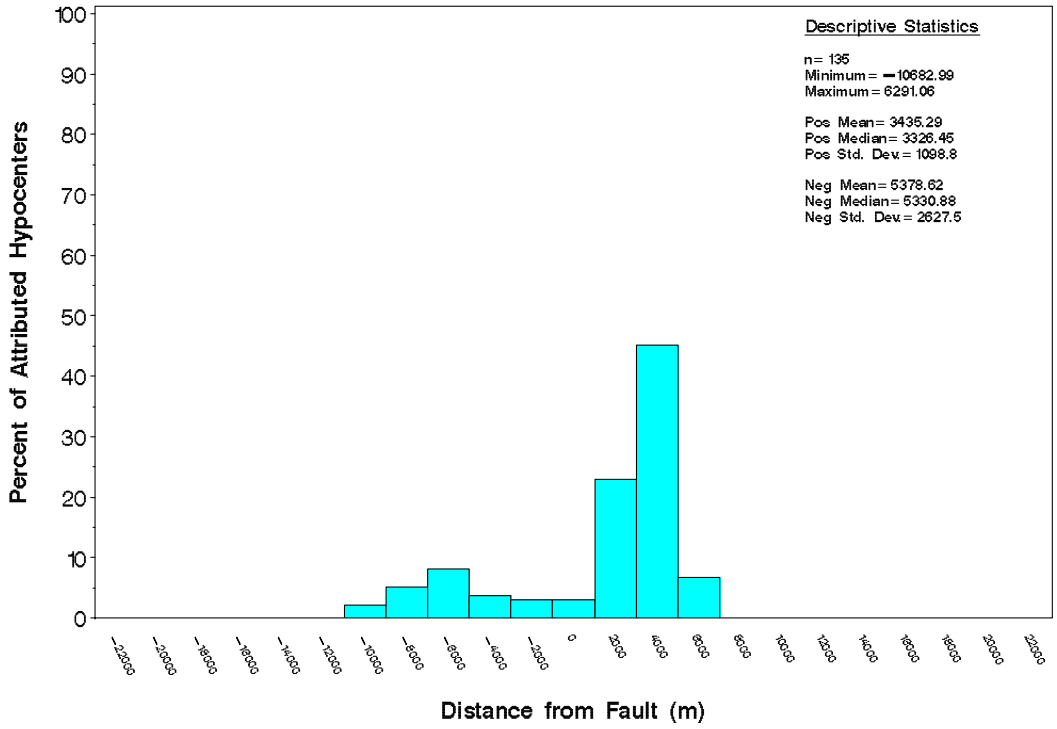

System = Aizu−bonchi−seisn
Fault= Aizu−bonchi−seien−nanbu (A44−4)

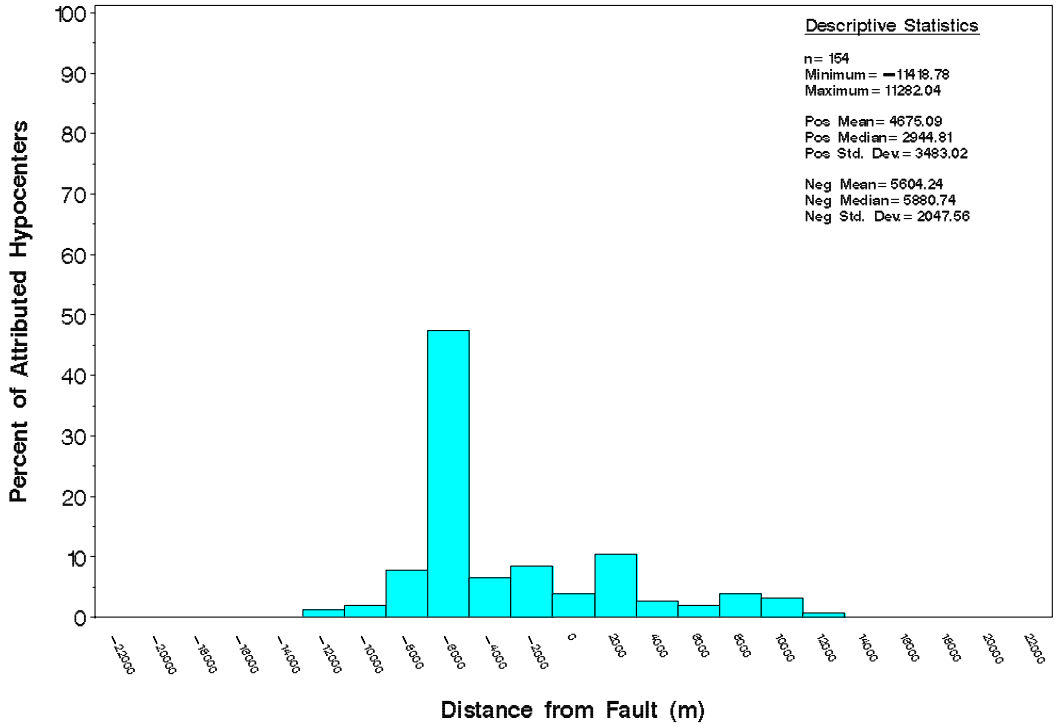

System = Tsukioka
Fault= Tsukioka (A44—5)

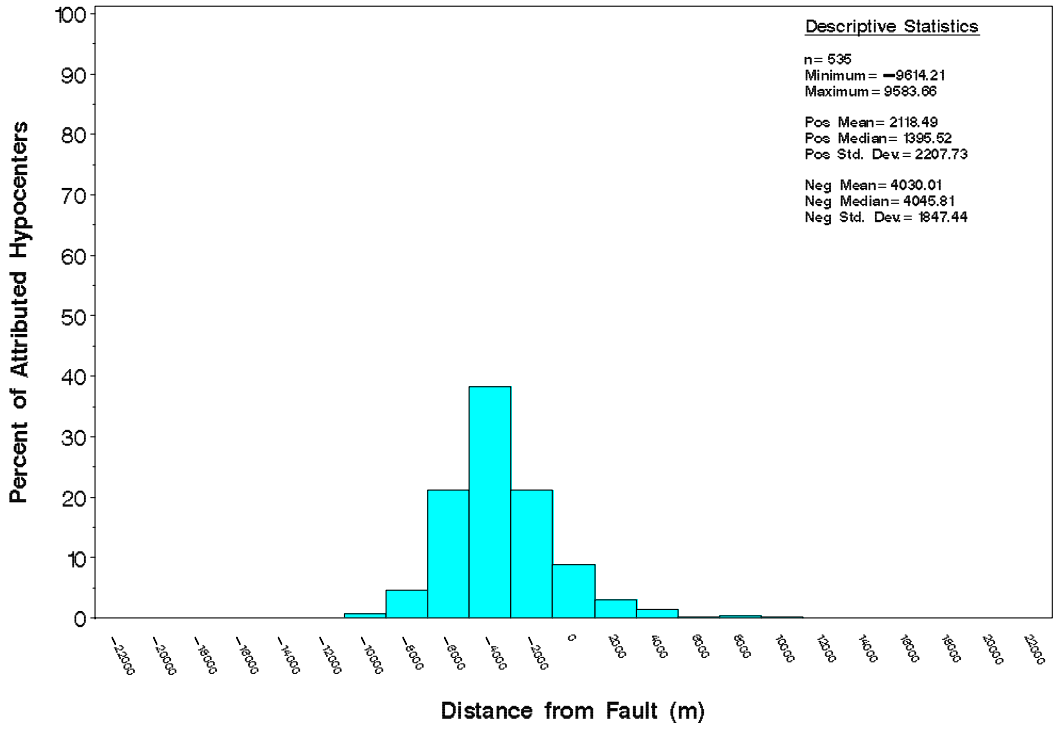

System = Sekiya
Fault= Sekiya (A50—1)

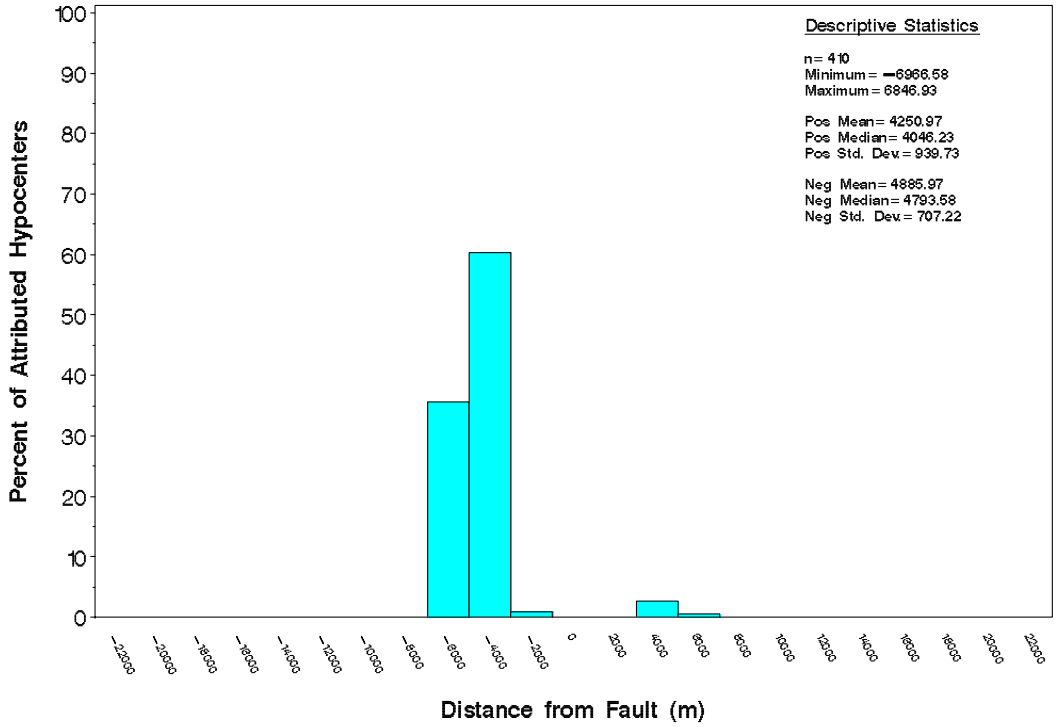

System = Unknown
Fault= Unnamed (A50—2)

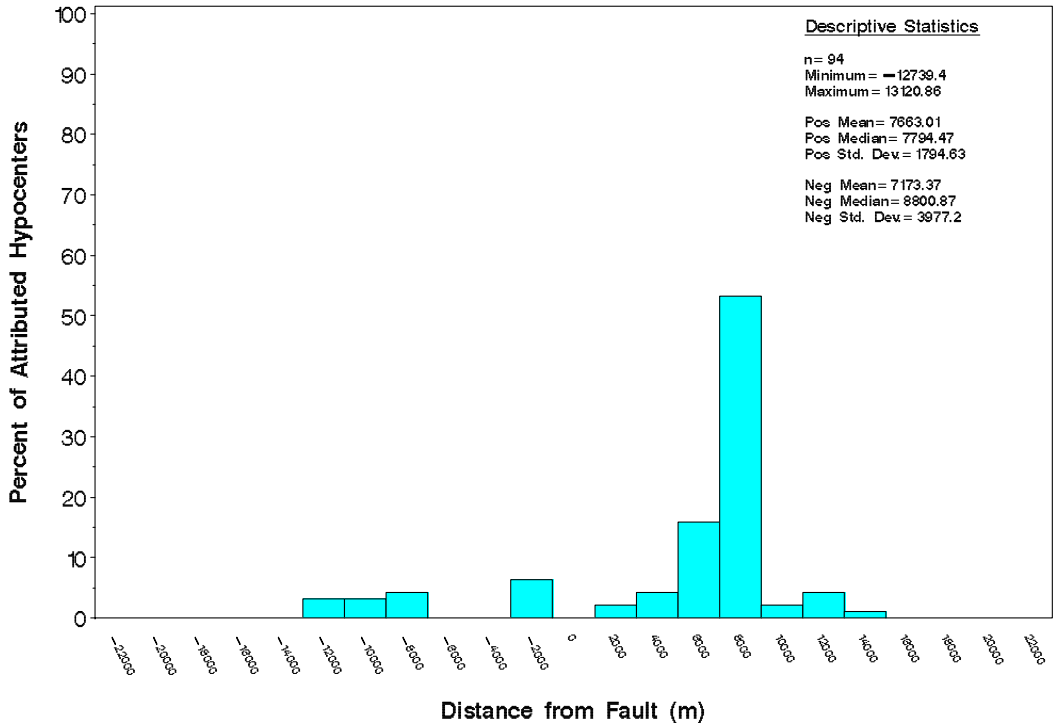

System = Kanto—heiya—hokuseien
Fault= Unnamed (A51—1)

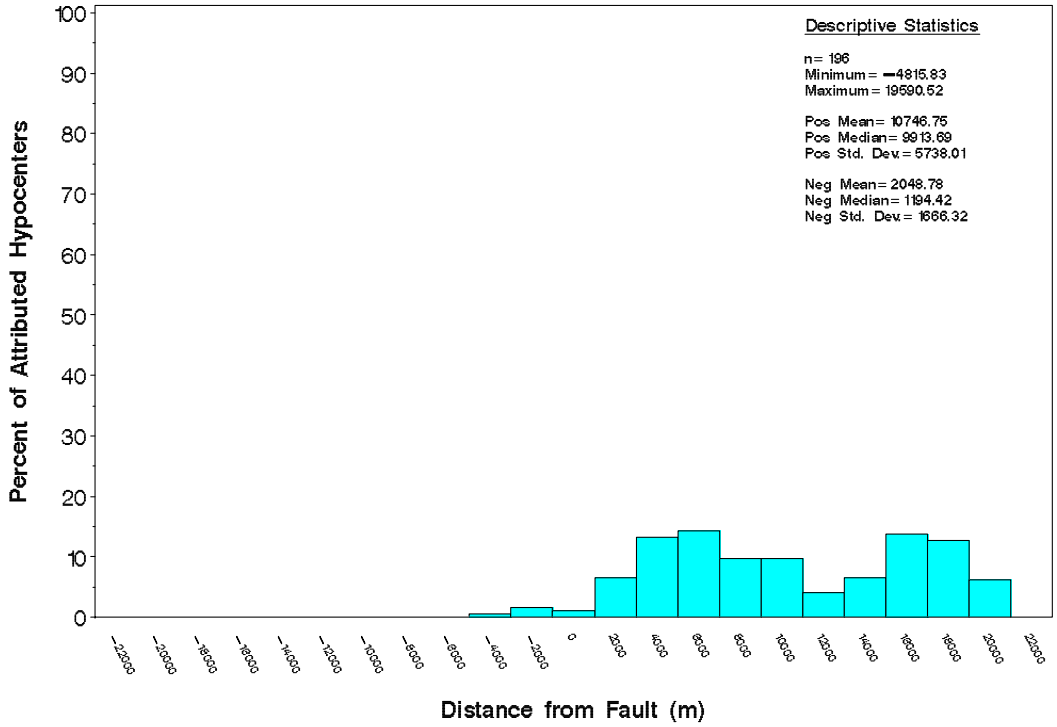

System = Hirai—Kushihiki
Fault= Unnamed (A51—2)

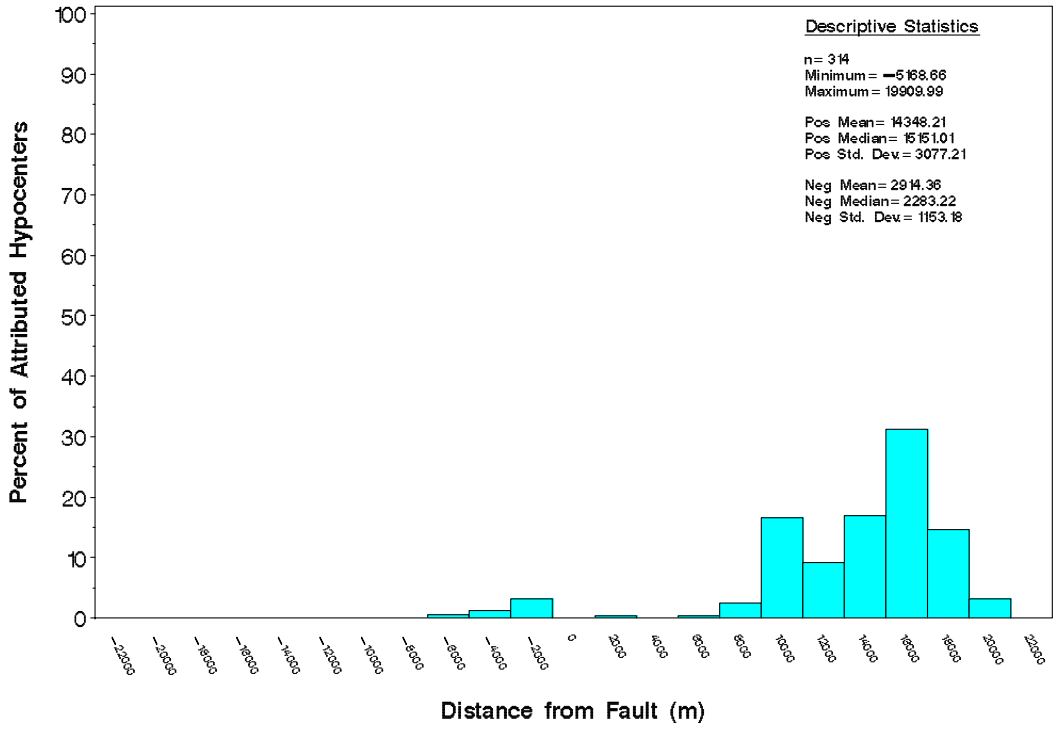

System = Tachikawa
Fault= Unnamed (A52—1)

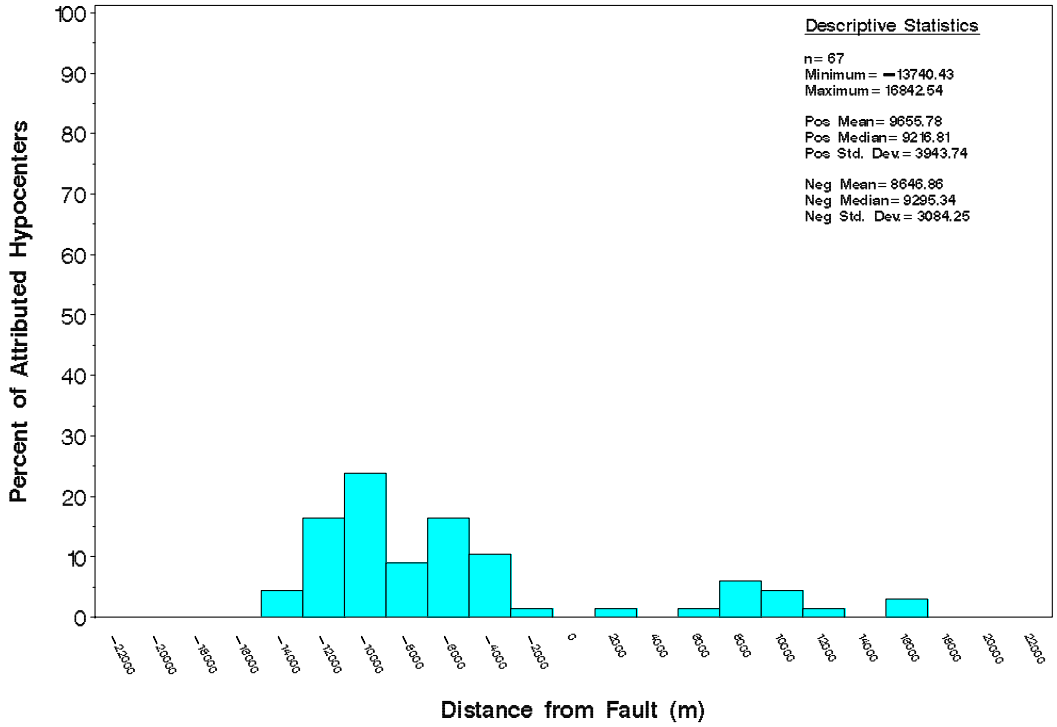

System = Isehara
Fault= Isehara (A52−2)

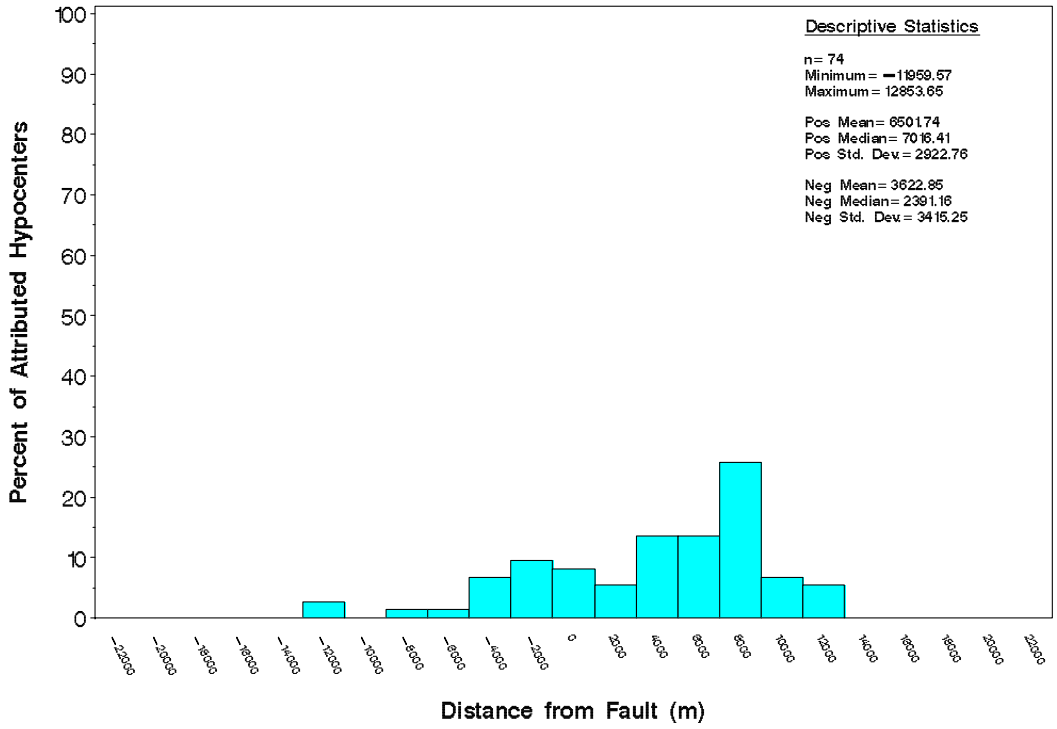

System = Kannawa/Kouzu−Matsuda
Fault= Kouzu−Matsuda (A52−3)

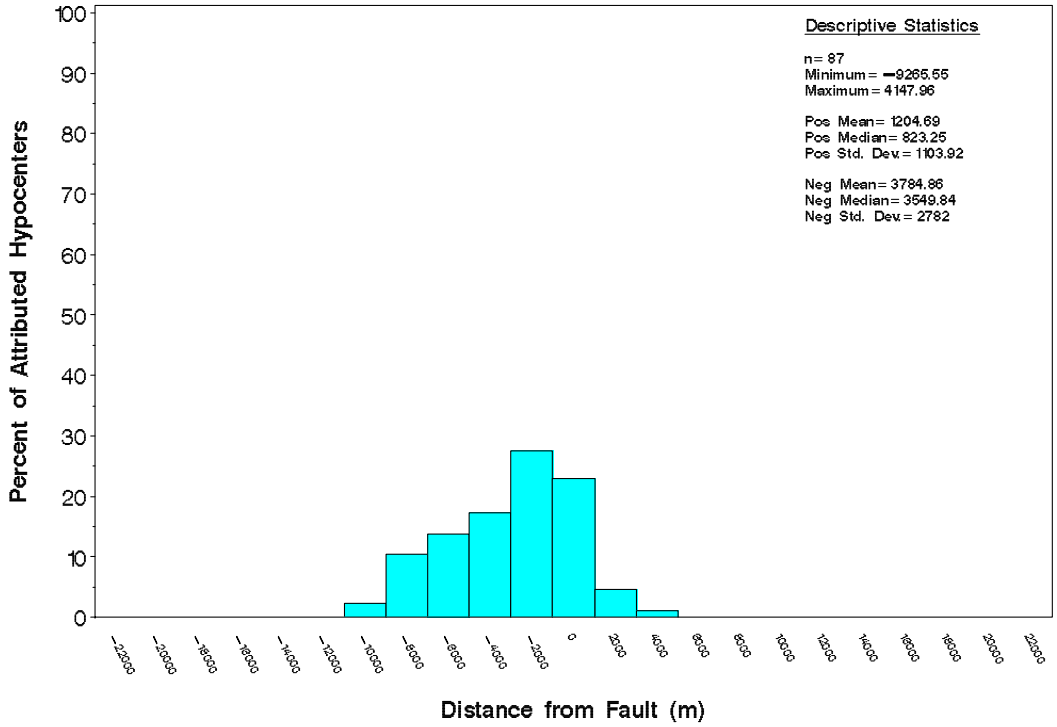

System = Tanna
Fault= Unnamed (A53−2)

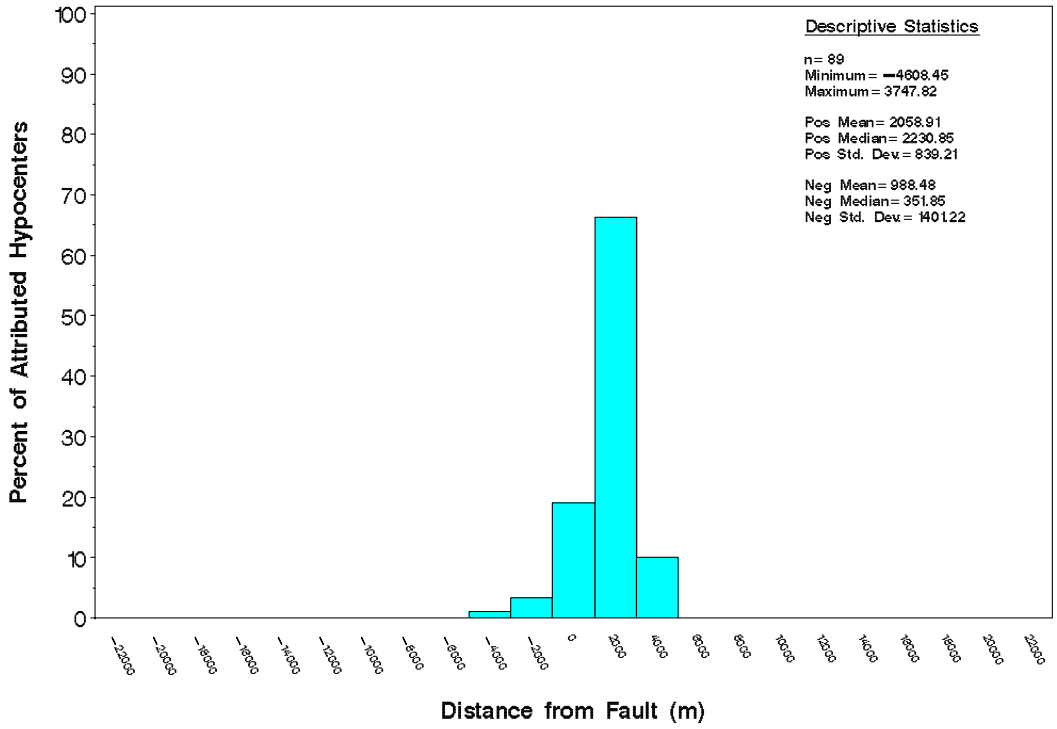

System = Muikamachi−bonchi−hokuen Tectonic Line
Fault= Ishiuchi (A58−1)

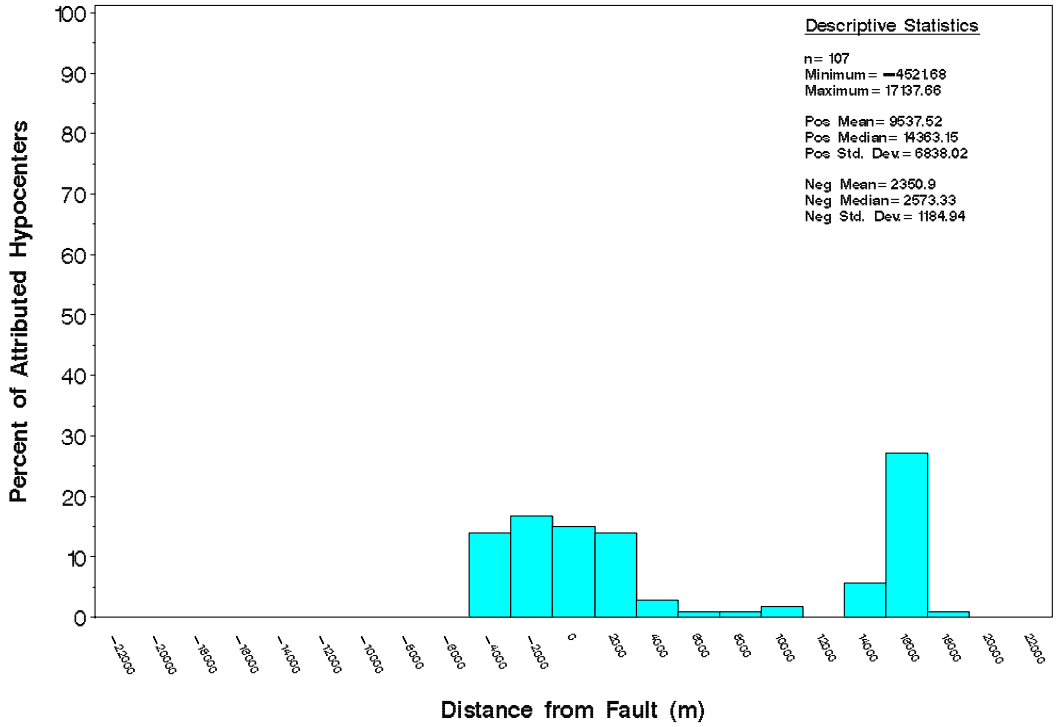

System = Tokamachi
Fault= Tokamachi (A58−2)

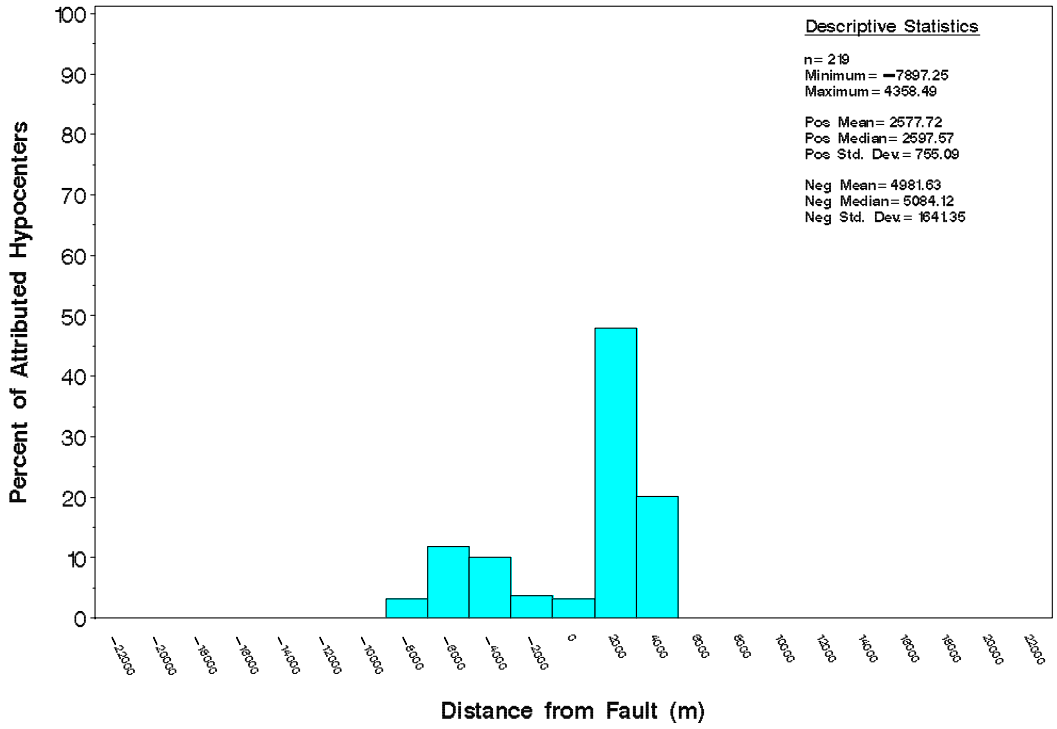

System = Shinanogawa
Fault= Asano, Sansai, Nagaoka, Toyono, Iriishi, Minamigo (A58−6)

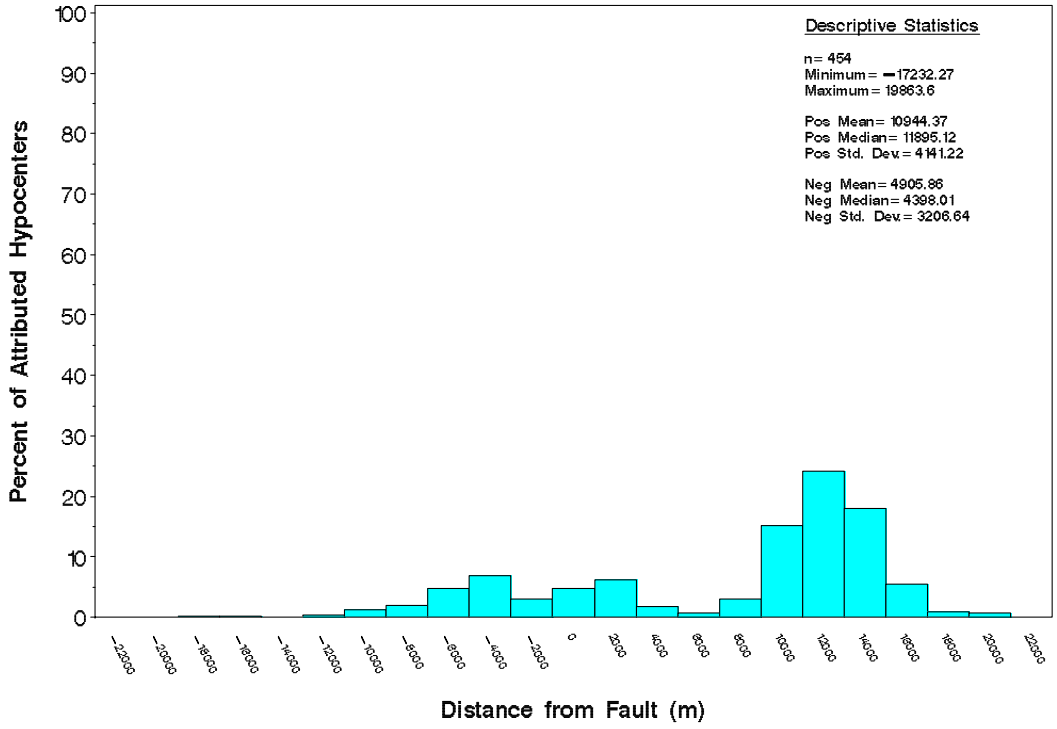

System = Shinanogawa, Nagano—bonchi—seien Tectonic Line
Fault= Shiroyama, Zenkoji, Komoatsubara, Amori (A59—1)

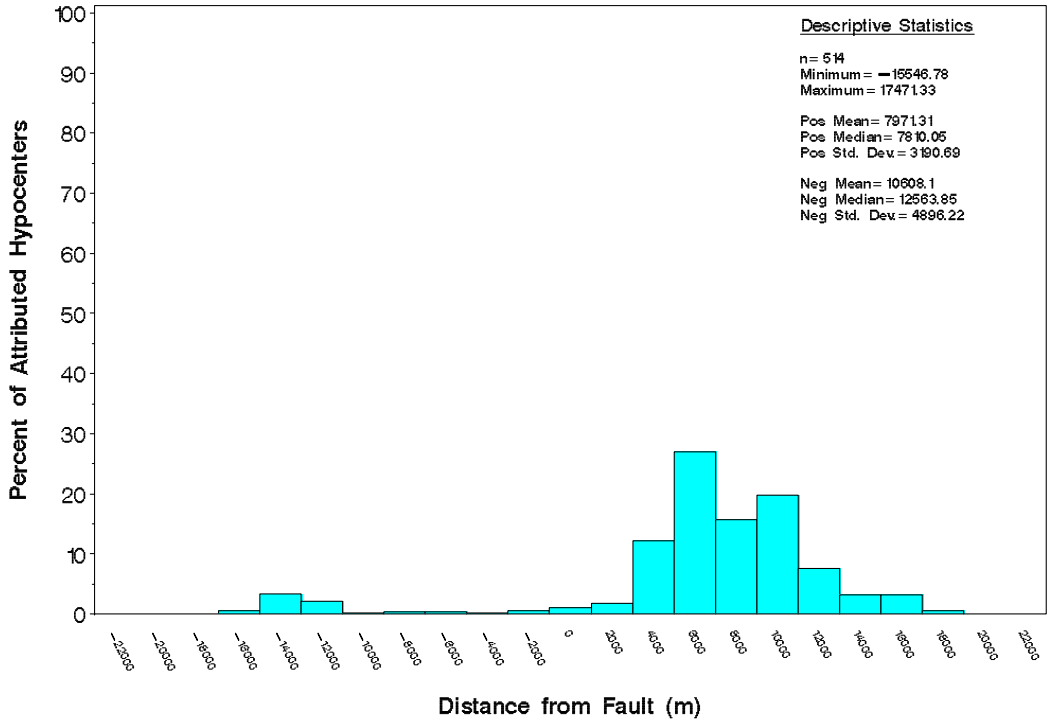

System = Itoigawa—Shizuoka Tectonic Line
Fault= Suwako—minami (A59—3)

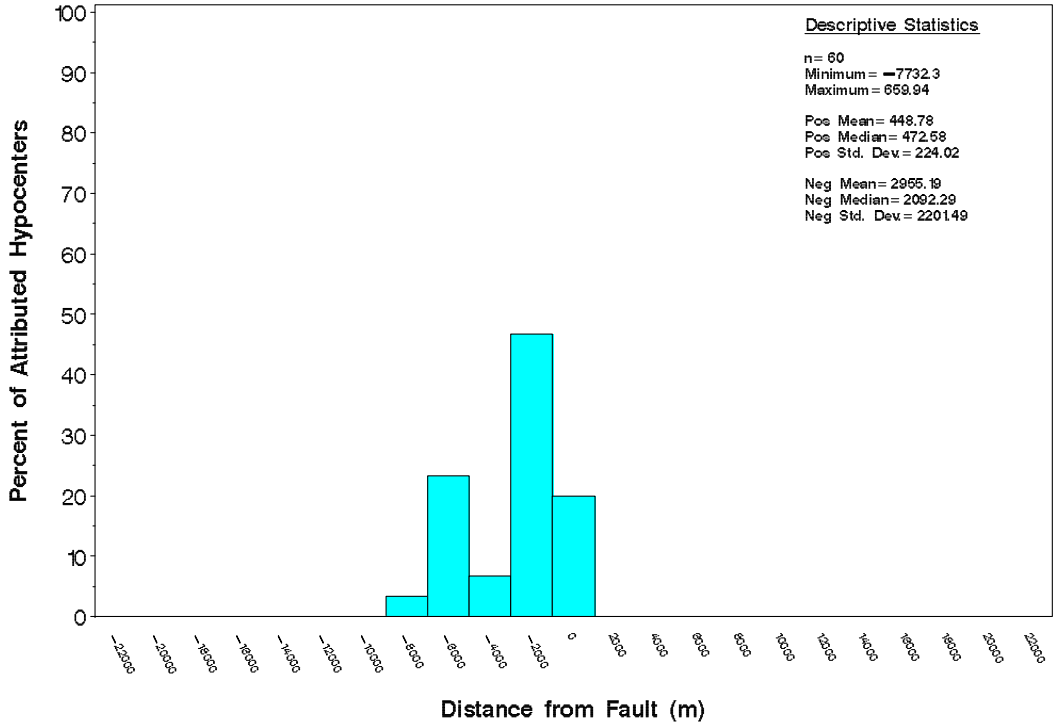

System = Itoigawa—Shizuoka Tectonic Line
Fault= Simotsugi, Hakusyu (A60—2)

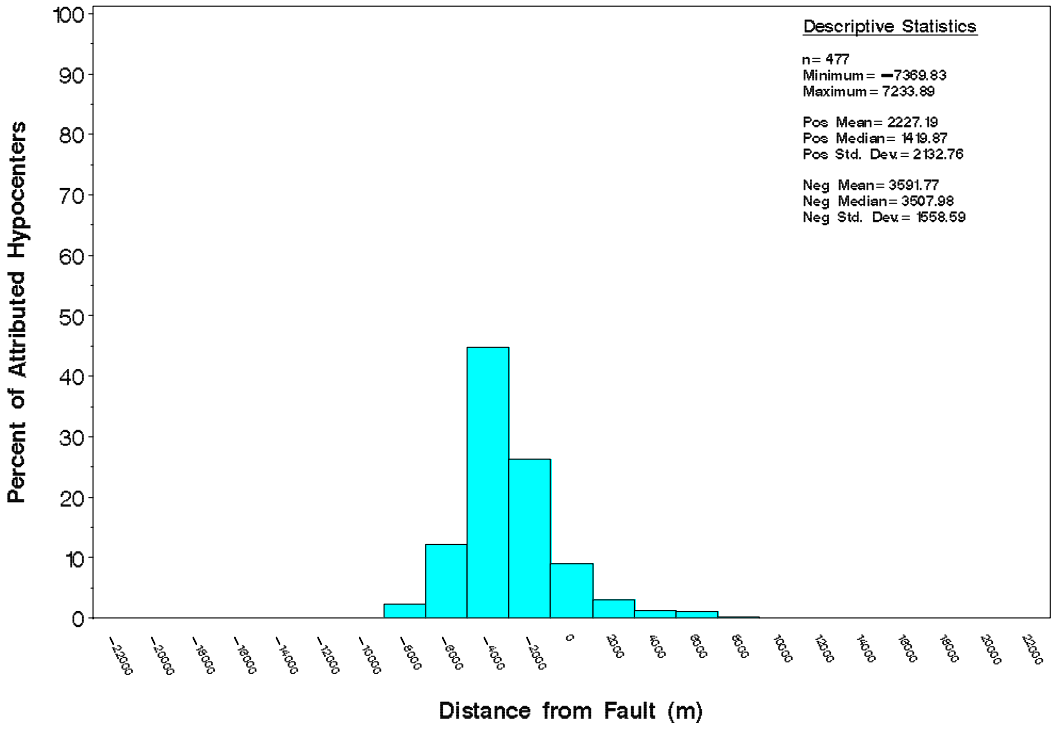

System = Fujigawa—kako
Fault= Ankyoyama (A61—1a)

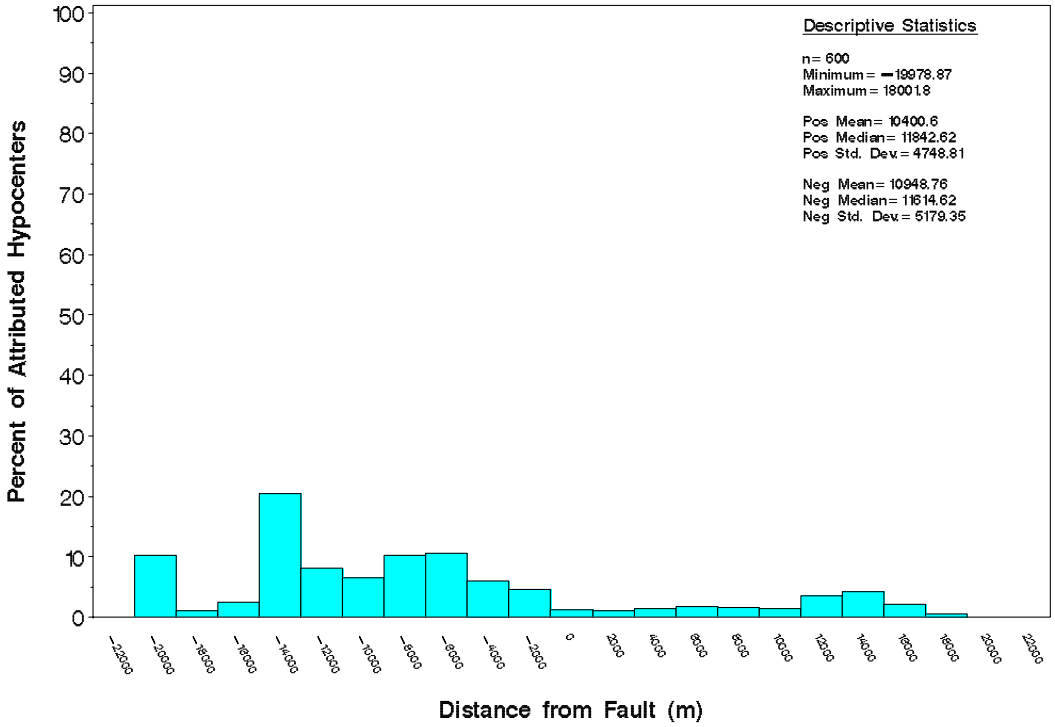

System = Itoigawa−Shizuoka Tectonic Line
Fault= Shinsiro, Matsumoto−bonchi−touen (A64−1)

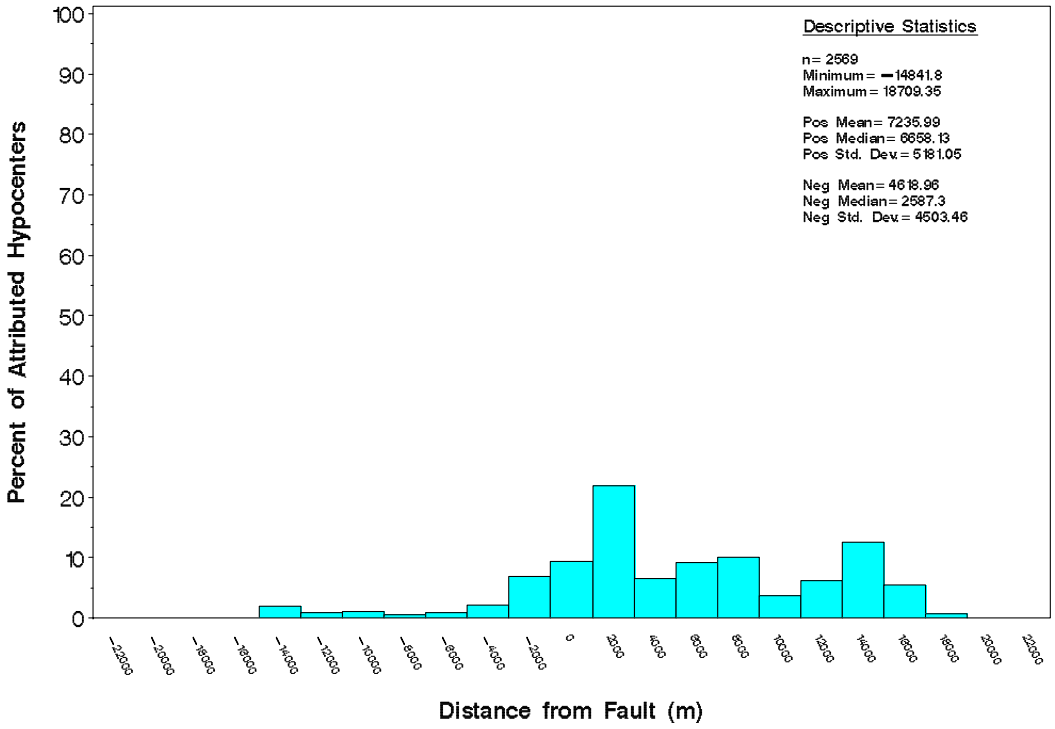

System = Itoigawa−Shizuoka Tectonic Line
Fault= Ushifuseji (A64−2)

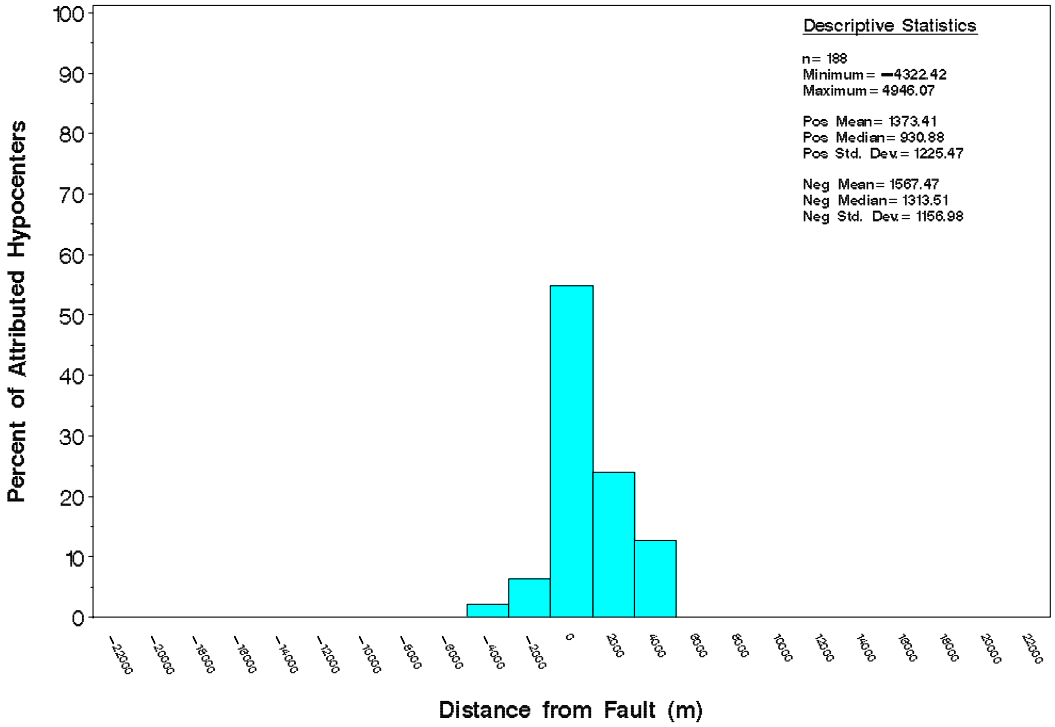

System = Sakai−toge−Kamiya
Fault= Sakai−toge (A64−4)

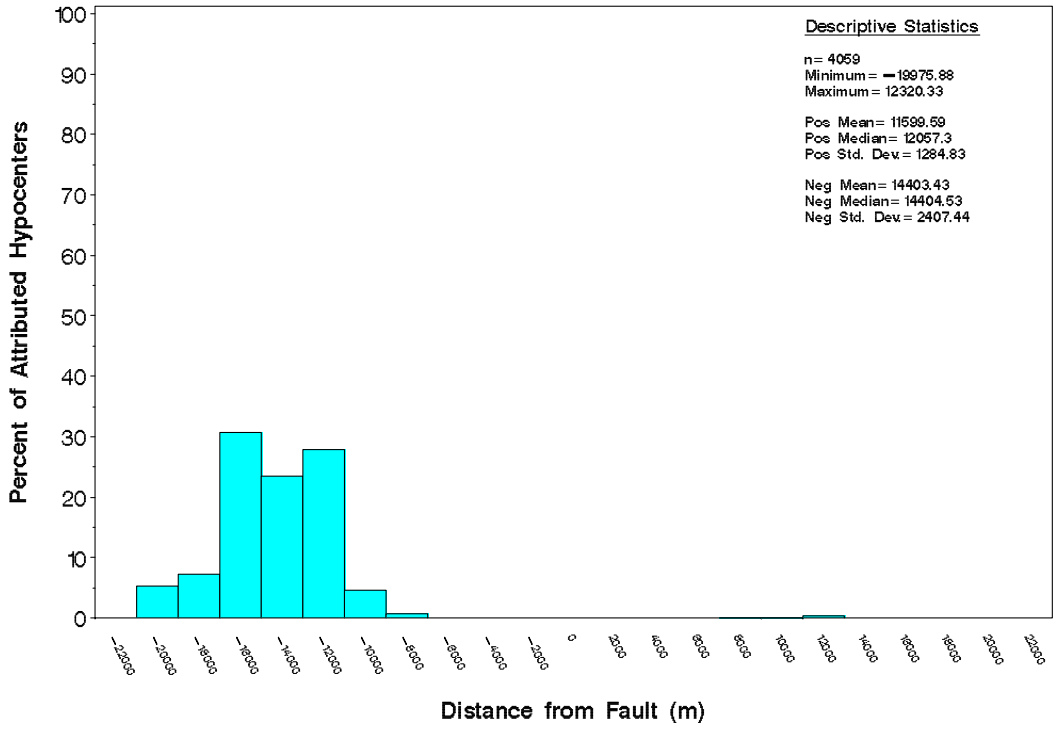

System = Enago
Fault= Atotsugawa (A64−5)

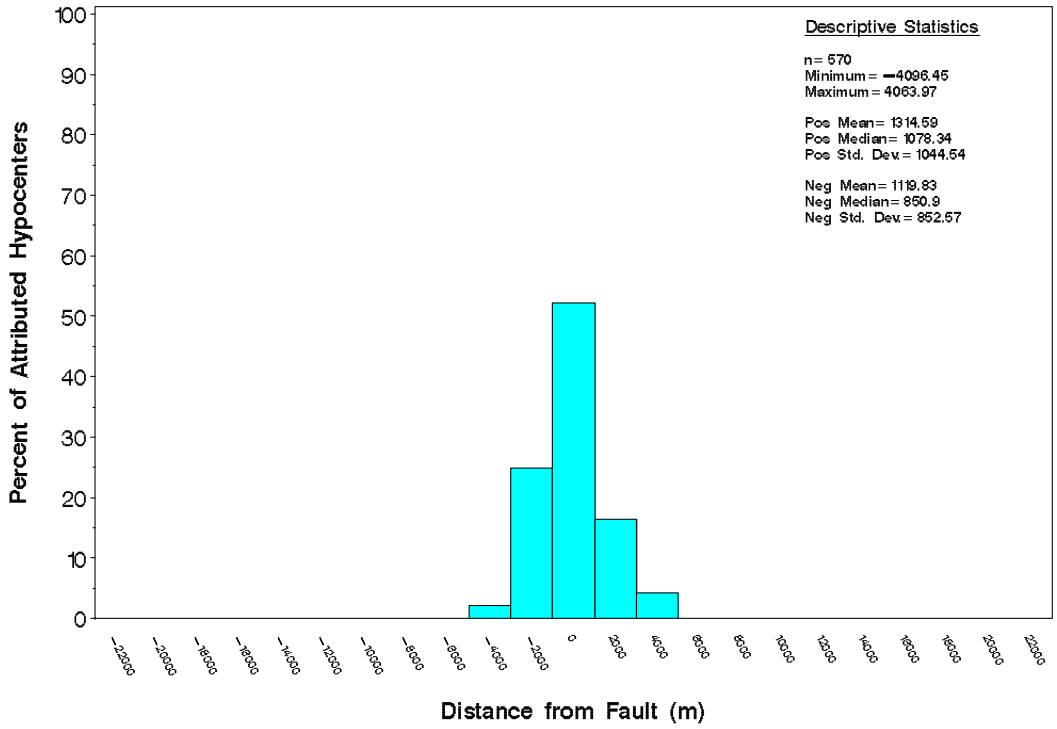

System = Ushikubi
Fault= Ushikubi (A64−6)

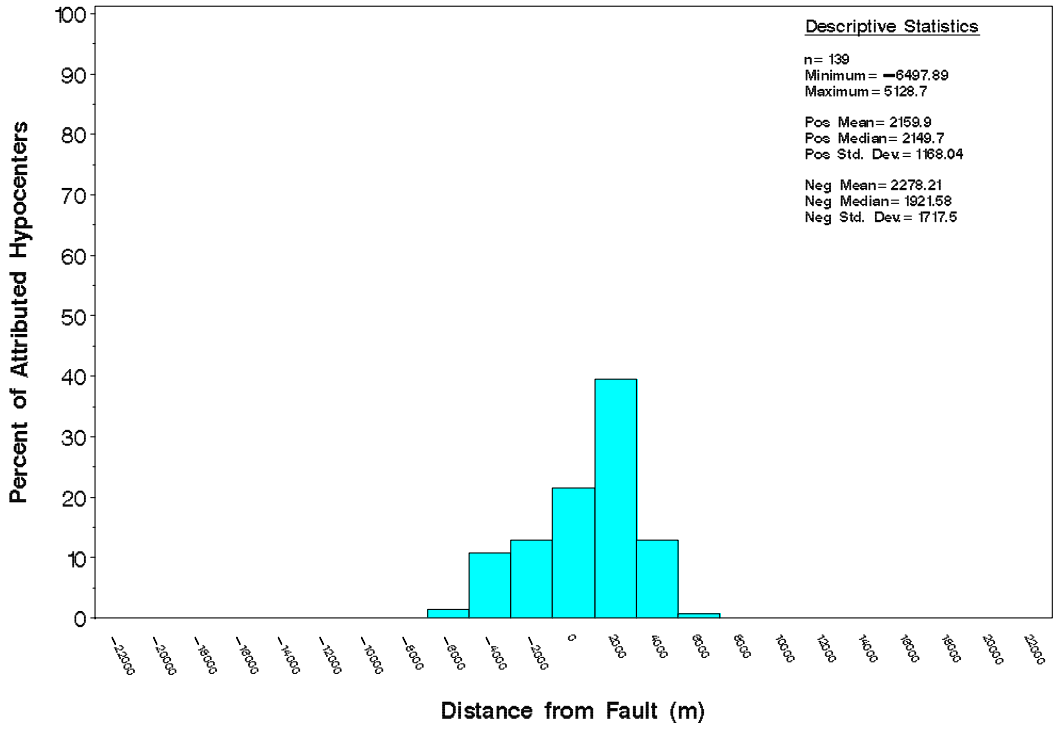

System = Enago
Fault= Enago (A64−7)

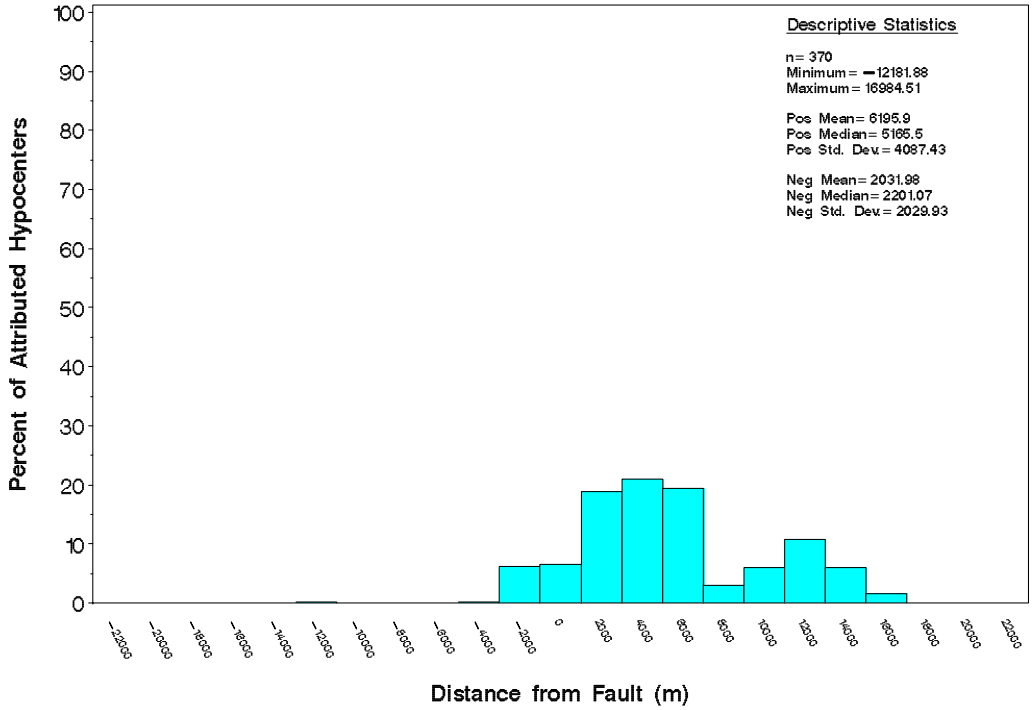

System = Takayama – Ohara
Fault= Makigabura (A64 – 8)

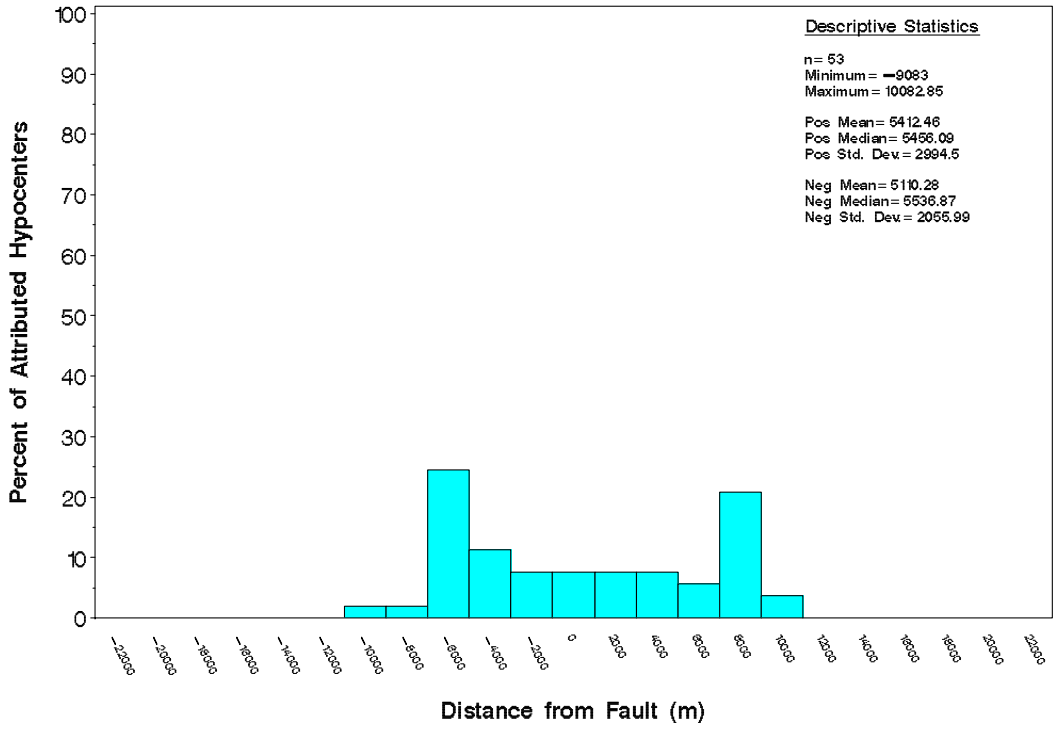

System = Inadani
Fault= Ogurogawa, Tagiri (A65 – 2)

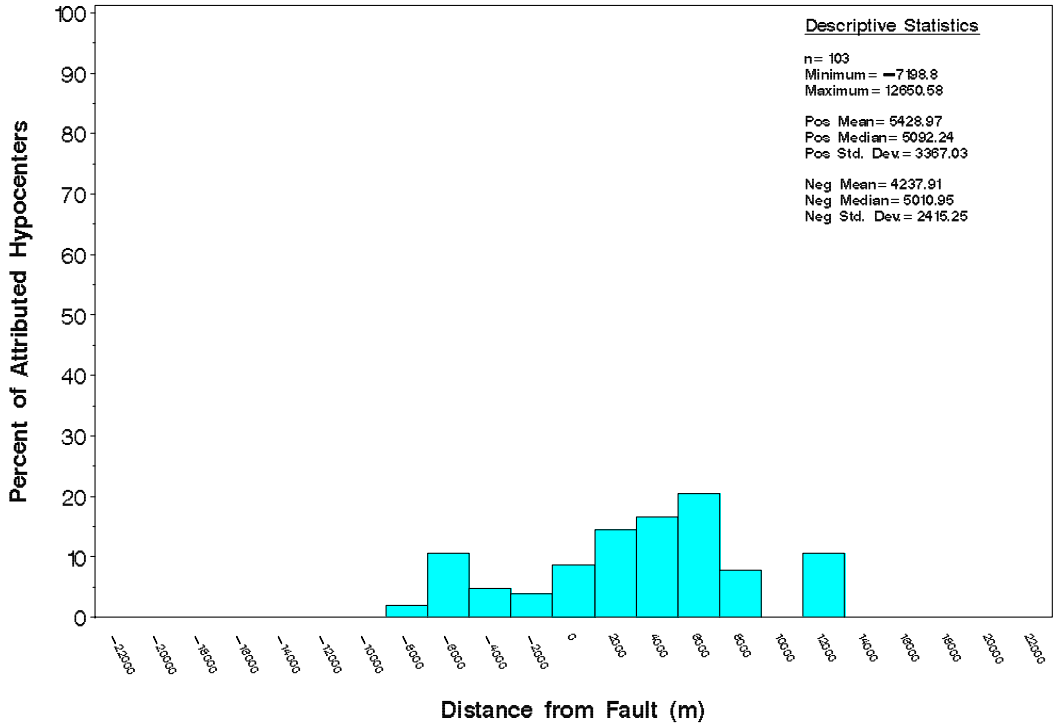

System = Inadani
Fault= Tagiri (A65−3)

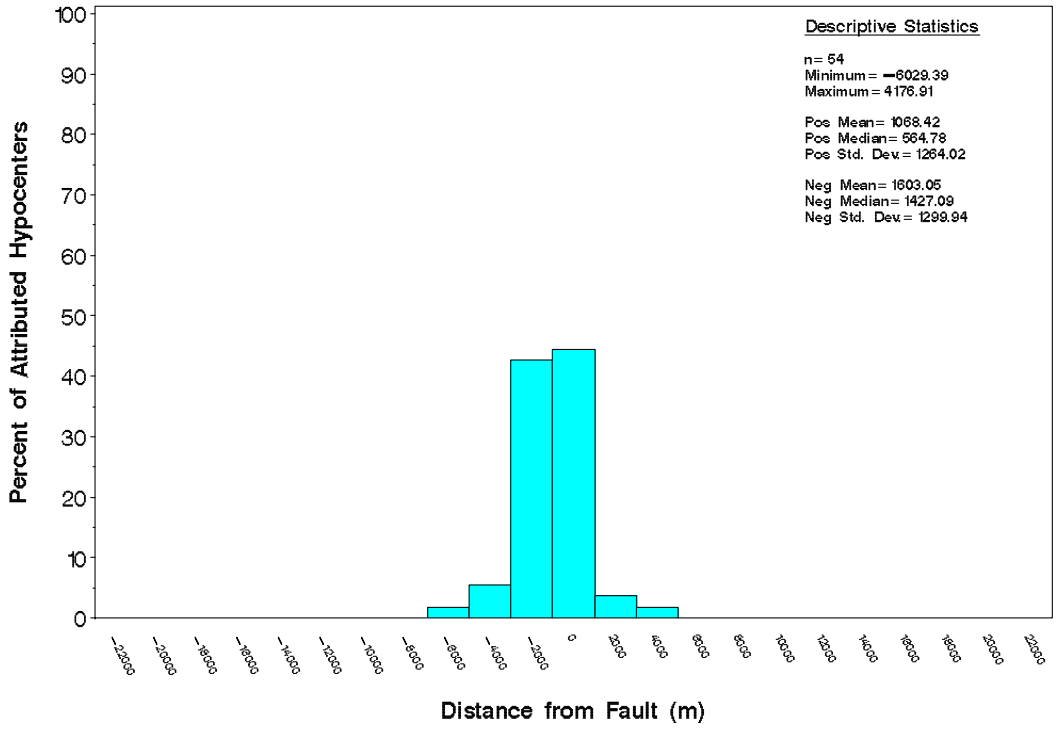

System = Inadani
Fault= Sansyu (A65−5)

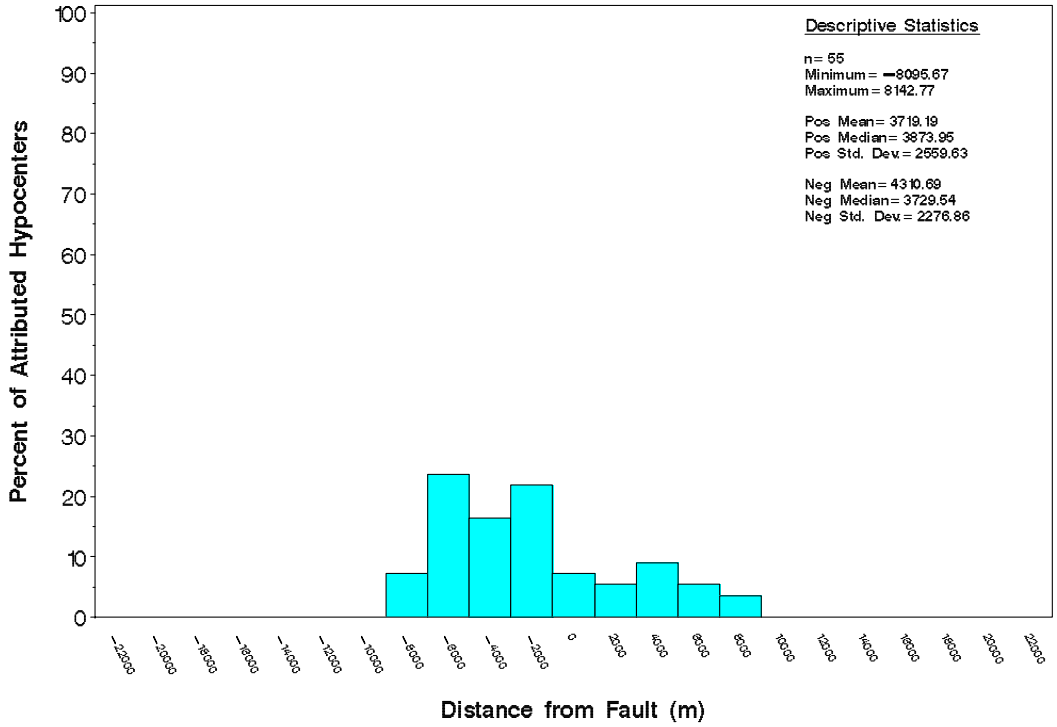

System = Kisogawa
Fault= Seinaiji−toge (A65−6)

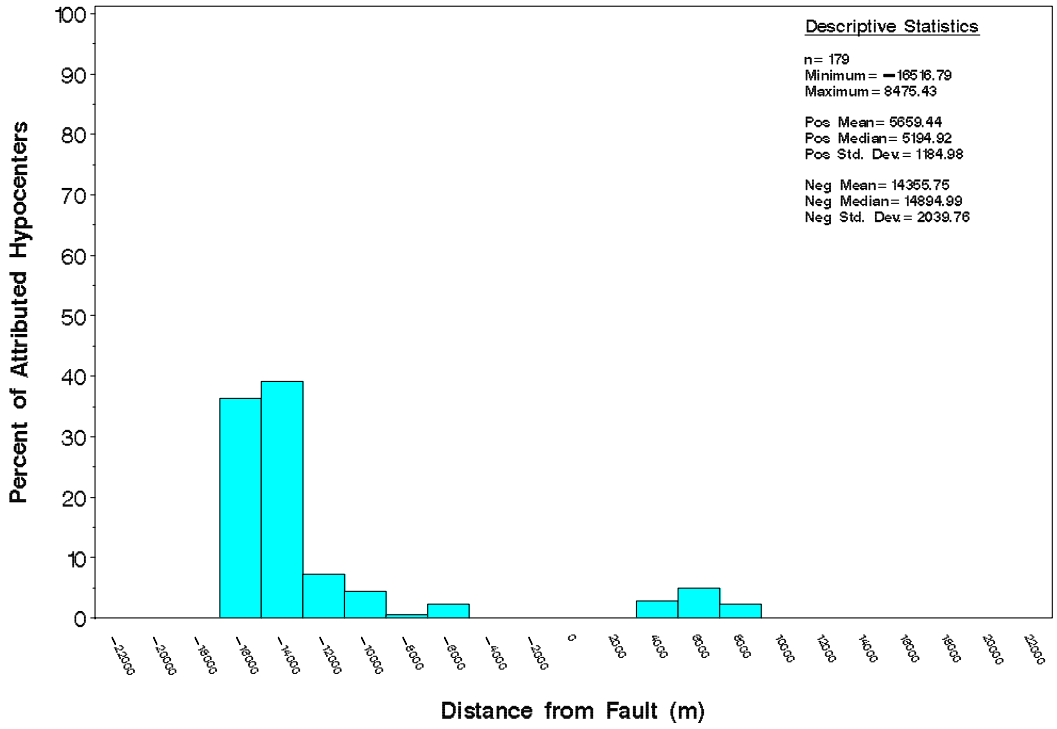

System = Atera
Fault= Atera, Ogiwara−higashi, Gero, Ogiwara−nishi (A65−8)

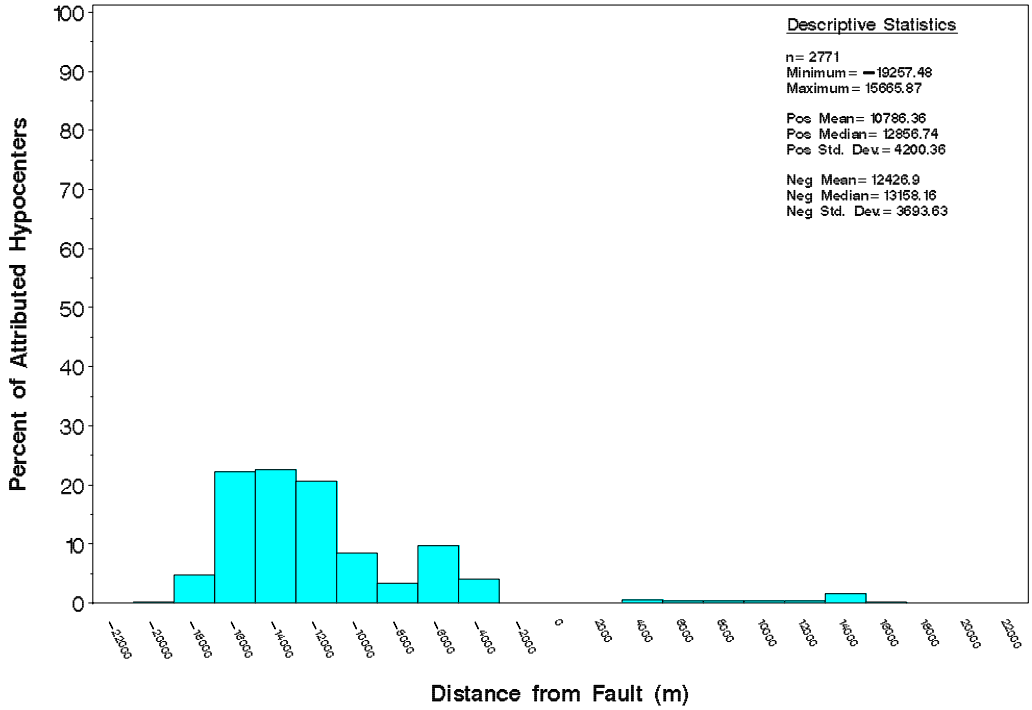

System = Takashimizu
Fault= Takashimizu (A70−1)

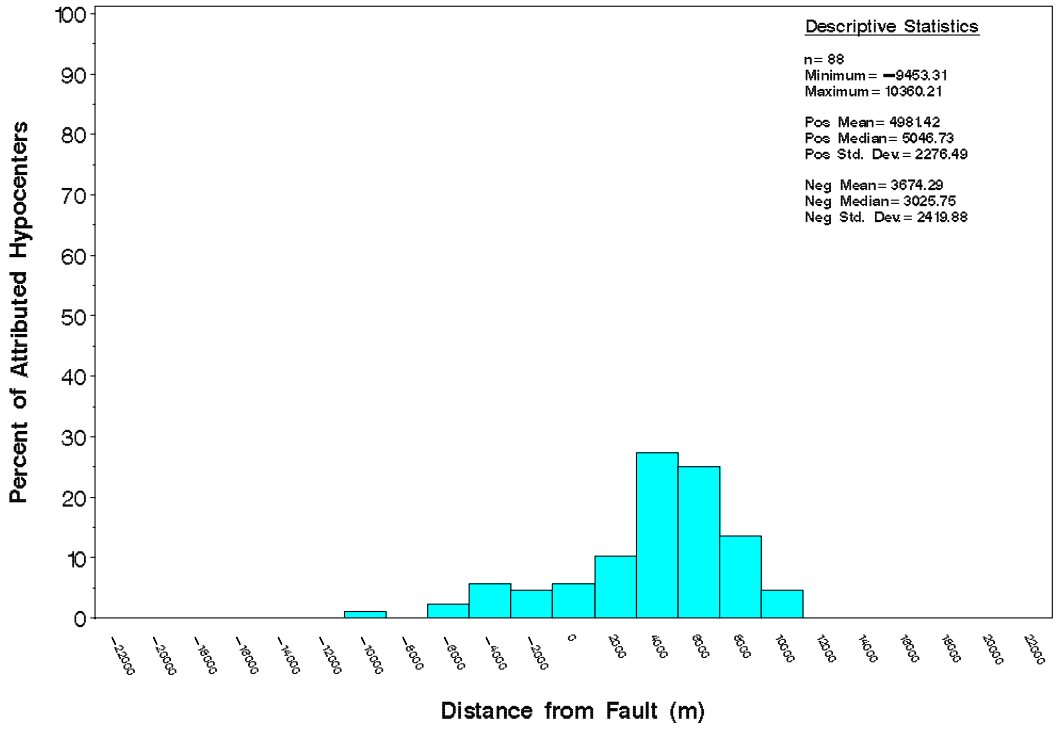

System = Shokawa
Fault= Kzura, Shirakawa, Miogawa (A70−4)

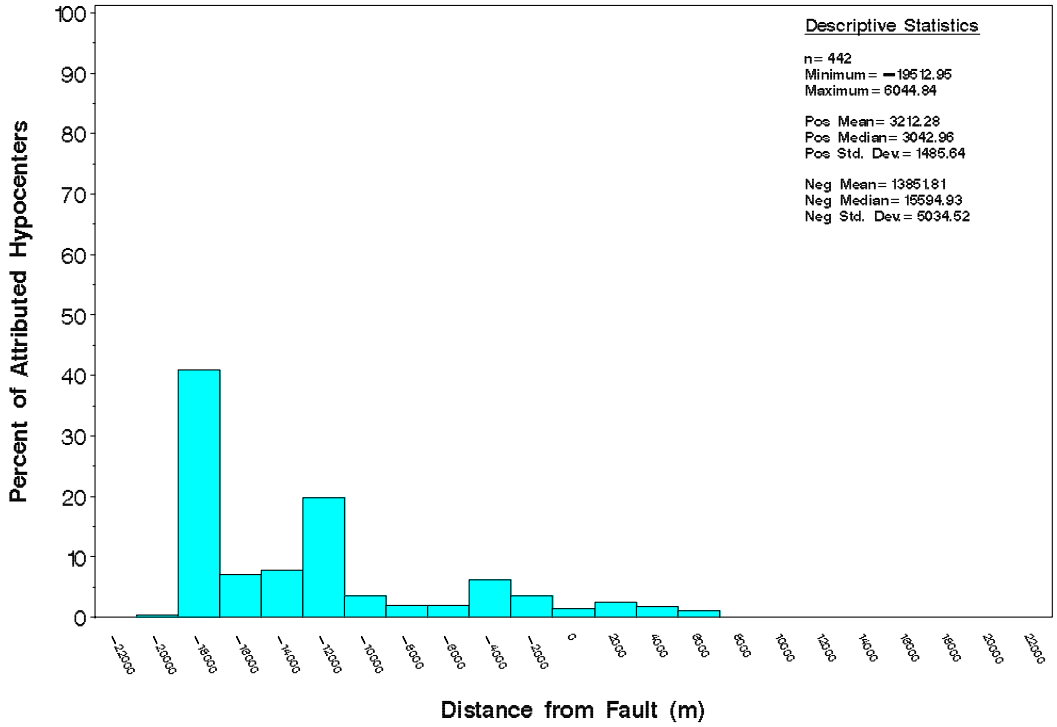

System = Neodani
Fault= Atsumi (A71−1)

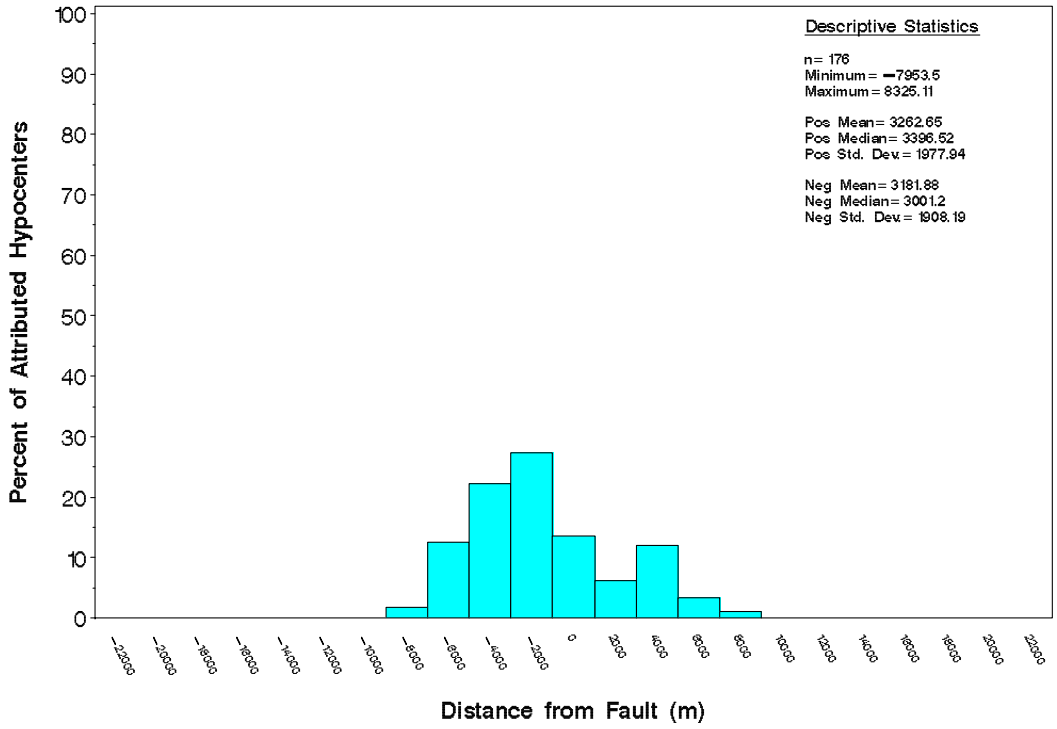

System = Neodani
Fault= Mugigawa (A71−2)

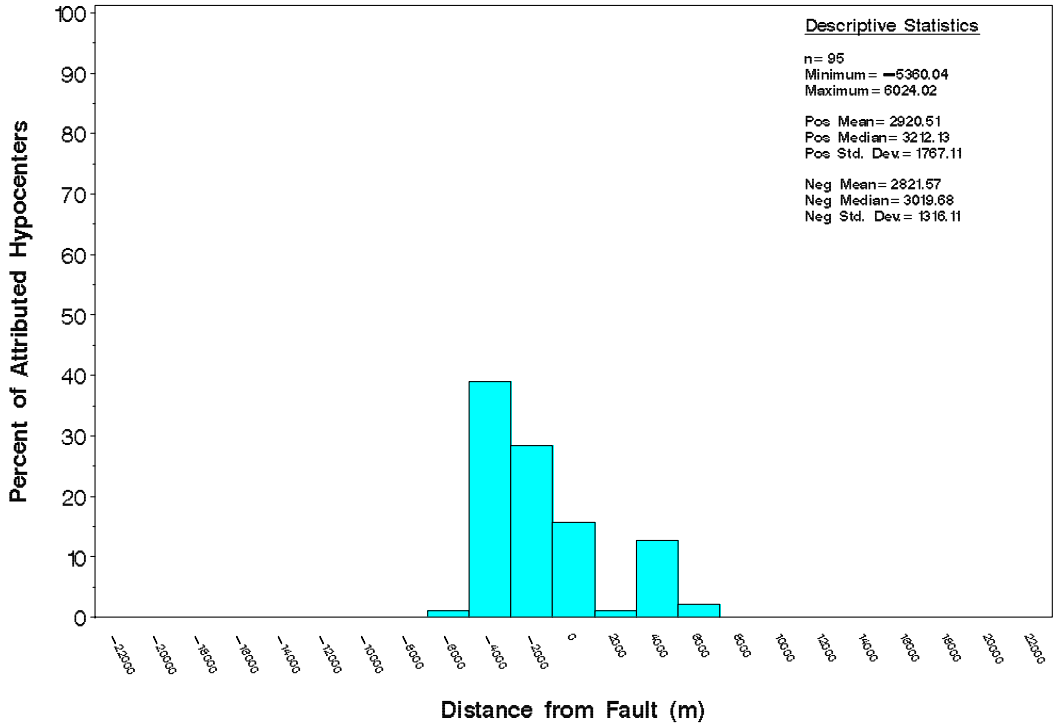

System = Neodani
Fault= Neodani (A71—3b)

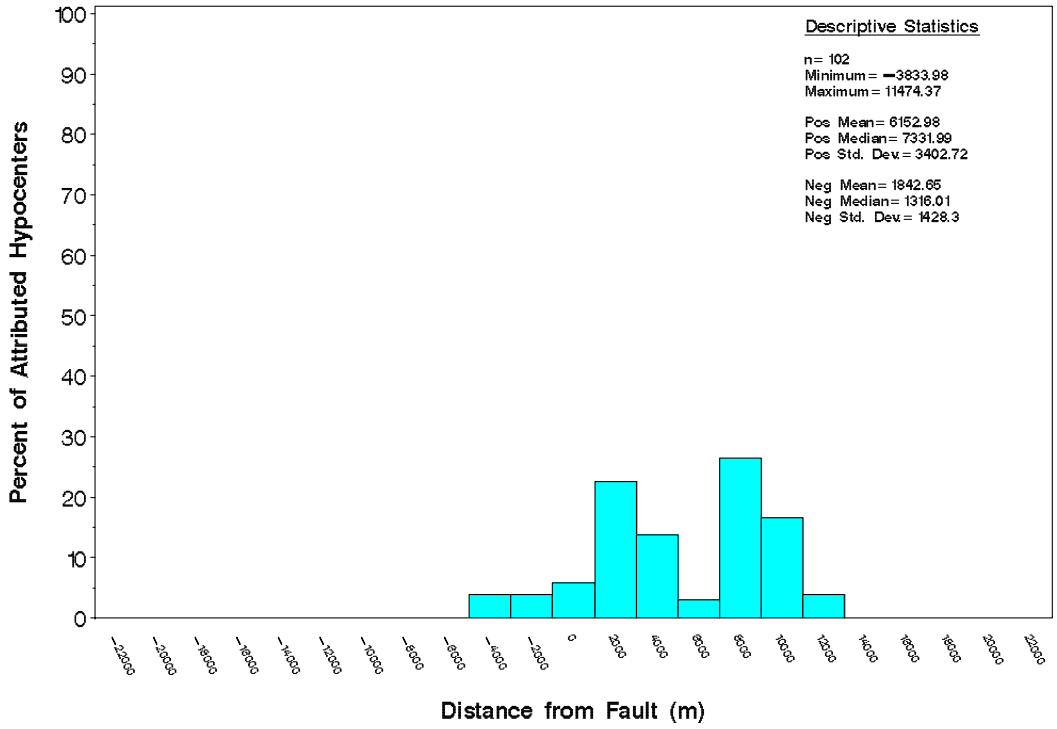

System = Neodani
Fault= Umehara (A71—4)

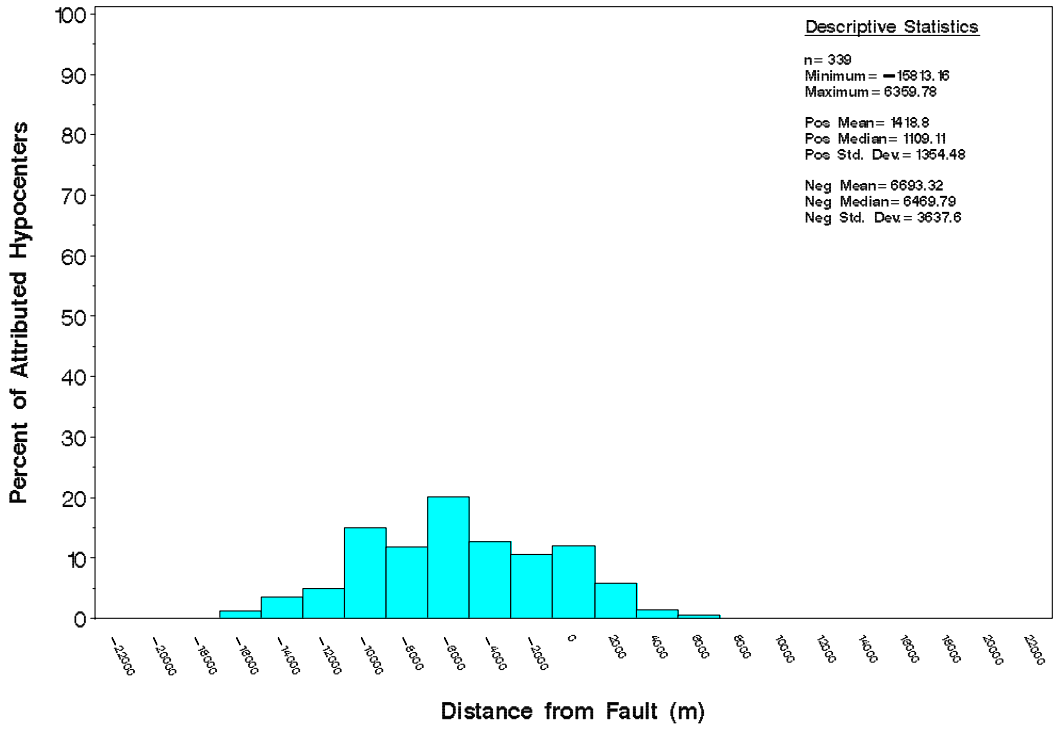

System = Kinsoudake
Fault= Kinsoudake (A71—5)

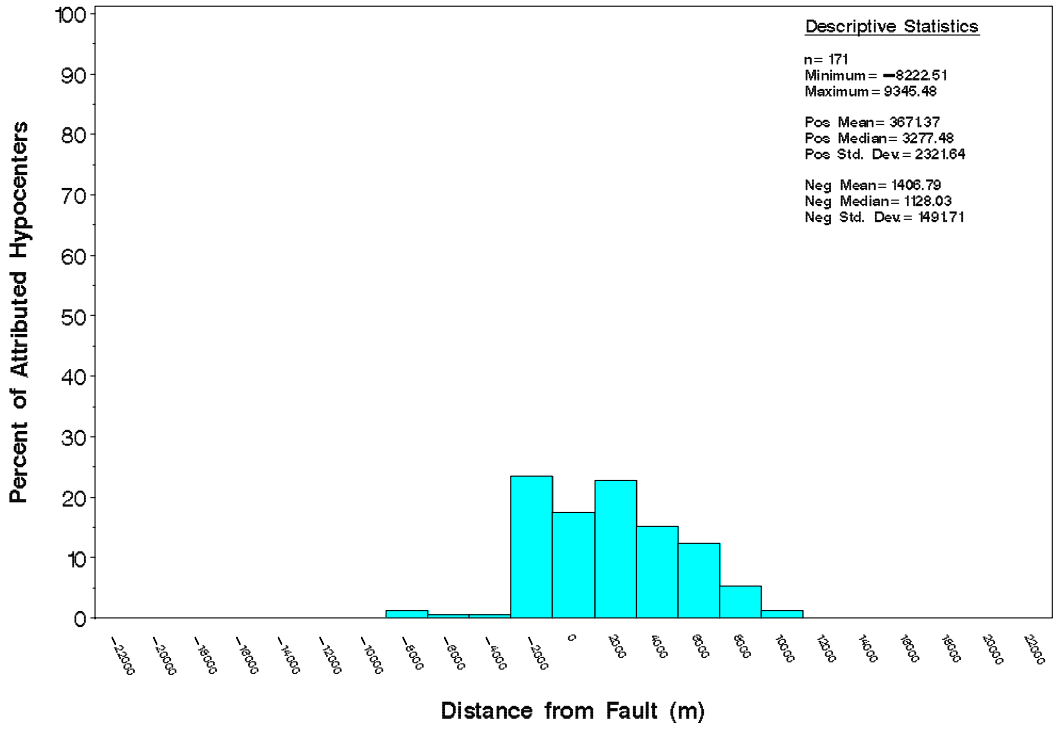

System = Yoro—Kuwana—Yokkaichi
Fault= Ikedayama (A71—6)

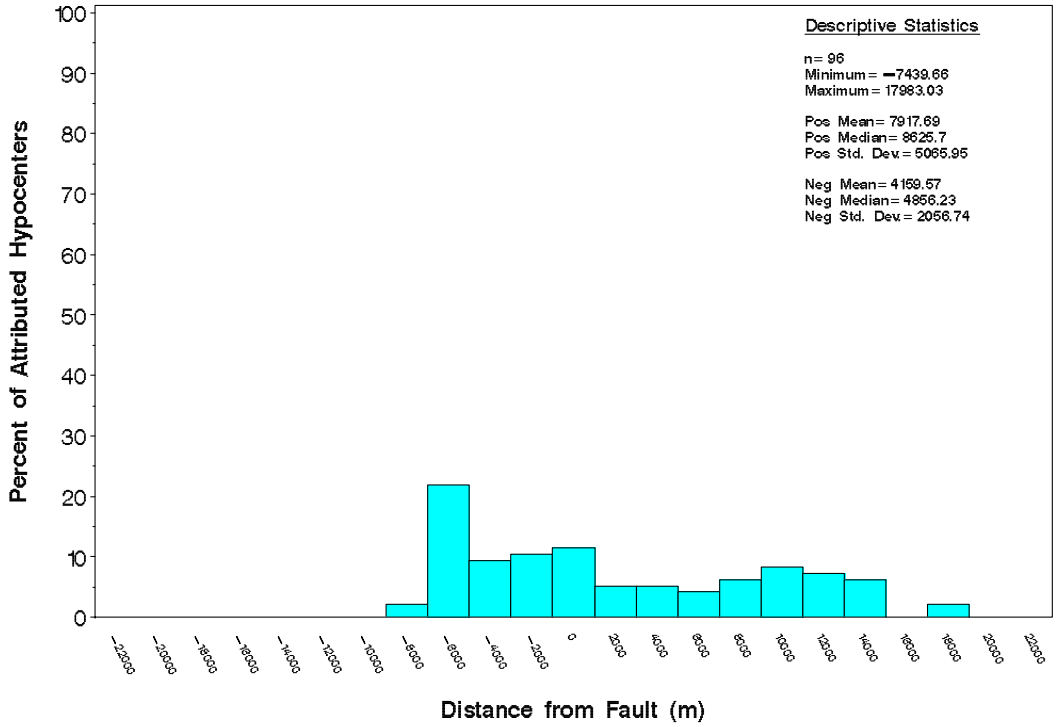

System = Yanagase
Fault= Yanagase (A71—7)

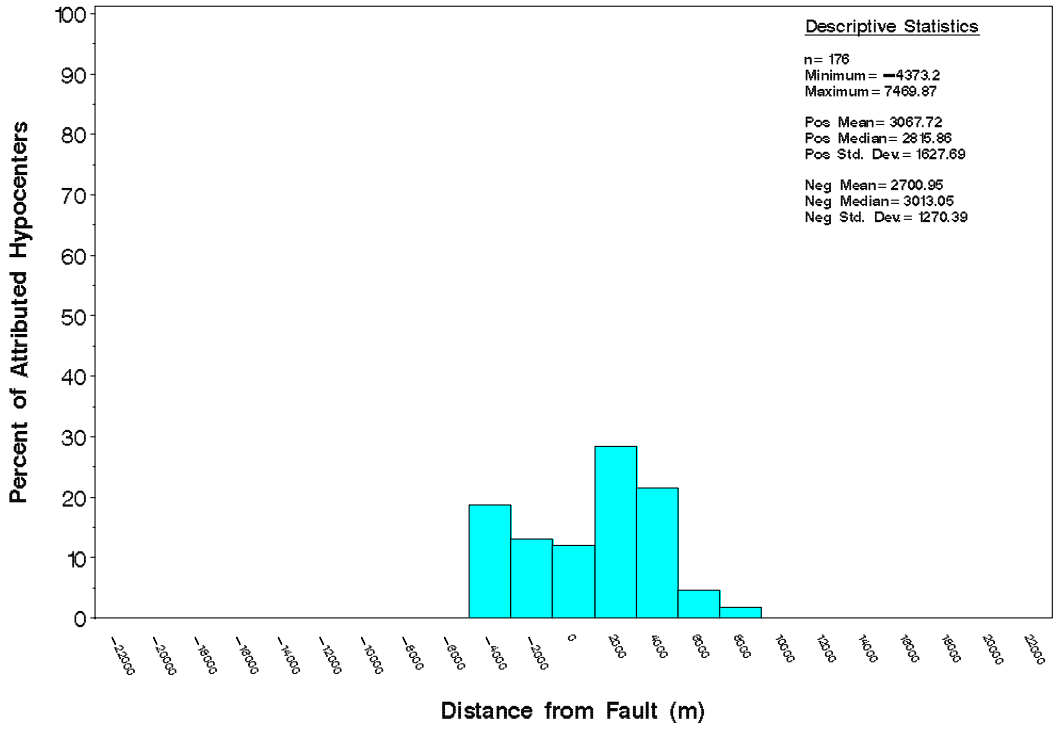

System = Sekigahara
Fault= Kajiya (A71—8)

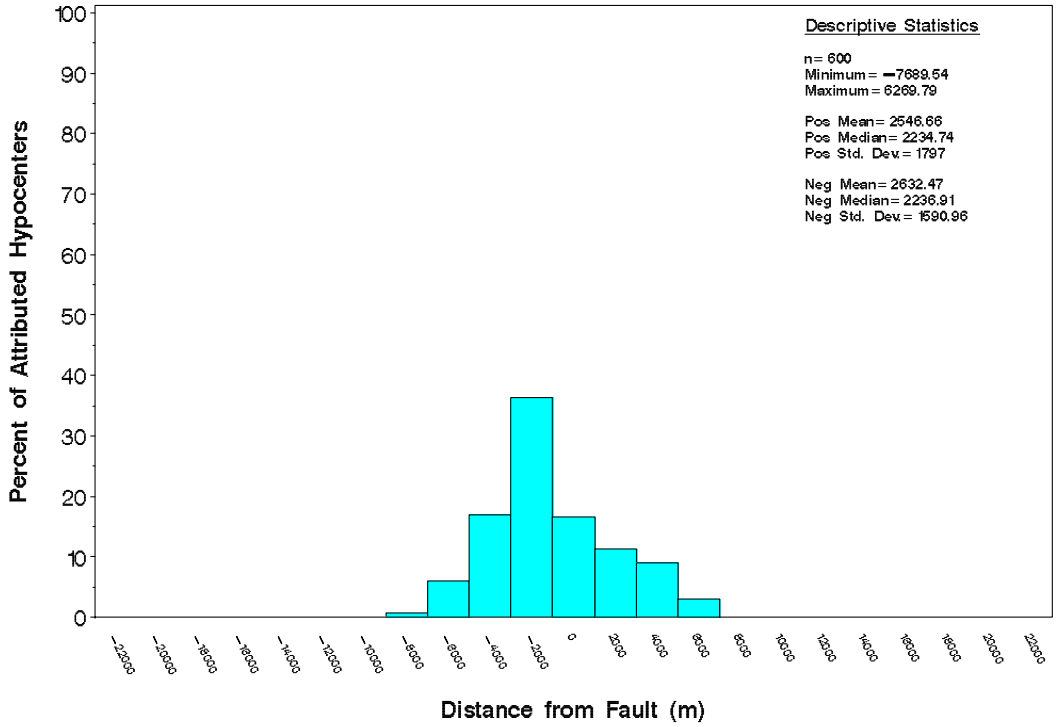

System = Sekigahara
Fault= Sekigahara (A71—9)

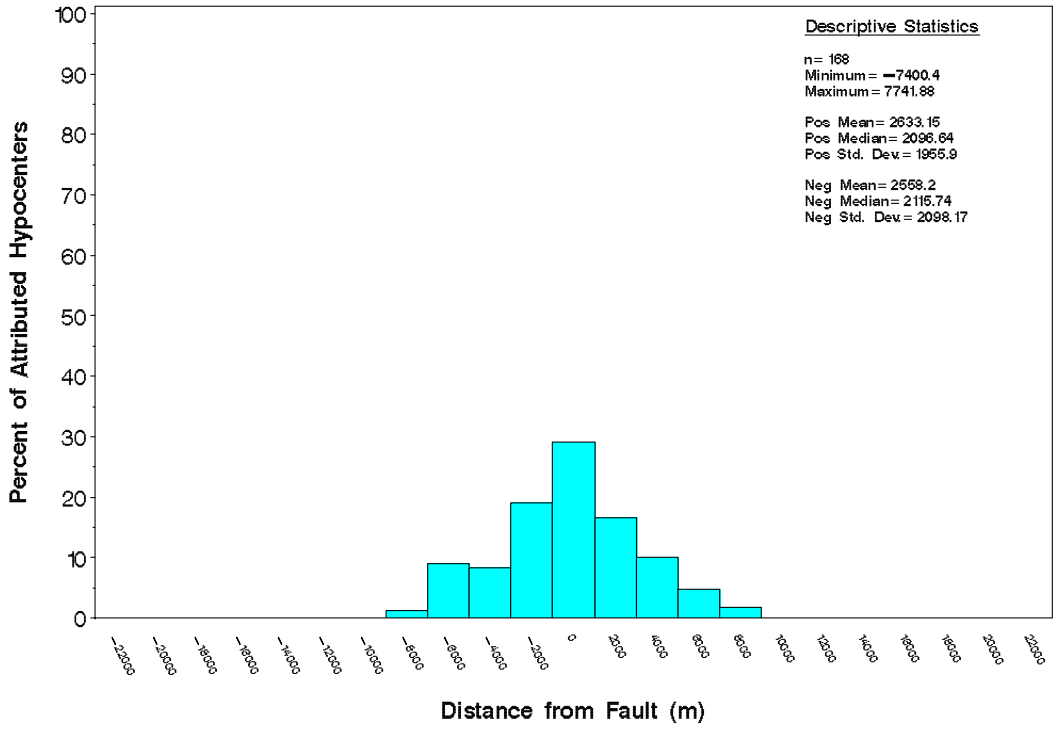

System = Biwako—seigan
Fault= Sakanami, Enbano, Kamitera (A71—12)

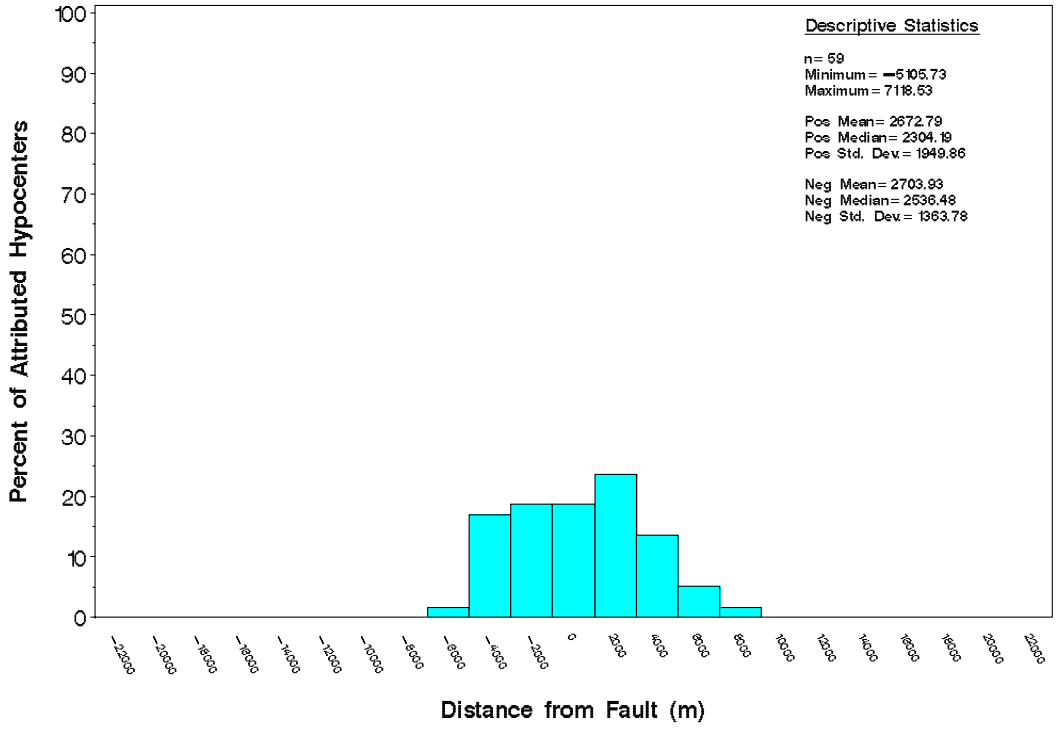

System = Yoro — Kuwana — Yokkaichi
Fault= Kuwana — Yokkaichi,?Tarusaka (A72 — 1)

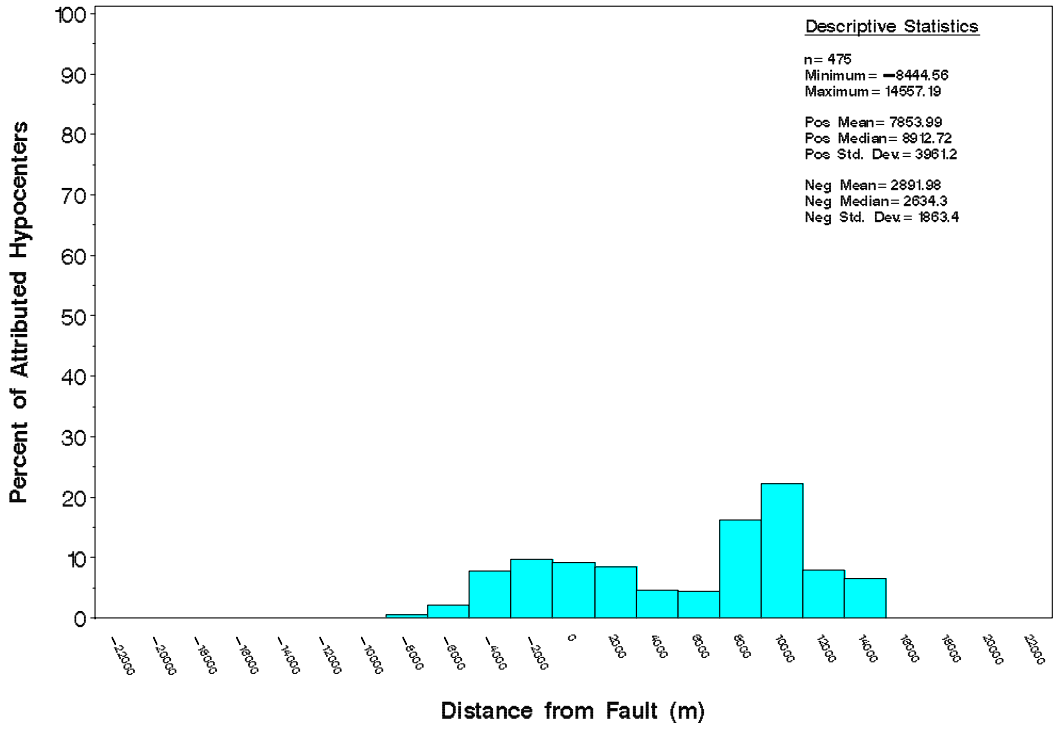

System = Yoro — Kuwana — Yokkaichi
Fault= Yokkaichi (A72 — 2)

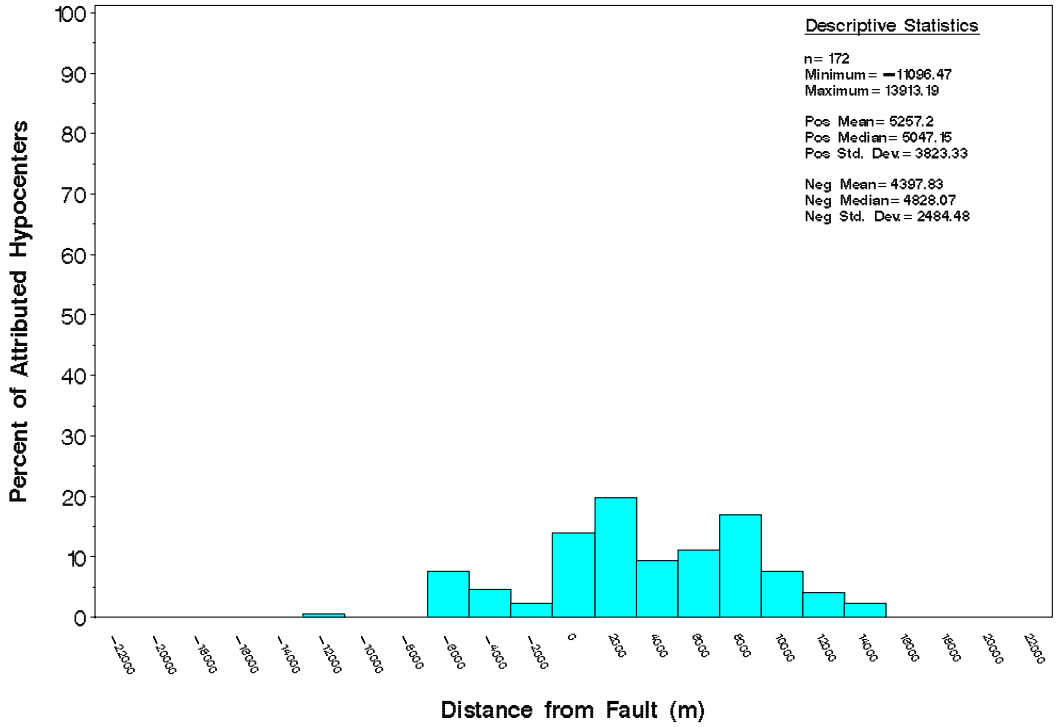

System = Suzuka−Sakashita
Fault= Suzuka−Sakamoto (A72−3)

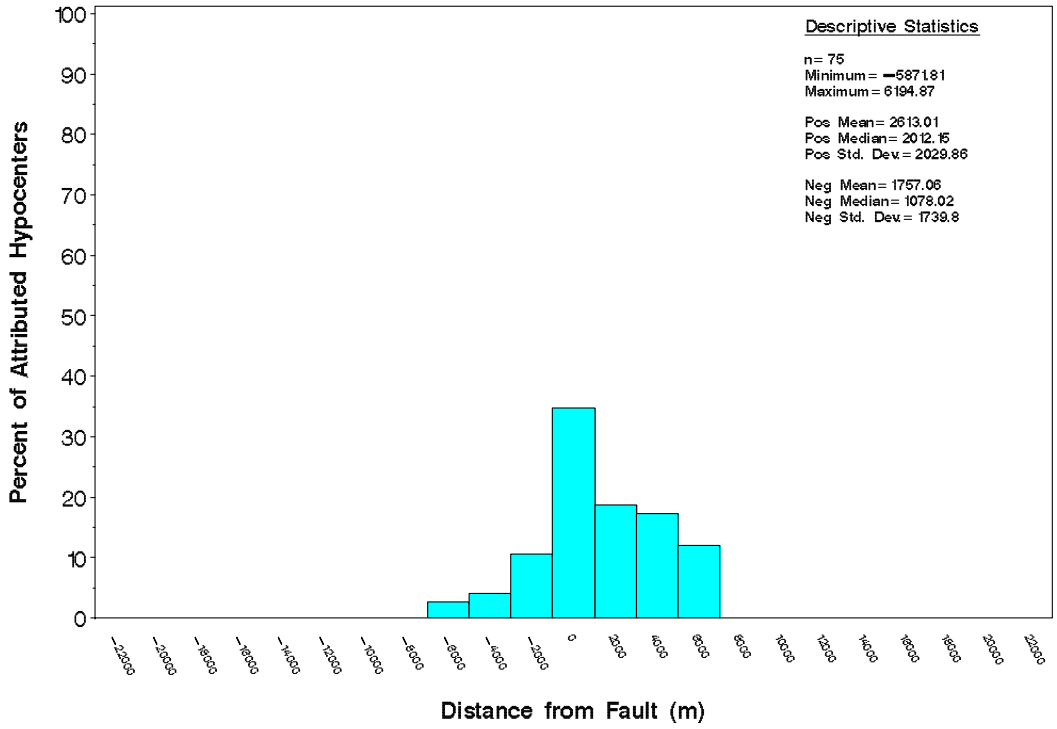

System = Kizugawa
Fault= Kizugawa−seibu (A72−4)

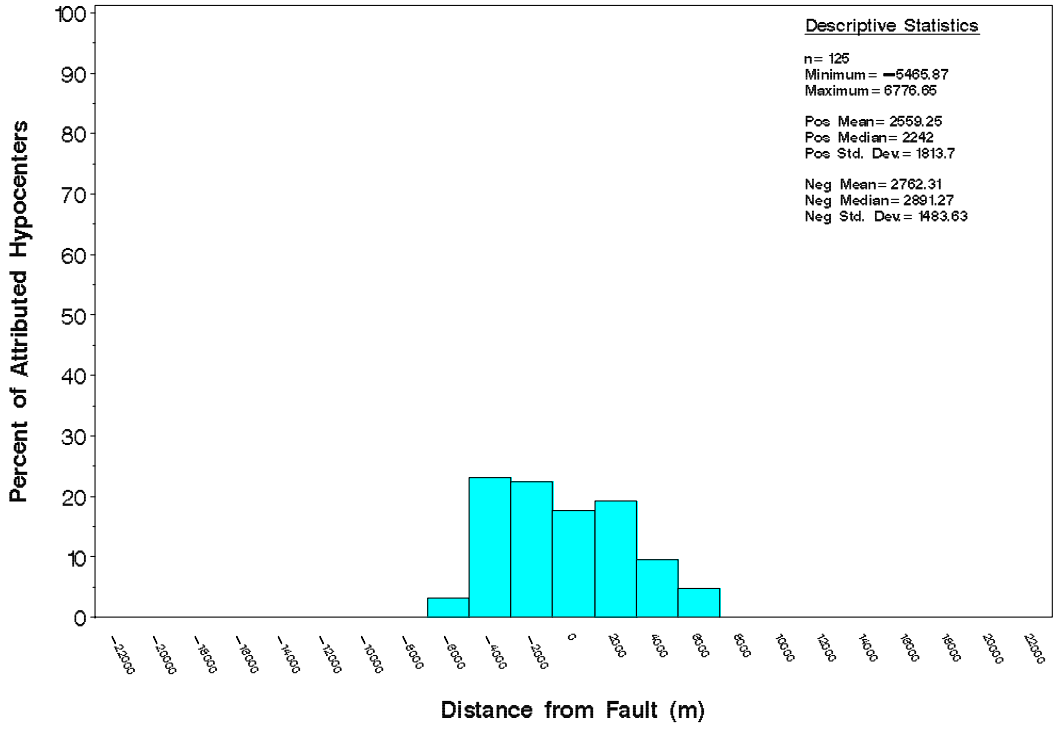

System = Kumagawa
Fault= Kumagawa (A75−2)

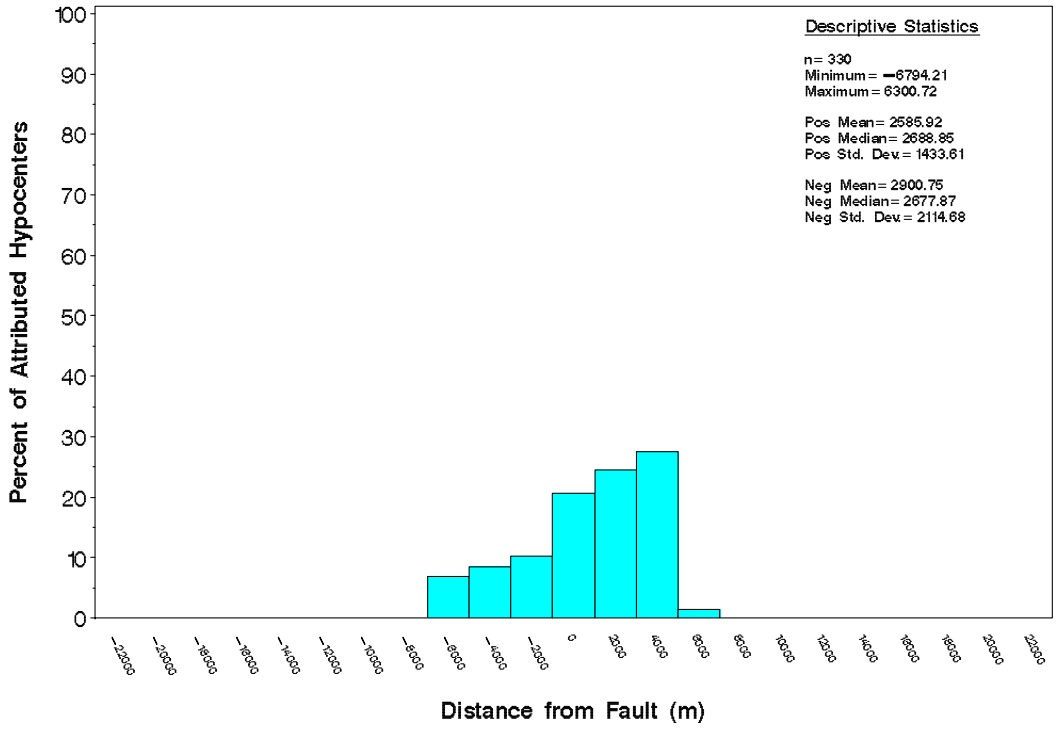

System = Mikata−Hanaore
Fault= Hanaore (A75−3)

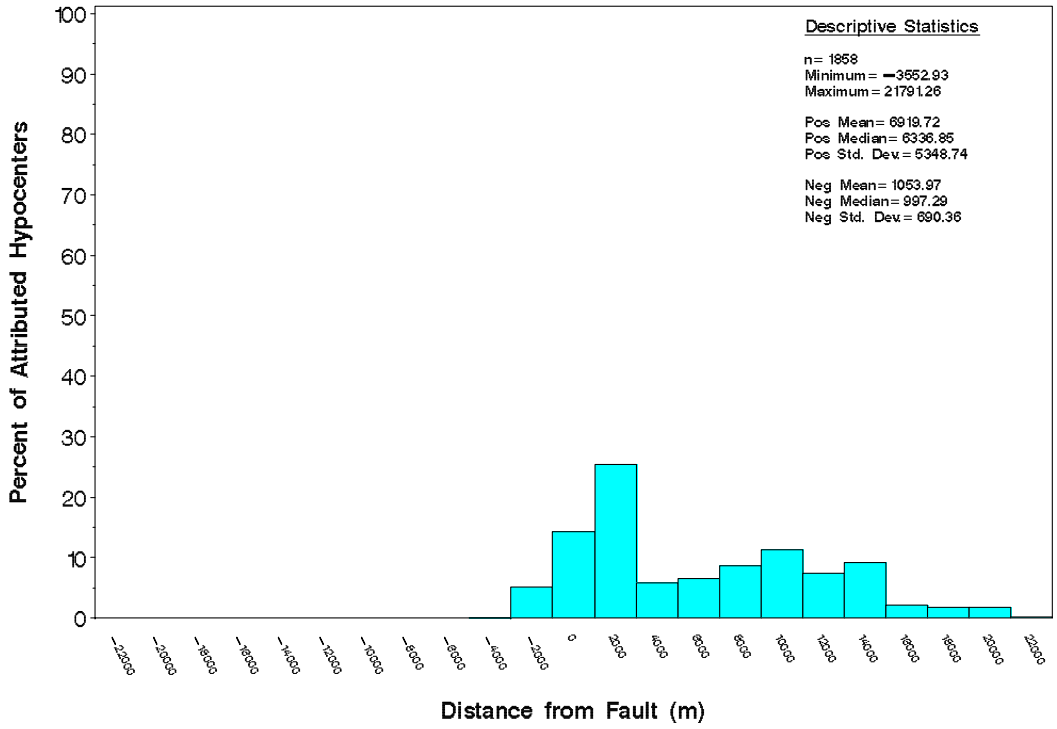

System = Joringawa
Fault= Joringawa (A75−4)

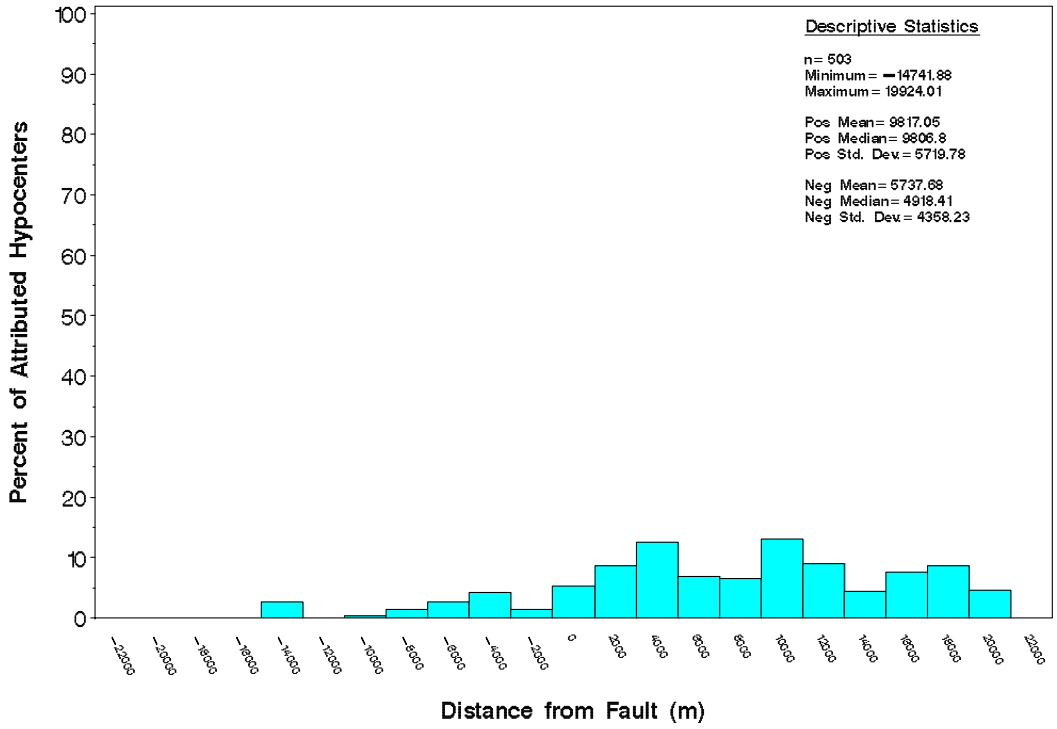

System = Yamada
Fault= Yamada, Yasukeyakma−nishi (A75−5)

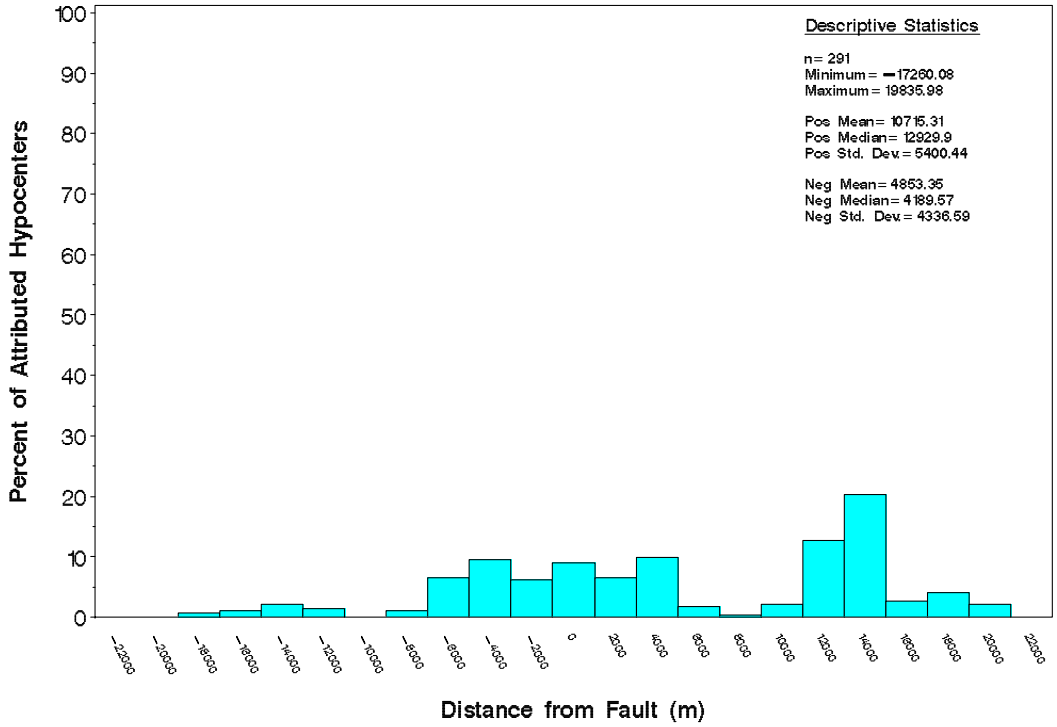

System = Satomura
Fault= Satomura (A75−7)

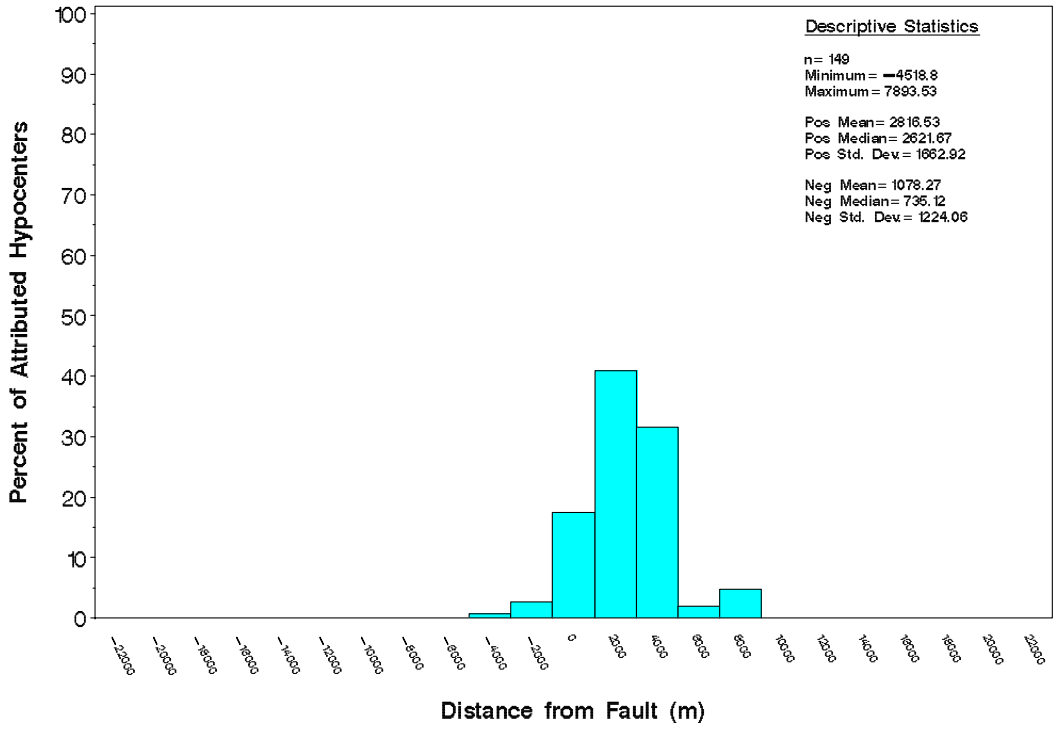

System = Biwako−seigan
Fault= kasida (A76−1)

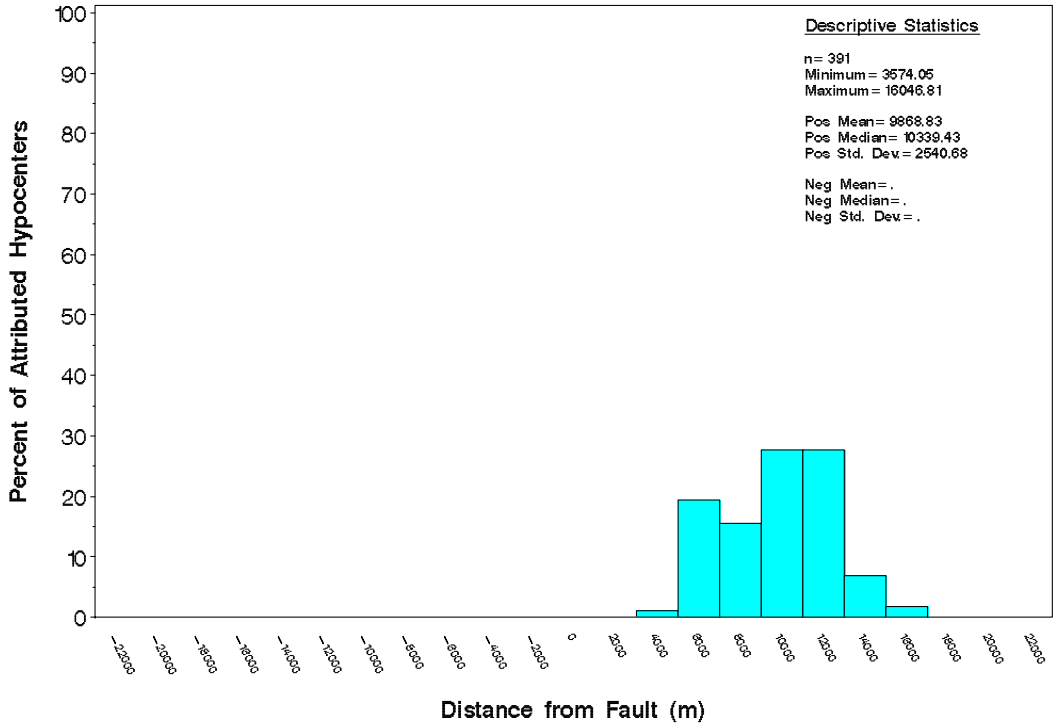

System = Biwako−seigan
Fault= Hiei (A76−2)

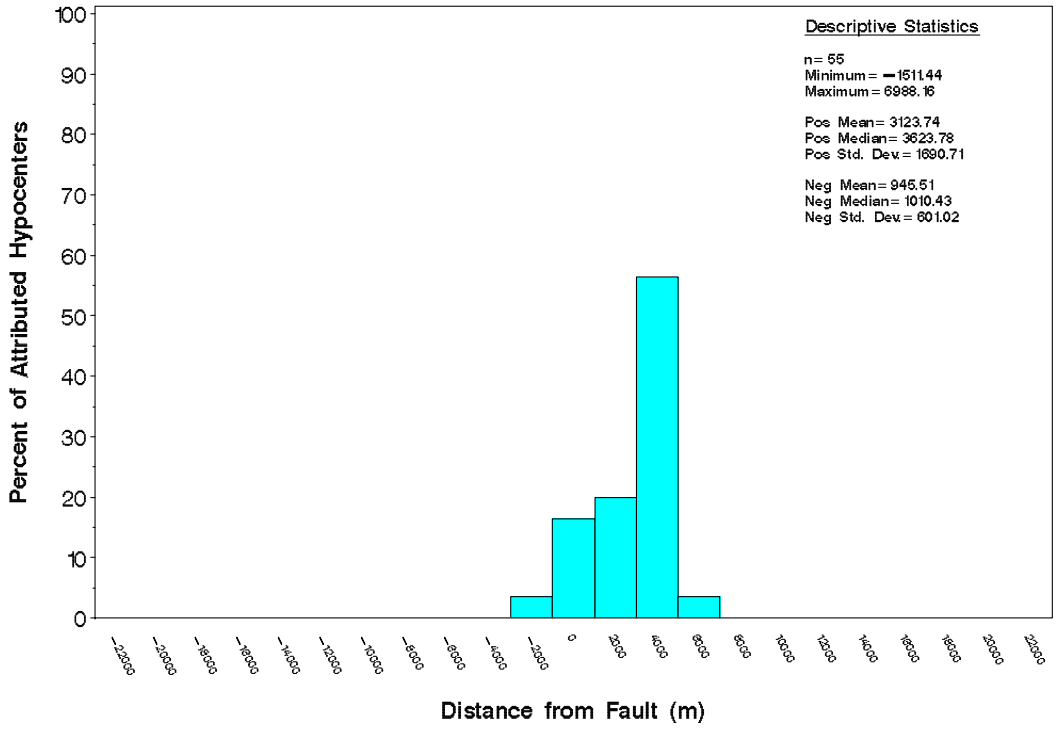

System = Mikata−Hanaore
Fault= Kouheki (A76−3)

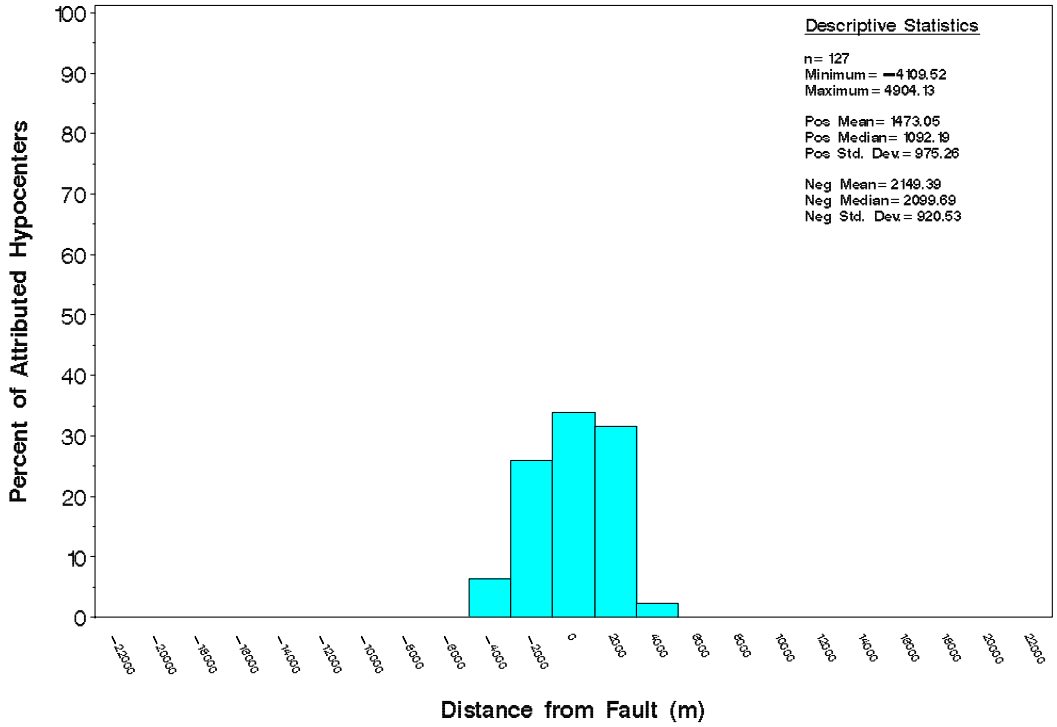

System = Mitouge—Kyoto—Nishiyama
Fault= Mitouge (A76—5)

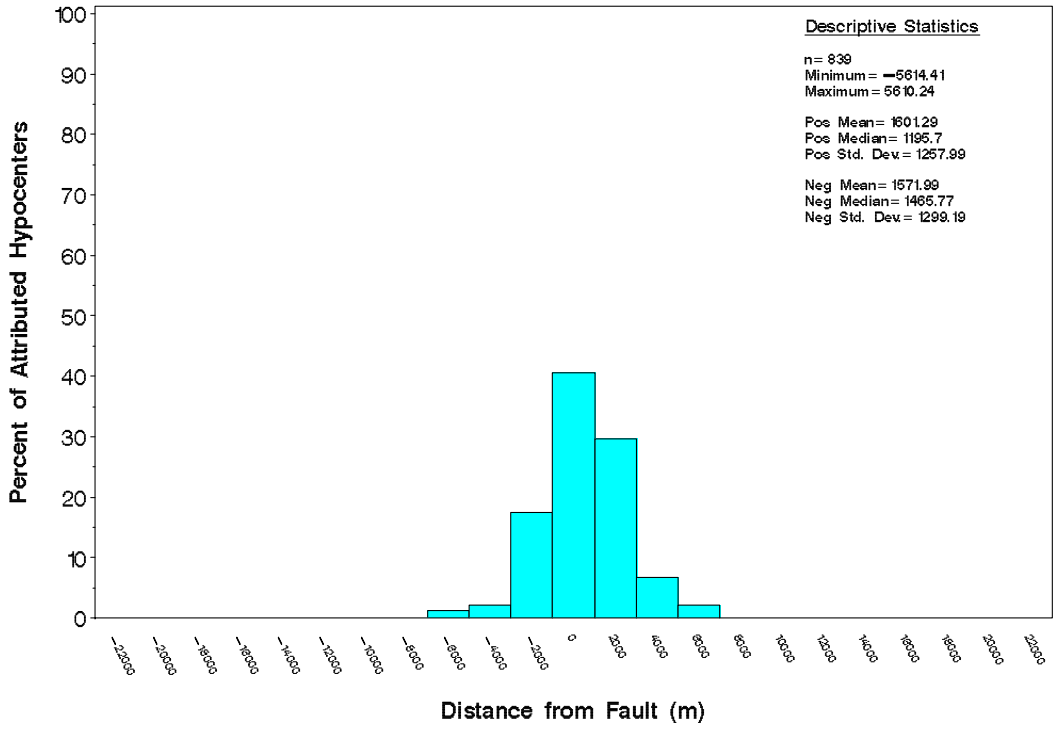

System = Mitouge—Kyoto—Nishiyama
Fault= Kashihara (A76—8)

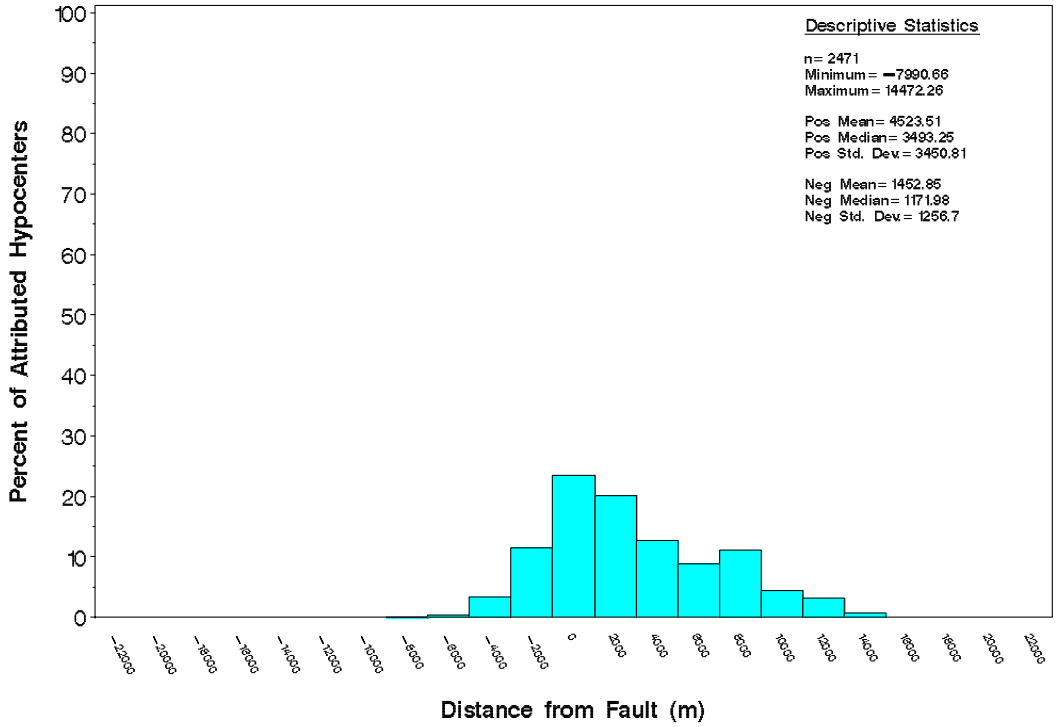

System = Kameoka
Fault= Kameoka (A76—9a)

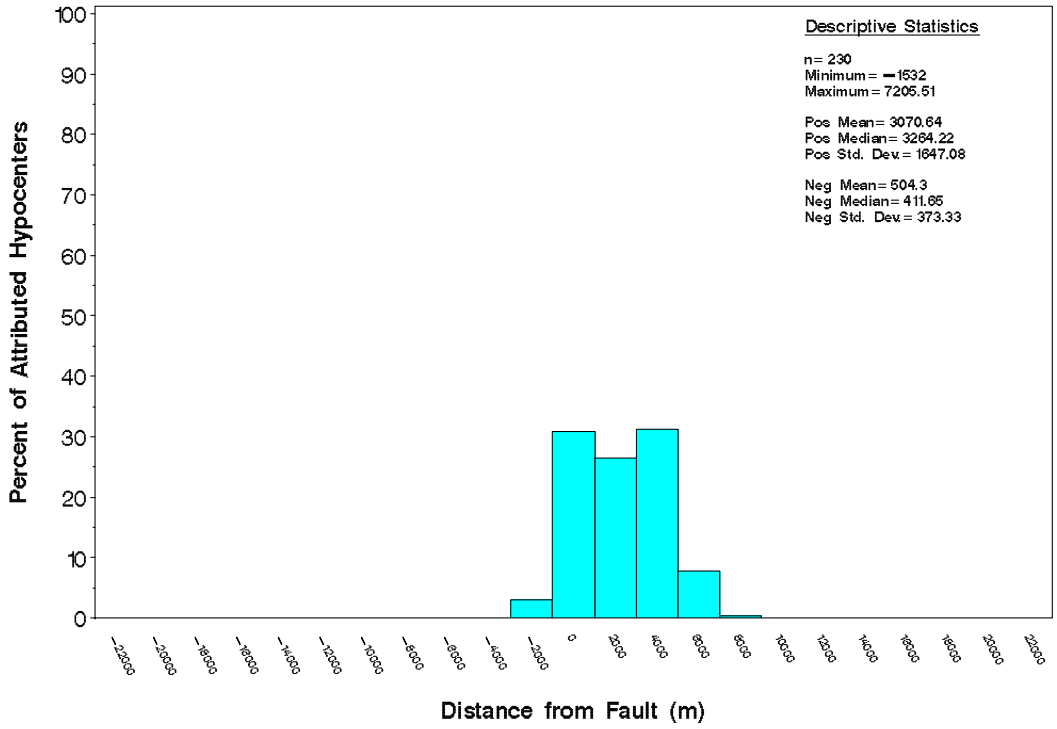

System = Kameoka
Fault= Koumyoji, Taguchi (A76—9b)

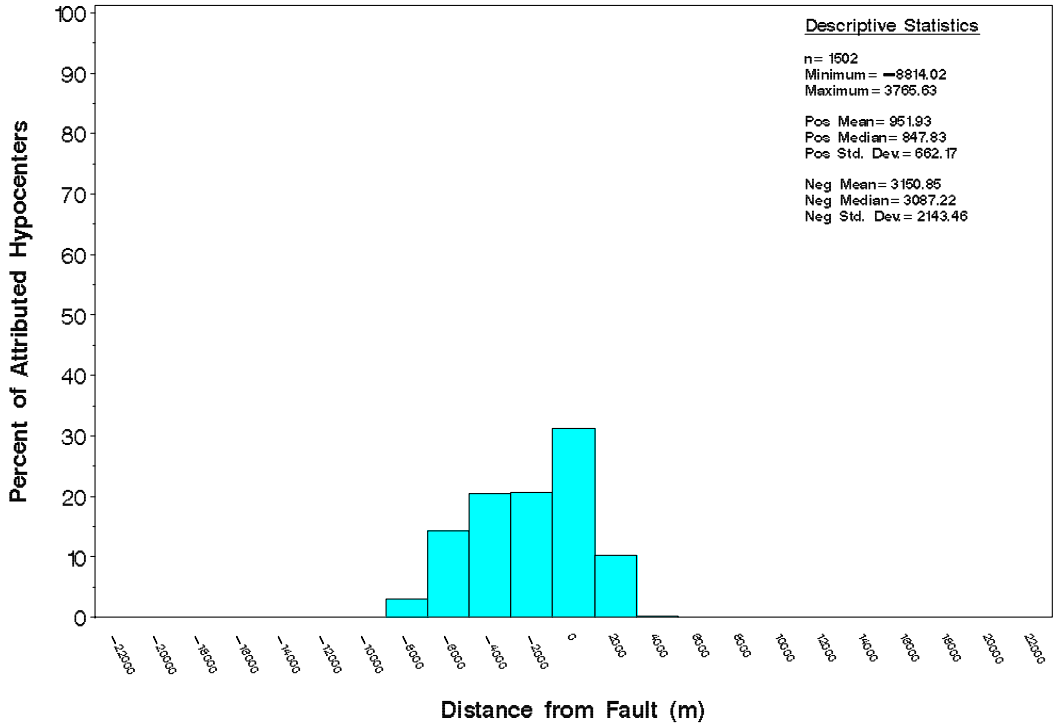

System = Arima—Takatsuki
Fault= Arima—Takatsuki (A76—14a)

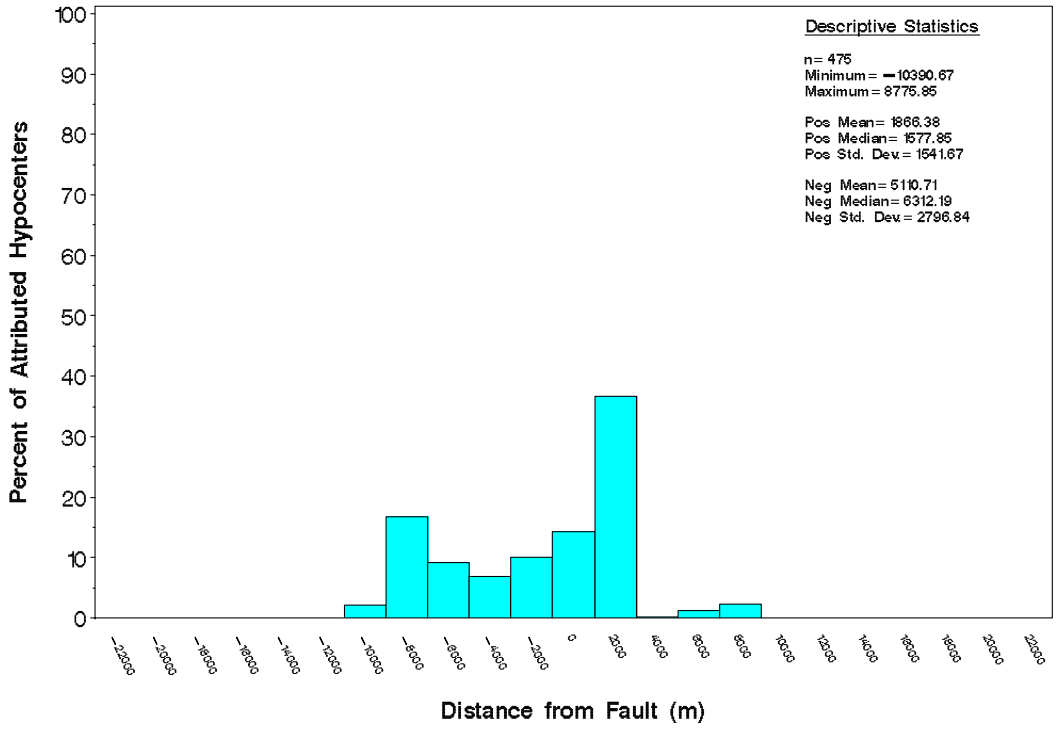

System = Arima—Takatsuki
Fault= Onohara (A76—15)

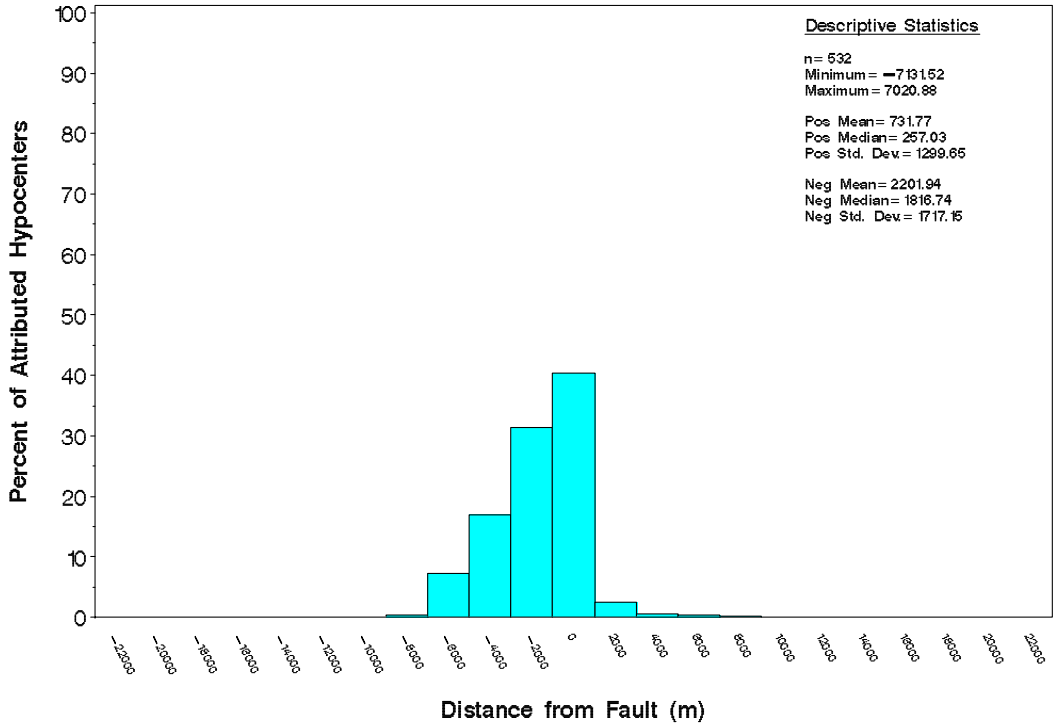

System = Rokko, Awaji−shima
Fault= Gosukebashi, Suwayama (A76−17)

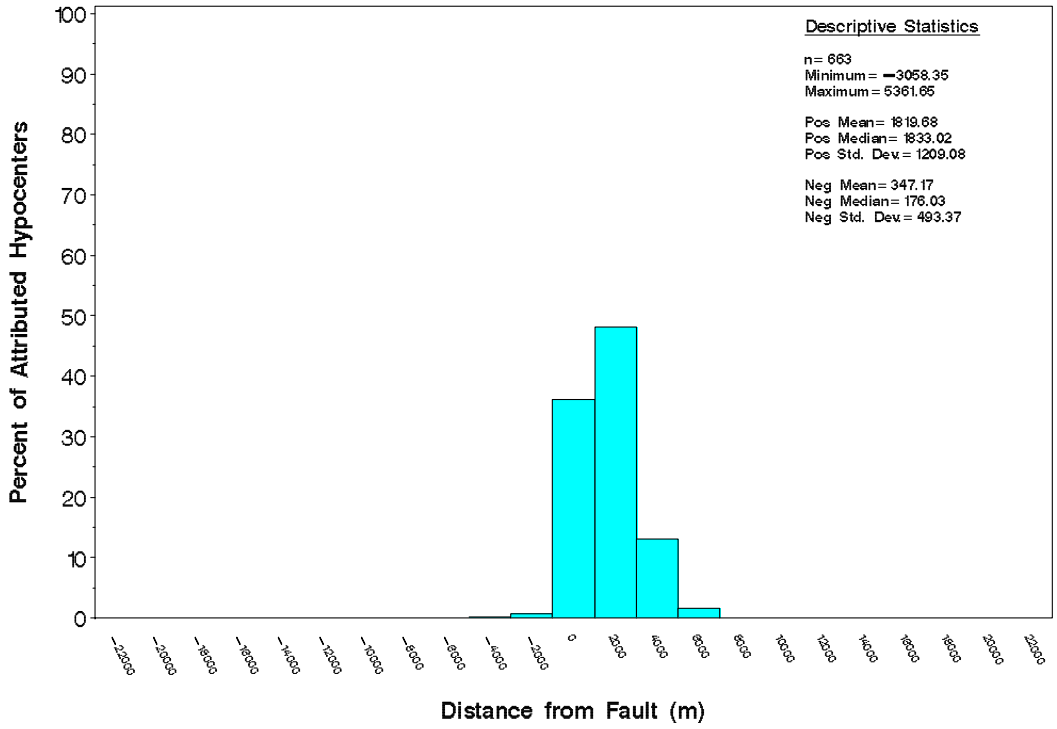

System = Ikoma
Fault= Ikoma, Tamateyama (A77−2)

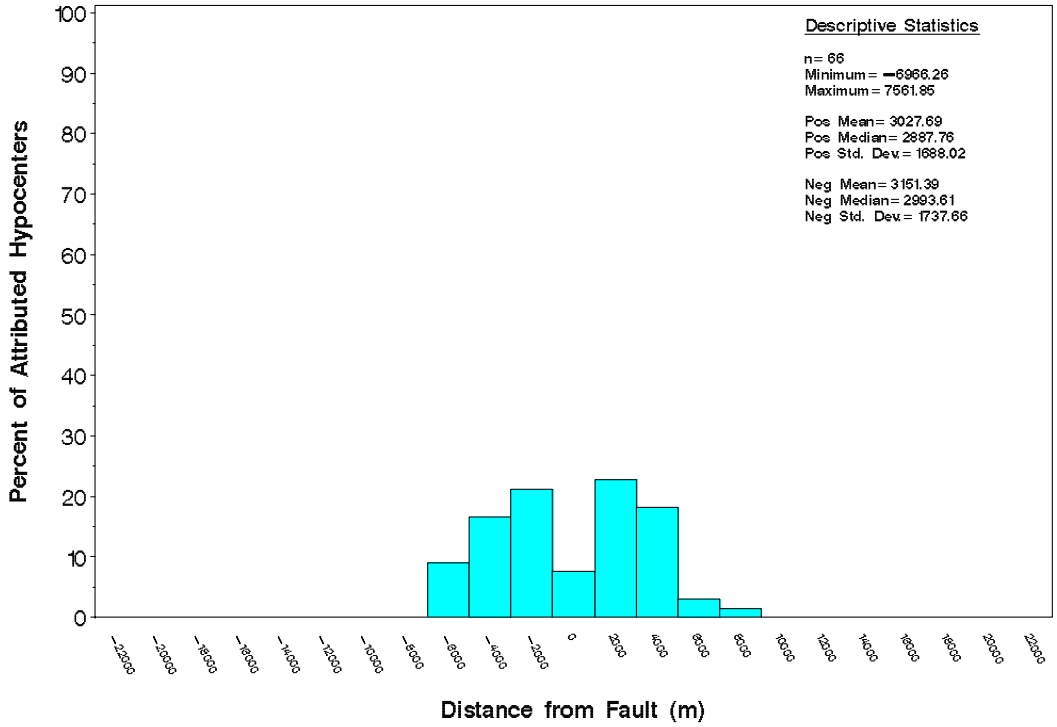

System = Uemachi
Fault= Sakamoto (A77−5)

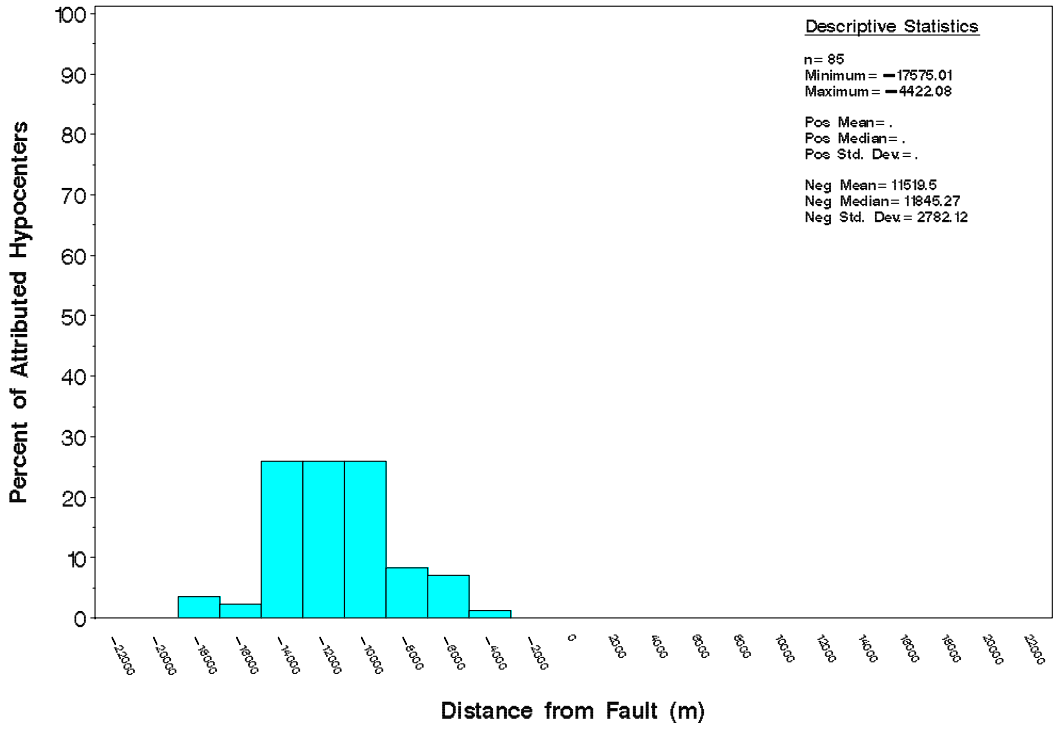

System = Median Tectonic Line
Fault= Kougo, Gojodani, Negoro (A77−6)

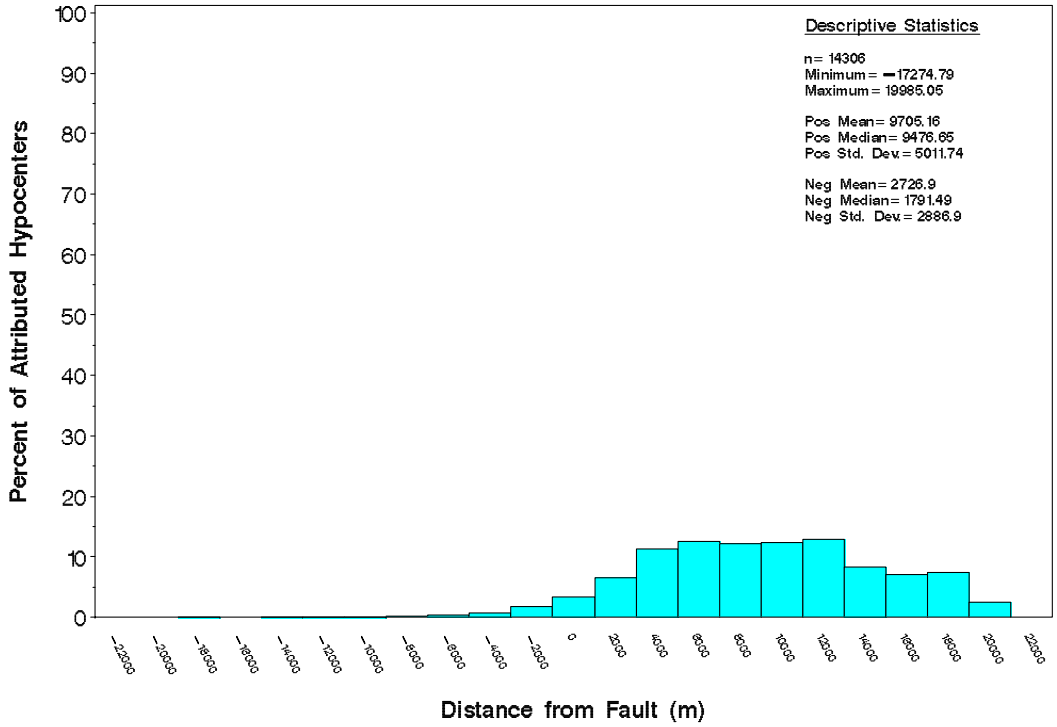

System = Rokko—Awaji
Fault= Kusumoto, Higashiura, Nodao (A77—8)

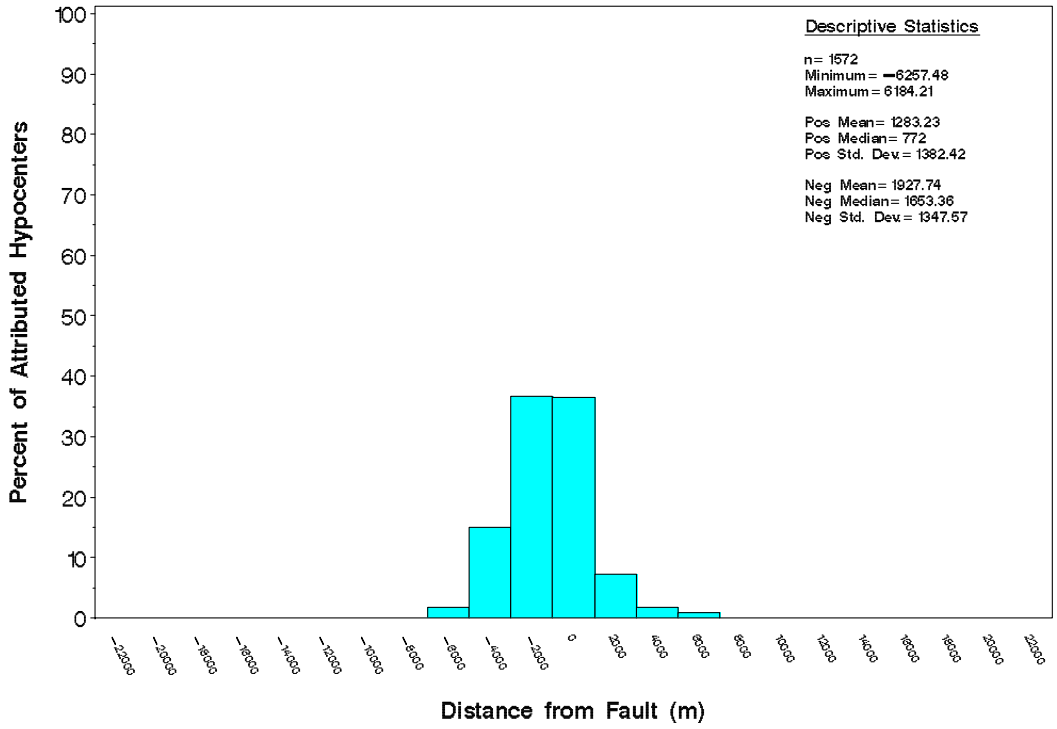

System = Unknown
Fault= Youhu (A79—1)

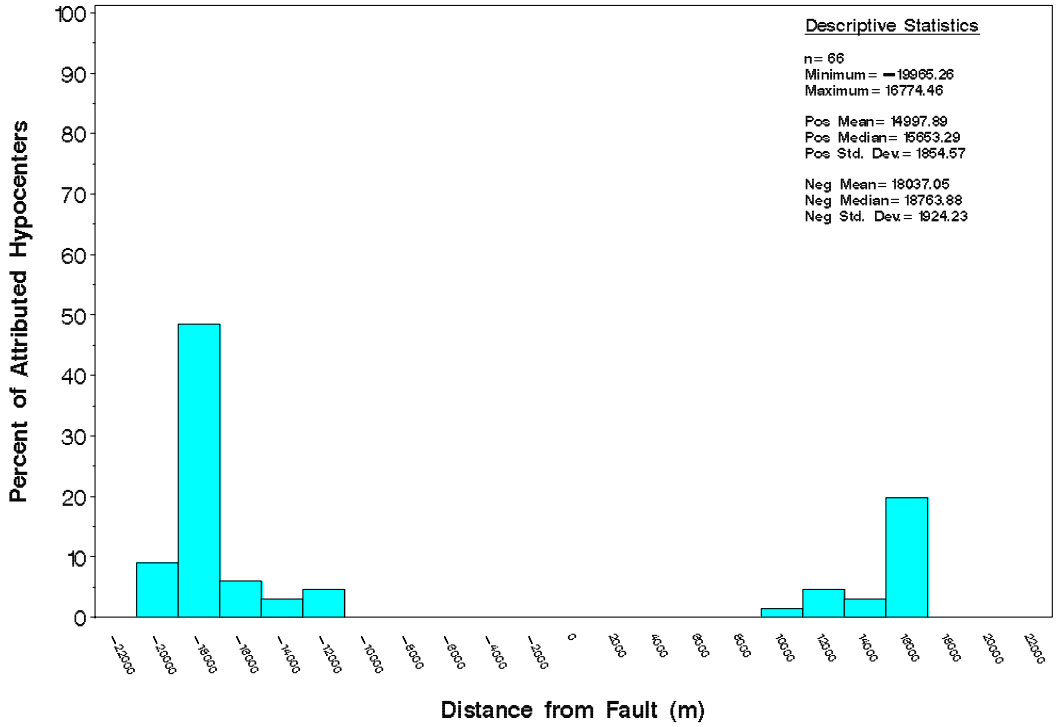

System = Yamasaki
Fault= Ohara (A80—1)

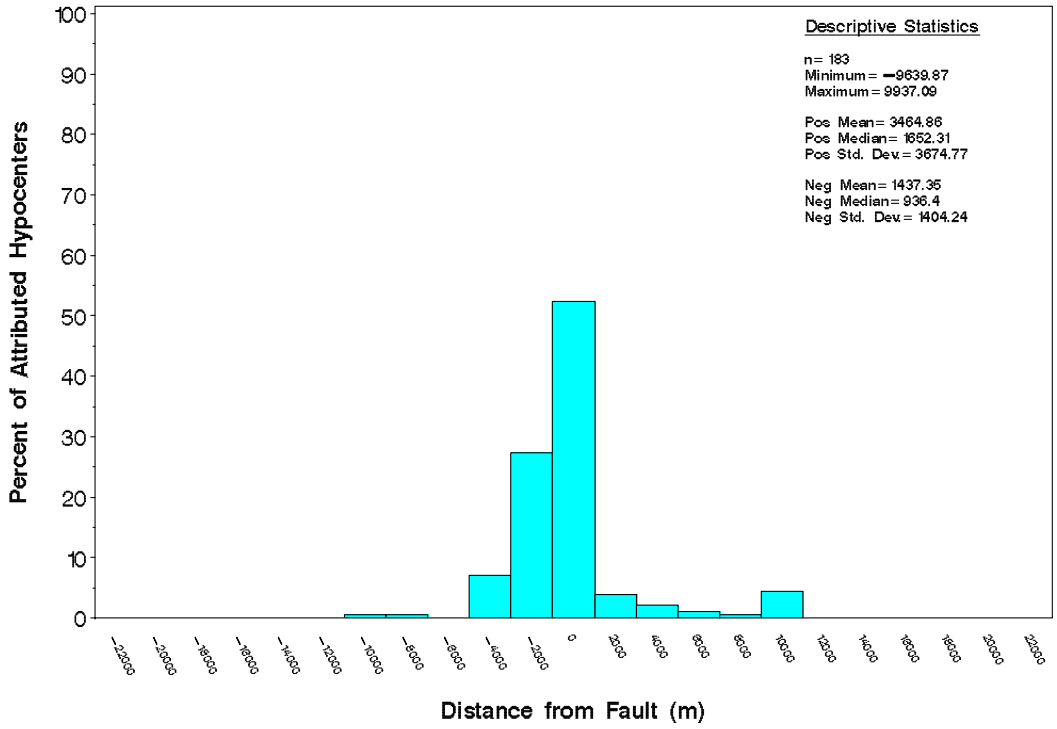

System = Yamasaki
Fault= Doman—Yasutomi (A80—2)

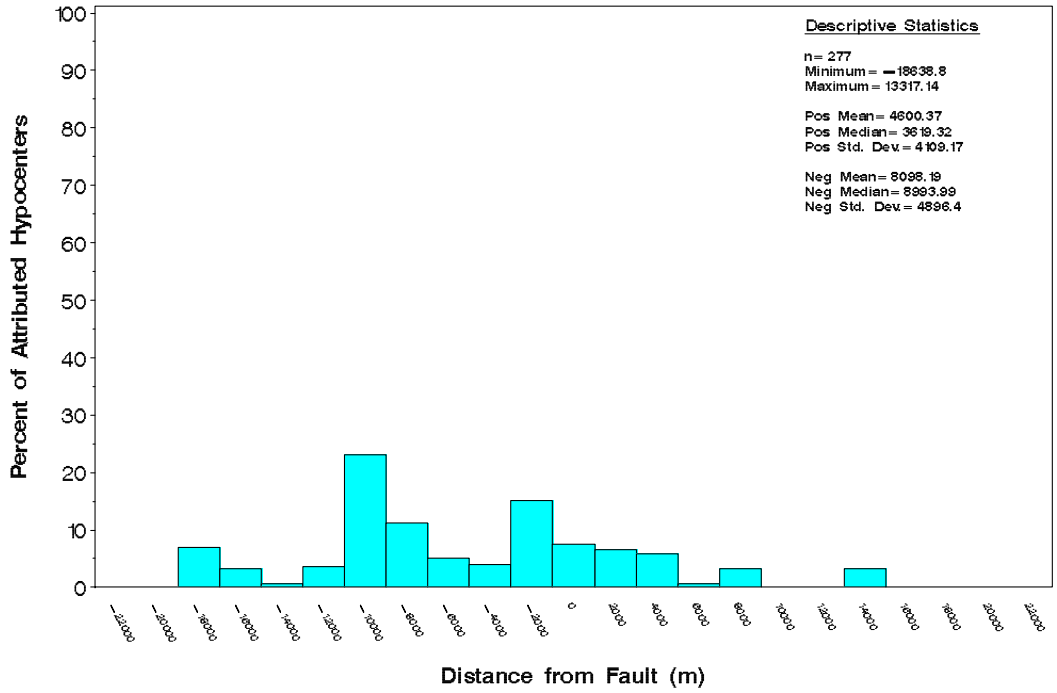

System = Yamasaki
Fault= Yasutomi (A80—3)

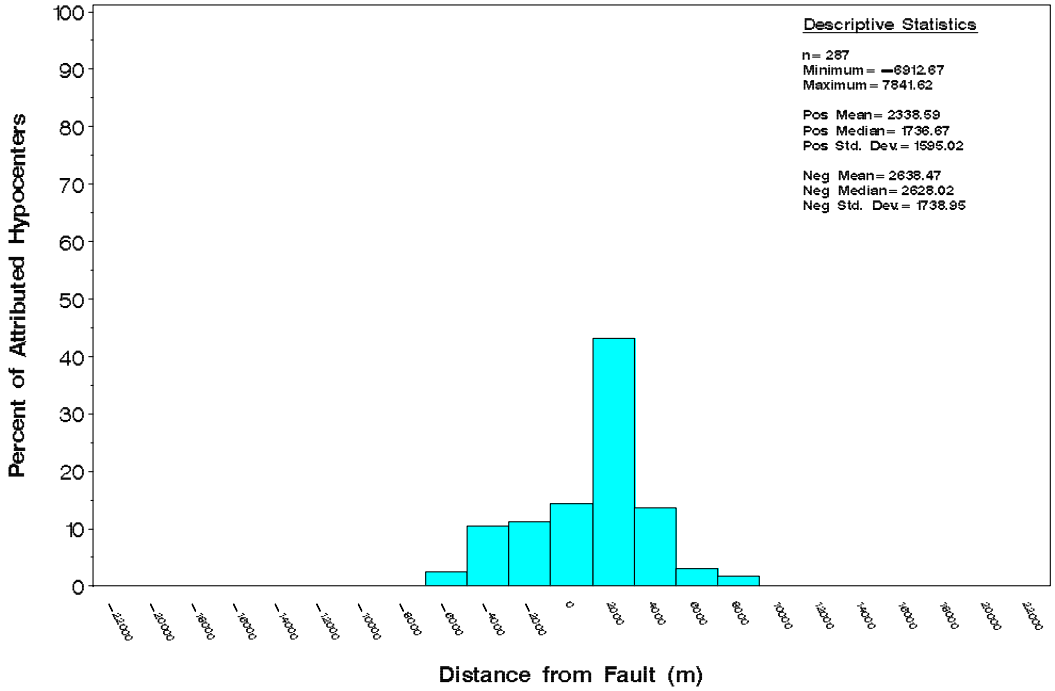

System = Rokko—Awaji
Fault= Nojima (A81—1)

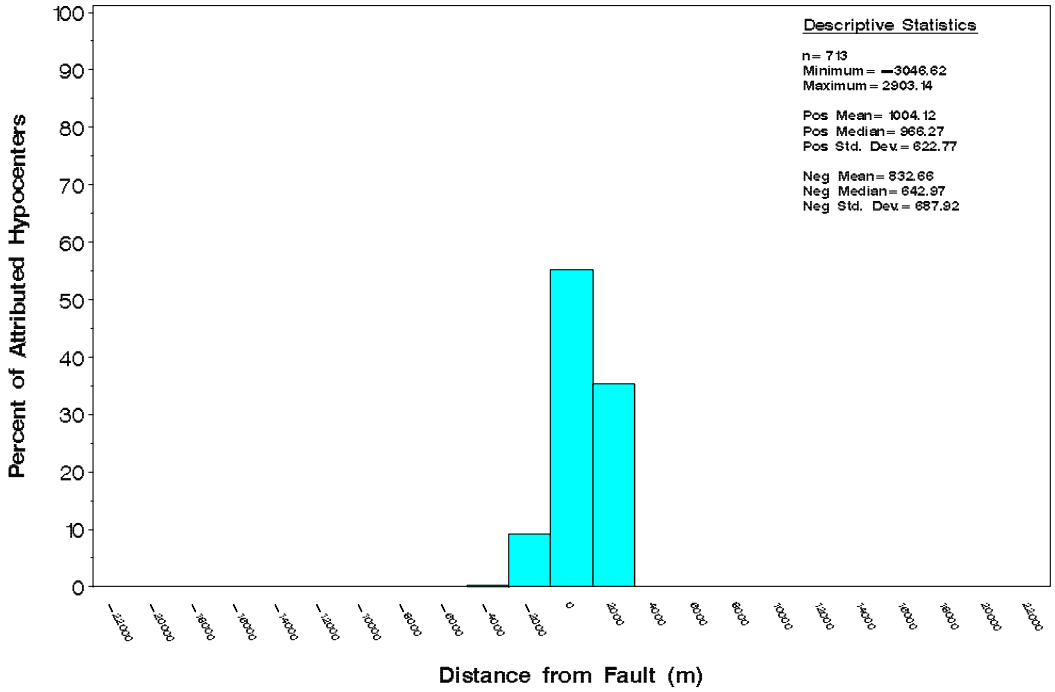

System = Median Tectonic Line
Fault= Unnamed (A81—2)

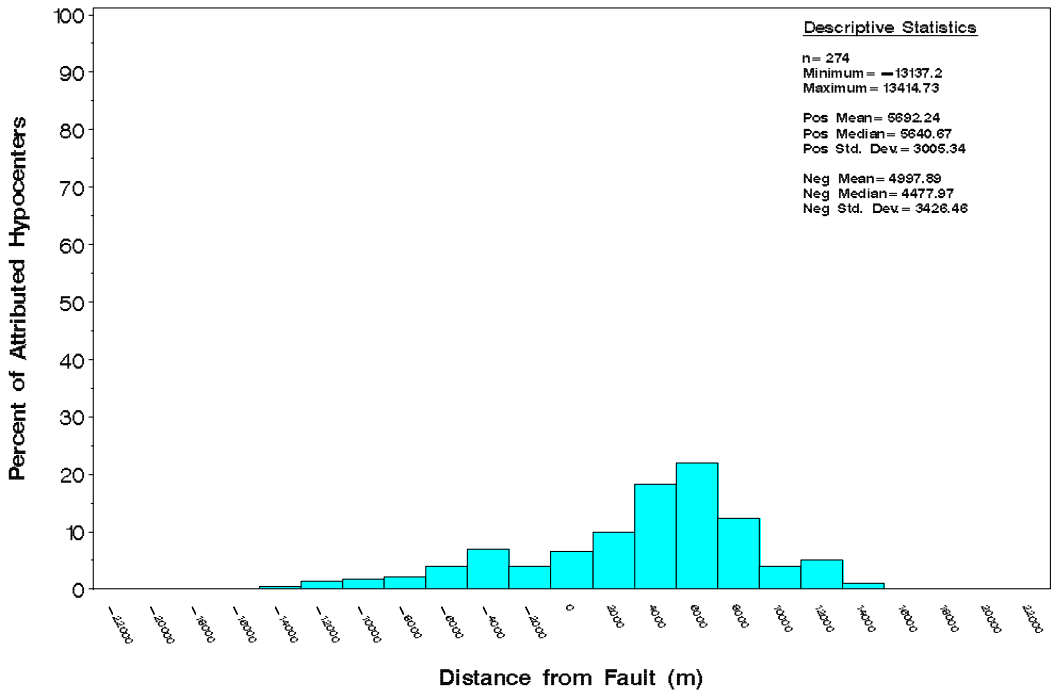

System = Nagao
Fault= Unnamed (A81—3)

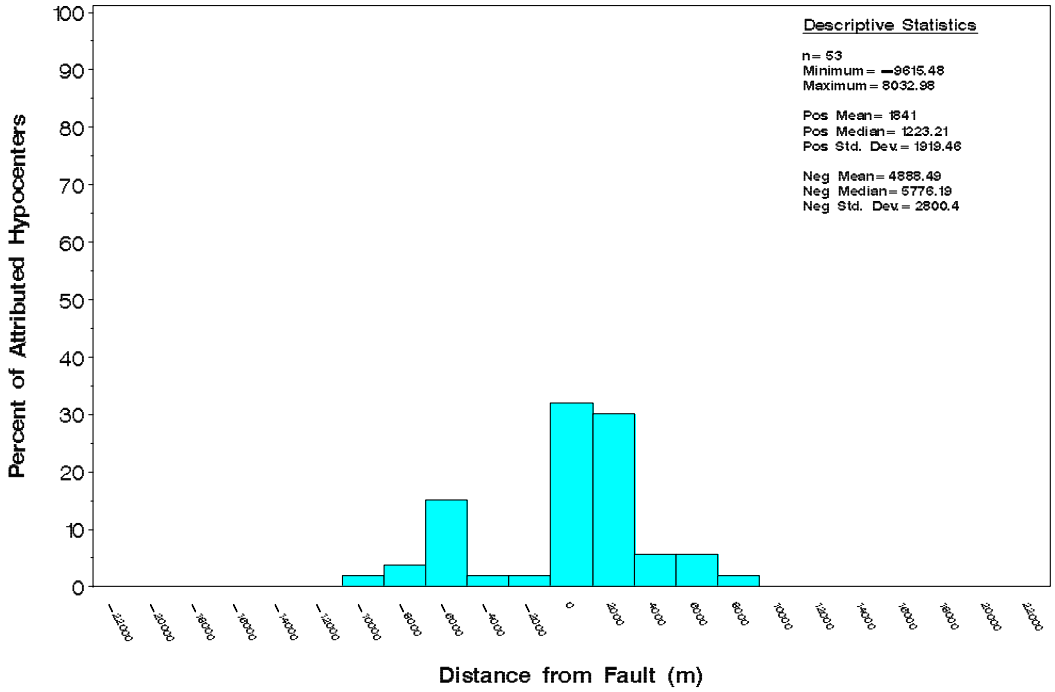

System = Unknown
Fault= Chyojagahara (A86—1)

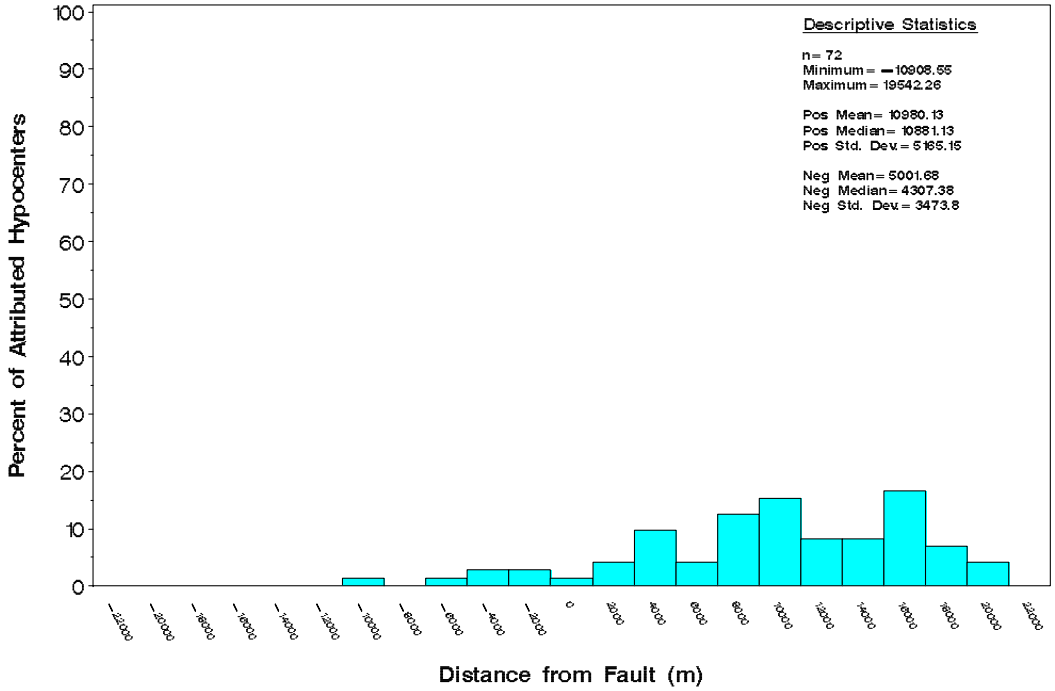

System = Median Tectonic Line
Fault= Ishizuchi (A87—2)

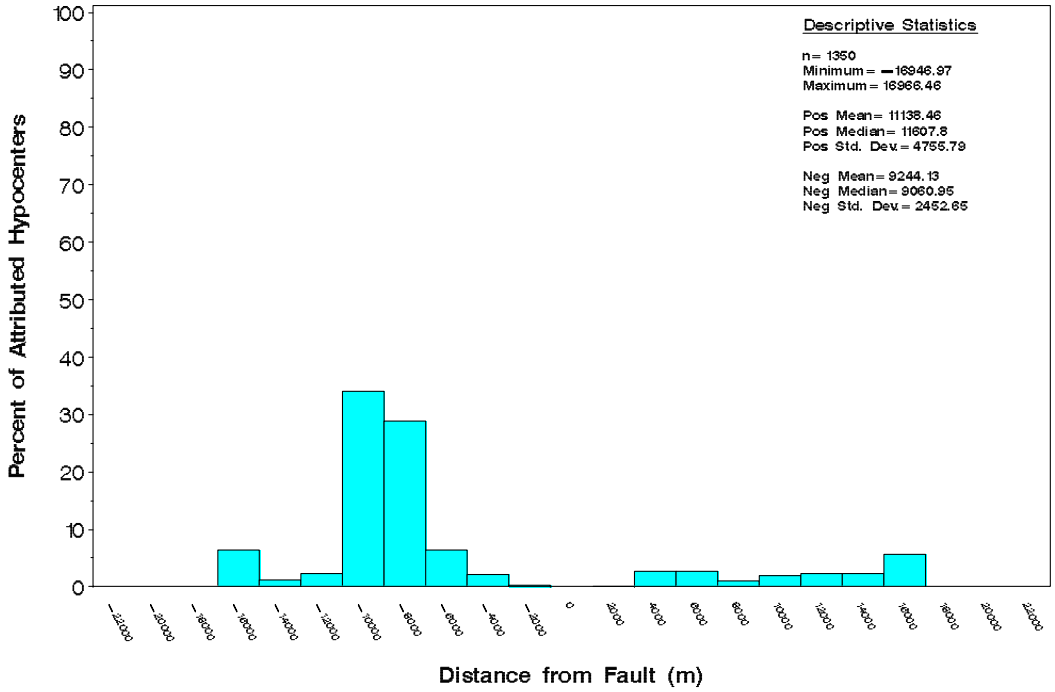

System = Median Tectonic Line
Fault = Okamura (A87—3)

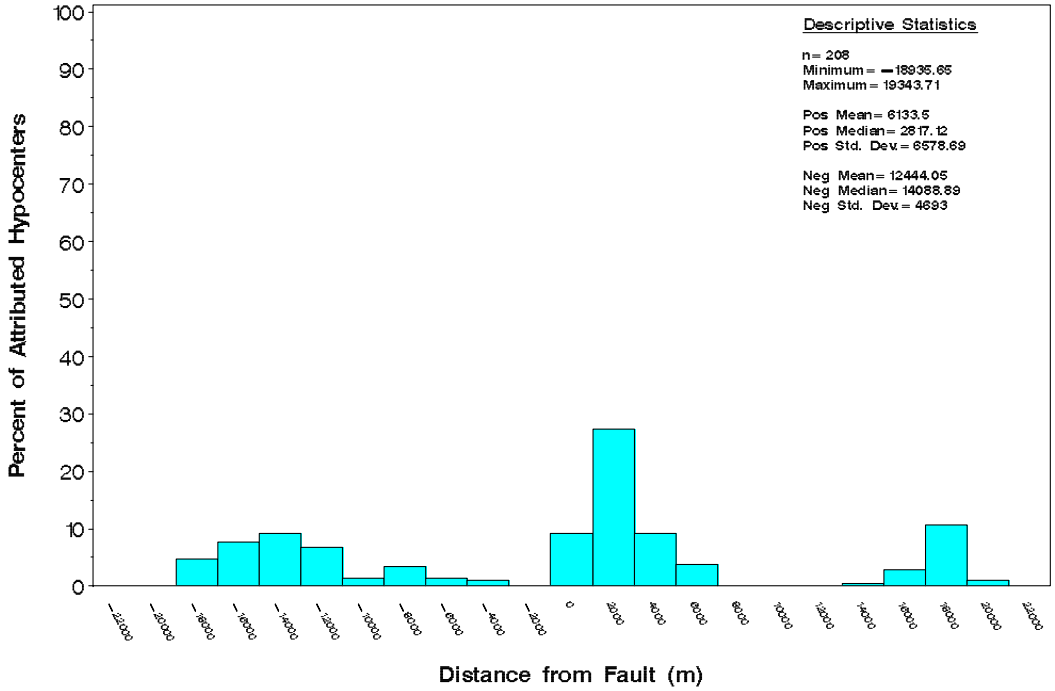

System = Median Tectonic Line
Fault = Kawakami, Kitagata (A87—4)

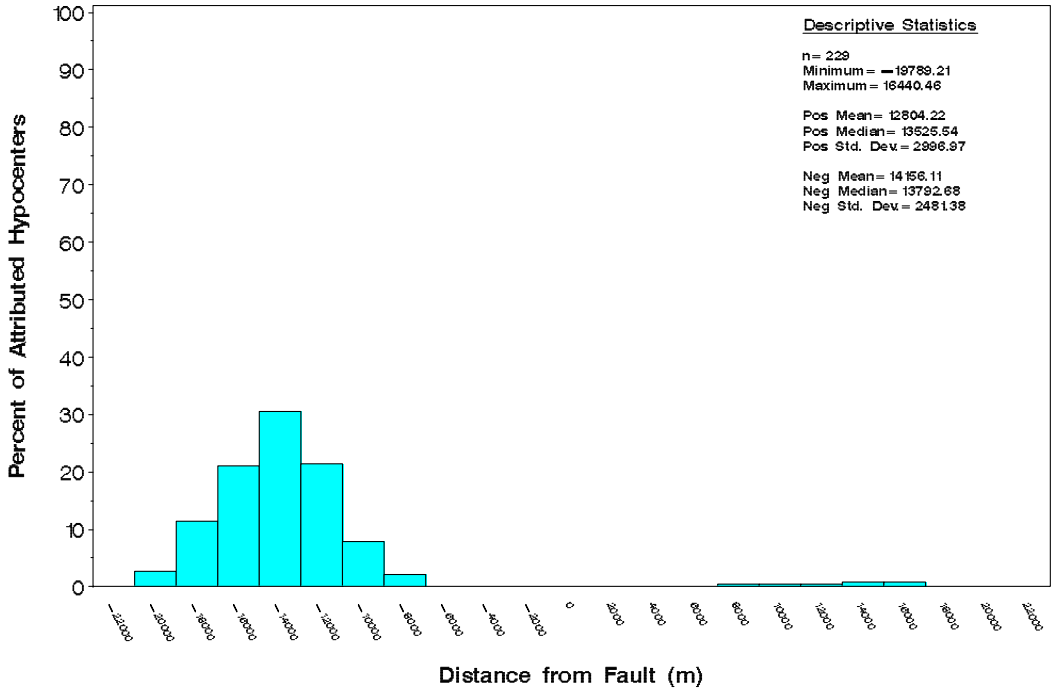

System = Iwakuni
Fault= Ogata—Oze (A91—3)

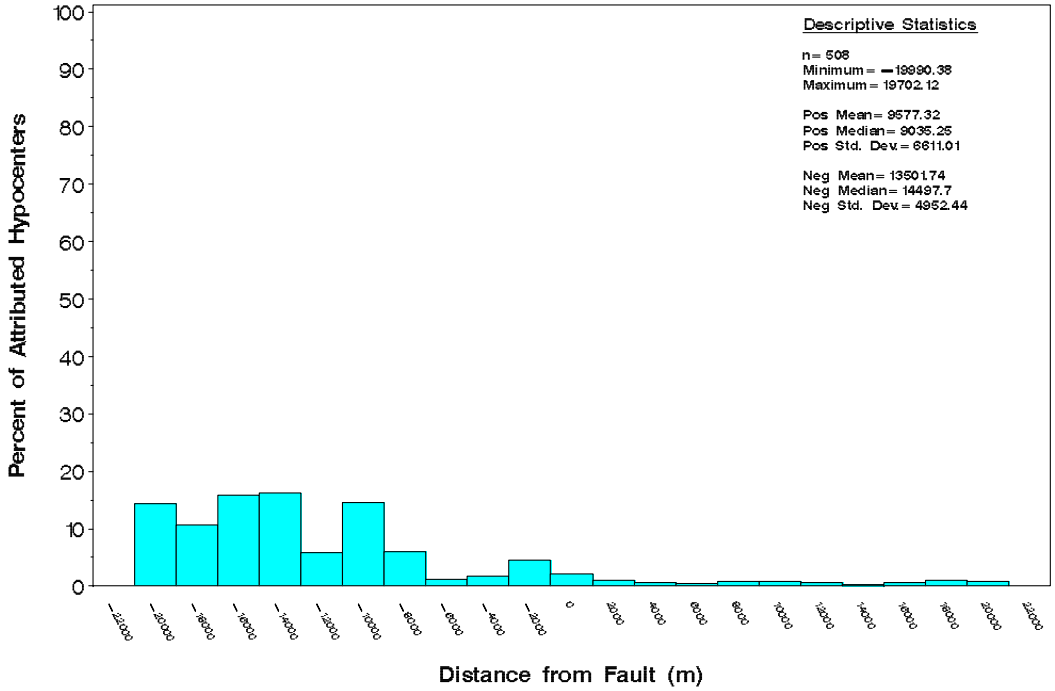

System = Kikugawa
Fault= Kikugawa (A95—2)

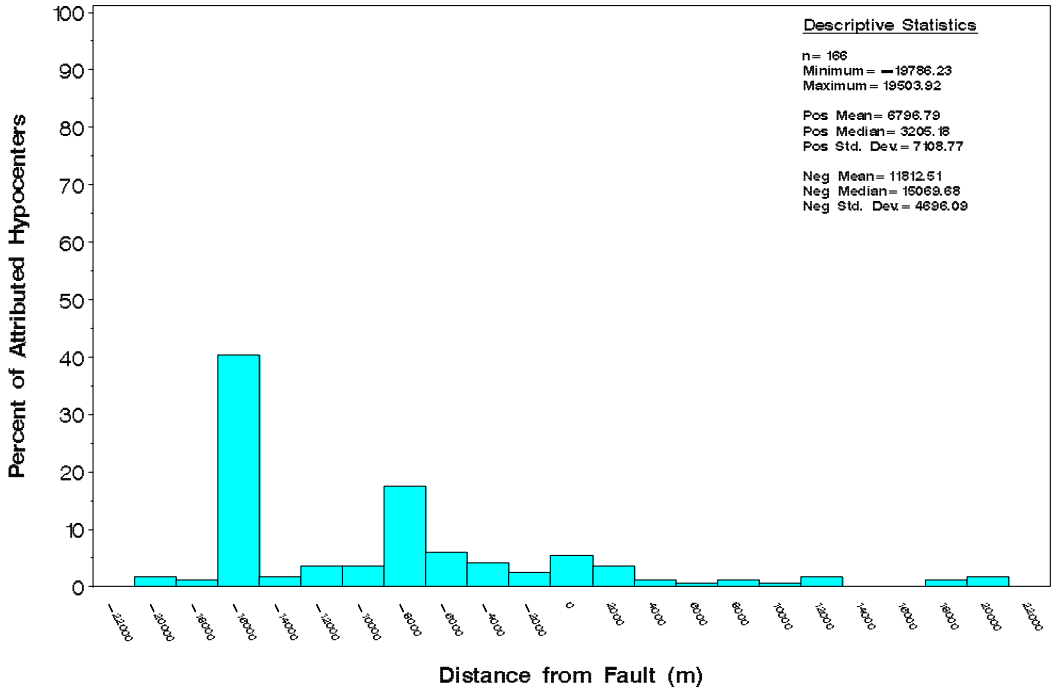

System = Beppu—Mannenyama
Fault= Unnamed (A98—1)

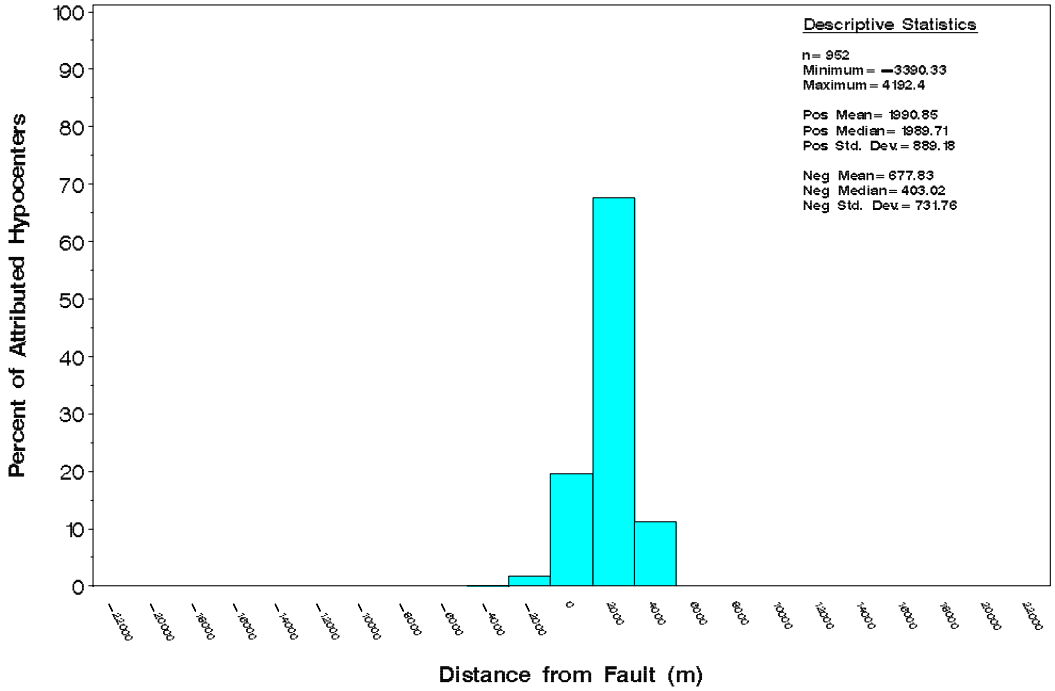

System = Hukuchiyama
Fault= Hukuchiyama (A99—2)

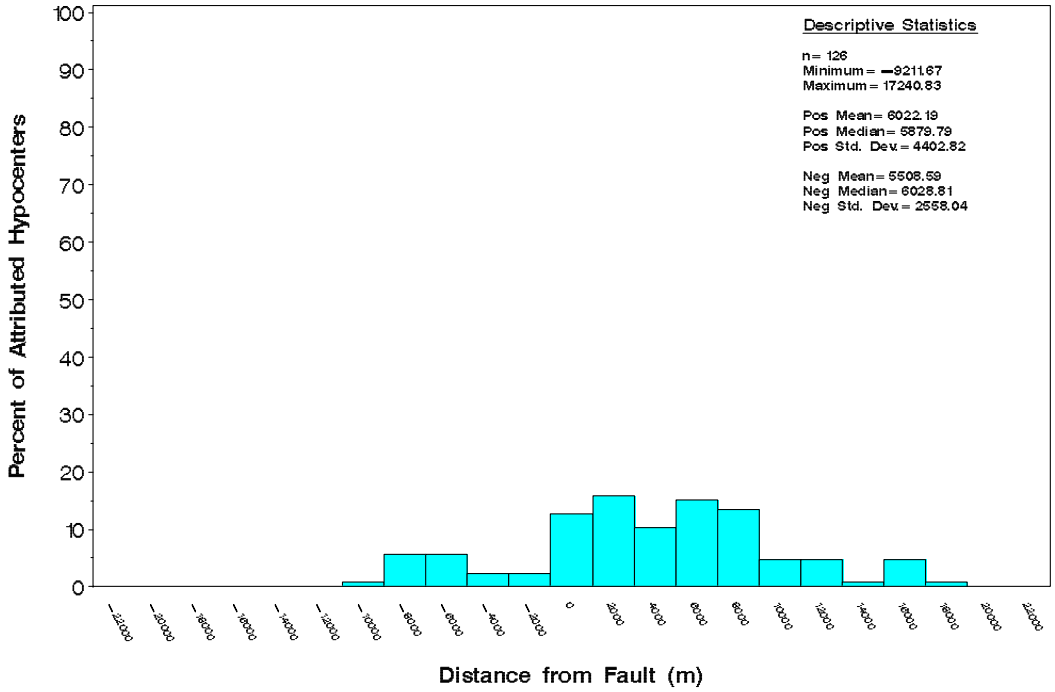

System = Nishiyama
Fault= Hukuyama—Wakamiya (A99—3a)

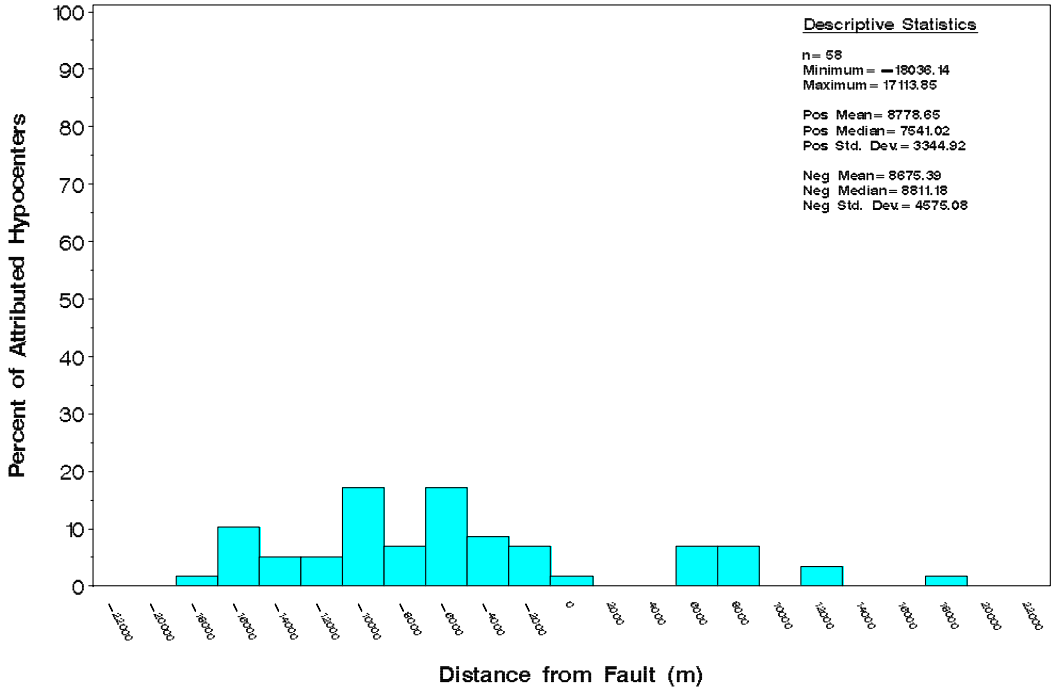

System = Nishiyama
Fault= Iizuka—nishi (A99—3b)

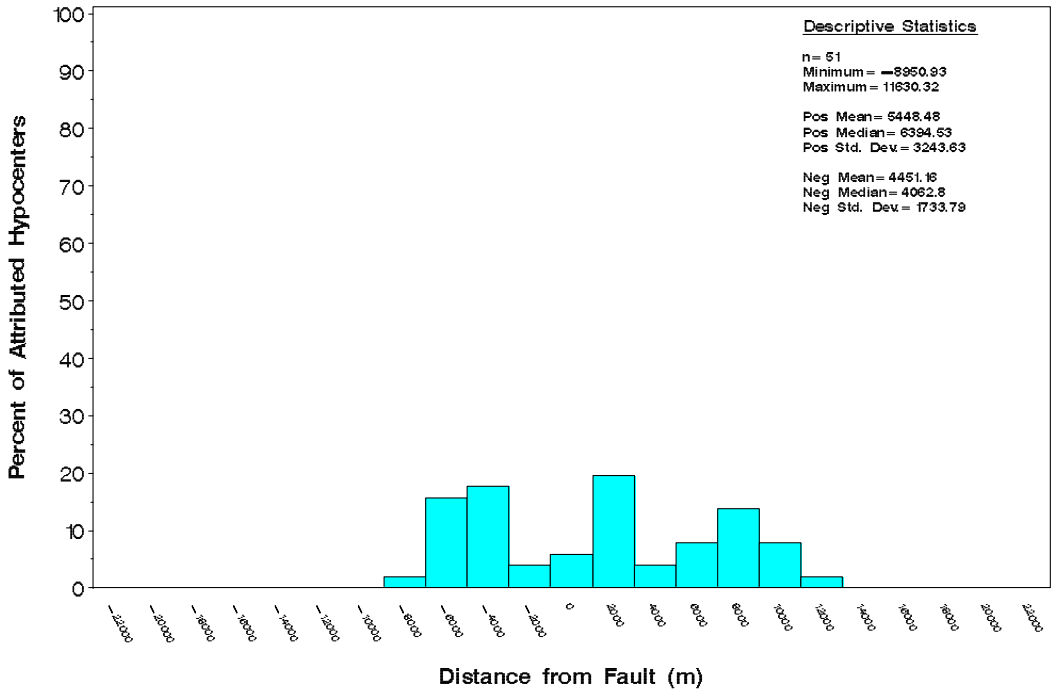

System = Kwiko
Fault= Keiko (A99—4)

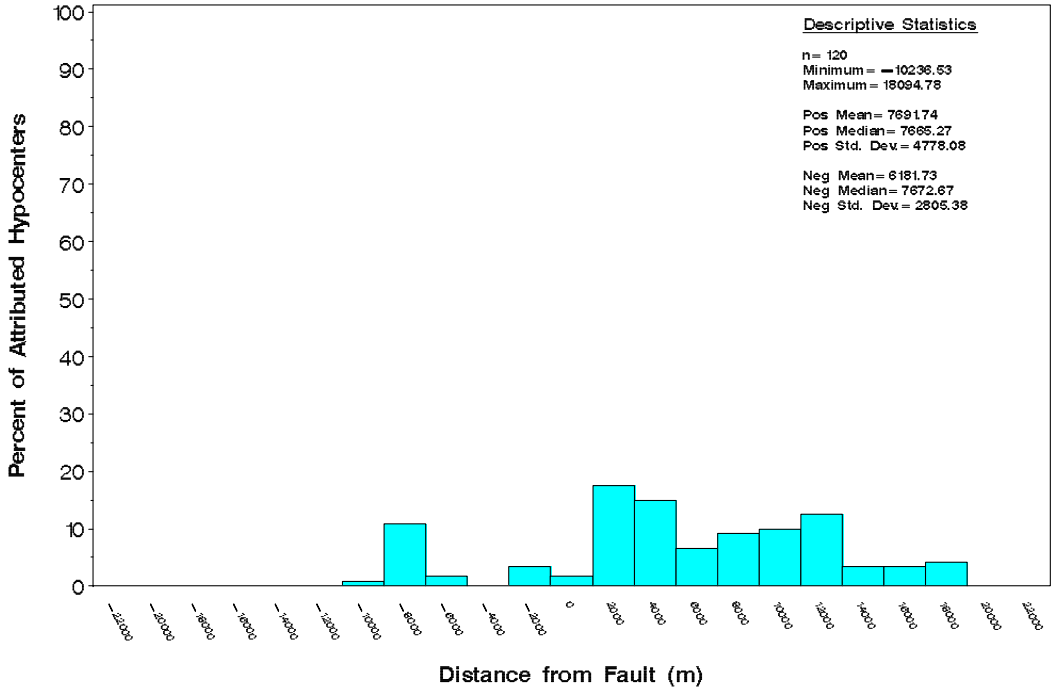

System = Beppu—Mannenyama
Fault= Kurotake (A101—1b)

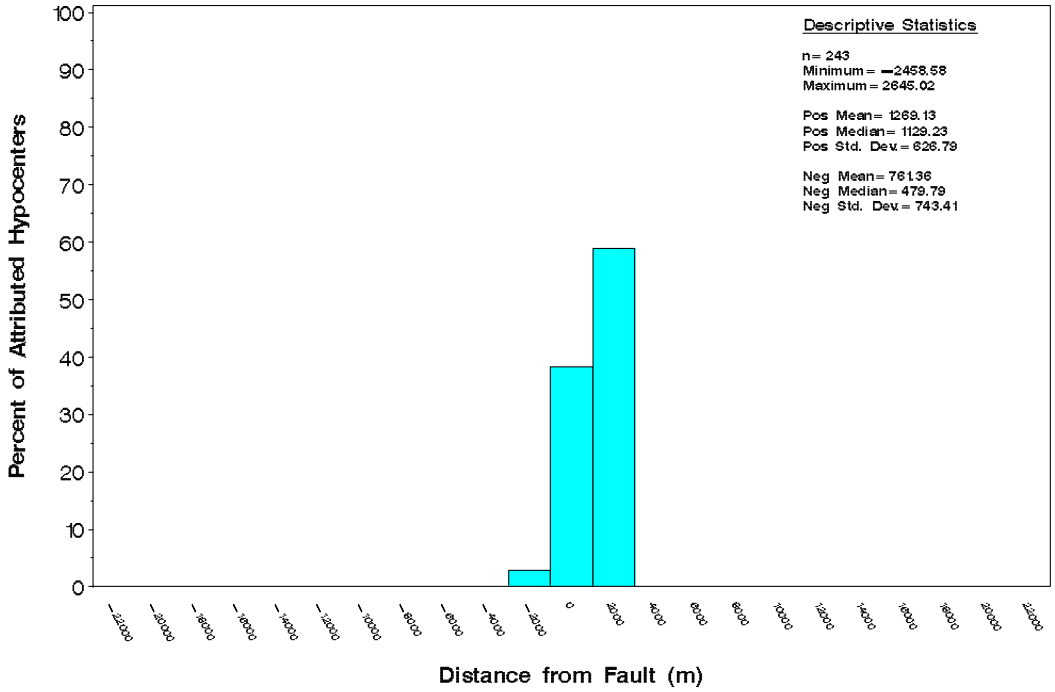

System = Beppu—Mannenyama
Fault= Hanaka (A101—2)

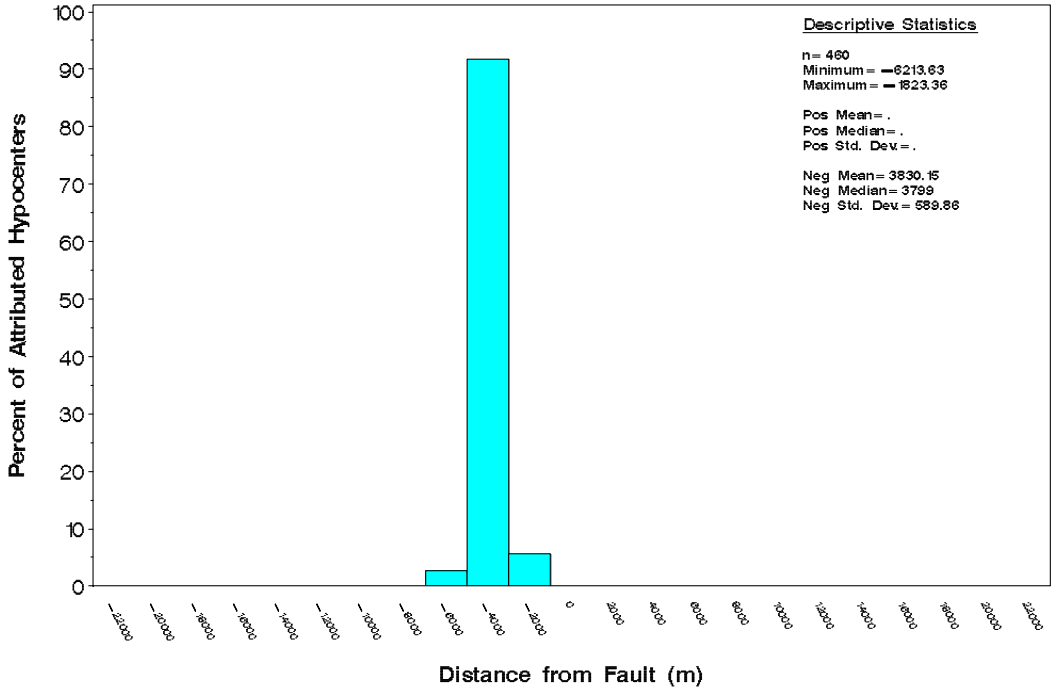

System = Unzen
Fault= Chijiishi (A102—4)

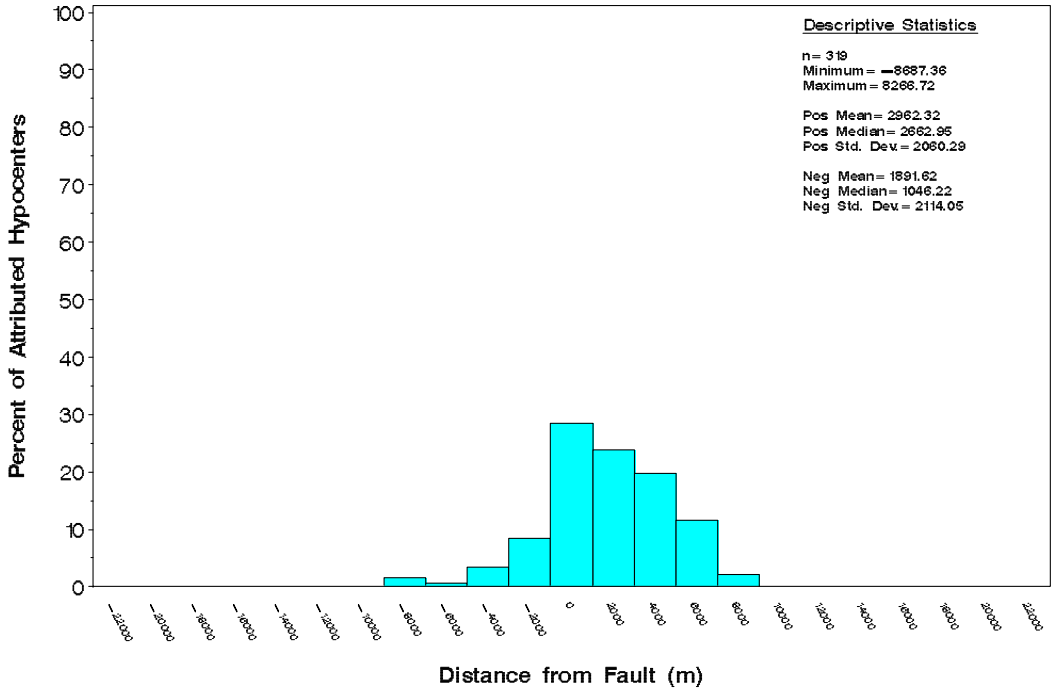

System = Unzen
Fault= Nunotsu (A102—5)

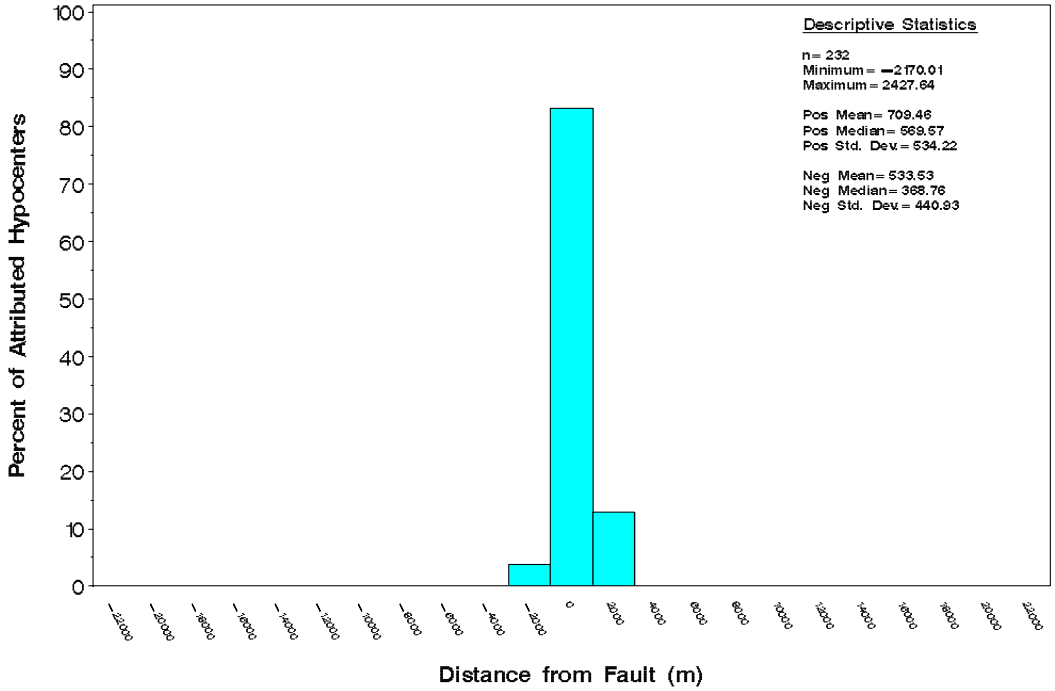

System = Hutagawa—Hinaku
Fault= Ono, Hinaku (A106—1)

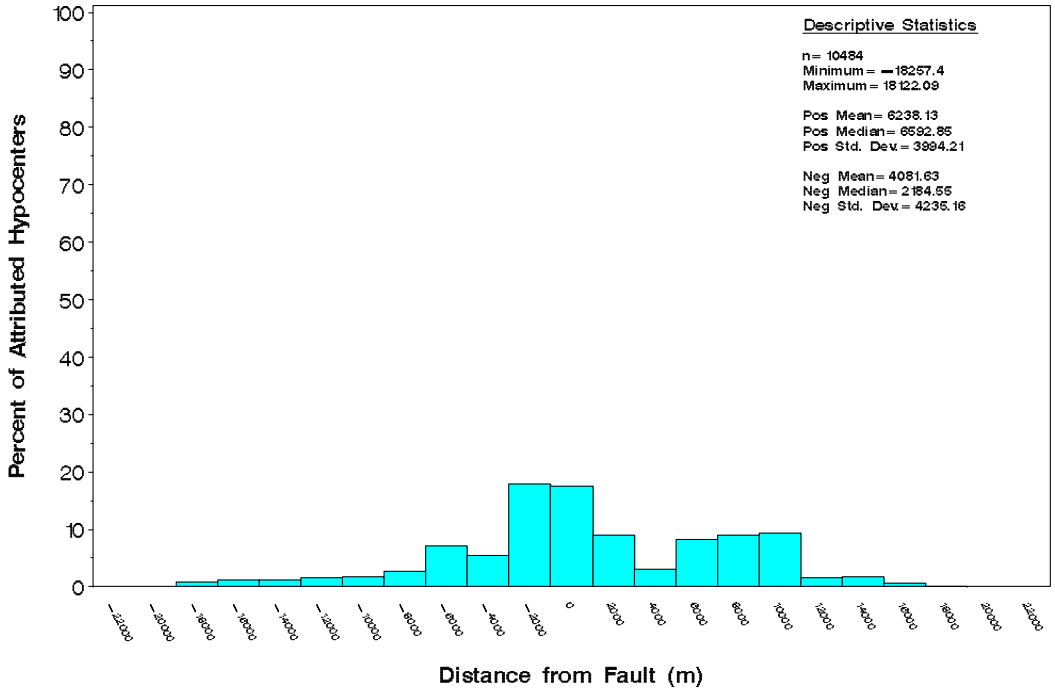

System = Hitoyoshi—bonchi
Fault= Touhou—Tabata, Motobeppu (A106—3)

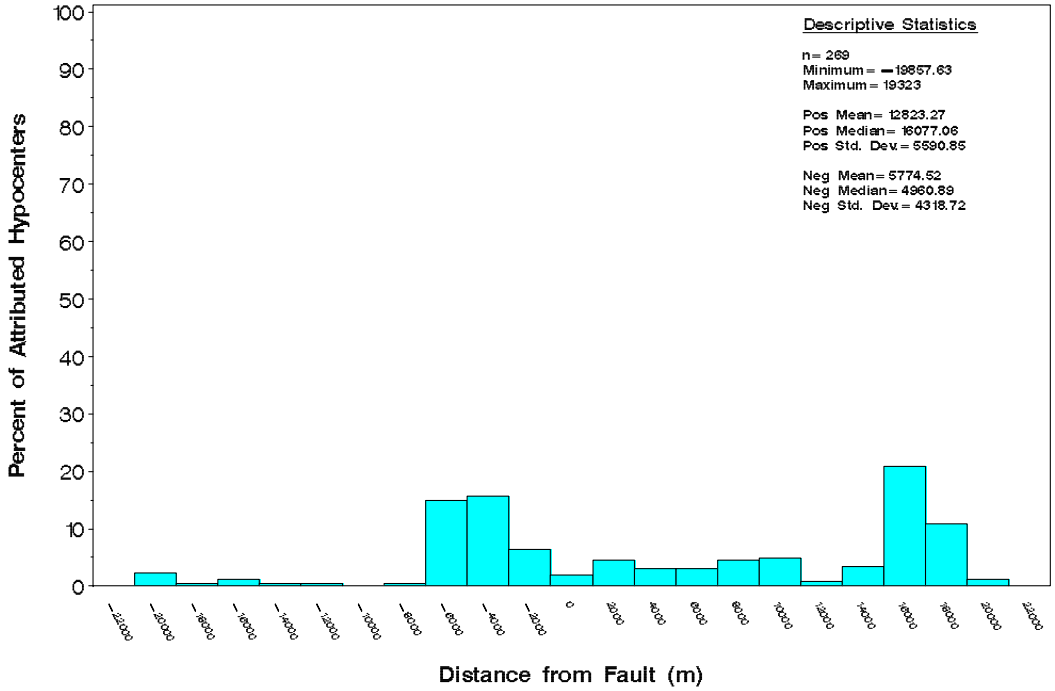

System = Demizu
Fault= Yhazutoge, Kiminagawa, Uchikiba (A106—4)

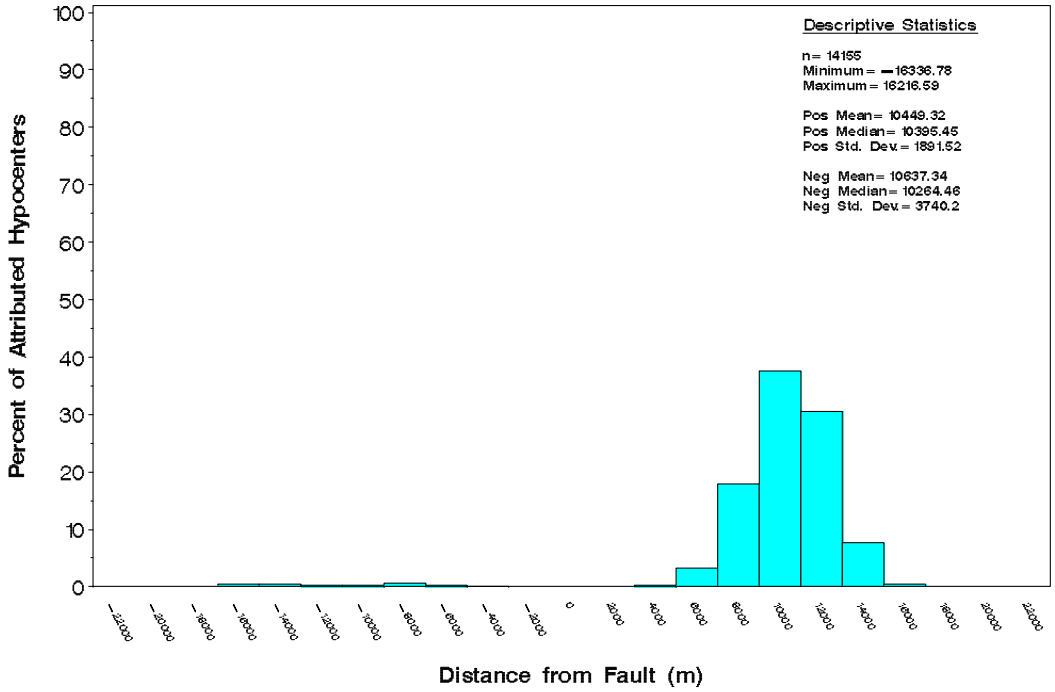

System = Tanegashima
Fault= Hnasatozaki—Tanosaki (A112—1)

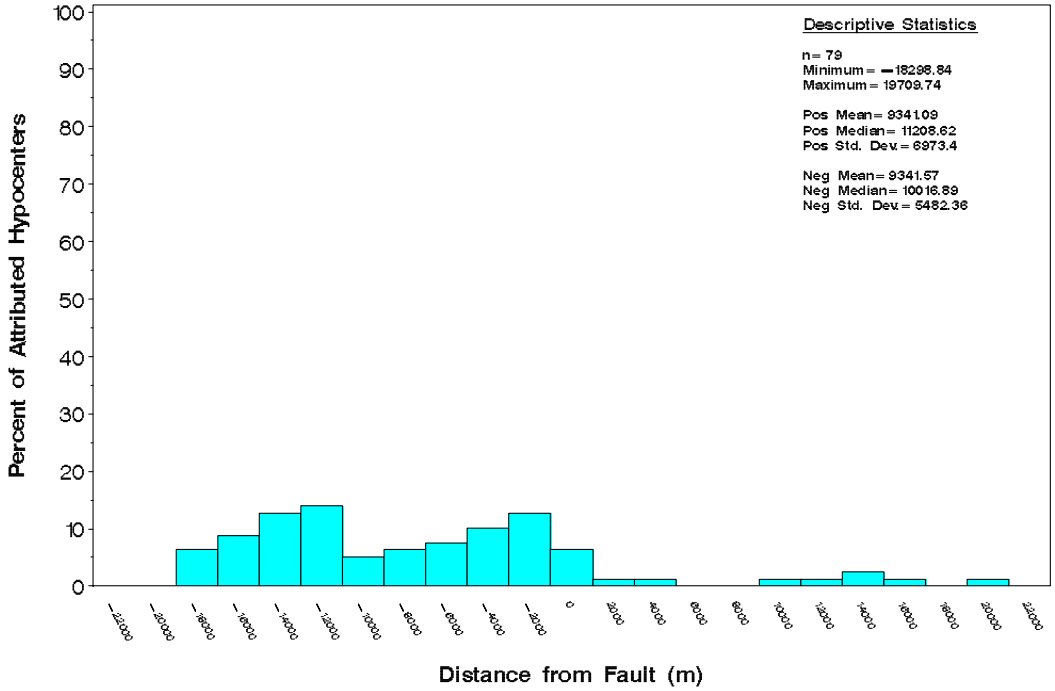

System = Oritsume
Fault= Oritsume (B30—1)

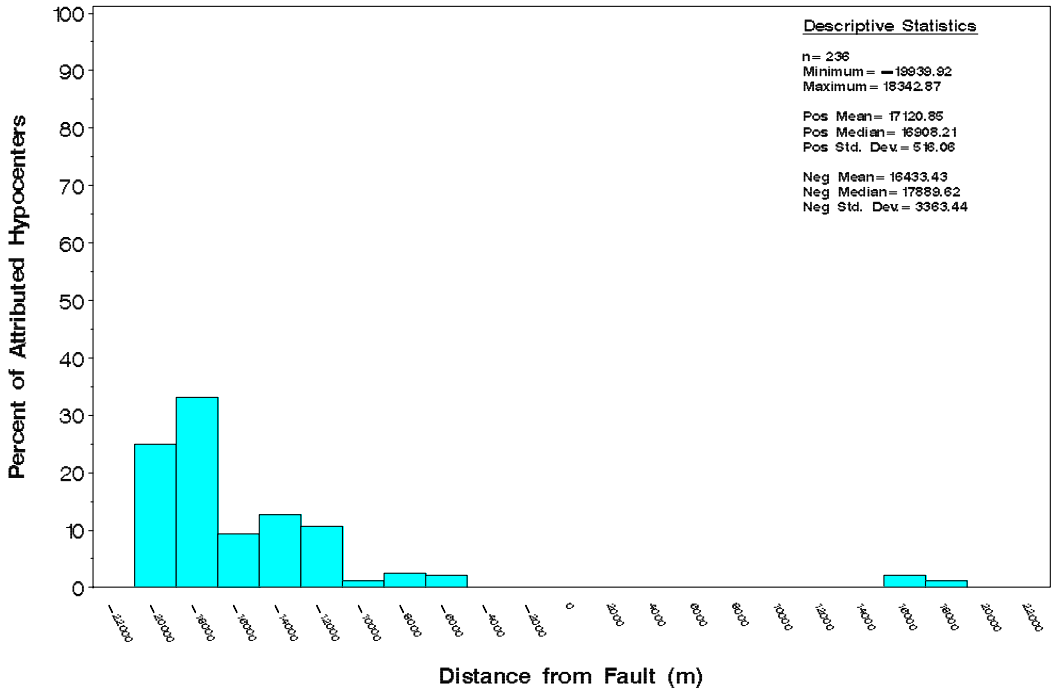

System = Yakushima—nangann
Fault= Onoma (A114—1)

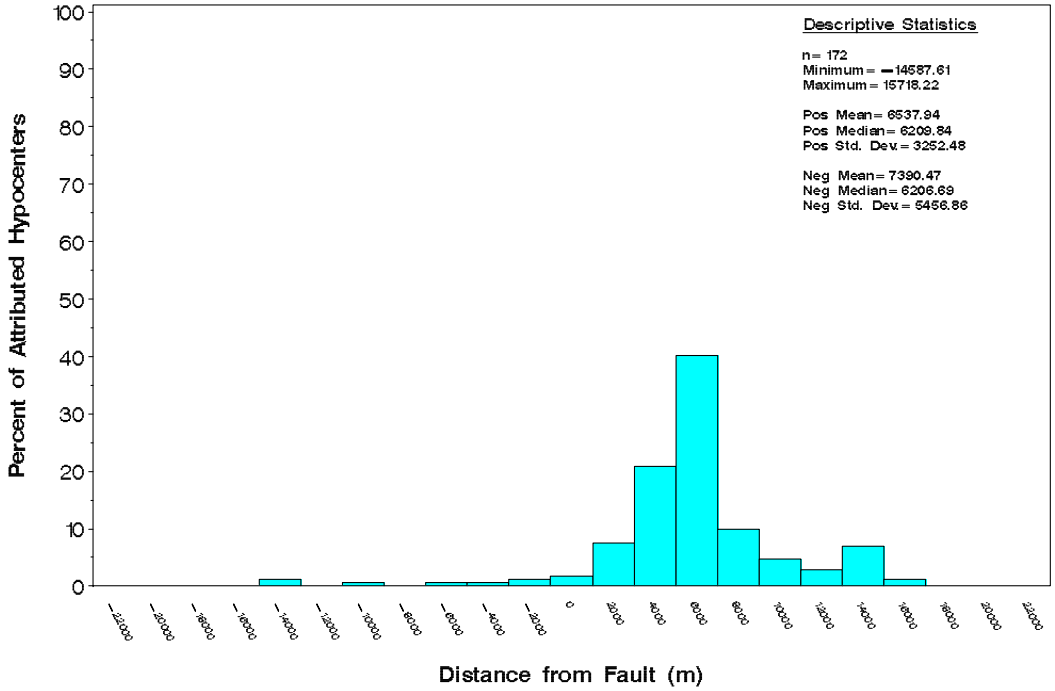

System = Unknown
Fault= Murata (B40—2)

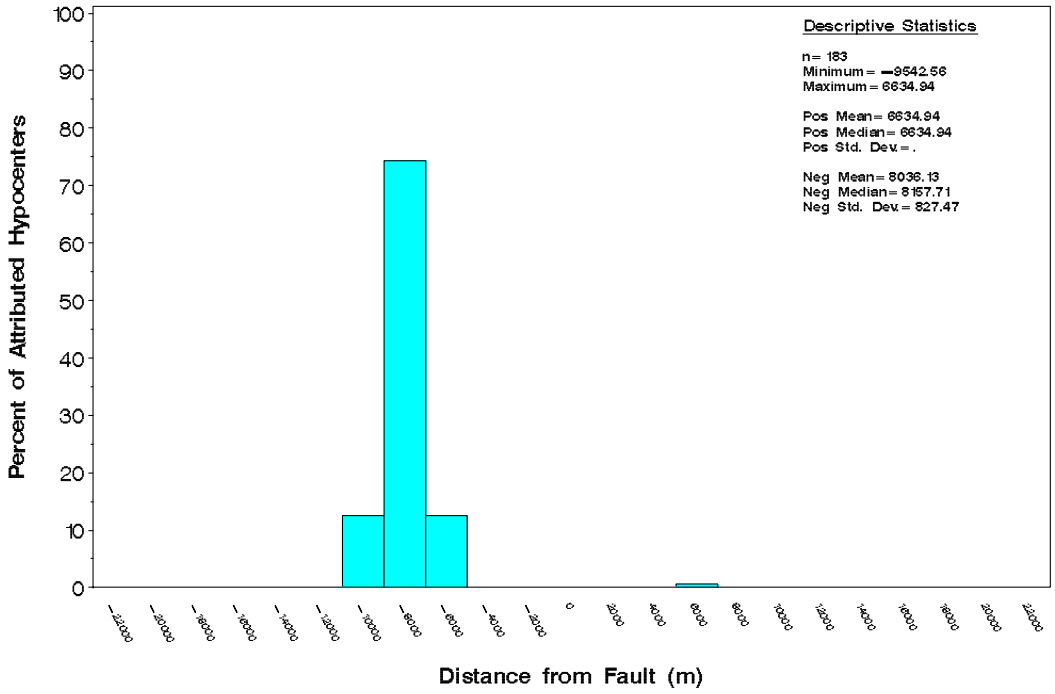

System = Unknown
Fault= Unnamed (B40—3)

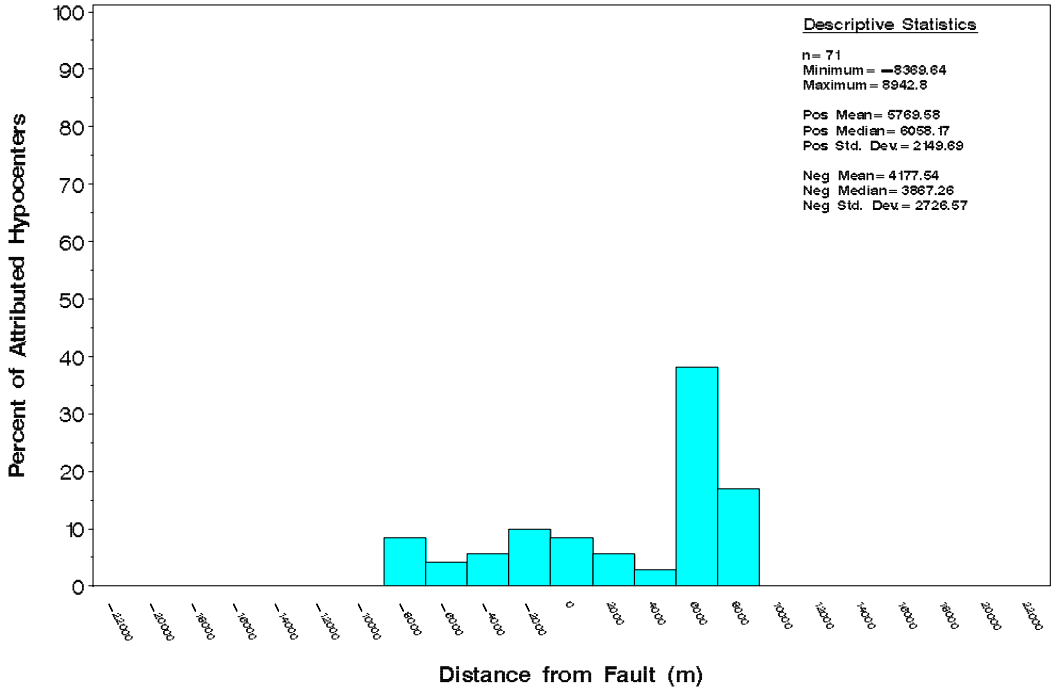

System = Unknown
Fault= Kannawa Thrust, Fujisawa (B52—4)

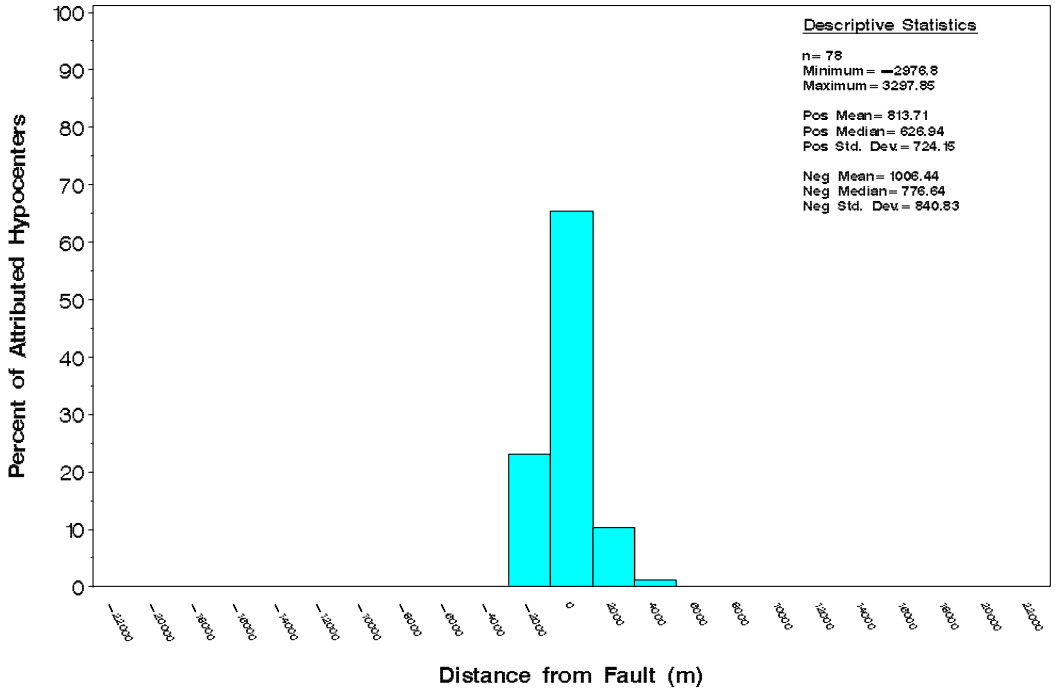

System = Median Tectonic Line
Fault= Unnamed (B60—1)

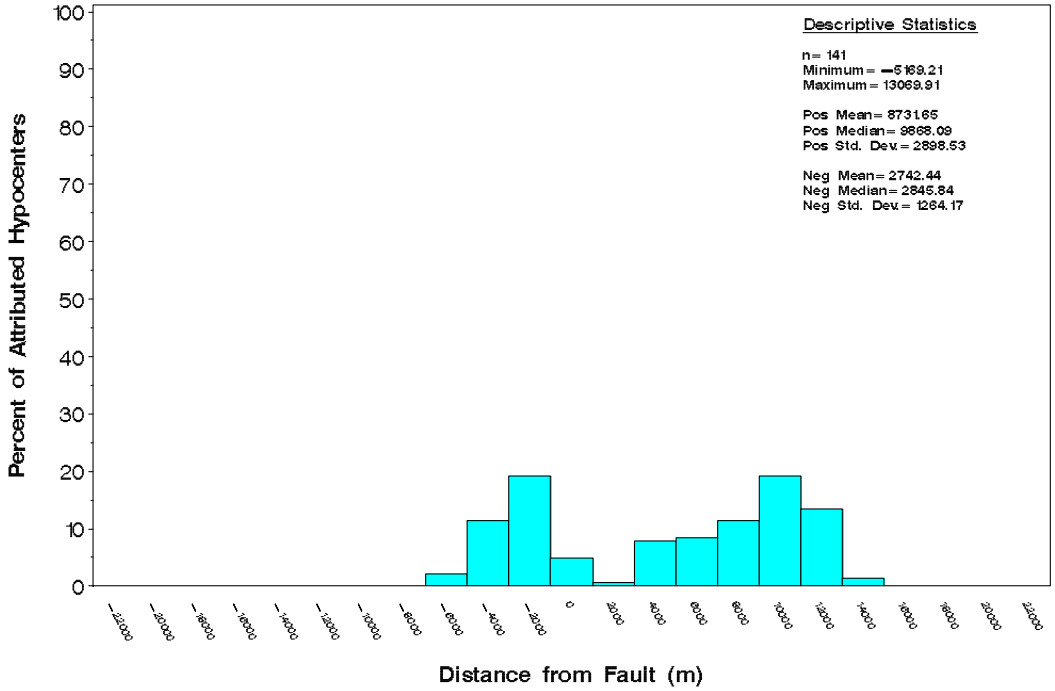

System = Unknown
Fault= Jonendake, Kashimamanganji (B64—1)

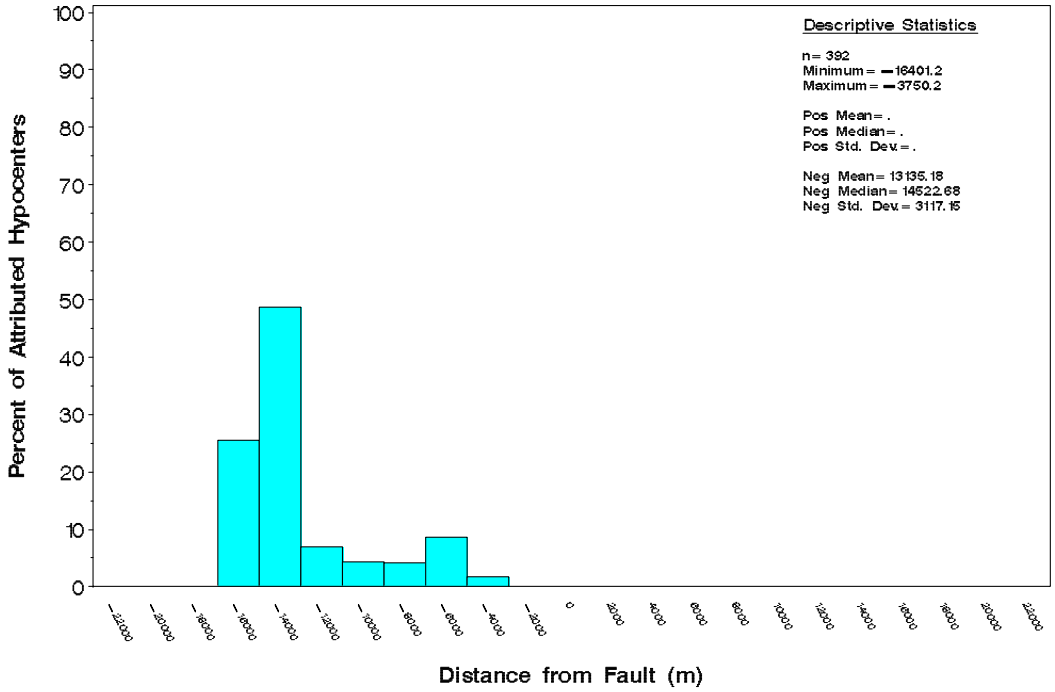

System = Unknown
Fault= Shinanozaka (B64—2)

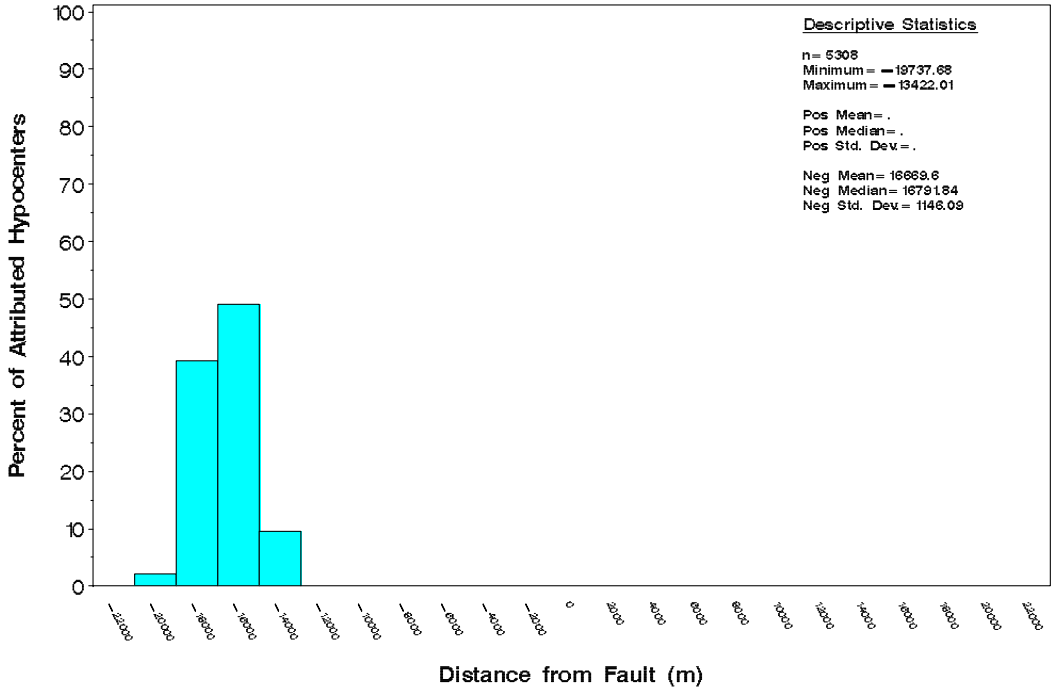

System = Unknown
Fault= Mozumi—Hironobe (B64—3)

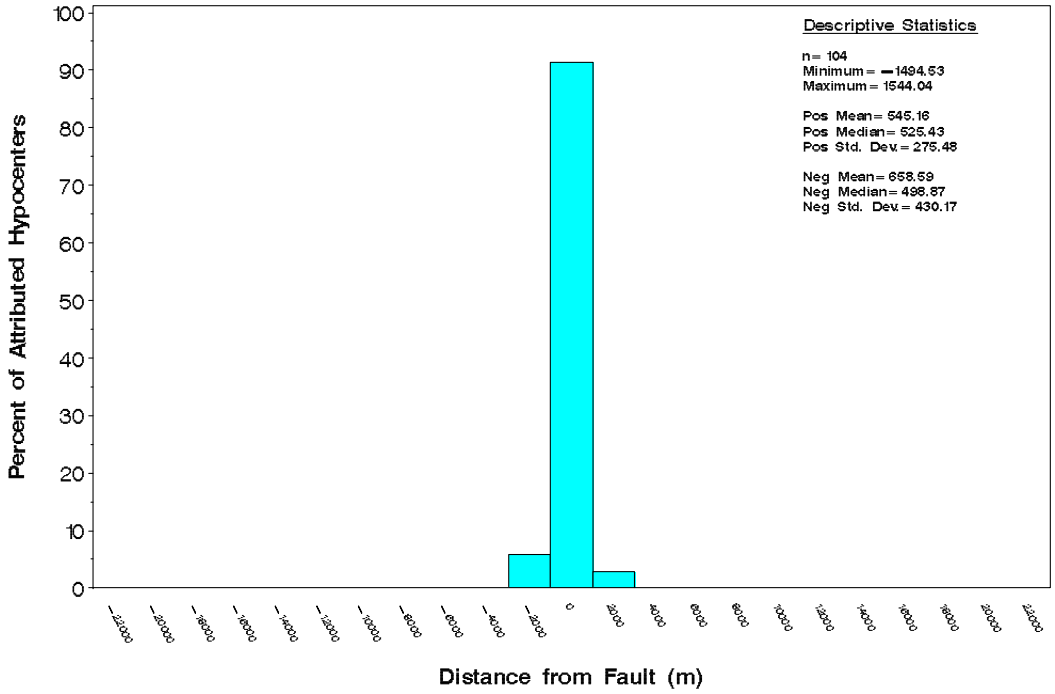

System = Unknown
Fault= Kunogawa (B65—2)

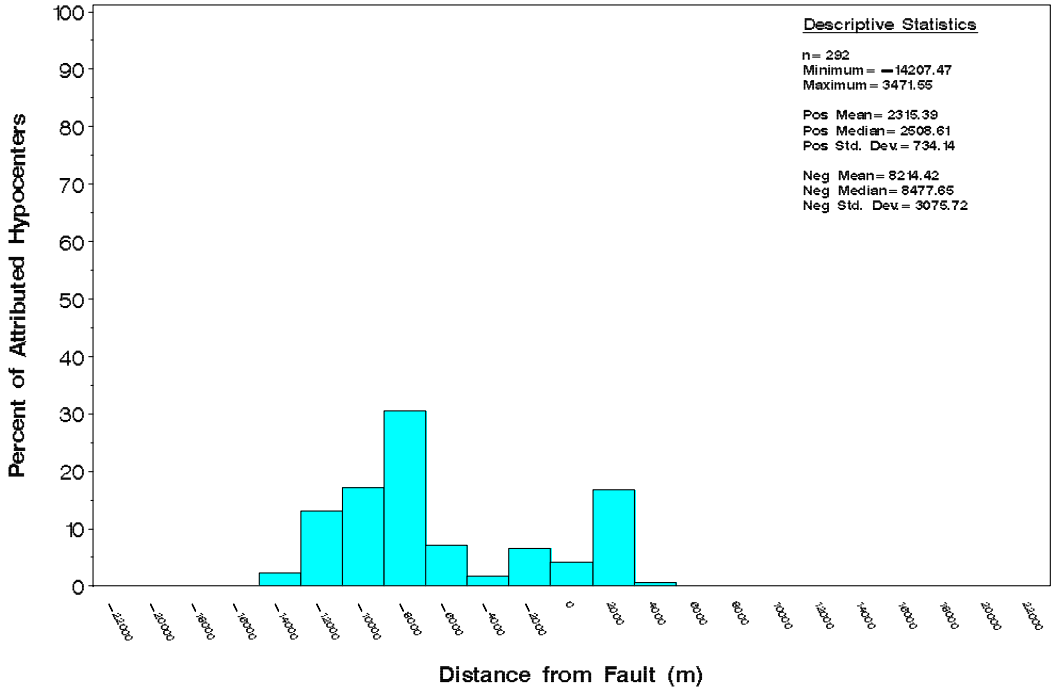

System = Ohara
Fault= Ohara (B65—4)

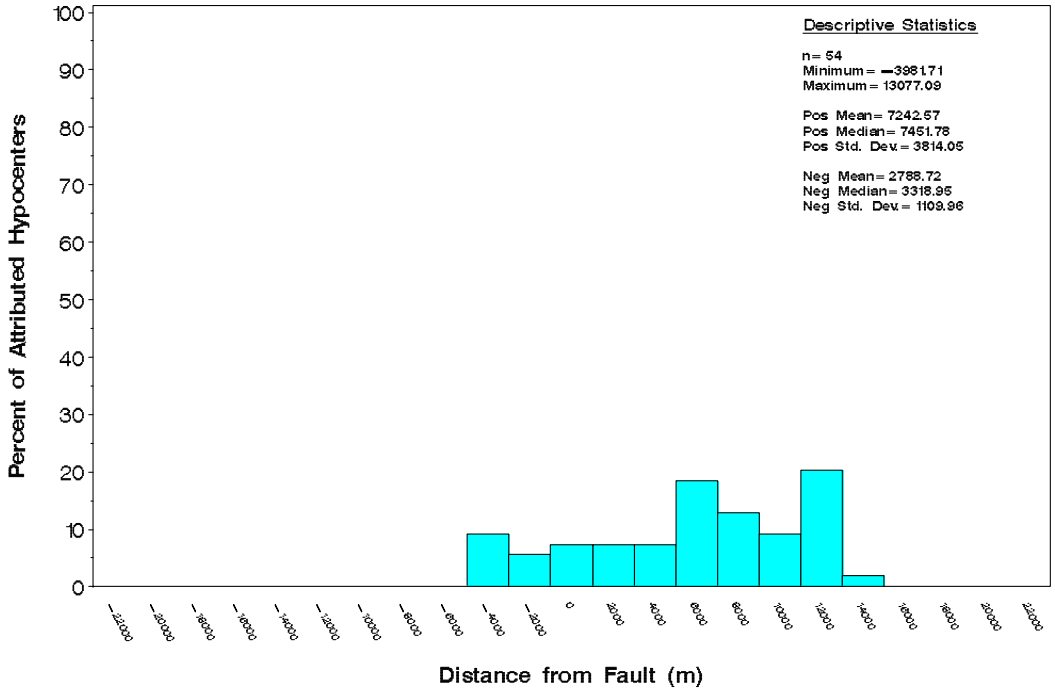

System = Nagaragawa—jouryu
Fault= Hachiman (B71—1)

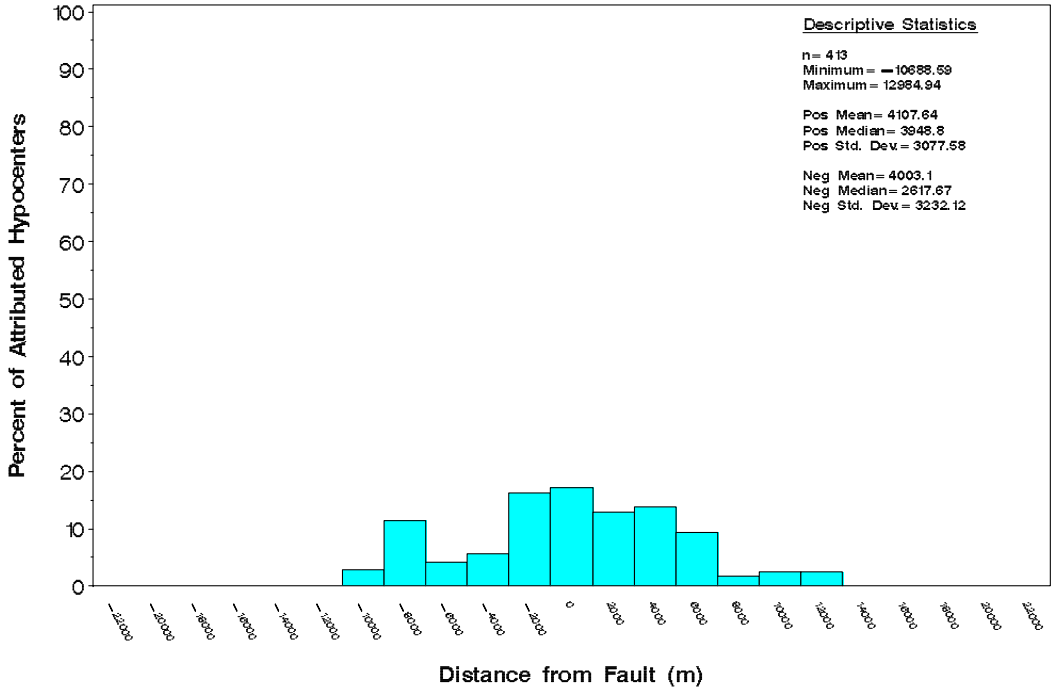

System = Unknown
Fault= Kakiya, Nawa—Kaki (B72—2)

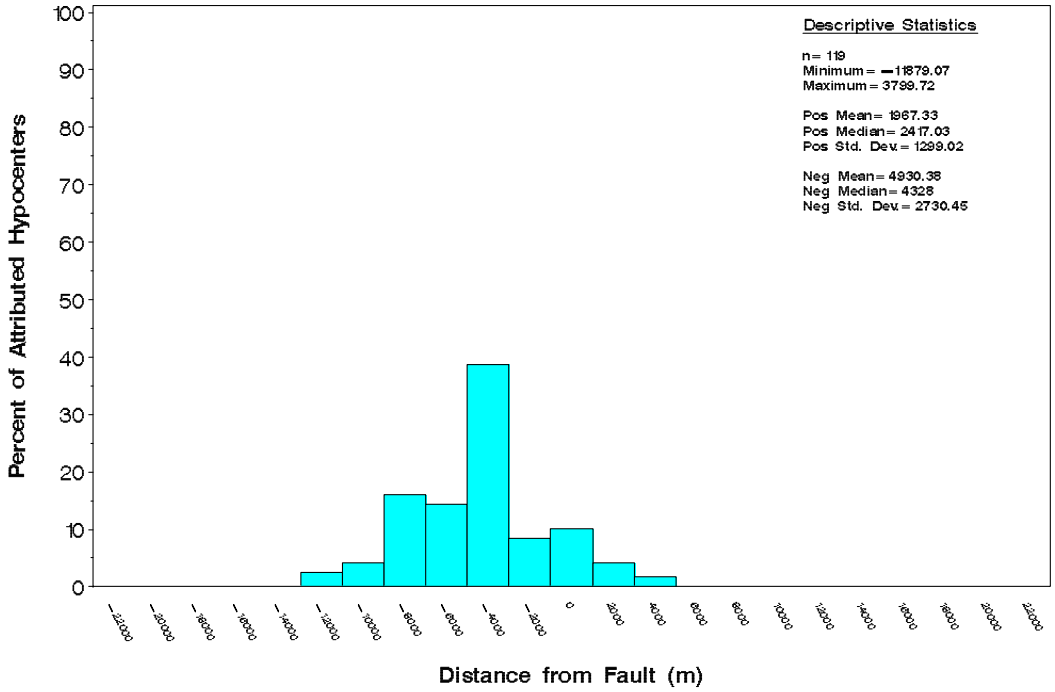

System = Unknown
Fault= Ootorii (B72—5)

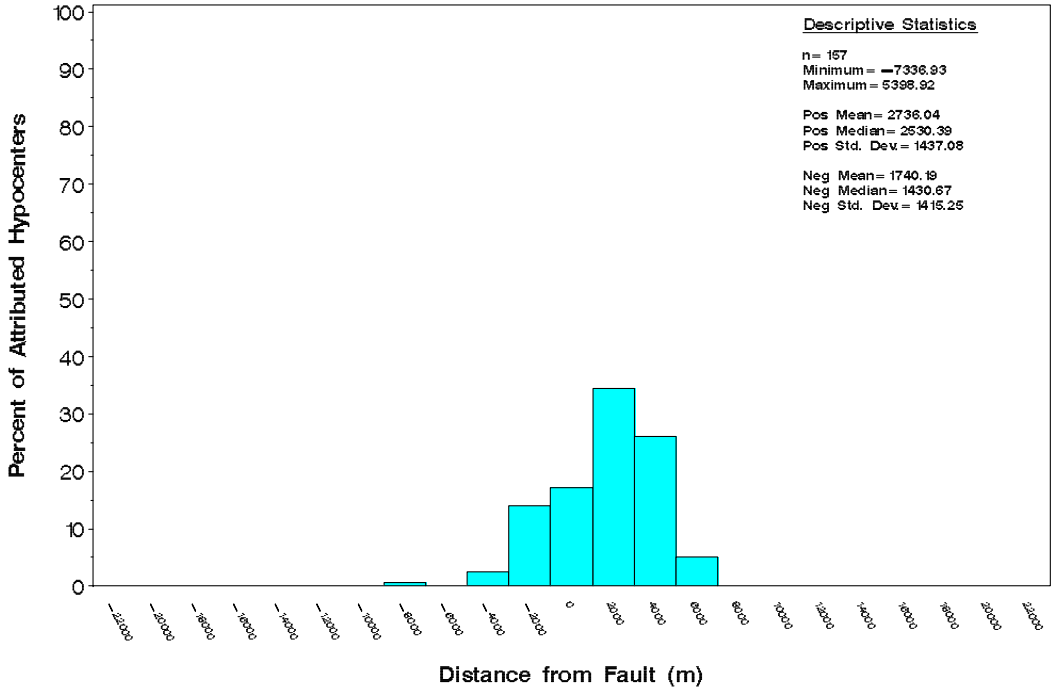

System = Biwako—seigan
Fault= Hira (B76—1)

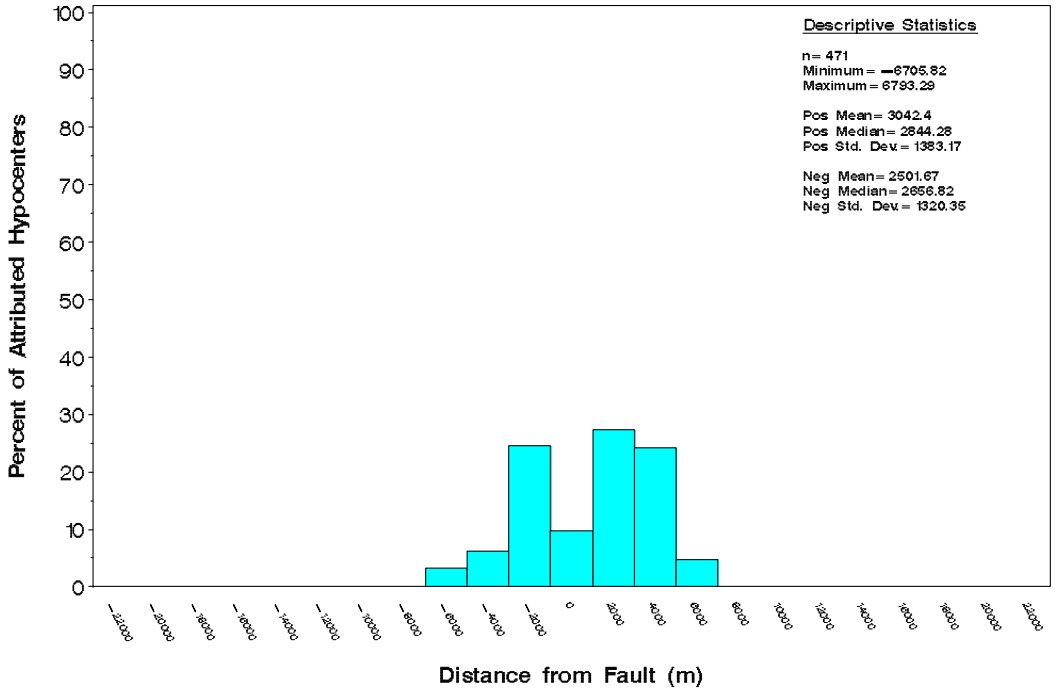

System = Unknown
Fault= Tahara (B76—4)

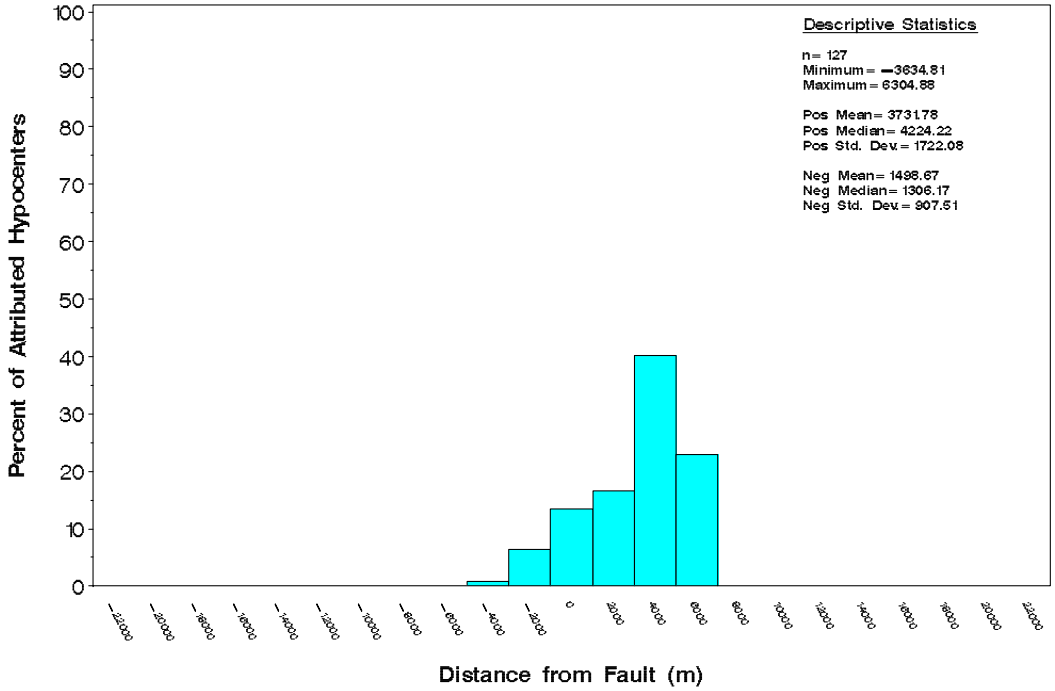

System = Rokko—Awaji
Fault= Otsuki, Numobiki (B76—6)

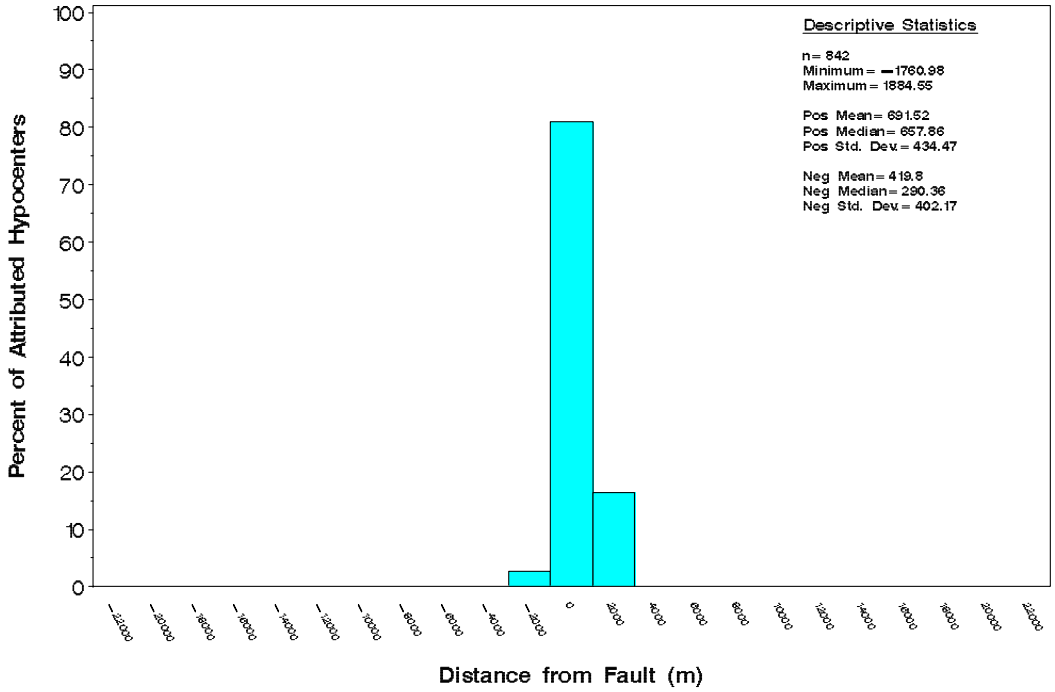

System = Arima — Takatsuki
Fault= Arino — Dango (B76 — 7)

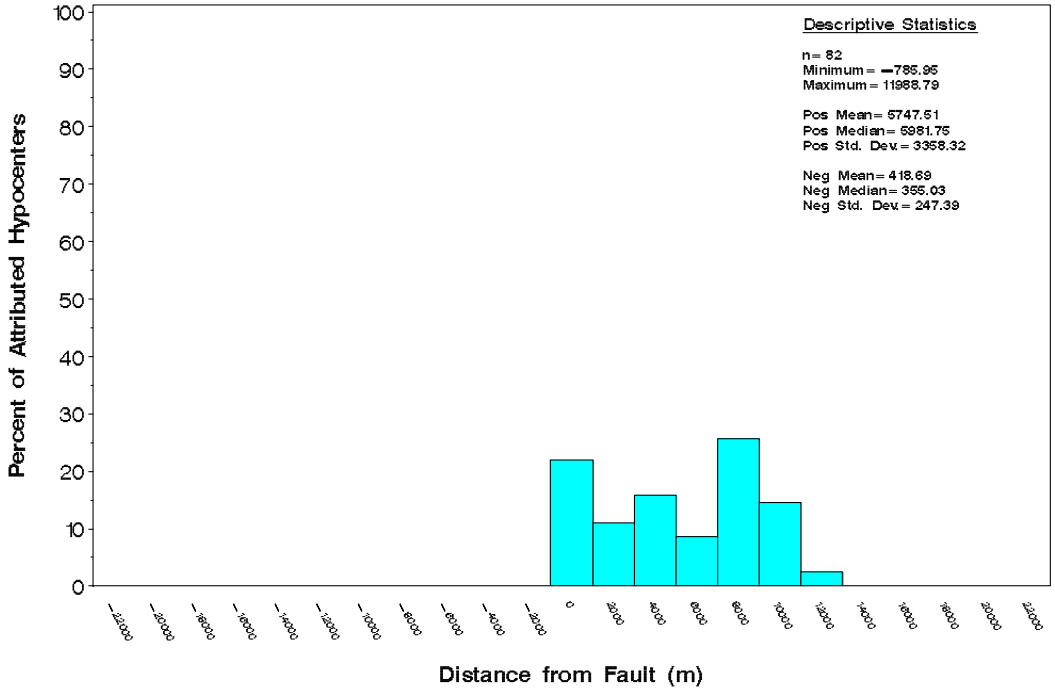

System = Unknown
Fault= Furuichi (B76 — 9)

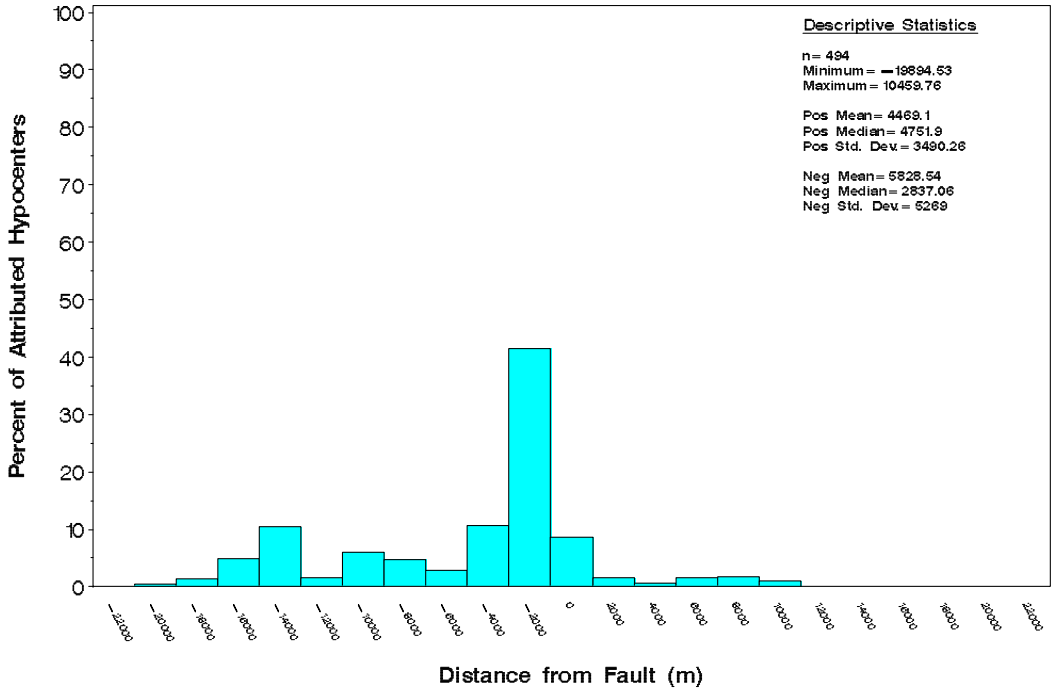

System = Unknown
Fault= Ametaki—Kamado (B79—1)

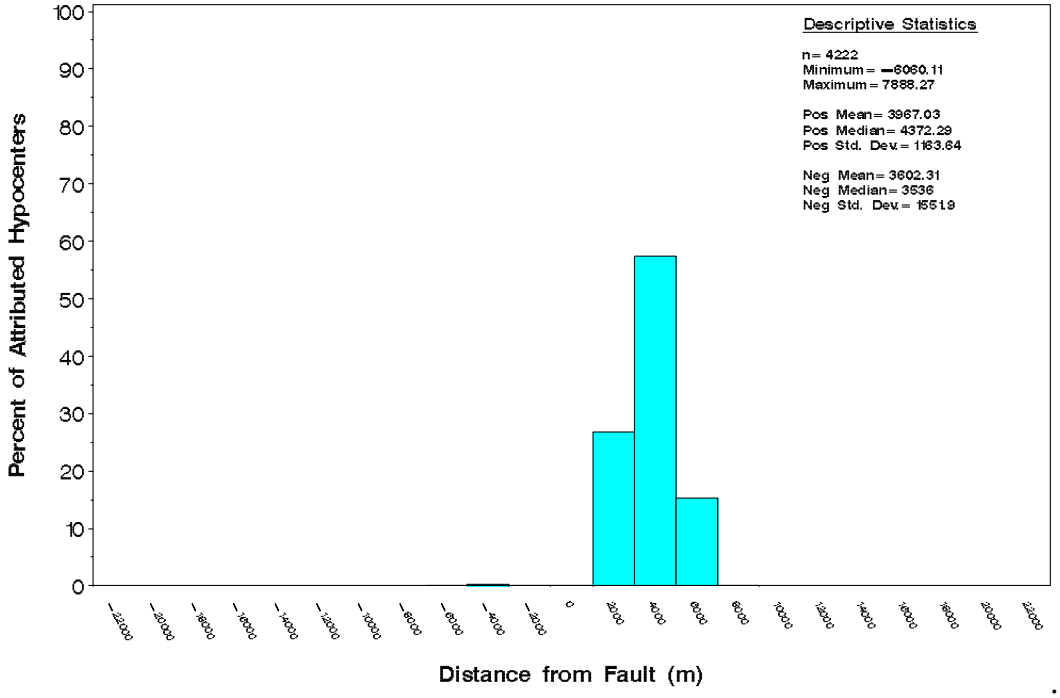

System = Yamasaki
Fault= Gobantoge (B80—1)

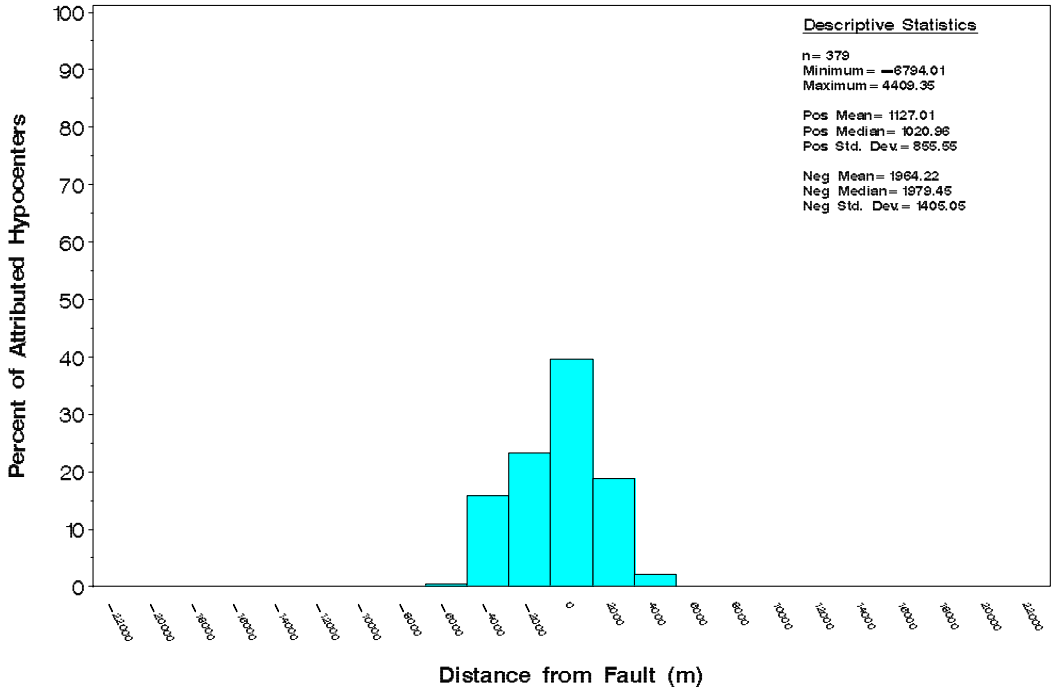

System = Ayukuigawa
Fault= Miyamae, Nanzan (B82—1)

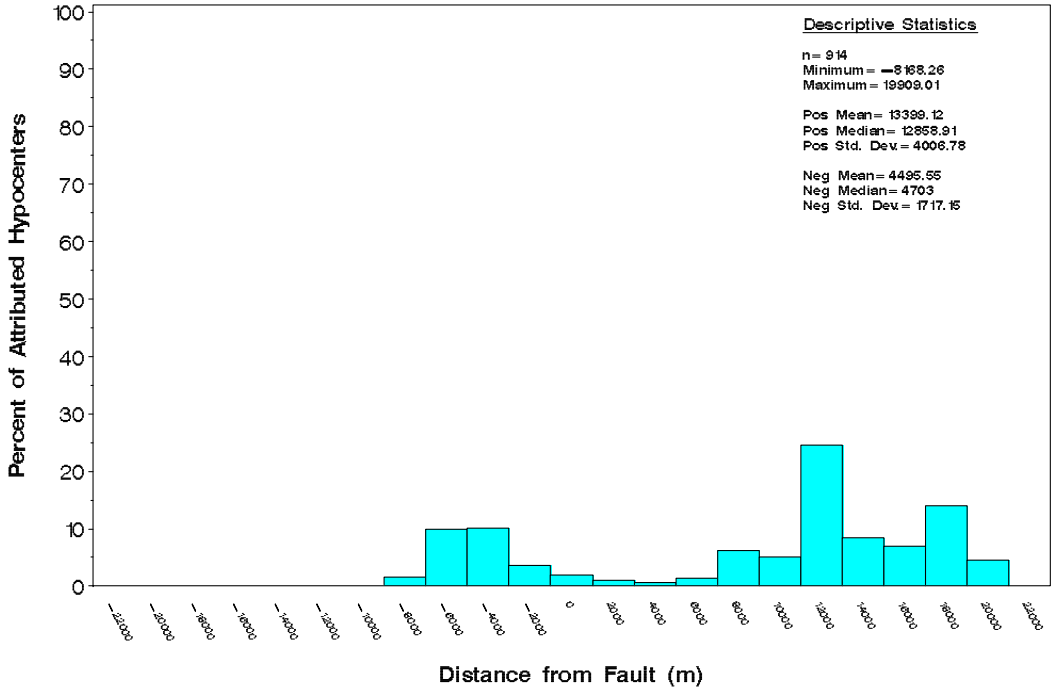

System = Unknown
Fault= Mitate (B101—2)

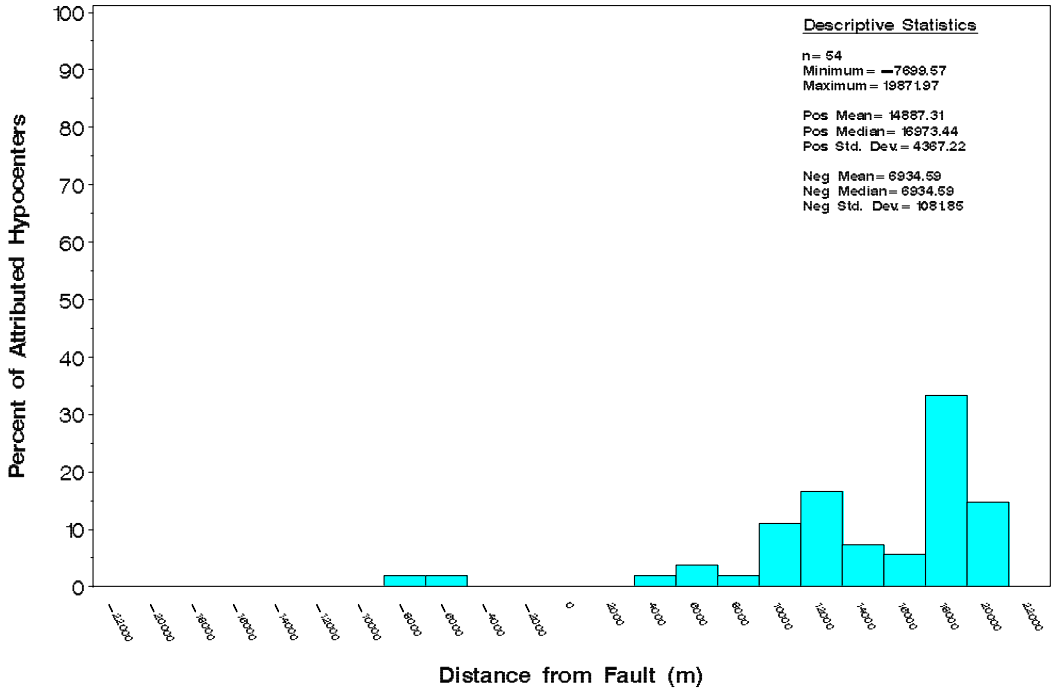

Appendix D

Errors in the Location of Earthquake Hypocenters

The estimated location of an earthquake hypocenter is a combination of the true location of the hypocenter (x,y,z) and two types of error: 1) error due to using an earth velocity model that is not the true model as well as non-uniqueness in the hypocenter location caused by non-optimal sensor network geometry (referred to as *geologic/geometric error* and denoted as (dx_G, dy_G, dz_G)) and 2) error within the actual sensors themselves, such as timing errors, errors caused by the coupling of the sensor to the earth and noise within the sensor electronics (termed as *sensor error* and denoted (dx_S, dy_S, dz_S)). The two types of error are independent in that if one type of error was removed, the other type would not be affected. The estimated locations of the hypocenters (x',y',z') as given in the database are a combination of the true locations and the two types of error:

$$x'=x + dx_G + dx_S \qquad y'=y + dy_G + dy_S \qquad z'=z + dz_G + dz_S$$

No information is provided on the magnitude of the sensor error and typically this is not something that is easily quantified; however, standard errors of the estimated locations that are mainly a function of the geologic/geometric error are given in the hypocenter data set. The estimated hypocenter locations were reported along with standard errors of the estimate in the directions of the longitude, latitude and depth. If we ignore the unknown sensor error, these three components of the standard error of location define an error ellipse that is centered on the estimated location of the hypocenter (Figure D-1). No such estimates of the standard errors are available for individual locations along the fault trace. In fact, not all the actual locations defining the fault traces are known (see the section titled "Fault Endpoint Polyline Creation" in main text). However, uncertainties in the locations of faults are not considered in this discussion.

Figure D-1 presents a planimetric view of an estimated hypocenter location (red circle) and the error ellipse around that location (blue ellipse) along with the straight-line distances that are orthogonal to each of three different faults: A, B and C. In Figure D-1, the distance from the estimated hypocenter to each of the three faults is exactly the same. Although the distances to the hypocenters are exactly the same, the amount of the standard error along each distance line is quite different depending on the orientation of the fault relative to the ellipse. From the hypocenter to Fault A, the magnitude of the standard error is roughly 20 percent of the best estimate of the total distance. The distance from the estimated hypocenter to Fault C is the same as to Fault A, but the standard error is 100 percent of the total distance to Fault C. The error along the line to Fault B is an intermediate proportion of the distance between that of the Fault A and Fault C proportions.

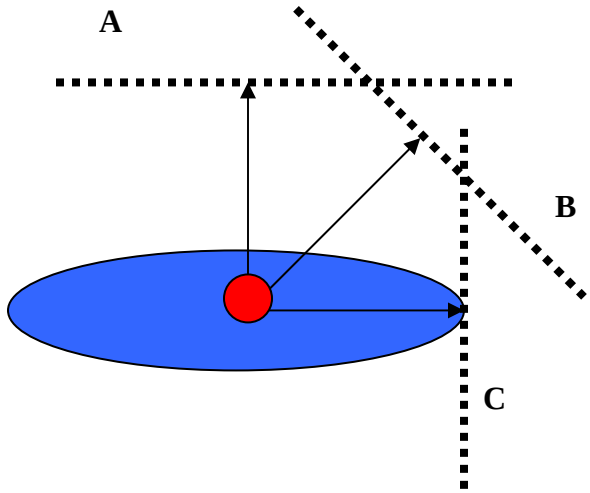

Figure D-1. Map View of the Error Ellipse Around an Estimated Hypocenter Location and the Normal Distances to Three Faults, All the Same Distance Away from the Hypocenter.

Given all of the available data on the estimated hypocenters, the three components of the standard error and the fault dips and orientations, it would theoretically be possible to calculate the error term along the vector from each hypocenter to each fault. However, this would not be a correct characterization of the error because the sensor error has been ignored. Additionally, the actual location of the hypocenter within that ellipse is unknown and therefore it is not possible to accurately determine the effect of the standard error in hypocenter location on the calculated distances between the estimated hypocenter and the nearest fault. The hypocenter locations are presumed to be the best available estimates, with the uncertainty of those estimates expressed in terms of the standard errors.

The accurate calculation of the effect of the standard error of the hypocenter location is not possible. However, some intuitive feeling for the effect of this error, if it was possible to calculate, can be gained by a simple set of one-dimensional calculations. In general, for a normal, or near normal, probability distribution, the total variance of the distribution is the sum of the component variances. The total mean is also the sum of the component means. These relationships can be rearranged as:

$$Var_{Combined} - Var_{Uncert} = Var_{Offset}$$

$$Mean_{Combined} - Mean_{Uncert} = Mean_{Offset}$$

This situation specifically concerns the offset distances from the center of a fault zone in one direction. As such, these distributions of offset distances have a mean value of zero because the hypocenters are expected to be uniformly distributed on both sides of the active fault. Additionally, the uncertainty in the hypocenter location is expected to be unbiased –that is, the location of a hypocenter relative to the distance from a nearby fault is just as likely to be

overestimated as underestimated. Therefore, the mean value of all distributions in the equations above should be zero and it is not necessary to examine the relationship between means of distributions any further.

The distribution of one-dimensional distances from an estimated hypocenter location to the closest fault is a combination of the true distance between the hypocenter and the fault and the error in the actual location of the hypocenter. This relationship is illustrated with an example calculation. A total of 2000 random distances were drawn from a Gaussian distribution with a mean of 0.0 and a standard deviation of 1000.0 to represent the observed distribution. Here the standard deviation represents the sum of the true offset and hypocenter location uncertainty. A second set of random numbers was drawn from a Gaussian distribution with a mean of zero and standard deviation of 250.0 to represent the unknown distribution of errors in hypocenter location alone. For each pair of random numbers, the error value was subtracted from the combined value and the difference is the true offset distance. The distributions are shown in Figure D-2 and the actual values of the mean, variance and standard deviation of the three distributions are given in Table D-1.

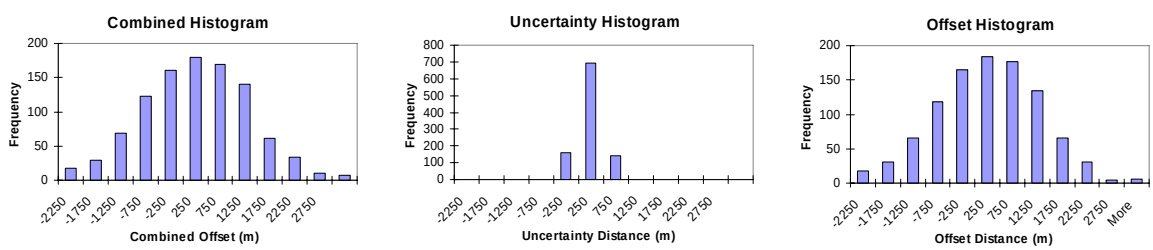

Figure D-2. Distributions of Offset Distances Showing the Combined (Left), Uncertainty (Middle) and Offset Distributions (Right)

TableD-1. Mean, Variance and Standard Deviation of the Three Distributions Representing the Combined Offset Distances, the Errors in Hypocenter Location and the True Offset Distances for the Example Calculation. All units are in m or m^2.

	Combined	Uncertainty	Offset Distances
Mean	18.1	-2.3	20.4
Variance	1,115,798	60.227	1060705
Standard Deviation	1056.3	245.4	1029.9

The combined distribution of both true offset distances and the uncertainty, or error, in estimating those offset distances is shown by the distribution in the left image of Figure D-2. The distribution of uncertainty in estimates is shown in the center image of Figure D-2 and the true distribution of offset distances is shown in the right image of Figure D-2. The effect of the uncertainty distribution on the true offset distances is seen by comparing the observed combined

distribution (Figure D-2, left) to the distribution of true distances (Figure D-2, right). For this example calculation, the differences between the combined distribution and the true offset distribution are nearly indiscernible.

These results indicate that when the uncertainty distribution is roughly one-fourth the width of the combined distribution (compare standard deviations), the true offset distribution has an only slightly narrower width than the combined distribution. In other words, for this example calculation where the uncertainty in the hypocenter locations was one-fourth of the width of the observed combined distribution, the differences in the combined and true offset distance distributions was relatively small (true offset standard deviation is 97.5 percent of the standard deviation of the observed combined distribution).

The equation above defines the differences in distributions in terms of variances. However, in practical use, it is often the standard deviation of the distribution that is used to define the spread of values about the mean value. Therefore, the relationship between the ratio of the observed offset distance standard deviation, which combines both the true offset and the hypocenter location error, to the true offset distances standard deviation as a function of the proportion of the combined distances standard deviation that is due to the hypocenter location error is shown in Figure D-3. From Figure D-3, it can be seen that the standard deviation of the combined distribution of offset distances is essentially the same as the standard deviation of the true distribution when the standard deviation of the hypocenter location error is 10 percent or less of the standard deviation of the combined offset distances. Even as the error grows to be 50 percent of the overall combined distribution standard deviation, the difference between the combined distribution standard deviation and the true offset standard deviation is only 15 percent. These results are for one-dimensional results only. The effect for multi-dimensional distances is not treated here.

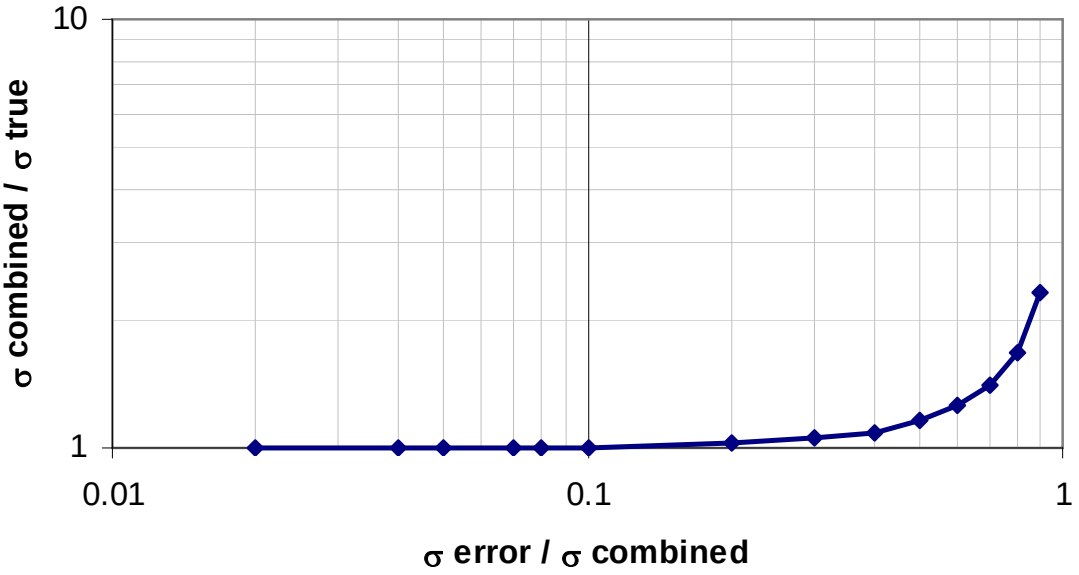

Figure D-3. Relationship Between Ratio of the Observed Distribution of Offset Distances and the True Offsets as a Function of the Hypocenter Error Normalized by the Standard Deviation of the Combined Distribution

Distribution List

Internal

1	MS 0735	Ray Finley, 6115
1	MS 0735	Tom Lowry, 6115
1	MS 0735	Sean McKenna, 6115
4	MS 0735	Barry Roberts, 6115(4)
1	MS 0778	Bill Arnold, Dept. 6851
5	MS 0731	NWM Library, 6805
1	MS 9018	Central Technical Files, 8945-1
2	MS 0899	Technical Library, 9616

External

Kazumi Kitayama
NUMO Headquarters
MitaNN Bldg., 1-23 Shiba 4-Chome,
Minato-ku, Tokyo, Japan, 108-0014.

Hiroyuki Tsuchi (3)
NUMO Headquarters
MitaNN Bldg., 1-23 Shiba 4-Chome,
Minato-ku, Tokyo, Japan, 108-0014.

Junichi Goto (3)
NUMO Headquarters
MitaNN Bldg., 1-23 Shiba 4-Chome,
Minato-ku, Tokyo, Japan, 108-0014.

Dr. Katsuhiko Ishiguro
NUMO Headquarters
MitaNN Bldg., 1-23 Shiba 4-Chome,
Minato-ku, Tokyo, Japan, 108-0014.

Keiichiro Wakasugi
NUMO Headquarters
MitaNN Bldg., 1-23 Shiba 4-Chome,
Minato-ku, Tokyo, Japan, 108-0014.

Dr. Tim Coburn (2)
Department of Management Science
Abilene Christian University
ACU Box 29315
Abilene, TX 79699

Dr. Erik Webb
201 3rd Street NW, Suite 710
Albuquerque, NM 87104

Sandia National Laboratories